The study of Stray Magnetic Fields from Digital Recording heads for Tape Applications

Tommy Munro

UNIVERSITY
of
GLASGOW

Submitted for degree of Doctor of Philosophy at the Department of Physics and Astronomy, University of Glasgow.

December 2000

ProQuest LLC.
789 East Eisenhower Parkway
P.O. Box 1346
Ann Arbor, MI 48106 – 1346

Acknowledgements

This thesis was enabled by a scholarship funded by the Engineering and Physics Science Research Council, whose support I acknowledge. This thesis also would not have been possible without the help of many others throughout the course of this work. Foremost I would like to thank Prof. R. P. Ferrier for his excellent supervision and help at all times during the last few years and Prof. J. N. Chapman for his encouragement and provision of the research facilities in the Solid State Physics Group at the University of Glasgow. I am grateful to Dr. S. McVitie for his assistance in learning to operate the JEOL 2000FX (S)TEM, and to Dr P Aitchson for his assistance in learning to operate the Philips CM20. Thanks to Jamie for the training on the Magnetic Force Microscope and for printing and binding this thesis.

To the management and personnel at Onstream for preparing and supplying the samples, thank you.

I would like to offer thanks to Dr. W. A. P. Nicholson for his encouragement, support and the odd motivation speech. Thanks to the technical support team Sam, Colin, Billy and the fourth Musketeer Ian.

Thanks to Margit for recording Friends on a Friday night while I was in Tenants having a swift char with the group social club, they know who they are. Little Miss Morgans (AKA Beverly) needs a mention for keeping me on the straight and narrow during our groups little adventures out and about in Glasgow.

Thanks everybody.

Declaration

This thesis is a record of the work carried out by me in the Department of Physics and Astronomy at the University of Glasgow during 1996-1999. The work described herein is my own apart from the preparation of the electron microscope samples; the Emboss head and the Data head (chapter 3) were modified by Onstream™, the Radon transform tomography program which was initially provided by colleagues at the University of Duisburg in Germany and was modified by Prof. R. P. Ferrier, and the Algebraic reconstruction program was written by Yan Liu and supplied by Prof. R.P Ferrier.

This thesis has not previously been submitted for a higher degree.

TS Munro

Summary

The study of stray magnetic fields from magnetic recording heads for tape applications was undertaken using the Differential Phase Contrast (DPC) mode of Lorentz microscopy and Magnetic Force Microscopy (MFM). Electron Beam Tomography (EBT), at Glasgow was derived from the DPC technique and this was carried out in a highly modified Philips CM20 (S)TEM; previous EBT work had been carried out using a modified JEOL 2000 FX. A Digital Instruments MFM 3100 equipped with an Extender™ Electronics Module was used to study a production data head and an experimental Emboss head supplied by Onstream™.

This thesis starts with a brief discussion of the basics of ferromagnetism and the application of magnetic materials in magnetic recording technology. Development trends and some recent advances in magnetic recording head design for tape applications are also discussed.

Chapter 2 gives a review of quantitative techniques developed for magnetic stray field measurement. The Differential Phase Contrast (DPC) mode of Lorentz microscopy is presented as is an introduction to Electron Beam Tomography. The second method used to study the Onstream samples namely Magnetic Force Microscopy is discussed with particular attention given to the novel features that Digital Instruments employ in making their instrument an effective tool for the study of magnetic samples. There were several types of tip available and they fell into two categories, magnetically hard or soft; in the final section their characteristics are presented.

The results of the electron beam studies on the Emboss head and on the modified data head are discussed in Chapter 3. This chapter starts with a brief description of the samples. The preparations of the samples were carried out by Onstream to adapt them for electron microscopy and is discussed in this chapter. The remaining sections concentrate on the

results obtained from the JEOL 2000 FX on which the Emboss head was studied and Electron Beam Tomography carried out on the data head on the Philips CM20.

In Chapter 4 the Magnetic Force Microscope method is applied to study the stray field from inductive heads. The microscope was operated exclusively in Tapping Mode™ and with Interleave™ mode engaged. Three samples were studied, two Emboss heads, one of which was experimental and a production data head. One of the aims of this study was to determine which type of tip would be most suitable for the study of the stray field and we found that a CoPt coated tip had the magnetic characteristics suitable for the study of stray field.

Conclusions and suggestions for further work are given in Chapter 5.

In an Appendix the topic of noise in the DPC data for tomographic reconstruction is discussed. This was inspired by the major problems encountered with the stability in the JEOL2000FX gun output. The influence on tomographic field reconstruction of increasing noise added to DPC data for a model recording head is analysed.

Chapter One

1 Ferromagnetism and Magnetic recording

1.1 Introduction

This chapter deals with the basic principles of ferromagnetism and leads on to the principles behind magnetic recording. The reasons why some materials exhibit ferromagnetism will be discussed and the formation of magnetic domains will be covered. In the section on magnetic recording, the fundamental theory will be described including the development of magnetoresistance elements for the read-back function. The final section is concerned with the design of recording heads, which are suitable for the linear tape systems, used in the data backup market.

1.2 Ferromagnetism

A ferromagnetic material is one which may possess a spontaneous non-zero net magnetic moment in the absence of an applied magnetic field. Known ferromagnetic substances include transition metals, rare earth elements and their alloys and oxides. They all display ferromagnetism below a critical temperature called the Curie temperature (T_C), for example for nickel this is below 356^0C. Elemental ferromagnetic materials have a magnetic dipole moment associated with each atom. This is caused by the angular momentum which, due to the quenching of orbital angular momentum, arises predominantly from the spin of unpaired electrons in the 3d or 4f shells. In a ferromagnet the magnetic dipoles are aligned parallel to each other below the Curie temperature, unlike a paramagnetic material where the dipoles are randomly aligned due to thermal agitation. To account for this cooperative phenomenon, Weiss (1907) [1] proposed the presence of an internal molecular field. This internal field, H_m, is proportional to the magnetisation (M) and produces the parallel alignment of the atomic dipole moments.

The presence of the molecular field was accounted for by Heisenberg [2], who proposed a quantum mechanical interaction, known as the exchange force, acting between each atom and its nearest neighbours. Due to the Pauli [3] Exclusion Principle the total wavefunction for a quantum mechanical system comprising electrons must be antisymmetric. The wavefunction can, however, be thought of as the product of spatial and spin wavefunctions and for a two electron system the electrostatic energy is dependent on the relative angle between the two spins. When the spins are parallel a minimum in the electrostatic energy is obtained when the spatial part of the wavefunction is antisymmetric. The exchange force tends to align the atomic magnetic dipoles to lower the energy and is therefore the phenomenon responsible for ferromagnetism.

1.3 Energy Considerations

The spontaneous magnetisation and domain structures arise due to the fact that, a material will always seek to be in a state in which its potential energy is a minimum. By considering the various macroscopic energy terms it is possible, in certain cases, to predict the magnetic state of a system by minimising the total energy. However, for many systems the energies of different states are finely balanced and micromagnetic calculations are required.

1.3.1 Exchange Energy

As discussed in Section 1.2 the exchange energy is responsible for the spontaneous alignment of atomic magnetic dipoles in a ferromagnet. The interaction energy between two individual particles takes the form;

$$E_{ex} = -2J\mathbf{S}_i \bullet \mathbf{S}_j \tag{1.1}$$

where J is the exchange integral for the two interacting particles, and $\mathbf{S}_i$ and $\mathbf{S}_j$ are the spin parts of the wavefunctions describing the particles. Equation (1.1) is seen to favour parallel alignment and thus ferromagnetism if J is positive.

In terms of a finite volume of magnetic material, the exchange energy is more completely described by,

$$E_{ex} = A\int_V \left[(\nabla\alpha)^2 + (\nabla\beta)^2 + (\nabla\gamma)^2\right] dV \qquad (1.2)$$

where α, β and γ are the directional cosines of the magnetic vector and A is the exchange constant of the material and is defined by,

$$A = \frac{kJS^2}{a} \qquad (1.3)$$

k is a constant whose value depends on the crystalline structure, a is the lattice constant, J and S are respectively the exchange integral and the magnitude of the spin of magnetic moment. Since J is positive for a ferromagnetic material so also is the exchange constant. From equation (1.2), E_{ex} is a minimum when the atomic dipoles align parallel to each other and is therefore the phenomenon responsible for the spontaneous magnetisation of ferromagnetism.

1.3.2 Anisotropy Energy

If a magnetic material has preferred magnetisation directions, along which the specimen is much easier to magnetise, it is said to be anisotropic. The preferred direction are often referred to as the easy axis and in the case of magnetocrystalline anisotropy are related to crystal lattice directions. Deviations of the magnetisation vector from an easy axis results in an increase in the anisotropy energy.

For a single cubic crystal, the anisotropy energy is well defined by the first two terms of a series expansion of the directional cosines,

$$E_K = \int_V \left[K_1(\alpha^2\beta^2 + \beta^2\gamma^2 + \gamma^2\alpha^2) + K_2\alpha^2\beta^2\gamma^2 \right] dV \qquad (1.4)$$

where K_1 and K_2 are the first two anisotropy constants of the material. For transition metals $K_1 >> K_2$ and the anisotropy energy can be approximated to just a single term.

In uniaxial crystals such as Cobalt, which has a hexagonal crystalline structure, the anisotropy energy is described by,

$$E_K = \int_V \left[K_1(1-\gamma^2) + K_2(1-\gamma^2)^2 \right] dV \qquad (1.5)$$

Anisotropy energy explains certain orientations of domain magnetisation.

1.3.3 Magnetostatic Energy

The magnetostatic contribution to the energy of a magnetic system arises from the interaction between magnetic 'free poles'. These are generated either within the volume of the magnetic material or at its surface where there is a divergent component of magnetisation. These free poles give rise to both an internal field and an external stray field, which is in the opposite sense to the magnetisation. These can be described in terms of an integral over the volume and surface of the source. The field is often termed the demagnetising field, H_d, and is given by,

$$\mathbf{H_d} = \frac{1}{4\pi}\int_V \frac{-\nabla\bullet\mathbf{M}}{r^2}\, dV + \frac{1}{4\pi}\int_S \frac{\mathbf{M}\bullet\mathbf{n}}{r^2}\, dS \qquad (1.6)$$

where r is the position vector for the points in space where the field from the charge is evaluated (field points) and **n** the outward pointing unit vector, normal to the surface. The term $\nabla.\underline{M}$ is equivalent to the magnetic volume charge and $\underline{M}.\underline{n}$ is the magnetic surface charge. This integral is easily evaluated for an ellipse but for other common shapes, such as rectangles, the integral has no simple analytical form.

The energy contribution due to the demagnetising field is called the magnetostatic energy and takes the form,

$$E_m = -\frac{1}{2}\mu_0 \int_V \mathbf{M} \bullet \mathbf{H}_d dV \tag{1.7}$$

where μ_0 is the permeability of free space. The most effective way to decrease the magnetostatic energy is to divide the magnetic specimen into magnetic domains, which is discussed next. The free pole density gets less as the specimen is divided to create more domains and may even vanish on the surface when closure domain structures are present.

1.3.4 Magnetic Domains

The observed net magnetisation of a ferromagnetic body is often substantially less than the saturation magnetisation of the magnetic material from which it is made. To explain this, Becker [4] introduced the concept of magnetic domains. This hypothesis, which was later confirmed by Bitter [5], assumes that there are many different regions of spontaneously aligned magnetisation within a sample, each with a different direction of magnetisation. These different directions of magnetisation result in a lowering of the overall net magnetisation of the body.

An example is shown in Fig. 1.3.4.1, which shows schematically the development of domains in a magnetic specimen. Originally the sample was all magnetised in the same direction and there is a large amount of magnetostatic energy (equation 1.7) stored in the free space around the material. As the specimen is demagnetised the magnetisation distribution is divided into progressively narrower domains of opposite magnetisation leading to a reduction in the magnetostatic energy. If the loss in the magnetostatic energy is greater than the increase in the exchange energy and the anisotropy energy due to the formation of the domains, the magnetisation in the specimen will be subdivided into more domains until a minimum energy state is reached.

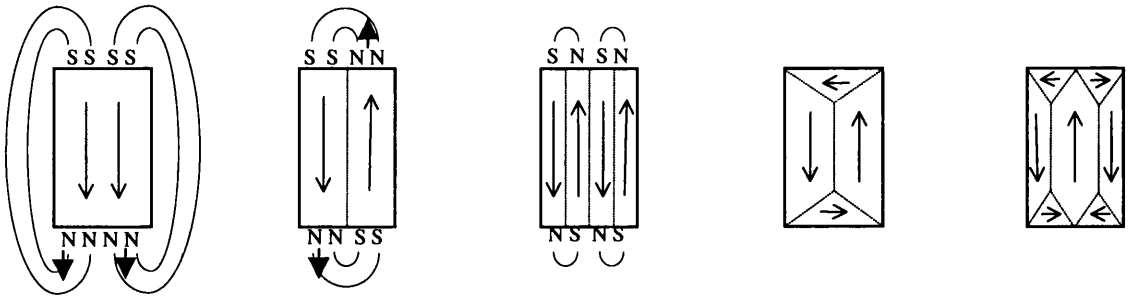

Fig. 1.3.4.1. The Emergence of the domains as a result of the demagnetisation

The boundaries between domains are known as domain walls and the magnetisation vector smoothly rotates within a wall between the two directions of magnetisation in the adjacent domains. In iron this domain wall can be ~300 times the lattice spacing in width. The domains in the thin films, as demonstrated in Fig. 1.3.4.2(a) are mainly the results of minimising the magnetostatic energy. For bulk cubic materials, in Fig. 1.3.4.2(b) the domains tend to form 90° and 180° domain walls as the cubic anisotropy ensures that the directions at right angles to the magnetisation in a given domain are also magnetically easy axes. Provided that the edges of the sample are along the {100} or {111} directions. Depending on how the magnetisation vector rotates, the wall is either referred to as a Bloch [6] or a Néel [7] wall. In a Bloch wall the magnetisation rotates out of the plane of the film as shown schematically in Fig 1.3.4.3. A Néel wall however has an in-plane rotation of magnetisation.

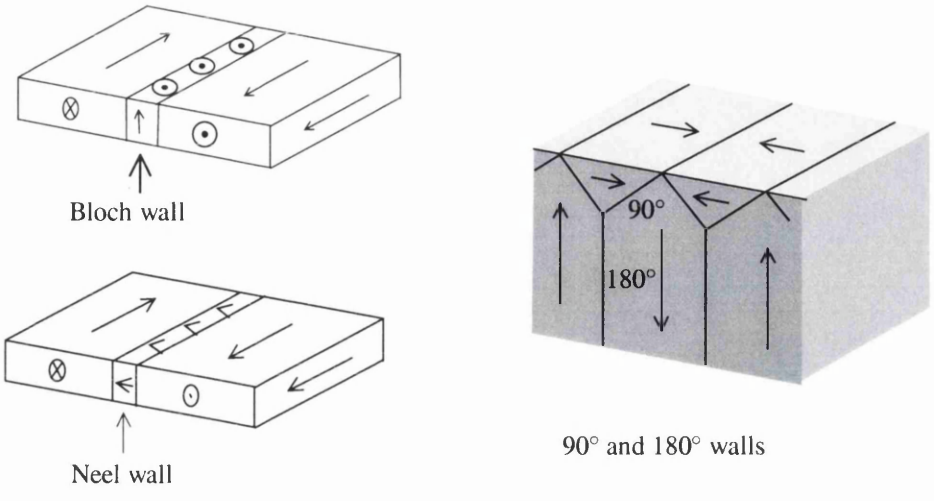

Fig. 1.3.4.2. Schematic of domains and domain walls found in (a) magnetic thin films and (b) cubic materials.

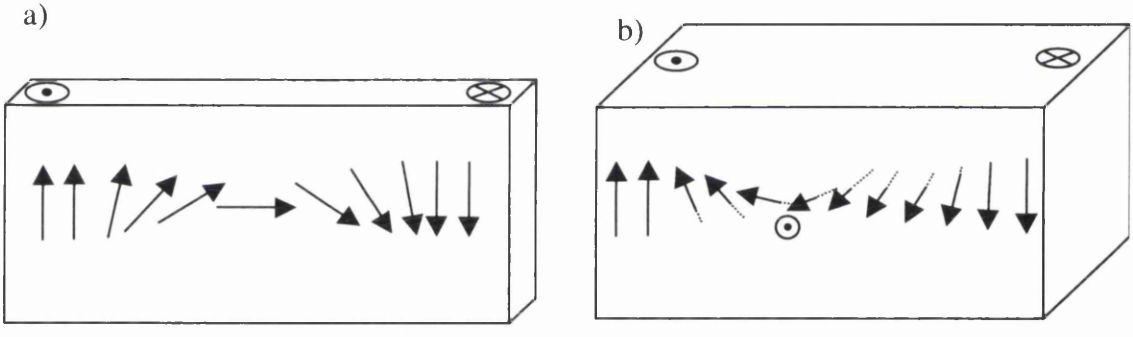

Fig. 1.3.4.3. **:** *Schematic representation of (a) the Néel wall and (b) the Bloch wall. For a Néel wall the magnetisation rotates in the plane of the sample and for the Bloch wall the magnetisation rotates out of the plane of the sample. The plane of the film is the plane of the paper*

The rotation of magnetisation through a domain wall results in a contribution to the exchange energy, the anisotropy energy and in some cases also the magnetostatic energy. For a Bloch wall in a bulk material it is possible to define the domain wall energy per unit area of the wall as,

$$\sigma_{wall} = 4\sqrt{AK} \qquad (1.8)$$

Although wall energy is a combination of previously introduced energies it is valid to consider it as a separate entity, E_W

1.3.5 Total Energy

The total energy of a magnetic system, E_{tot}, is given by the summation of all the energies introduced above viz.:

$$E_{tot} = E_{ex} + E_K + E_m + E_W \qquad (1.9)$$

To determine the final magnetic state of the system, the total energy must be minimised. The four energy terms are however inter-related and the balance between them is the factor which controls the magnetic state of the sample. For example, in many cases the magnetostatic energy may be lowered, or even nulled by the formation of closure domains. This however has the consequence of increasing other energies, E_W is increased due to the closure domain walls and E_K is increased since the closure domains may be orthogonal to the easy axis direction. In a fully demagnetised state the magnetic system will be such that there is a global minimum in the total energy. When, however, the system has not been demagnetised the remanent state is only a local minimum. Thus the energy of the system is dependent on the previously applied field. This "memory" of the last applied field is called hysteresis and is fundamental to magnetic recording technology.

1.4 Magnetic Recording Principles

Magnetic storage has been around for over a 100 years. The first working apparatus in which information was stored in a steel piano wire was described by Poulson [8] in 1900. Over the last few decades there has been unrelenting pressure to increase the amount of information and its spatial density, which can be stored using magnetic media. The combination of an inductive element for the write/read processes and the magnetic recording media on which the data is written is still the main platform of this rapidly developing technology. Almost all the revolutions in recording density and data rate are the

result of the minimisation in the size of the inductive element and the development of improved magnetic materials for recording heads and media. A newer addition to this technology is the inclusion of a separate non-inductive element to read the stored information. This element utilises the magnetoresistance effect, which is defined as " *A change in the resistance of a metal due to the presence of a magnetic field.*" [9]. This enables heads to be designed for specific tasks, either writing or reading the data; in earlier years of magnetic recording an inductive head performed both tasks.

1.4.1 Hysteresis

Hysteresis is the phenomenon in which two physical quantities are related in a manner that depends on whether one is increasing or decreasing in relation to the other. This was first observed in a magnetic material by Warburg [10] in 1881. The hysteresis loop, shown in Fig.1.4.1.1, results from irreversible magnetisation processes. To determine the hysteretic characteristics of a magnetic material a field is applied in one direction, which is sufficiently large to align all the domain magnetisations to the direction of the applied field. Then the field is reduced to zero, reversed and finally increased to saturation in the opposite direction. By sweeping the field in the opposite sense a similar curve is obtained thus completing the loop. The remanent magnetisation M_r acts as a type of memory of the last field maximum, both in magnitude and direction, experienced by the magnetic material. The hysteresis effect is used in magnetic recording technology to store information in digital form for computers and related devices, or in analog form in some audio and video signal recording.

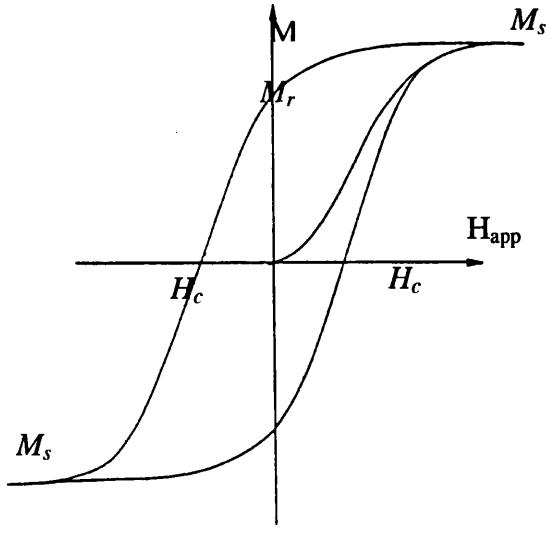

Fig. 1.4.1.1 A typical hysteresis loop for a hard ferromagnetic material.

From the above graph three quantities, M_s, M_r and H_c, provide the principal characterisation of a magnetic material. These determine the suitability of a ferromagnetic material for application in write or read heads and for media fabrication. Another important property of ferromagnets is their high relative permeabilities, especially for use as soft magnets as in recording heads. The permeability of a ferromagnet is not a constant but varies as a function of the magnetic field and the operating frequency. Quantification of this property is rather difficult but it can be described by the following relationship

$$\boldsymbol{B} = \mu_0 \mu_r \boldsymbol{H} \tag{1.10}$$

where μ_0 is permeability of free space and μ_r is the relative permeability of the material.

For applications such as recording media, where the recorded information must be easily retrieved whenever necessary with minimum distortion, the materials must have sufficiently large coercivities to prevent the loss of or change to information due to extraneous fields. On the other hand, the coercivities have to be sufficiently small to allow the material's "memory" to be erased and new data recorded by the recording head. The magnetic recording media ideally should have as large saturation and remanence magnetisations as possible to provide a large signal during the reading process; this is

especially true with the continuing scaling down of the area of an information bit necessary to achieve increased recording density.

A recording head material on the other hand should have high permeability and high saturation magnetisation to generate high magnetic induction for a given magnetic field and leave a large imprint on the media. Also the head must have a low remanence to ensure that there is no writing field when the current in the coil is zero. Other properties for head core material, which must be considered, include the electrical resistivity ρ, the thermal coefficient of expansion and the mechanical hardness [11].

1.4.2 Magnetoresitance (MR)

Lord Kelvin discovered the MR effect in iron in 1856 and in the following year in nickel [12]. However it was not until the end of the 1960's that its potential was realised for reading information from magnetic media [13]. MR materials are characterized by the property that their electrical resistance changes when a magnetic field is applied. In 1988 giant magnetoresistance, GMR, was reported by Baibich et al [14] in a multilayer Fe/Cr superlattice; the increased sensitivity which this provides in the read back of digital data has had a major impact on the recording industry.

The GMR phenomenon is present in multilayer structures consisting of conducting ferromagnetic and non-magnetic layers just a few nanometres thick [15]. One such GMR multilayer structure is the spin-valve multilayer, and is shown schematically in Fig 1.4.2.1. Exchange-biased spin valve layered structures were first described in 1990 by Dieny et al[16]. The simplest spin valve includes a ferromagnetic layer (called the pinned layer) in contact with an antiferromagnet layer, which fixes the magnetization direction in the presence of fields from the tape. A conducting non-magnetic layer separates the pinned layer from a second ferromagnetic layer (called the free layer), whose magnetization is free to rotate in response to the field from the tape. In this way, the magnetisation changes between being parallel, (shown by the two solid blue arrows in figure 1.4.2.1) a low resistance state to antiparallel, (the top solid blue arrow and the dotted blue arrow) a high resistance state, as the magnetic flux transition pass under the head.

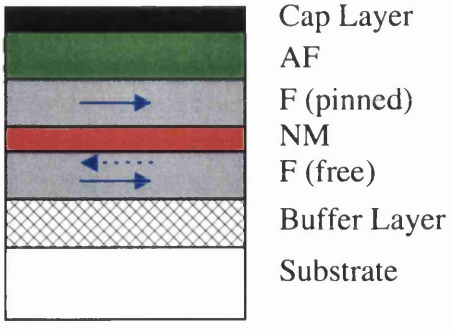

Fig.1.4.2.1 A schematic cross section of a Spin-valve structure. The key for layers is as follows:- AF- anti-ferromagnetic, F- ferromagnetic, NM-non-magnetic

A typical MR response for a FeMn biased spin-valve is shown in Fig 1.4.2.2. The relative directions of the two permalloy layers are indicated on the figure. The curve may be divided into three main sections; 'A' the 1st low resistance state where there is a parallel alignment between the two ferromagnetic layers, 'B' the high resistance plateau where there is anti-parallel alignment between the two ferromagnetic layers and finally 'C' the 2nd low resistance state where the biasing is overcome and there is again parallel alignment.

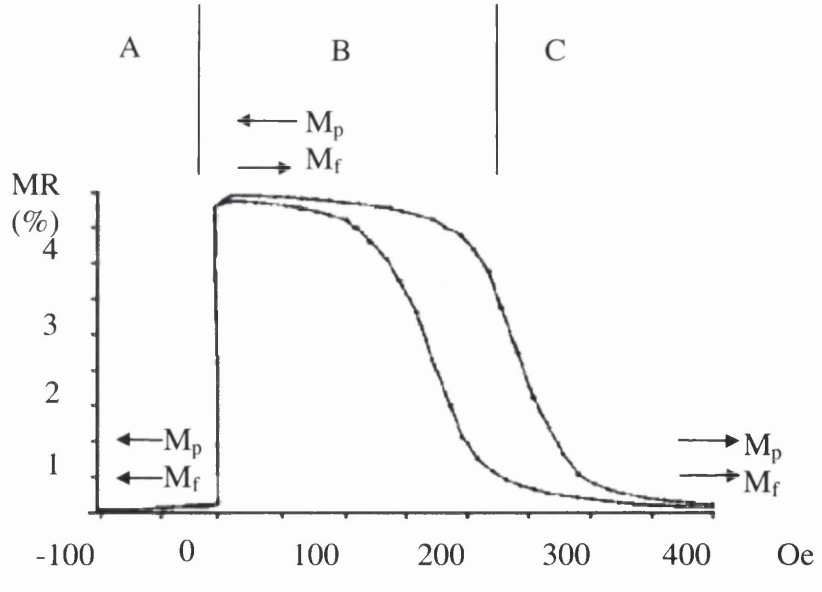

Fig 1.4.2.2: Typical MR response of a spin-valve biased by FeMn, with relative orientations of pinned and free layer magnetisation indicated.

Choosing and improving materials for spin valves continues to be an area of active research in industry and university.

Philips and later Onstream utilise MR and GMR materials in a read back sensor in which the material bridges the gap in the yoke of a thin film head. This construction of read sensors is known as Yoke Magnetoresistance Element (YMRE) form and they were introduced for tape recording applications around 1983.

1.4.3 Inductive Recording Heads

The utilisation of hysteresis for magnetic storage is easily implemented using an inductive read/write head. An early form is the "ring-head", which is illustrated in the simplified schematic of Fig 1.4.3.1.

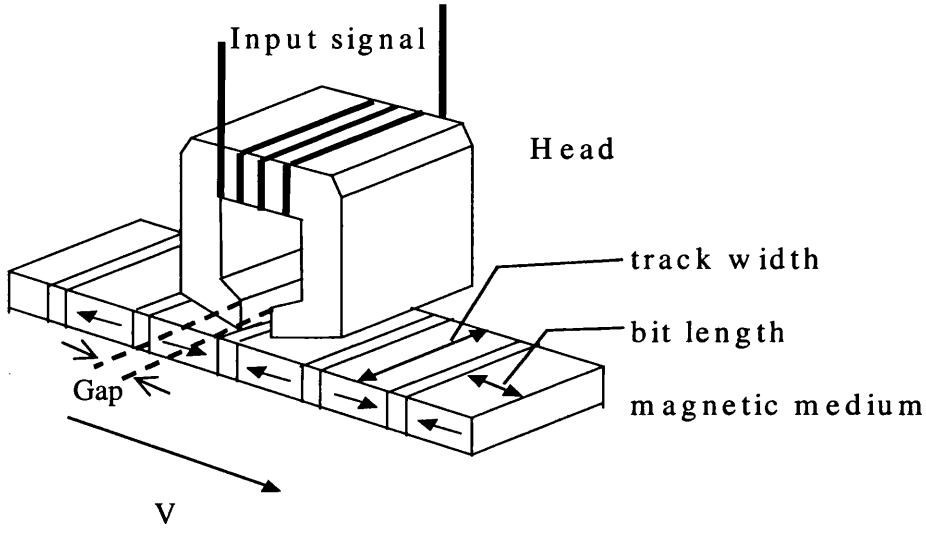

Fig. 1.4.3.1. Schematic of the recording process of a ring head in tape recording.

The signal to be recorded is applied via the coil, which is wound around a magnetic core. This has the effect of generating a magnetic field, along the axis of the coil, which then magnetises the core of the head. In turn this leads to the generation of a magnetic field at the narrow gap; this is proportional to the input signal provided saturation effects are not present. The stray field from the head gap magnetises the recording medium as it passes in front of the head. The stray magnetic fields emanating from the magnetic media after recording, are representative of the recorded signals and can be detected using an inductive head. Detailed analysis of the magnetisation in the medium is very difficult as the

magnetic fields at different depths in the recording medium are different and the writing field is a function of time.

An inductive head, working in read mode, provides a flux closure path for stray fields emanating from the magnetic media. The variation of magnetisation within the magnetic core, which results from this flux closure, induces an output voltage in the coil, given by Faraday's Induction Law. This law states that the e.m.f. induced in a circuit is equal to the rate of change of flux linking the circuit,

$$V = -N\frac{d\phi}{dt} \tag{1.11}$$

where, V is the induced e.m.f., N is the number of turns in the coil and ϕ the magnetic flux. This process is analogous to that of writing but with the input and output roles reversed.

The introduction of thin film technology has allowed inductive heads to be deposited layer by layer. This has resulted in smaller pole tips and consequently inductive heads can now write much higher bit densities. Unfortunately, however, the present bit densities which can be written do not result in a sufficiently large stray field for inductive data recovery. This has been a principal reason for the rapid development and introduction of GMR read heads. This does however enable inductive heads to be optimised for the single task of writing data. Another benefit of designing heads only for writing information is that they require fewer copper coils, materials, photolithographic masking operations, and dimensional tolerance requirements are relaxed.

The recording media can be either in the form of a spinning disk or a passing magnetic tape and inductive recording can be used to record either analogue or digital signals. In Fig. 1.4.3.2 below the current I(t) represents the information to be recorded. The shape of the output signal waveform via the head depends on the head's geometry. . In all electronic systems there are sources of noise and in tape recording there is also media noise. However, in a digital system, the electronics has to decide only if a transition is present or not, unlike an analogue system where the signal should ideally be reproduced exactly. This gives digital recording an advantage over analogue recording in that there is

the vast improvement in signal to noise ratio. Digital recording format also has the ability to store a greater amount of information on a smaller area of magnetic material.

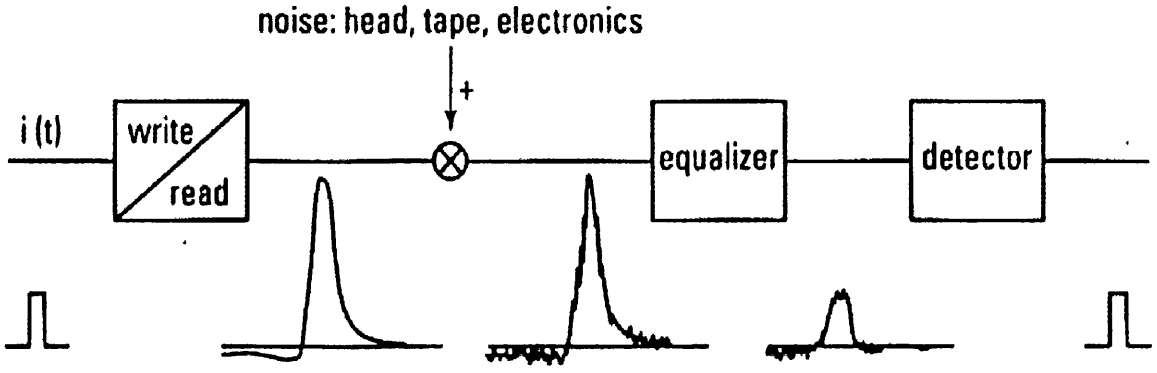

Fig.1.4.3.2. Digital Recording Schematic.

1.4.4 Magnetoresistive Heads for Data Reading

As stated previously a magnetoresistive (MR) sensor exhibits a change in resistance in the presence of a magnetic field. Recording heads using this phenomenon can provide higher read sensitivity than traditional inductive elements. In addition the output of a MR sensor is proportional only to the magnetic flux and is independent of the head-tape velocity. These types of sensors can only be used to recover information, which has previously been written by an inductive head. Consequently a recording system which utilises magnetoresistive readback must either have separate read/write heads or, as is more common, a single composite structure which incorporates both an inductive write coil and an MR sensor.

To linearize the output from a MR sensor there are two options. The first is to provide a bias conductor close to but separate from the MR sensor, this technique is currently employed in the Onstream heads. Secondly to construct a 'barber pole' metallization structure on top of the magnetoresitive element (MRE), (see fig.1.4.4.1). The name barber pole is given to this design due to the conductor stripes that are constructed on the MRE at an angle <45 degrees to the long axis of the MRE. The current in the MRE flows almost perpendicularly from one conductor stripe to the other. Since the magnetization, at the zero applied field, is in the length direction, the angle between the current and magnetization varies around 45 degrees and maximum linearity is obtained.

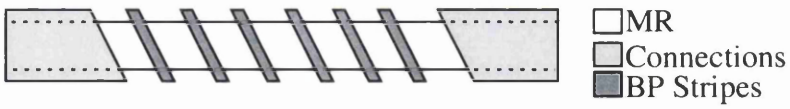

Fig. 1.4.4.1. A schematic of a barber pole biased MRE.

In figure 1.4.4.2 a schematic of the Philips DCC^{TM} tape head is presented. In practice the MR head is constructed on top of the write head, but this will be discussed in greater detail in section 1.5. This type of head is called a Yoke-Type Magnetoresistive Head (YMRH) [17,18] and is employed in digital recording systems. To realise a linear and stable response, appropriate biasing of the MR element is required. The current generation of MREs don't have barber poles to bias the MR element since the new tape systems are digital recording systems [18].

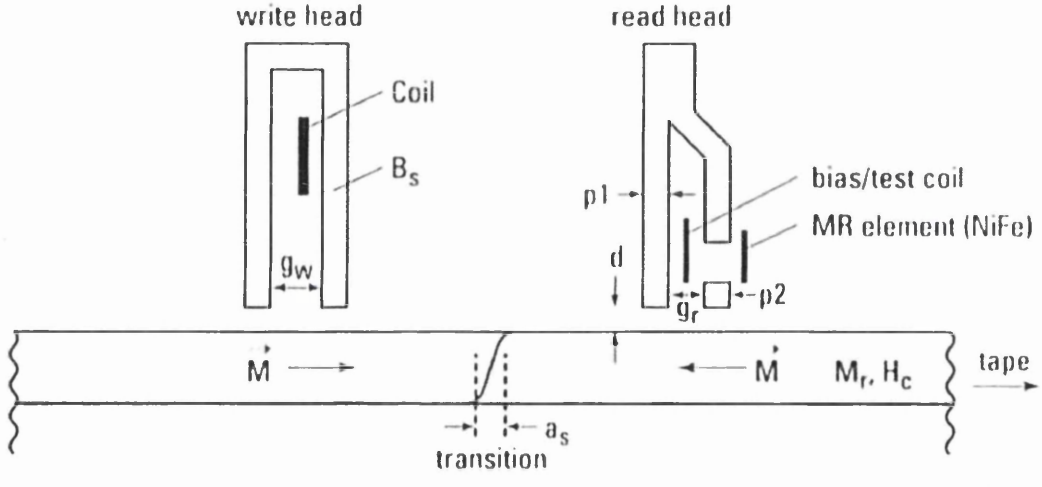

Fig.1.4.4.2 A schematic view of an inductive and MR head in the Philips DCC^{TM} data head from which the Onstream heads were developed.

These MR heads exploit the anisotropic magnetoresistance (AMR) effect in thin permalloy films to convert flux changes into resistance changes. The magnetoresistive element bridges the gap in the yoke of a thin film head, as shown above. In tape applications, the tape is abrasive and would wear down the MRE if it were allowed to come into contact with the media. By using the above design it is less susceptible to noise, wear, corrosion and has a lower sensitivity to electrostatic discharge damage. A disadvantage with the above design compared to that used in hard disk heads, where the MRE is much closer to the media and utilise soft magnetic shields, is a lower output signal.

For high density tape recording, GMR materials have improved sensitivities compared to AMR materials and they can be made with an intrinsically linear MR curve [18].

1.5 Recording head design and construction

The Ontream tape system utilises a cartridge containing pre-formatted tape and a tape drive unit which has a data head that can read/write eight tracks simultaneously [19]. The tape media is pre-formatted with servo information that the data head uses to keep on position and to find data on the tape. This servo information is "buried" in the lower depths of the tape media coating and the data is written on top. An advantage of this system is that all of the tape area can be used to store data and a simple filter arrangement separates the data from the servo signal on readback.

In this system there are two separate types of head required to make it viable. The first is the servo head and is called the Emboss head; it is used by the tape manufacturer prior to the sale of the tape to the customer. The second is the data head in the tape unit which reads and writes the data to the tape file. Both of these heads are unique in their structure, which will be described briefly here. A more complete description of the heads which were studied, is given in Chapter 3.

1.5.1 Emboss Heads

Figure. 1.5.1.1 shows the lay out of the poles in an Emboss head. The 'W' represents the smallest pole width and it can be seen from the image that there are three sizes in the structure of widths W, 1.5W and 10W.

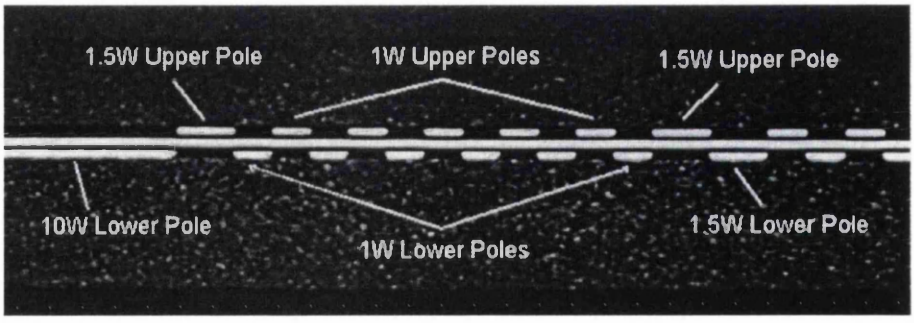

Fig.1.5.1.1 Tape bearing surface of the head which contains the poles. The scale shows the size relationship between the three 'types' of poles within the head.

This type of stacked multi- head writer with limited distance between the lower and upper gaplines is difficult to construct in a conventional thin-film process with relatively thick polymer layers. Hence the head is processed in a dedicated planer thin-film process without polymer isolation layers to eliminate any undesired topographical steps. Applying chemical/mechanical polishing after the deposition of each of the layers in the following sequence planarises the thin-films [19]:

- Poles of the lower write circuit
- First winding layer
- Shared pole of both write circuits
- Second winding layer
- Poles of the upper write circuit.

In the Emboss heads studied in the microscope there were 157 poles and an overall width of 8.8 mm; in future generations of the device it is expected that the number of parallel tracks will rise significantly, whilst retaining the current tape width.

1.5.2 Data Heads

The data head consists a parallel array of 8 inductive write heads and 8 YMRE heads for readback. Below (Fig.1.5.2.1) is a "3D" schematic of the layout of a data head, only a single write coil winding is shown.

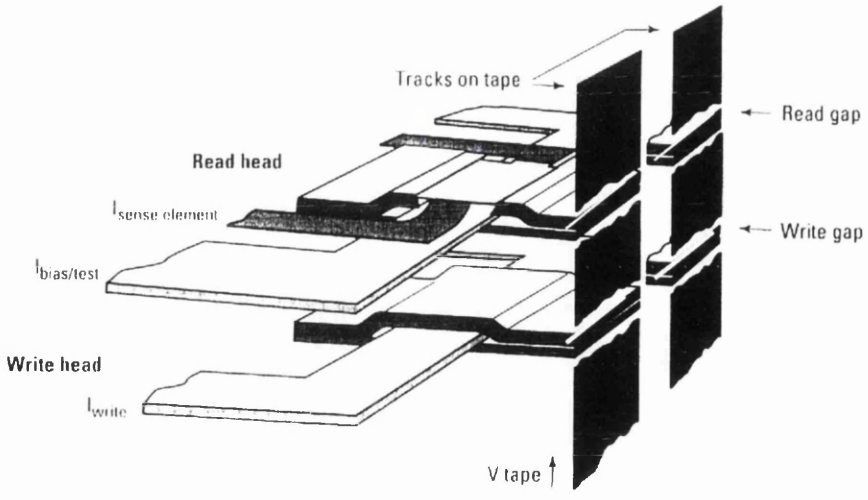

Fig.1.5.2.1 A 3D schematic of a multi read/write data head for use in a linear tape storage systems.

In this construction the MRE is embedded relatively deep in the head assembly and is substantially farther away from the media than in hard drive MR heads. Whereas in hard drives the heads "fly" over the surface of the magnetic media, tape recording is a "contact" technique. Hence heating of the head must be considered as this can also cause a change of resistance in the MRE [20] and (together with wear considerations) determines the deeper location within the structure. The head in addition to writing/reading the data information has to pick up the long wavelength signal from the servo information. This requires the gap spacings to be optimised for efficient operation. This head has been studied in the (S)TEM and with the MFM: the results are presented in Chapters 3 and 4 respectively.

1.6 References

1. Weiss P., (1907), *J. Phys.*, **6**, 661.
2. Heisenberg W., (1928), *Z. Physik*, **49**, 619.
3. Weiss P., (1907), *J.Phys.*, **6**, 661
4. Becker, R. Z.,(1930) Physik, **62**, 253
5. Bitter F., (1931), *Phys. Rev.*, **38**, 1903

6. Bloch F, (1932), *Z. Physik*, **74**, 295.
7. Neel L, (1955), *Compt. Rend.*, **421**, 533.
8. Poulsen, V.(1900), *Annales der Physik*, **3**, 754
9. Oxford Dictonary of Physics, Oxford University Press, 1996
10. Warburg E, (1881), *Ann. Physik,* **13**, P 141.
11. Mee C. D. and Daniel, E. D. (1987), *Magnetic Recording Vol. I: Technology*, McGraw-Hill.
12. Thomson W. (Lord Kelvin) (1884), *Mathematical and Physics Papers (part 2),* 307
13. Hunt R.P. (1971), *IEEE Trans. Mag.* **7**, 150
14. Baibich M.N. et al, *J. Phys. Lett.* **61**, 2472 (1988)
15. Gurney B. and Grochowski, E., (1998), *Data Storage*, **59**
16. Deny B., Sperious V.S., Parkin S.S.P., Gurney B.A., Wilhoit D.R. and Mauri D., (1991) *Phys. Rev B,* **43**, 1297
17. Ruigork J.J.M., Draaisma H.W. and van Kesteren H.W., (1998), *Philips Journal of Research*, **51**, 21
18. Luitjens S.B., van Kesteren H.W. and Ruigork J.J.M., (1998), *Philips Journal of Research*, **51**, 5
19. Internet publication, Onstream web site.
20. Sawatzky E., (1998), *Data Storage*, Feb. edition, 49-54

Chapter Two

2 Methods to Characterise the Stray Magnetic Field from Recording Heads

2.1 Introduction

In this chapter the techniques used to study the stray magnetic fields from the Onstream recording heads will be described. A brief review of the range of techniques, which can be used to investigate recording head magnetic fields, will be presented first. This is followed by a more detailed discussion on the first of the experimental methods used in this thesis study. This method required the acquisition of electron deflection data using the Differential Phase Contrast (DPC) mode of Lorentz electron microscopy followed in some cases by tomographic reconstruction. The microscopy facilities used in these studies will be described. The final section of the chapter deals with Magnetic Force Microscopy (MFM), the second technique applied to the study of stray magnetic fields from heads described in this thesis.

2.1.1 Review of Investigative Methods

As the search continues for ways to increase the areal storage density in hard disks and linear tape storage systems, new methods are being developed to study the next generations of recording heads and magnetic media. Although information on the nature of the head field can be obtained indirectly, for example by studying the detailed structure of the magnetisation distribution in the written tracks they create, we are concerned with direct studies of the field distribution. Given the relatively high spatial resolution which is required, electron microscopical methods are an obvious approach. Several research groups have been involved [1,2,3,4] in applying Lorentz electron microscopy to the problem. Of the four methods explored to date, three have utilised the Scanning Electron Microscope (SEM) and the other, that used in our studies, a modified (Scanning)

Transmission Electron Microscope ((S)TEM. All of these methods involve recording the deflection of an electron beam as it is scanned through the head field; by obtaining many different projections of the field, the data may then be reconstructed by methods of tomography to give the 3-D field distribution. Ideally the electron deflection data [1,2,3] should come from a distance no more that a few nanometres from the plane of the polepieces (i.e. as close to the plane of recording as possible), but experimentally this is very hard to achieve. The fourth of these methods [4] analyses the electron deflection following reflection from the polepiece surfaces; however the physical basis for this method is almost certainly incorrect [5]. We now discuss more direct methods of exploring the nature of recording head fields.

In the recording industry the standard instrument for the study of written tracks on magnetic media is the MFM; MFM has also been used to study the fields from thin film heads directly [6] and is the second method used in our investigations (details are given in Section 2.5). Commercial MFM's can provide high-resolution (~50nm) images with minimal sample preparation. They operate at room temperature and an operator can be trained to use one in a relatively short period of time. This makes this method very attractive when studying written magnetic data. The principal challenge in this area of research is to find a way to quantify the data collected. So far most methods that have been proposed have been based on modelling the tip magnetisation to calibrate the image data [7,8].

Oral et al in 1996 [9] developed a scanning Hall probe microscope (SHPM) system using a patterned sub-micron Hall probe prepared by electron beam lithography [10]. The probe is mounted on the piezotube of a custom manufactured low-temperature scanning tunnelling microscope (STM). A STM tip is positioned close to the Hall probe to enable positioning on the sample. The Hall probe is raster scanned over the surface of the sample collecting the normal component of the magnetic field. Since the STM tip is integrated in the system, the topographic data can be collected simultaneously. This system has a magnetic field sensitivity of 30 $nT/\sqrt{Hz}$ at 77k and a spatial resolution of 0.8μm. A complex bit track with a repeat pattern of 10μm has been imaged successfully with this system at 77K [10]. The relatively poor spatial resolution compared to standard MFM is a distinct limitation.

However the development of higher resolution Hall probes is proceeding. For example Hall crosses have been manufactured as small as 100nm, but they had a short operating life span [11]. If the size of the Hall probe can be reduced further, then this method would be ideal to study tape heads where the writing pole is generally much larger than for hard disk heads.

Scanning Magnetoresistive Microscopy (SMRM) is one of the newer scanning "probe" microscopy techniques. In the SMRM developed by Yamamoto and Shultz, commercially available MR readback heads are raster scanned across a magnetic sample [12]. The combined MR/inductive element is mounted on a standard head/gimbal assembly. The slider is brought into physical contact with the sample, which is mounted on a high-resolution flexure stage for scanning. This stage is piezo driven and linearized through the use of capacitance displacement sensors for closed loop operation. The above system was designed for the study of magnetic media but could also be used to study the stray magnetic fields from recording heads. It is claimed that this system has a spatial resolution of 100nm in the "downtrack" direction and 2μm in the "crosstrack" direction of the head. The resolution will improve as MR or GMR elements are made smaller. To collect quantitative data with this type of microscopy, calibration of the MR element response to known magnetic fields is required [13]. Side reading of magnetic tracks, written by experimental heads, have been studied with this technique [14].

We now proceed to discuss the main features of the first of the methods used in this thesis to study magnetic fields viz. DPC Lorentz electron microscopy combined with electron tomography.

2.2 Lorentz Modes in (S)TEM

The Lorentz deflection of an electron beam by a magnetic specimen may be utilised in an electron microscope to image magnetic structures. This was first achieved in 1959 by Hale et al [15] and since then other magnetic imaging modes have been developed. In the earliest experiments, a defocused beam revealed the position of domain walls as dark or

light bands in a magnetic sample situated in magnetic field free space. This Fresnel contrast arose due to small deflections of the electron beam as it passed through the magnetic sample. The Lorentz force acting on the electrons as they pass through the sample is:

$$\underline{F} = (e\underline{v} \times \underline{B}) \qquad 2.1$$

where, e is the charge on an electron and $\underline{v}$ is the electron velocity in the region of magnetic induction $\underline{B}$. The deflection of the electron beam due to the Lorentz force can be described classically from the transfer of transverse momentum and the Lorentz deflection angle β_L is given by:

$$\beta_L = \frac{e\lambda B_\perp t}{h} \qquad 2.2$$

where λ is the electron wavelength, h is Planck's constant, and $B_\perp t$ represents the total (x, y) -plane component of magnetic induction integrated along the electron trajectory.

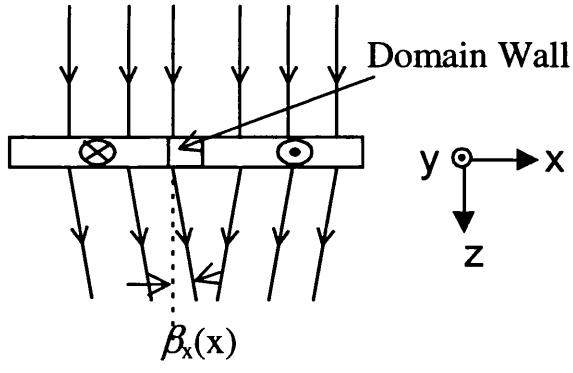

Fig.2.2.1 Deflection of electrons transmitted through a thin magnetic film with a domain wall.

If the magnetic induction varies with x and z in the vicinity of a domain wall (see Fig.2.2.1) then the local component of deflection is given by:

$$\beta_x(x) = \frac{e\lambda}{h}\int_{-\infty}^{\infty} B_y(x,z)dz \qquad 2.3$$

Contributions to $B_y(x,z)$ can arise from stray fields beyond the surfaces of the magnetic sample as well from contributions within the sample.

In 1959 Aharonov and Bohm [16] provided a quantum mechanical description of the electron-specimen interaction and this is best described by considering Fig 2.2.2. They showed that the presence of magnetic induction introduces a phase shift in the electron wave.

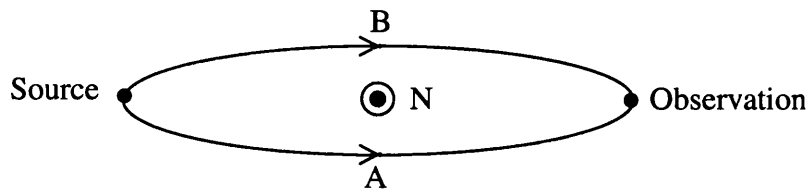

Fig 2.2.2: Illustration of two electron paths, 'A' and 'B' which enclose magnetic flux N

The electrons, emitted from the same source, travel over different paths enclosing a magnetic flux N and finally arrive at the same observation point; the phase shift introduced between the electron waves is,

$$\phi = \frac{2\pi e \mathrm{N}}{h} \qquad 2.4$$

The phase shift between an arbitrary position (x_o) and an end point (x) in the same horizontal direction is,

$$\Delta\phi(\mathrm{x}) = \frac{2\pi e}{h} \int_{x_o}^{x} \int_{-\infty}^{\infty} B_y(\mathrm{x},\mathrm{z}) dz dx \qquad 2.5$$

It is therefore correct to think of ferromagnetic specimens as pure phase objects and thus Lorentz microscopy as a branch of phase contrast electron microscopy.

There are three imaging modes of Lorentz electron microscopy viz. Fresnel, Foucault and DPC (see reviews of these modes by Chapman [17,18]). Only the third of these will be discussed here, as the first two methods were not used in the thesis studies.

2.2.1 The Differential Phase Contrast Mode

DPC microscopy was introduced by Dekkers and de Lang [19] and subsequently applied to the study of magnetic domain structures by Chapman *et al* [20,21,22]. Because of its high resolution and linearity, it has also been developed for the study of recording head fields [2, 23, 24].

In our laboratory DPC can be performed in both the JEOL 2000 FX and the Philips CM20 instruments; the major differences between these two microscopes will be discussed later. These are (S)TEM instruments and their design is such that the magnetic samples can be situated in magnetic field free space, a feature essential for the study of magnetic materials and stray magnetic fields. They are both fitted with 4 or 8 segment quadrant DPC detectors.

The implementation of DPC imaging is shown schematically in Fig. 2.2.1.1. The electron beam is focussed in a plane corresponding to the middle of the head polegap. A quadrant detector is situated in the far field (in this case it is a 4 segment device). In the absence of any drive current in the head, the beam will experience no Lorentz deflection and the spot on the detector should be central for all points in the raster scan. To achieve this it is essential to have post-specimen optics to provide this descan condition. Ideal descan conditions are very difficult to achieve with great accuracy at the low magnifications used in recording head studies and to date this has proved a significant limitation to the accuracy of the technique.

The electron beam is scanned over the area of interest and as it propagates through the stray magnetic field from the driven head it will suffer Lorentz deflection and this will lead to a displacement of the disc on the detector. The difference in the electron distribution on opposite quadrants provides information on the (x,y)-plane component of induction integrated along the electron trajectory. Provided that the deflection is small compared to the probe angle, then the difference signal of A-C is proportional to the component of in-plane magnetic induction in the direction of the line T in the figure. Similarly the D-B signal is proportional to the component of magnetic induction along the line M. These two difference signals provide maps of orthogonal horizontal components of magnetic

induction integrated along the electron trajectory. For electron tomography there is an additional requirement and that is the ability to carry out DPC imaging of the head field as the head is rotated about the an axis parallel to y and through the centre of the polegap. Images at 5° angular intervals over a total angular range of 180° must be collected to give us the required range of field projections. Linescans from each pair of DPC images are then extracted as close as possible to poleface and these serve as the input for tomographic reconstruction of the head field.

There is a limit to the linearity of the imagining system's response determined by the ratio of the Lorentz angle to the probe angle; the limiting condition has been determined as $\beta_L/\alpha < 0.1$ [25] for an annular detector. This ratio can be relaxed for a solid detector, as used in our studies of recording heads, and the system may be assumed linear provided $\beta_L/\alpha < 0.5$ [23].

The data from the DPC detector is collected and stored digitally. On the JEOL signal pairs are normally collected due to the storage space limit on the AN1000 Data Acquisition system. This system controls the scan function during image acquisition. The Philips CM20 has a more advanced data collection system, with more storage space. A benefit of this is that one can collect individual signals from the quadrants and via image processing obtain the DPC images. The potential advantage of this is a reduction in electronic noise from the signal mixer unit. However, in practice the signal combinations rather than individual quadrant signals are collected, due to time constraints.

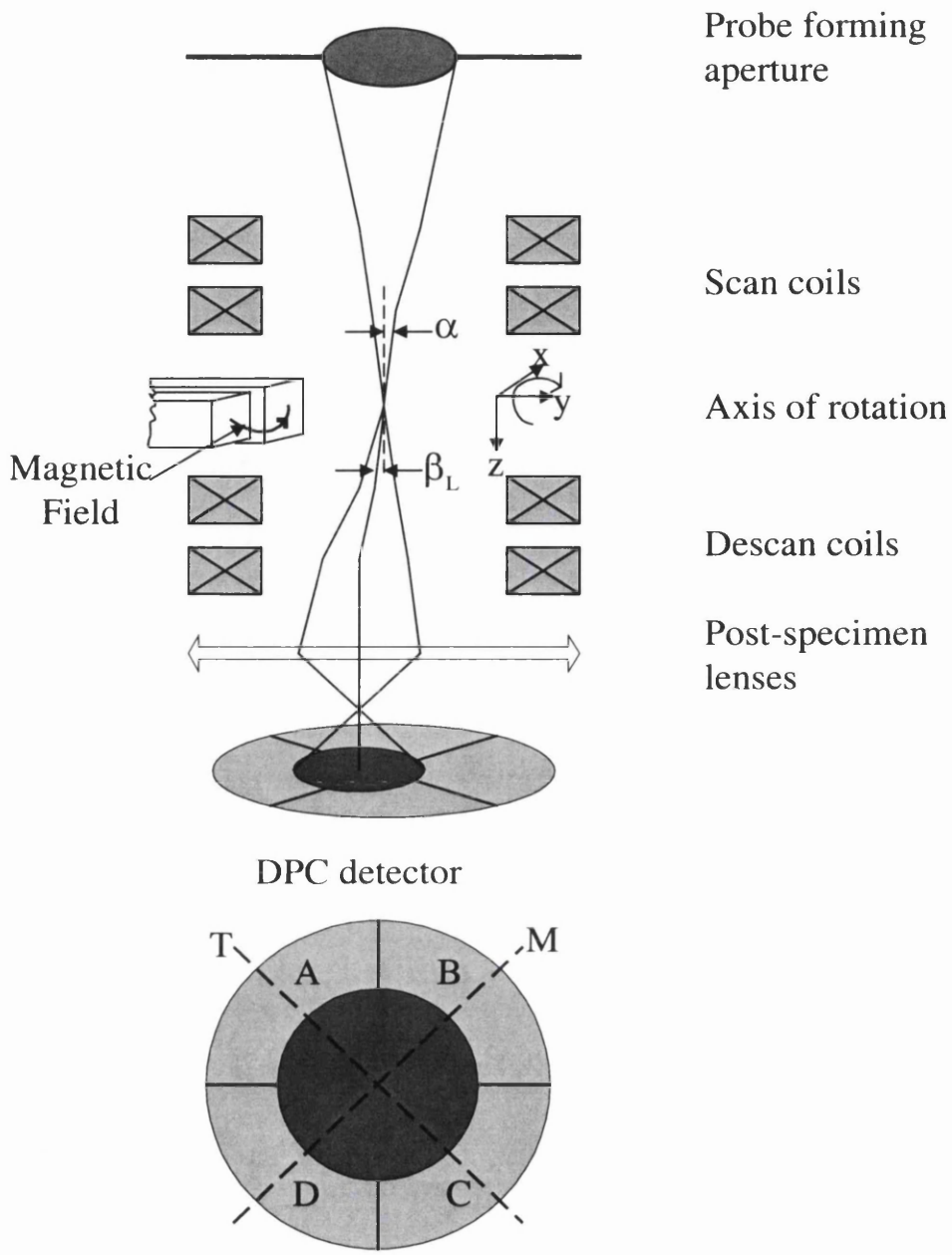

Fig 2.2.1.1. Schematic of the DPC mode of Lorentz Microscopy

2.3 Electron Beam Tomography

Tomography is the reconstruction of the interior of an object from the images of the object in a series of different projections. Electron beam tomography (EBT) is a technique, which employs an electron microscope to collect the projections (in the case of magnetic fields it is the magnetic induction integrated along the electron trajectory) and uses these

projections to reconstruct the object of measurement in its entirety. The first research group to develop an EBT system for the investigation of stray fields from recording heads was in Duisburg [1,26]. A SEM was used and the recording head samples were mounted on a high precision scanning stage. In this system the electron beam was raster scanned in front of the pole surface and the deflection due to the magnetic field at each point in the scan was measured by a 2D spatially resolving electron detector. The precision specimen stage was required to maintain the axis of rotation centred on the middle of the polegap as the head was rotated through the required 180° angular range to collect the data set. Apart from the post specimen optics required in (S)TEM to set a suitable camera length and to provide beam descan, the basic set up is the same. The sample is rotated incrementally to build up a series of different 'views' of the projection of the stray field. Apart from the reflection method [3], about which doubts have been cast [5], a stroboscopic method has also been developed [4].

The data for the field reconstruction are the orthogonal components of the electron deflection parallel/normal to the poleface of the head. In the case of the SEM these are determined from 2-D detector and in the case of (S)TEM they are given by the difference signals on the two sets of opposite quadrants of the detector which are suitably aligned relative to the specimen. The geometry of the EBT method is illustrated in Fig. 2.3.1. We require to measure the deflection data for a line in the image which is at a small distance from the polefaces. This is repeated for each of the images obtained as the head is rotated about the y(η)-axis at angular intervals $\Delta\theta$-for heads this is normally 5° - over a total angular range of (180 - $\Delta\theta$)°. For the given angular interval these constitute the totality of independent projections of the integrated magnetic induction and the 36 pairs of deflection components, each at the same distance from the head, are our raw data for tomographic reconstruction.

There are two reconstruction algorithms, which can be used to reconstruct the magnetic field of the recording head from the data on electron beam deflections. These have been designated the Radon Transform Method (RTM) [27] and the Algebraic Reconstruction Technique (ART) [28]. The RTM algorithm arises from the relationship between the Radon Transform [29] and the Fourier Transform and it requires convolution of each line

of experimental data with a mathematical function of the experimental parameters. The form of this function depends on the component of $\boldsymbol{B}$, which is to be reconstructed and the plane in which it is to be reconstructed. In practice this plane is as close to the sample as possible and our case the distance from the sample is determined by the pixel size 'a'. This means that the data is reconstructed at a plane y = a as shown in figure 2.3.1. However, the field can be reconstructed in any plane provided y > a. A filter function is applied to reduce the effects of noise in the data set. The values of $\boldsymbol{B}(x,y,z)$ can then be extracted by summing selected components from the convolved data set. Thus this is a real space back projection method. An advantage of the algorithm is that each data set provides an independent determination of **B** over the plane of reconstruction. Reconstructions using both sets of initial data then permit a check on the internal consistency of the reconstructions and of the original data.

With ART the plane of reconstruction is the plane y = a and both deflection data sets are required to determine the three components of $\boldsymbol{B}$. The y component is determined from the data set in the ξ direction and the x, z components from the data set for deflections in the η direction (see fig. 2.3.1.). The reconstruction plane is split into n^2 points on a square mesh and $\boldsymbol{B}(x,y,z)$ at each point is taken to represent the elemental square area surrounding it. The deflection value at any point in the reconstruction data set arises from the contributions of relevant components from a restricted set of values of $\boldsymbol{B}(x,y,z)$, for example those along the electron path and are weighted to take into account the length of the electron path in each elemental area. The end result is a set of simultaneous linear equations, which have to be solved. An iterative procedure is used to solve the problem and in the first instance the induction is assumed to be zero everywhere. The measured value of deflection at the first point of the first line of the deflection data set is then assigned in proportion to the elemental values of $\boldsymbol{B}(x,y,z)$, which contributed to it. The revised field value of each element is then used when it next is needed in the calculation of the deflection value. Refinement of an individual value of $\boldsymbol{B}(x,y,z)$ is done during the iterative procedure by apportioning the difference between the calculated and measured deflection value to the contributing elements in proportion to their magnitude. In practice it is found that ten iterations will give satisfactory convergence for the calculated values [23].

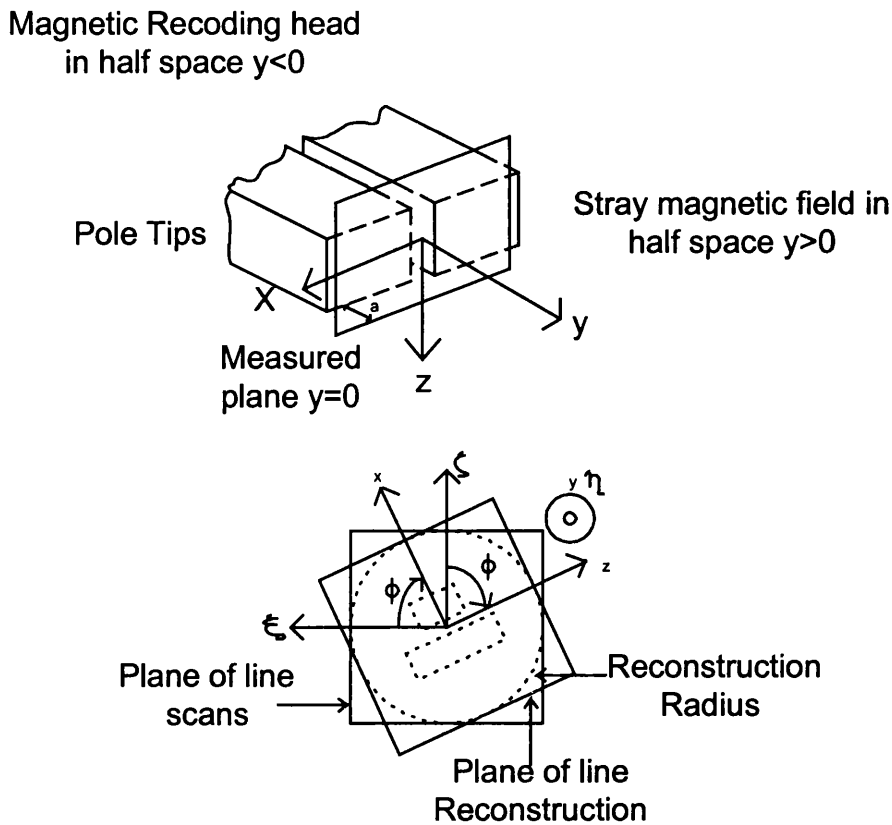

Fig.2.3.1 Co-ordinate systems used for Electron Beam Tomography

2.4 Modified Microscopes for Lorentz Microscopy

Most modern (S)TEM electron microscopes comprise(see fig. 2.4.1):

1) an electron gun which acts as the electron source,
2) two or three magnetic condenser lenses which control the illumination on to the specimen,
3) an objective lens and specimen stage – the objective lens is the most important lens for most imaging studies, since it normally determines the spatial resolution,
4) a series of post specimen lenses which serve in TEM mode to set the magnification at which the image is viewed or recorded; in STEM mode these lenses control the size of the scanned disc on the detector by determining the effective camera length.

In addition various coils, either air or magnetic cored, are situated along the length of the column to enable alignment of the electron optics and to provide the scanning facility for (S)TEM operation.

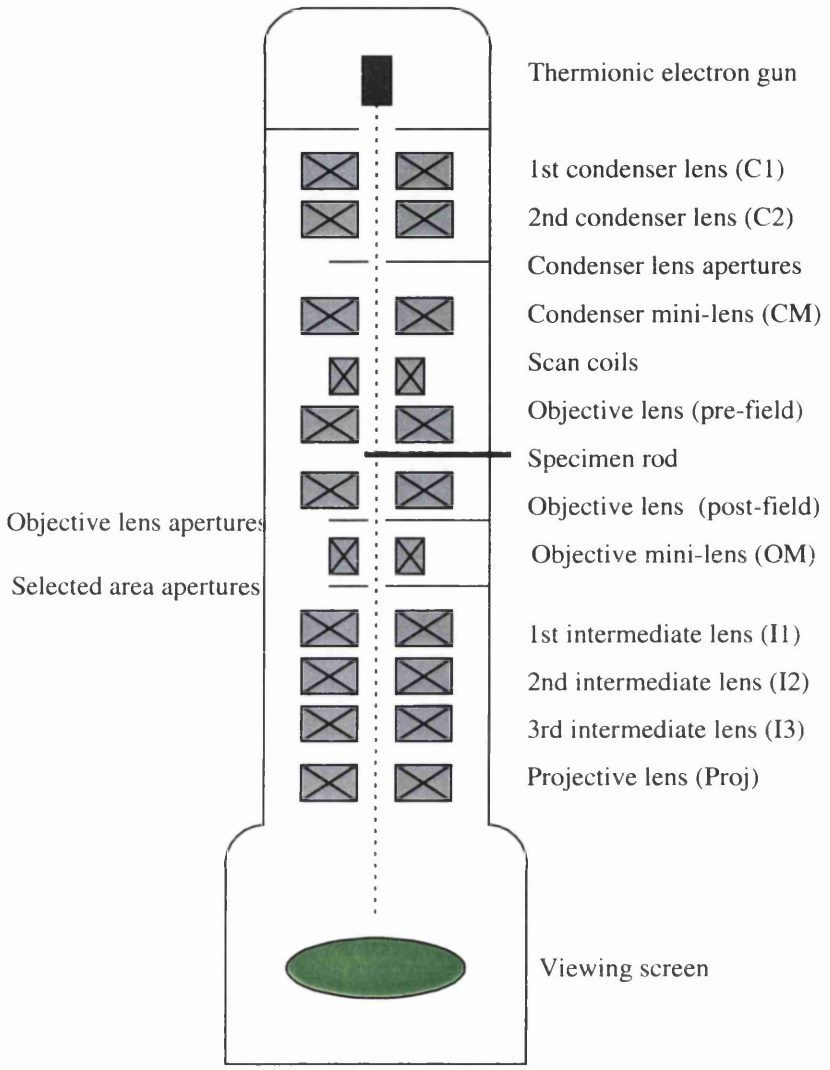

Fig.2.4.1 Schematic of the JEOL 2000 FX.

The two microscopes used in the investigation were of the same basic form i.e. they were both (S)TEM instruments. In the case of the JEOL 2000FX, the gun uses a thermionic tungsten emitter and hence has a relatively large effective source size ~40μm, resulting in a spatial resolution in scanning mode ≥100 nm in typical conditions for magnetic structure imaging. The Philips CM-20 is a much more sophisticated instrument (and of substantially more recent origin) and utilises a thermally assisted field emitter as the electron source. This provides a much smaller effective electron source and in consequence a spatial

resolution in STEM magnetic imaging ~10nm. In addition, the energy spread of the electron beam is ~0.6eV, compared to ~2eV for the JEOL – this means that the instrument is well suited to electron energy loss spectroscopy (EELS) and this together with energy dispersive x-ray microanalysis (EDX) are the available microanalytical facilities on this microscope.

For the study of ferromagnetic materials, the specimens must be placed in a zero strength magnetic field or more realistically in a field of very small magnitude; the strength of residual field which can be tolerated will of course be a function of the coercivity of the material under investigation. In our studies we are dealing with magnetically very soft materials and hence the residual field should ~10^{-3}-10^{-4} T. To achieve reasonable spatial resolution in magnetic STEM imaging therefore requires that the objective lens must be of a non standard form. This is true for both instruments under discussion. In the case of the 2000FX, the design solution is illustrated in Fig. 2.4.2. The objective lens polepiece was effectively split in to two field regions by a central soft iron core in which a gap housed the specimen rod [30], the objective aperture holder and a Back Scattered Electron (BSE) detector. This region was separated from the upper and lower field regions by two very narrow bores, which served to limit the magnetic field at the specimen to a value ~1 mT. With this configuration the upper part of the field acts like a third condenser lens and helps to reduce the electron probe size in scanning. The lower field acts as the objective lens in conventional TEM imaging.

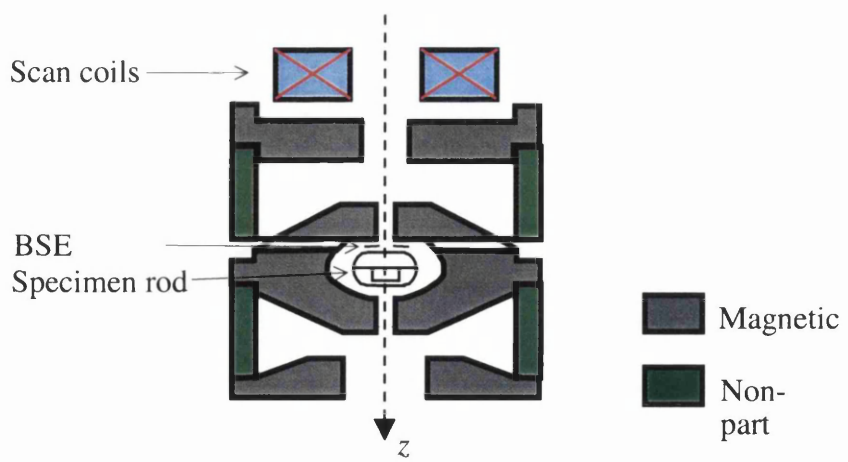

Fig.2.4.2. Schematic of the Objective pole piece in the JEOL 2000 FX (S)TEM

The solution to the problem of imaging at high spatial resolution, but with the specimen in magnetic field-free space, adopted by the Philips electron opticians is shown schematically in Fig. 2.4.3. In this case a very large gap objective lens was the basis of the design. This allows a great deal of freedom for the design and construction of ancillary equipment e.g. heating, cooling, magnetising straining etc stages. The lens however is fitted with non-standard mini lenses in the upper and lower objective lens bores. With the objective lens switched off for magnetic imaging, the upper mini lens is used to give a small electron probe ≥10 nm for STEM Lorentz imaging and the lower mini would be used as the effective objective lens for TEM magnetic imaging. The fact that these mini lenses are relatively close to the specimen means that their imaging performance, as determined by lens aberrations, is very good compared to the JEOL objective lens configuration. This objective lens arrangement combined with the FEG makes this microscope superior to the JEOL.

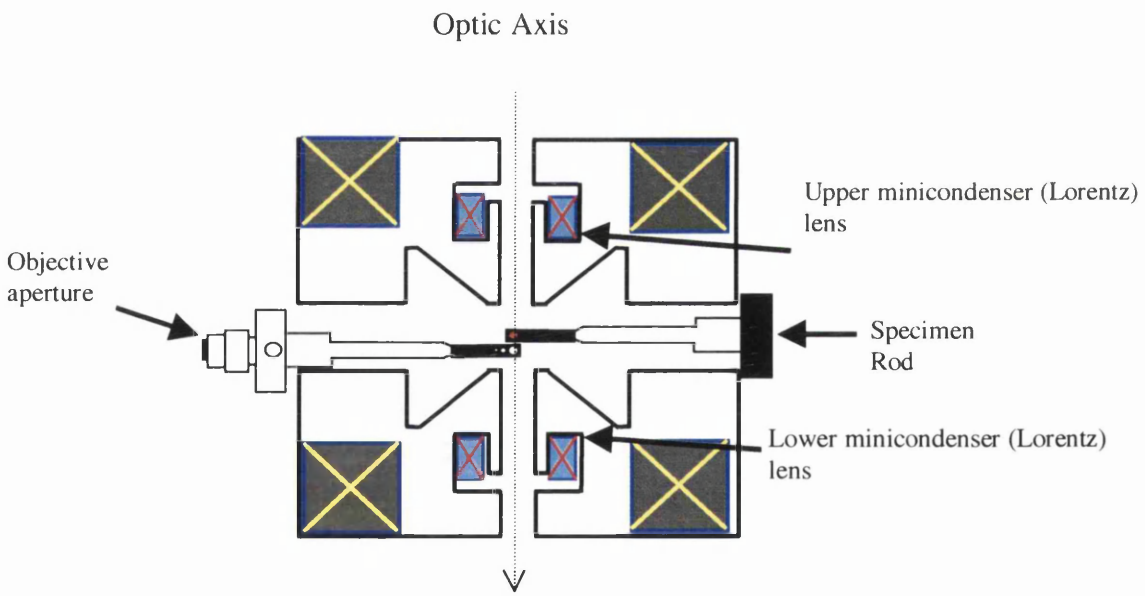

Fig. 2.4.3. A schematic of the lens arrangement in the Philips CM20 which provides a stray magnetic field free space.

2.4.1 The JEOL 2000 FX Problem's

During the second year of my Ph.D. programme the JEOL 2000FX developed a serious instability, which affected the instrument performance. The electron beam developed a "flicker" in intensity and an "oscillation" in the size of the electron probe (see appendix A).

This made any attempt to obtain quantitative data on the Onstream head fields impossible. Had the CM-20 not had a much smaller specimen rod diameter, this would have been a less severe difficulty particularly in regard to the study of the Emboss heads. In all, the identification of the source of the fault and its eventual cure took almost a year to achieve. It was a major setback since there were many false "cures" along the way and a great deal of time and experimental data was wasted.

2.5 Magnetic Force Microscopy

2.5.1 MFM Theory

In its simplest form a MFM consists of a sensor which detects deflections of a cantilever whose movement is controlled by the interaction of the magnetic tip with the stray magnetic field from a magnetic sample, (see fig. 2.5.1.1.)

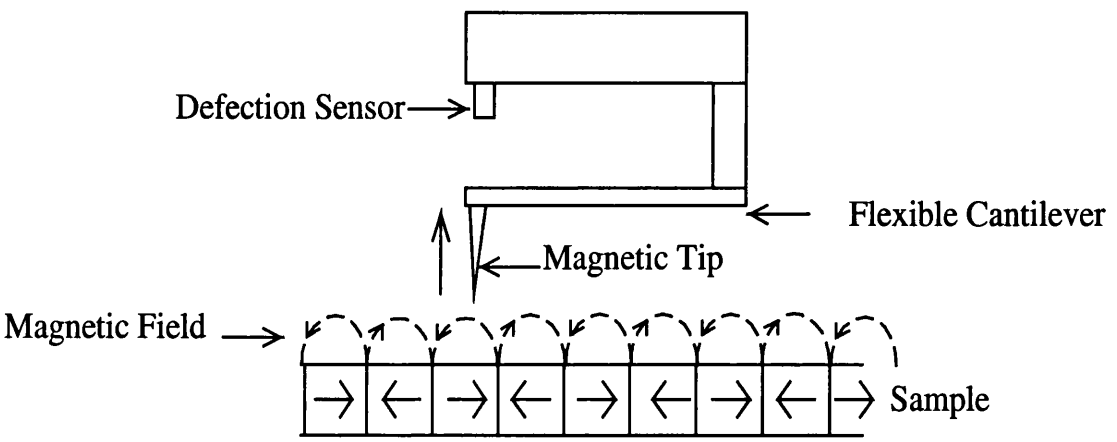

Fig.2.5.1.1 A schematic of the basic concept behind MFM

For pure force detection and if the tip is assumed to behave as a point dipole the force **F** acting on the tip is given by the gradient of the field,

$$\mathbf{F} = \nabla(\mathbf{m} \bullet \mathbf{H}) \qquad 2.6$$

where **m** and **H** are the magnetic moment of the tip and the field from the sample respectively. However, this technique is not commonly used, as force gradient detection offers significantly better sensitivity to long range forces such as magnetic fields. For force gradient detection, the cantilever is oscillated and the change in resonant frequency is measured. If the MFM is again treated as a point dipole and the drive frequency is kept constant then the phase shift ($\nabla\Phi$)of the tip oscillation near resonance is given by the following expression [31],

$$\nabla\Phi = \frac{Q}{k}\left(q\frac{\partial H_z}{\partial z} + m_x\frac{\partial^2 H_x}{\partial z^2} + m_y\frac{\partial^2 H_y}{\partial z^2} + m_z\frac{\partial^2 H_z}{\partial z^2} \right) \qquad 2.7$$

Tip contribution Stray magnetic field contribution

where Q is the quality factor of the MFM tip cantilever resonance, k is the spring constant of the cantilever, q is the effective magnetic charge of the MFM tip, m_i is the tip magnetic moment and H the field generated by the recording head. A real tip has an extended geometry and this has to be accounted for when trying to quantify any data collected.

Since the tips were mainly sensitive to the z component of the stray magnetic field then, taking into account that the phase shift can be positive or negative, the above expression simplifies to [32],

$$\nabla\Phi = -\frac{Q}{k}\left(-q\frac{\partial H_z}{\partial z} + m_z\frac{\partial^2 H_z}{\partial z^2} \right) \qquad 2.8$$

In the experiments presented later it was the phase shift that was measured and when the magnetically hard tips were used it is possible to differentiate between positive and negative phase shifts. The instrument used in our studies was a Digital Instruments 3100 with the Extender Module for phase imaging.

Despite the progress made in the application of MFM, quantitative interpretation of MFM images is still lacking at the time of this thesis, although the theoretical work on tip sample interaction, image simulation and micromagnetic modelling of MFM tips has aided the

understanding of image formation [33, 34, 35]. Experimental work [7, 8, 31, 32] to characterise and model MFM tip stray magnetic fields has helped to increase the understanding of the physics underpinning MFM. The high resolution of MFM compared to other methods (see section 2.1.1) makes it the most attractive method for the study of magnetic media and the method would be greatly enhanced if the data collected could be quantified.

2.5.2 The Digital Instruments MFM

The Digital Instruments (DI) Dimension 3100 AFM/MFM produces high-resolution, two-dimensional images by scanning a sharp probe over the sample surface. The probe is part of a flexible cantilever that is mounted on one end of a cylindrical piezoelectric tube. The piezo tube is rigidly mounted near the top of the microscope. Voltages applied to the X and Y electrodes on the piezoelectric tube deflect the tube horizontally to produce a precise raster scan over the sample surface. A voltage applied to the Z electrode on the piezo tube controls the vertical height of the probe. Stepper motors coupled to lead screws translate a x-y stage to which the sample is attached. A separate motor drive allows the z-height of the microscope and probe to be adjusted relative to the sample surface. A schematic of a AFM/MFM is shown Figure 2.5.2.1

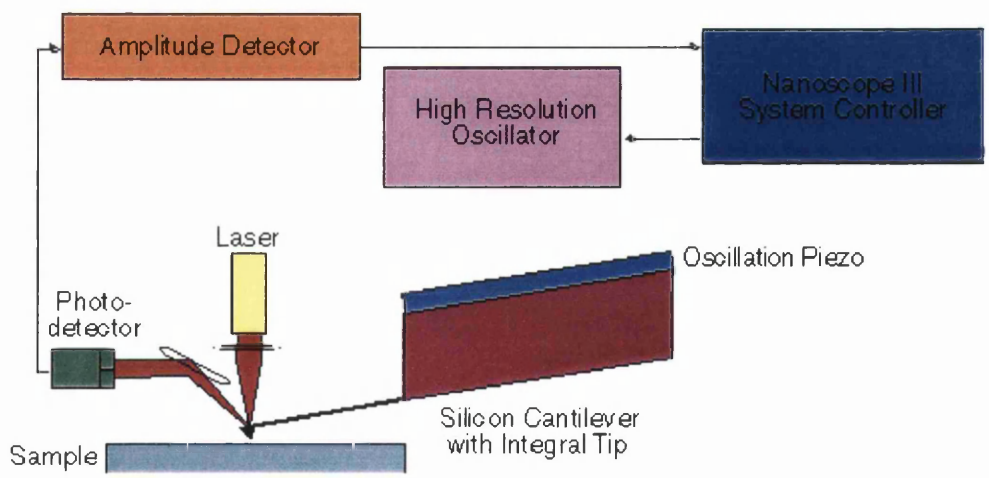

Fig.2.5.2.1. Schematic of the MFM.

In our studies the DI MFM was operated in TappingMode™ combined with LiftMode™ to collect magnetic information about the stray magnetic fields from the Onstream samples.

These operating modes enable the topographic data to be separated from the magnetic field data. They are fundamental to the operation of this type of MFM and so will be discussed briefly next.

For mapping the topography of a sample the probe tip can either be in constant contact with the sample surface, which has the potential for the tip to damage the sample, or the tip can be "tapped" across the sample. TappingMode™ operates by scanning a tip, which is attached to the end of an oscillating cantilever across the surface of the sample. The cantilever is oscillated at or near its resonance frequency. The tip lightly "taps" on the sample surface during scanning, contacting the surface at the bottom of its swing. A feedback loop maintains a constant oscillation amplitude by maintaining a constant RMS of the oscillation signal measured by a split photodiode detector. To maintain a constant "setpoint" amplitude the vertical position of the scanner at each (x, y) data point is stored by the computer to form the topographic image of the sample surface. By maintaining a constant oscillation amplitude, a constant tip-sample interaction is maintained during imaging.

LiftMode™ is invoked by selecting lift in the interleave option. By selecting Interleave an "interleaved" scan is fitted in between a normal raster scan (Fig 2.5.2) with the result that the vertical scan speed is halved giving twice as many scan lines.

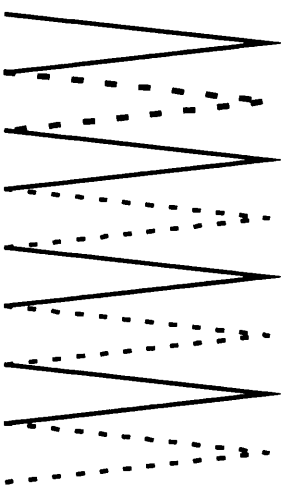

Fig2.5.2. A schematic of Interleave scanning, the solid lines represent the main scan and the dotted lines the interleave scan.

In LiftMode™ measurements are taken in two passes across each scanline with each pass consisting of one trace and retrace. In the first pass, topographical data is taken in TappingMode™ on one trace and retrace. The tip is then raised to a user defined lift scan height and a second trace and retrace are performed while maintaining a constant separation between the tip and the local surface topography. The magnetic interactions are detected during this second pass. For the best results the data from any magnetic interactions is collected on the retrace. Using LiftMode, (see Fig. 2.5.2.3.) topographical features are virtually absent from the MFM image (see Fig. 2.5.2.4.)

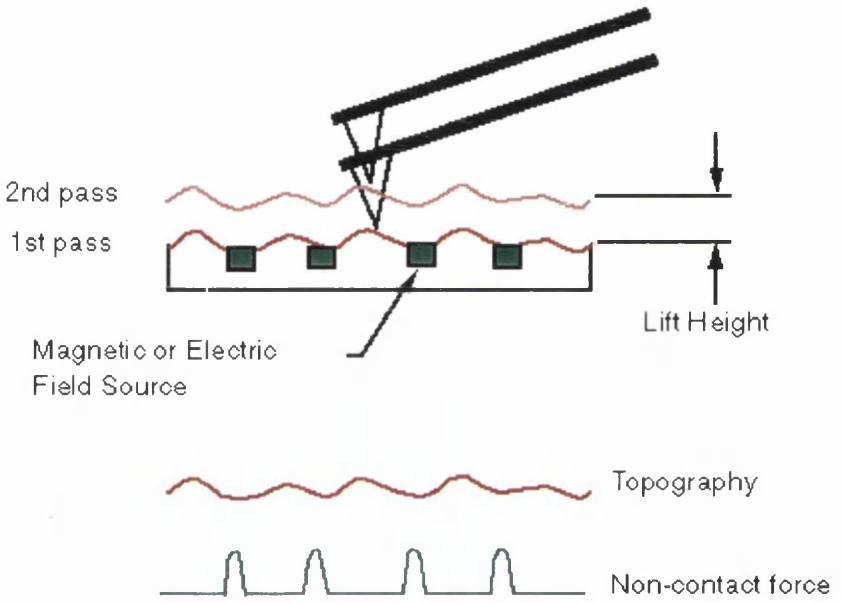

Fig.2.5.2.3. Schematic of the operation of the LiftMode and how the topographic data is "separated" from the magnetic data.

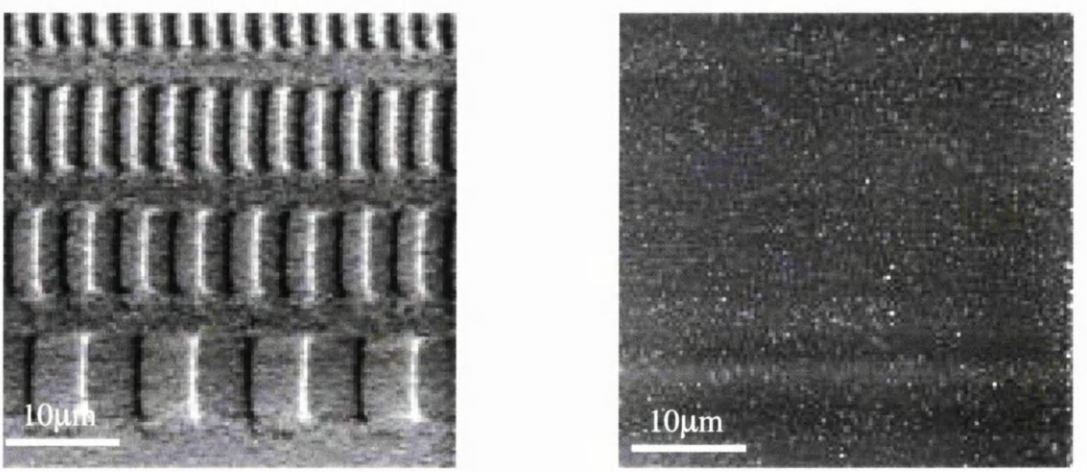

Fig.2.5.2.4. The image on the left is a typical phase image from the hard drive sample and to the right is the topographic data collected simultaneously. The lift height was 100nm

The magnetic influences are measured using the principle of *force gradient detection*. In the absence of magnetic forces, the cantilever has a resonant frequency f_o. This frequency is shifted by an amount Δf proportional to vertical gradients of the magnetic force on the tip. These frequency shifts can be detected three ways: phase detection; amplitude detection and frequency modulation. Phase detection and frequency modulation produce results that are generally superior to amplitude detection. Due to its ease of implementation, the method selected in these studies was phase detection. In phase imaging (see equation 2.7), the phase lag of the cantilever oscillation, relative to the signal sent to the cantilever's piezo driver is monitored and recorded. This phase lag is very sensitive to variations in magnetic field. However it should be noted that the Extender electronics give a measure of the phase lag of the cantilever oscillation relative to the piezo drive. This measurement is monotonic versus frequency, as is the true phase lag in degrees. The Extender measurement, however, has slightly different nonlinear characteristics *vs.* frequency. The measurement technique allows optimal signal-to-noise ratios; however, absolute values of phase data should be taken as approximate.

As important as the microscope are the probes which are used as the sensors. The probes consist of a silicon substrate with an integrated cantilever on which the tip is stiuated; the structure is coated with a magnetic thin film by sputtering or evaporation. SEM images showing the tip transducer are shown in Fig. 2.5.2.5. In the following section the characteristics of the tips selected for the study of the magnetic heads are discussed.

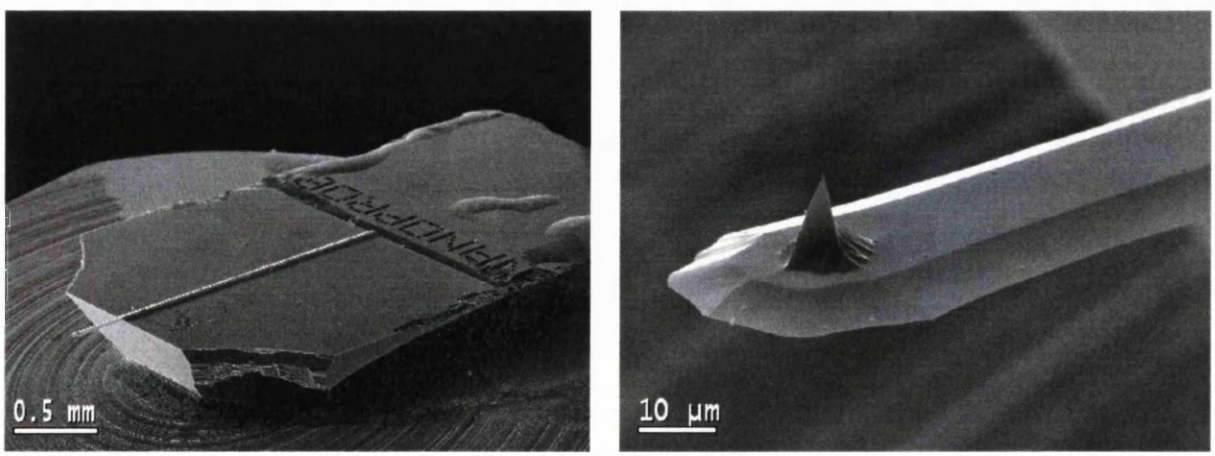

Fig. 2.5.2.5 Two SEM images of a typical MFM "head assembly".

2.5.3 The MFM tips available at Glasgow

For the study of the Onstream heads with the MFM we had a selection of tips to choose from; three standard commercial tips supplied by DI and a number of experimental tips. In this section the characteristics of the tips used for the experiments in Chapter 4 will be presented. Before any studies of the stray magnetic field from the tape heads was undertaken the tip selected was characterised using a standard magnetic sample to try to ensure it was responding in the expected manner.

A hard disk sample was used as the "standard" magnetic sample, and the particular area selected had tracks with bit separations of ~4.7 μm, ~2.5 μm and ~1.9 μm (later in the research period, a special recording sample was obtained from NIST, Boulder Co. and would be the preferred standard). The scan area was 40 microns square and a resolution of 128 samples per line was selected, which was adequate for this purpose. The tips were all magnetised prior to use to try to ensure they were sensitive to the perpendicular magnetic component of the stray field. The anticipated form of the stray field components from the sample are shown below in Fig. 2.5.3.1

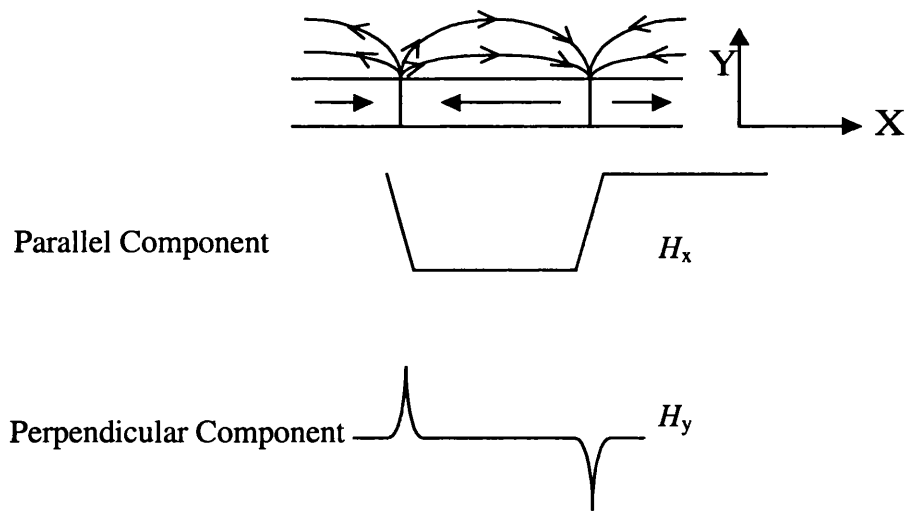

Fig. 2.5.3.1 An idealised sketch of the two components of magnetic field that can be studied using MFM.

The same section of the standard sample was used to characterise the various tips used in the studies. This enabled a comparison of their response to the magnetic tracks and acted as an aid to the interpretation of the phase images of the stay magnetic field from the tape

heads. The standard sample also proved useful in determining if the tip had become damaged during the course of an experiment and was also used to provide an insight into the magnetic state of the tip at the end of an experiment.

The tips may be divided into two main categories namely magnetically 'hard' or 'soft' categories and their characteristics are discussed under these general headings next.

2.5.3.1 The magnetically hard tips.

Three types of hard magnetic tips (see Table 3.5.3.1.1 below for details) were available for the study of the stray magnetic field from the tape heads, but the supply particularly of the CoPt type was limited. In Figure 2.5.3.1.1, the phase images taken with the individual tips and the corresponding linescans extracted from the track with a bit spacing of 4.7μm are shown.

Table 2.5.3.1.1 The Magnetically Hard Tips

Tip Designation	Magnetic Thin film Coating	Approximate Thickness (nm)
MESP	CoCr	50
CoPt	CoPt	40
Cobalt	Co	50

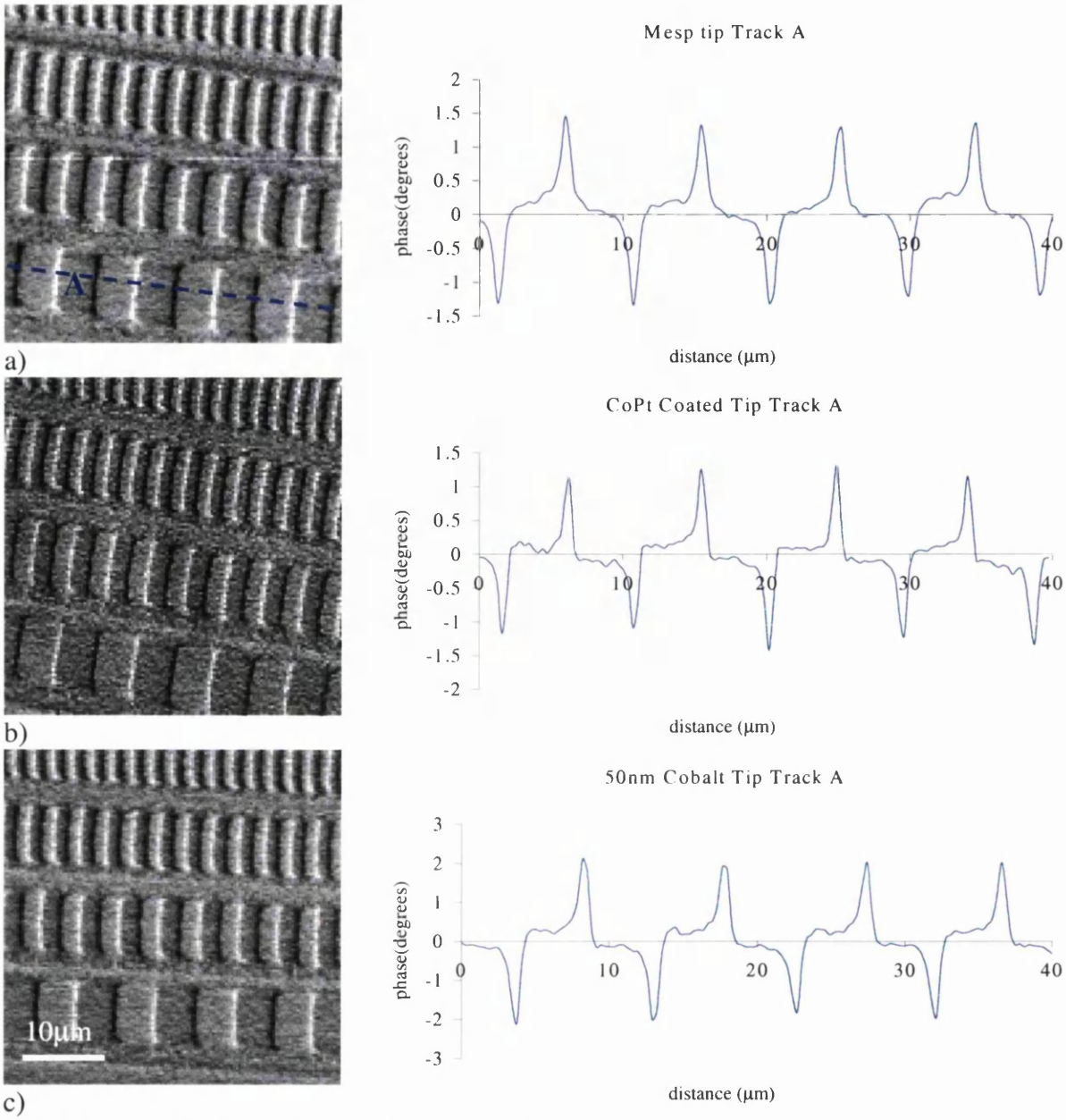

Fig. 2.5.3.1.1 The phase images of the standard hard disk sample collected using the three types of hard magnetic tips, the lift height being 100 nm. To the right of each image is the corresponding linescan extracted from position along 'A' as shown in the first image.

The first image was taken with the standard DI tip, which is coated with ~50nm of CoCr alloy. As the tip is scanned across the surface of the hard disk sample the shift in its resonant frequency is recorded as a phase lag relative to the piezo drive. If one follows the arguments presented by Lohau [32] and equation 2.8, then what is seen in the above linescans can be equated to positive and negative changes in the resonant frequency as the tip scans across the hard disk. In this case the white contrast arises due to a positive shift

and therefore a positive force gradient. Black contrast arises from a negative shift in the resonant frequency and hence a negative force gradient. This can be loosely interpreted as the polarity of the track transitions relative to the magnetisation direction of the tip.

From the extracted linescans it can be seen that all three tips have a similar response function in relation to the magnetic tracks on the disk section. The linescans for the images taken with the CoPt and the Co coated tips are very close in profile to those shown in Fig. 2.5.3.1 for the perpendicular component of the stay magnetic field. Of the three tips the largest phase signals were recorded for the CoPt coated tip.

When selecting a magnetically hard tip for the study of the stray magnetic fields from recording heads, ideally they should be sufficiently hard not to be influenced by the stray field. That is to say they should retain/maintain their magnetic characteristics under the influence of the stray magnetic field from the head. To increase the coercivity of a tip the shape anisotropy can be increased and/or the grain structure of the magnetic thin film altered. Therefore the ideal shape for a hard magnetic tip would be an elongated needle, which has a large shape anisotropy [36]

2.5.3.2 The magnetically soft tips

The ideal soft tip should always be attractive to the sample. This means that it will image the absolute value of the stray magnetic field from the sample [37]. However information about stray field direction will be lost. It has been suggested that the ideal soft tip would be a superparamagnetic particle [36].

Three soft magnetic tips were utilised and their details are given in Table 2.5.3.2.1 The corresponding phase images of the hard disk sample are shown in Fig. 2.5.3.2.1.

Table 2.5.3.2.1 The Magnetically Soft Tips

Tip Designation	Magnetic Thin film Coating	Approximate Thickness (nm)
Low Coercivity (LC)	NiFe	?
Metglas 10	FeBSiC	10
Meglas 50	FeBSiC	50

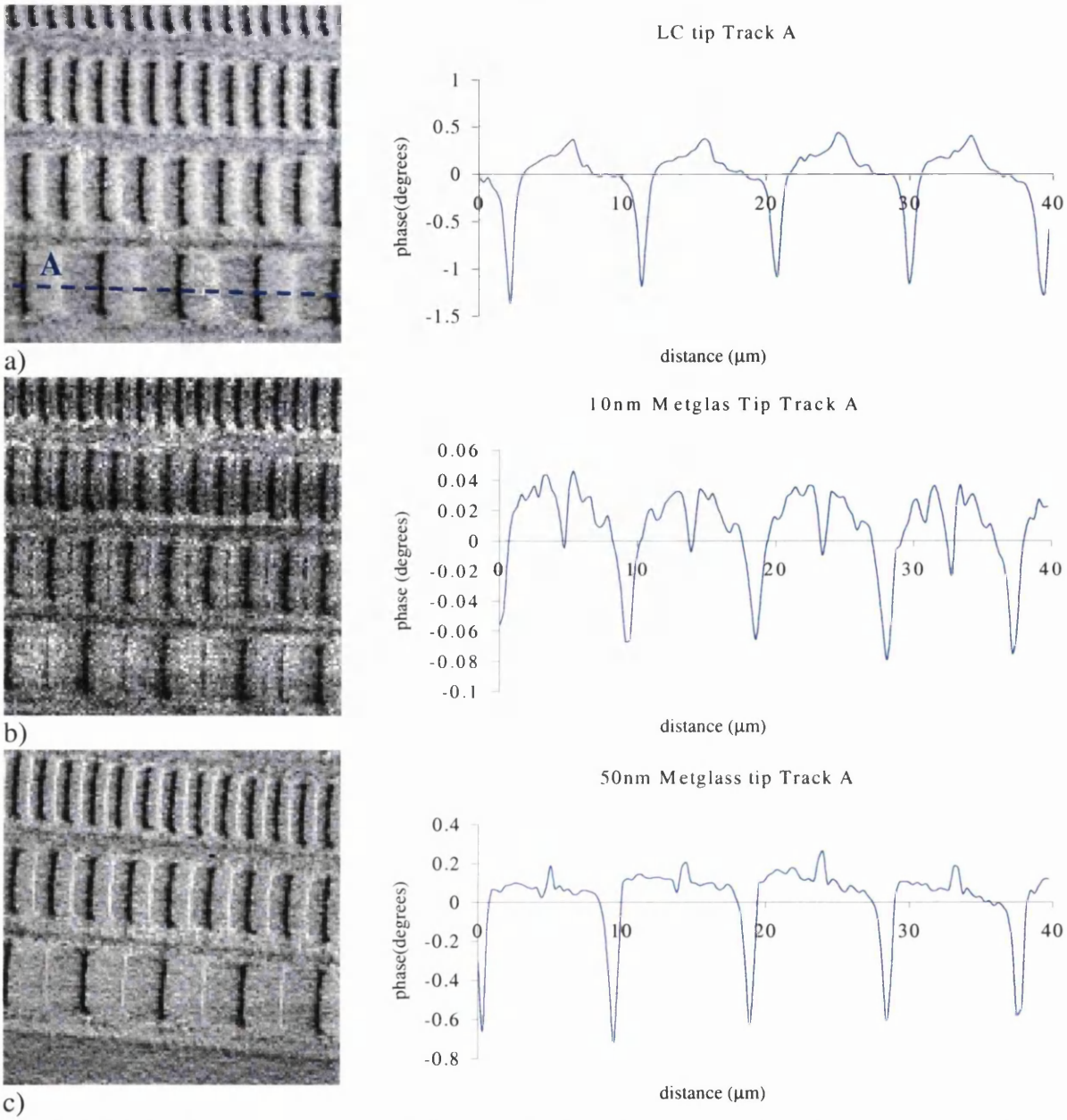

Fig 2.5.3.2.1 The phase images of the standard hard disk sample taken with the various soft magnetic tips as indicated in the title of the graphs to the right of the images and the corresponding linescans extracted from position along 'A' as shown in the first image.

Unlike the previous tips these three exhibit differing response functions for the magnetic track imaging. It was expected that they should 'follow' the magnetic transitions and not respond to the polarity of the transitions i.e. the transition region contrast would always be black. The LC tip and the 50 nm Metglas tip both show signs of a negative phase shift followed by a positive phase shift. The positive phase shift is not as large or as well defined as the negative phase shift, but this result indicates that these tips cannot truly be

considered as magnetically very soft. It is worth noting that the minima for the 50nm Metglas tip is approximately half that of the LC tip. The middle image, that taken with the 10nm Metglas tip, shows the type of response that was expected. The magnitude of the minima are very much lower than for the other two tips reflecting the substantially lower thickness of the film coating. This caused a problem when used to study the tape heads, due to a low signal to noise ratio in the image.

For the LC tip the linescan shown here is characteristic of this type of tip when used to image the hard disk sample. However the same cannot be said for the 50nm Metglas tips used with this sample. These did produce well resolved images but there was an indication that they could show some sensitivity to the in-plane magnetic component despite being magnetised vertically i.e. along the tip axis. The 10nm Metglas tip was very difficult to characterise using this sample.

2.5.3.3 The low moment tip

This tip (see Table 2.5.3.3.1) exhibits a low moment but has high coercivity. For this reason it is presented separately. The hard disk image taken with this type of tip is shown in Fig. 2.5.3.3.1. It proved to be very difficult to repeat this characterisation study with some of the other tips in this batch from DI and generally we have found these tips to be very unreliable in performance.

The reasoning behind using this tip was to reduce the tip sample interaction and thereby reduce the number of tips damaged when studying the stray magnetic fields from the Onstream samples.

Table 2.5.3.3.1 The low moment Tip

Tip Designation	Magnetic Thin film Coating	Approximate Thickness (nm)
Low Moment (LM)	CoCr	20

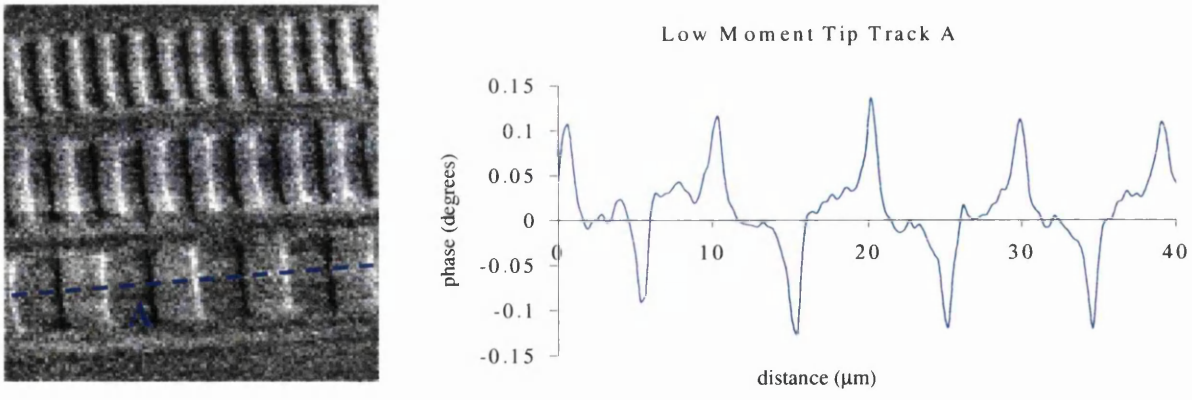

Fig 2.5.3.3.1 The phase images of the standard hard disk sample taken with the LM magnetic tip and the corresponding linescan extracted from position along 'A' as shown in the image.

It can be seen from the graph that it has a response function similar to the hard magnetic tip but the maxima and minima phase excursions are much lower in magnitude when compared to the graphs in figure 2.5.3.1.1. confirming the low moment categorisation.

2.6 Conclusion

The basic concepts behind the techniques used for the study of the Onstream tape heads have been presented. In the next two chapters these methods are applied and the results presented.

2.7 References

1. Elsbrock J.B., Schroeder W., and Kubalek E., (1985), *IEEE Trans. Mag.*, **5**, 1593
2. Ferrier R. P., Liu Y., Martin J.L. and Arnoldussen T.C., (1995), *J. Mag. Magn. Mater.*, **149**, 387-397.
3. Yin J., Matsuda J. and Nomizu S., (1996), *J. Phys. D –Appl. Phys.*, **29,** 1116-1123.
4. Shinada H., et al., (1992), *IEEE Trans. Mag.*, **28,** 1017.

5. R.P. Ferrier, (2000) Private Communication.
6. Wago K., Sueoka K., Sai F., (1995), *IEE Trans. Mag.*, **5**, 5178
7. Ferrier R. P., MacVite, S. Gallagher A,. Nicholson W.A.P, (1997) *IEEE Trans. Mag* **33(5)**, 4062
8. Scott J., MacVitie S., Ferrier R.P., (1999), *IEEE Trans. Mag.*, **35(5),** 3986
9. Oral A., Bending S.J., Henini M., (1996), *Appl. Phys. Lett.,* **69(9),** 1324
10. Howells G.D., et al (1999), *J. Magn. Mag. Matls.*, 196-197, 917-919
11. B. Milton (1999), Private Communication
12. Yamamoto Y., Schultz S., (1996) *Appl. Phys. Lett.*, **69**, 3263
13. Yamamoto Y., Schultz S., (1997), *J. Appl. Phys.*. **81**(8) 4696
14. Su J.L., Ju K., Vo L., (1992), *IEEE Trans. Mag.*, 28(5) 2722
15. Hale M.E., Fuller H.W., . Rubenstein H, (1959), *J. Appl. Phys.*, **30**, 789
16. Aharanov Y., Bohm D, (1959), *Phys. Rev.*, **115**, 485
17 Chapman J.N., (1984) *J.Phys D: Appl. Phys.* **7**, 623-647
18. McFadyen I.F., Chapman J.N., (1992) *Electron Microscopy of magnetic materials.* ESMA Bulletin, : p. 64
19. Dekkers N.H., de Lang H., *Optic*, **41**, 452 (1974)
20. Chapman J. N., Morrison G. R.,(1983) *J. Magn. Magn. Matls.*, **35**, 254-260.
21. Chapman J. N., McVitie S., . McFadyen I. R., (1987), *Scanning Microscopy Supplement 1, Scanning Microscopy International, Chicago (AMF O'Hare),* 221-228.
22. Chapman J. N., McFadyen I. R, McVitie S., (1990), *IEEE Trans. Mag*, **26**, 1506-1511.
23. Liu Y., 'Electron Beam Tomography Of Recording Head Fields', Ph.D Thesis, University of Glasgow (1996).
24. Liu Y., Ferrier R. P., (1995), *IEEE Trans. Mag.*, **31**, 3373-3375.
25. Gilles, M.F. Chapman J.N., (1995), *J. Appl. Phys.*, **78**(9), 5554-5562
26. Steck M. (1990), *Ph.D. thesis,* University of Duisburg.
27. Ludwig D., (1966) *Comm. Pure Appl. Math.*, 1966. **19**(4): 49.
28. Gordon R., (1974), *IEEE Trans. Nucl. Sci.,* 1974. **78**(4): p. 78
29 Radon J., (1917), *Math. phys. Klasse* **69**, 262-277
30. Tsuno, K. Inoue M., (1984). *Optik*, **67**(4): p. 363-376.
31. Kong L., Chou S.Y., (1997), *J. Appl. Phys.*, **81**(8) 5026

32. Lohau J., Kirsch S., Carl A., Dumpich G., Wassermann E.F., (1999), *J. Appl. Phys.*, **85(6),** 3410

33. Ishii I., Mukasa K., Kanai Y., (1998), *IEEE Trans. Mag,* **34**(5), 3455

34. Gomez R.D., Pak A.O., Anderson A.J., Burke E.R., Leyndecker A.J., Mayergoyz I.D., (1998), *J. Appl. Phys.* **83**(11), 6226

35 Wdowin M., Miles J.J., Middleton B.K., Aziz M.,(1998) *IEEE Trans. Mag,* **34**(4) 2324

36. Porthun S., Abelmann L., Vellekopp S.J.L., Lodder, J.C. Hug H.J., (1998), *Appl. Phys. A,* **66**, 1185

37. Grutter P., Rugar D., Mamin H.J., Castillo G., Lambert S.E., Lin C.J., Vallenta R.M., Wolter O., Bayer T., Greschner J., (1990), *Appl. Phys. Lett.,* **57(17)**, 1820

Chapter Three

3 The Study of Recording Heads using an Electron Probe

3.1 Introduction

The rapid increase in the size of hard drives in home computers, has resulted in the need for inexpensive high-capacity data storage systems for data backup. There are several technologies available, Iomega Zip/Jaz removable storage disks, Hewlett Packard and Onstream both have tape drive systems on the market, and finally there is optical storage media. The main considerations for choosing a storage system is data transfer speed, seek time, capacity and cost. If one is just looking for data archiving or backup for a single computer then CD-RW would be a good choice in terms of cost and capacity. With a CD-RW drive it is possible to re-write up to ~1000 times plus there is a storage capacity of 650MB and the cost of the media is ~ £2 per disk. However if a more versatile storage system is required then the Onstream option is very good in terms of cost and capacity. The entry level Onstream system is a 15/30GB internal IDE tape drive and uncompressed can hold up to the equivalent of 23 CD-RW disks at a cost of ~£28.00 per cartridge. If we compare the data transfer rate then the optical drive has a rate of ~700 KB/s and the tape drive 1 MB/s, hence the tape drive has the advantage. One of the great benefits of the tape drive system over the optical system is that it is a true drop-and-drag drive, i.e. you can just drag a file over the correct icon and drop the file onto the tape.

The current OnStream tape drive unit has evolved from the Philips DigaMax™ [1] tape system. In the tape drive there is a multi-array-recording head used in conjunction with pre-formatted media containing servo information. A novel design of servo head is used to write the servo information deep within the tape before it is sold. To help understand some of the challenges in studying the two heads, an understanding of the basic design of the heads is required and this will be addressed.

The read/write component of the tape drive comprises eight thin film write heads, and the same number of magnetoresistive (MR) elements for the read function. During normal operation, an actuator keeps the head on track using pre-recorded servo information in the lower depths of the tape coating. A dedicated servo head is used to define the position of the 192 data tracks on the tape. By writing the servo information to the full depth of the tape, the data can be overwritten in the upper part of the tape coating. The two signals are separated in the read-channels by low-pass and high-pass filtering. In contrast to hard disk heads which generally use shielded MR elements that are relatively insensitive to long wavelengths, the data head uses yoke type read heads, stacked on top of the write heads. The magnetic media is 8mm wide 72kA/m tape and the servo information is pre-recorded during a single pass of the servo head. A schematic of the servo head is shown in Fig.3.1.1 indicating the position of the poles relative to the tape bearing surface (TBS).

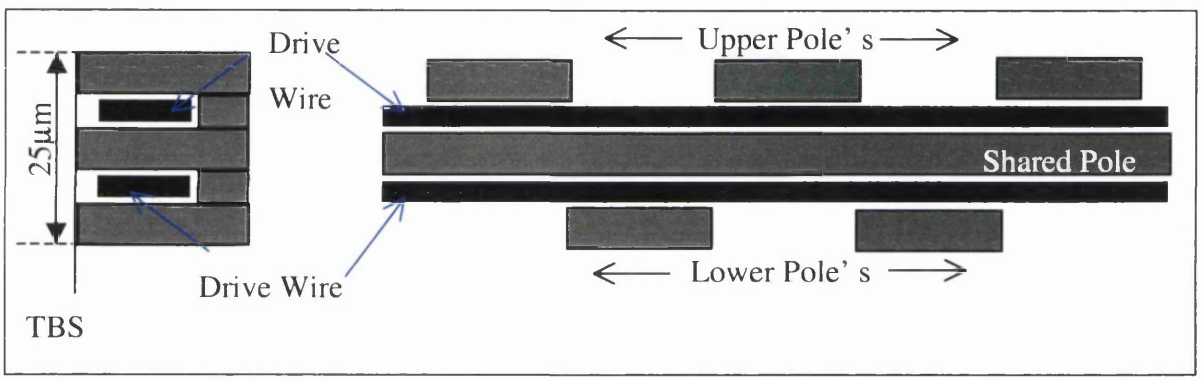

Fig.3.1.1 A schematic of a section of the Pole Layout in the Servo Head.

The total height of the pole stack is 25µm and the pole gap's of the head studied at Glasgow were 5µm. The upper and lower writers each have their own single turn common write wire by which servo tracks with a signal phase difference of 180 degrees between adjacent tracks are written. A combination of 0-180, 180-0 degree interfaces and two wide reference tracks keep the data head on position. Six of the read channels sense zero input from the servo tracks and the other two "see" the full signal to obtain phase and frequency signal. This servo format falls into the category referred to as boundary systems. The servo track is laterally divided into two or more regions separated by linear boundaries. These distinct regions have different properties, which can be detected by a data head. The head element straddles a boundary between regions, and the ratio of the amplitude of the

response of the head to each region provides the position signal upon which the track-following servo operates [2]. Next, the design of the data head is presented (see Fig.3.1.2).

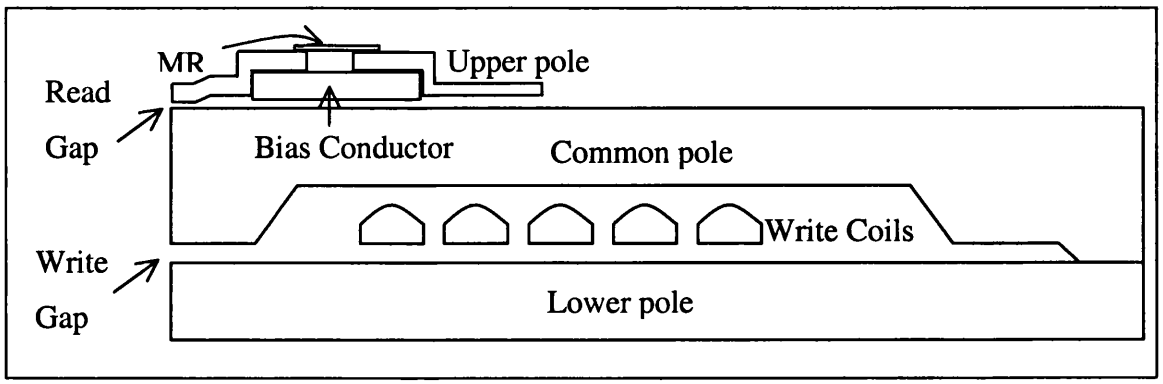

Fig.3.1.2 The cross section of the data head.

The read and write gaps of the data head are 0.25μm and 1.3μm wide, respectively. There are only five turns in each write head, which has led to a compact write head with a calculated head efficiency better than 80% [3]. The MR element bridges a gap in the yoke of a ring head which, sits on top of the write head. This design combined with the absence of a barber pole structure [4] and the small read gap enables the head to detect bit lengths as small as 0.35μm in the tape. A common MR head bias is incorporated, which is also used for test purposes during production. However, because of the specimen alterations needed to study the data heads in the electron microscope, we were unable to utilise this feature; this will be discussed in more detail in the section on sample preparation.

To maintain a competitive edge in the PC Desk Top and Server market, Onstream like all other data storage manufacturers have to keep developing their product by increasing the storage capacity of the system, whilst maintaining the selling price more or less constant. This has resulted in the need for a greater understanding of the nature of the stray field from the recording heads and the limitations on the areal recording density.

A method to characterise stray magnetic field has been developed at Glasgow University by Ferrier and Liu [4]. The method, which was introduced in Chapter 2, is Electron Beam Tomography (EBT), and has been used successfully to study the stray fields from both hard disk and tape heads[5,6]. In this chapter we will present the results obtained using

this method in studies of the stray magnetic field from the Servo head and also a modified data head. Due to the dimensions of the sample the experiments on the servo head were carried out on the JEOL 2000 FX microscope. The data head was studied in the Philips CM20.

3.2 The DPC Study of the Emboss Head in the JEOL 2000 FX

In this section the results of the DPC study of the Emboss head are in three sections covering sample preparation, the results of the experiments and the "simulated" DPC results.

3.2.1 Sample Preparation

The problem with studying the Servo head is its size and construction. It is not possible to isolate for study a single pole of the head due to the common central pole and the upper and lower drive wires, which run the length of the head. The "magnetic" circuit is a one-piece construction unlike the data head where the pole assemblies are individually connected to the drive electronics. To avoid overlap between the magnetic scattering from adjacent heads in the upper or lower pole distribution (driven separately), the maximum tilt angle that can be utilised with the goniometer is $\pm$ ~60^0 and the rotation axis is normal to the TBS. To carry out a full magnetic field reconstruction, strictly we need to be able to rotate the sample incrementally through a total rotation angle of 180^0. However, it was shown by Liu [7], that it is possible to obtain (to a reasonable accuracy) a head field reconstruction from a total angular rotation of 120 degrees. However this is only feasible if in the centre of the rotation range, the electron beam is parallel to the polegap - a situation which we cannot achieve with the servo head.

The individual pole sizes are given in Table 3.2.1.1 and in Fig. 3.2.1.1 is a schematic of the sample before and after part of the TBS has been removed. The gap between the poles is 5μm, as is the thickness of the individual poles, which makes the total height of the pole stack 25μm. In the diagram only a third of the pole layout is shown but this is repeated in

the other sections. In the Glasgow samples there are 157 poles, but due to the restrictions on the field of view in the (S)TEM only the central ~2mm of the head could be studied.

Table 3.2.1.1 Dimensions of the individual poles.

Pole type	Upper Pole	Gap between poles	Lower Pole	Gap between poles
1	38.7 μm	36.5 μm	41.6 μm	34.1 μm
2	58.1 μm	54.8 μm	62.4 μm	51.2 μm
3	387.2 μm			

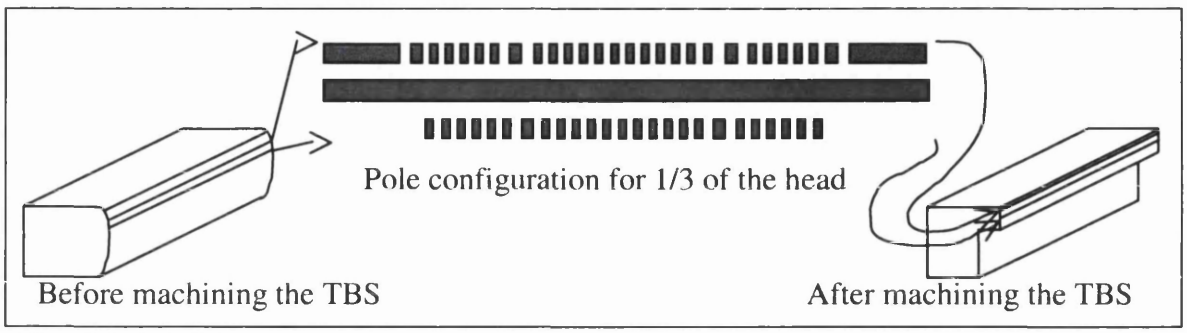

Fig. 3.2.1.1 Schematic of the Servo head before & after machining the tape-bearing surface, the arrows indicating the position of the poles within the TBS. Only a third of the total number of poles, which are not to scale, is shown in the diagram to give an indication of the complex pole configuration. The above layout is repeated three times to make up the compete head.

In the above diagram we see that in its initial form the tape-bearing surface is bevelled, this prevents us from getting close to the poles when carrying out EBT. The final thickness of the sample is ~1.0 mm and any mounting misalignment in the rod will result in significant shadowing of the poles as the specimen is rotated about the goniometer axis. To minimise this problem, part of the TBS was machined away and a step created so that the polefaces lie in the most prominent section of the sample (see Fig. 3.2.1.2).

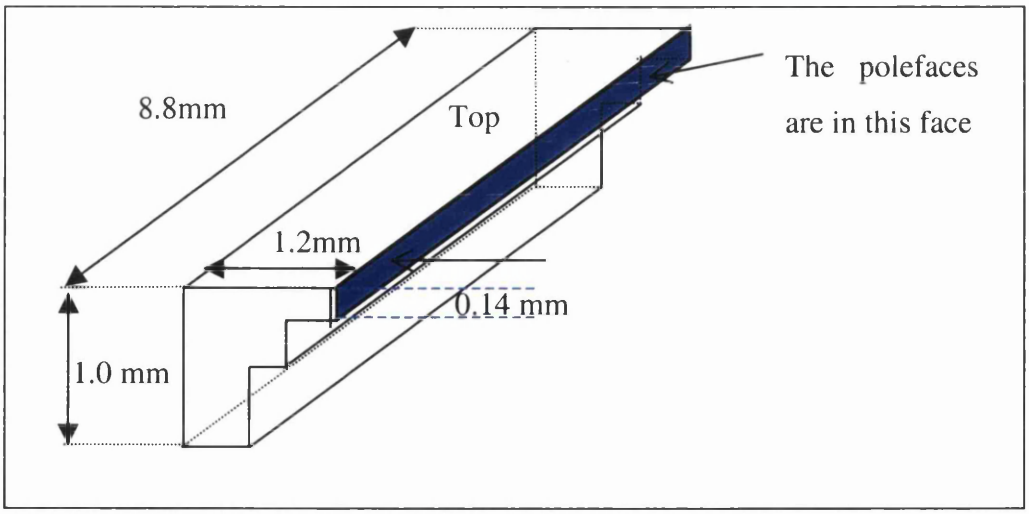

Fig.3.2.1.2 Schematic of the head shows an expanded view of the modified TBS. The diagram is not to scale but the dimensions are given.

Ideally we must mount the sample so that the poles are exactly parallel to the electron beam. However, no fully satisfactory method has been developed to achieve this. It is very difficult to achieve the required accuracy of alignment by mechanical means due to the fact that the sample rod diameter is 9mm (see fig.3.2.1.3) and the sample itself is 8.8mm wide. If the TBS face containing the poles, (shown as a coloured rectangular block in Fig. 3.2.1.2), is not precisely aligned parallel to the electron beam this will result in an effective reduction in the total angular rotation, due to shadowing of the electron beam by the sample and/or data set linescans which are at a greater distance from the pole centre than ideal.

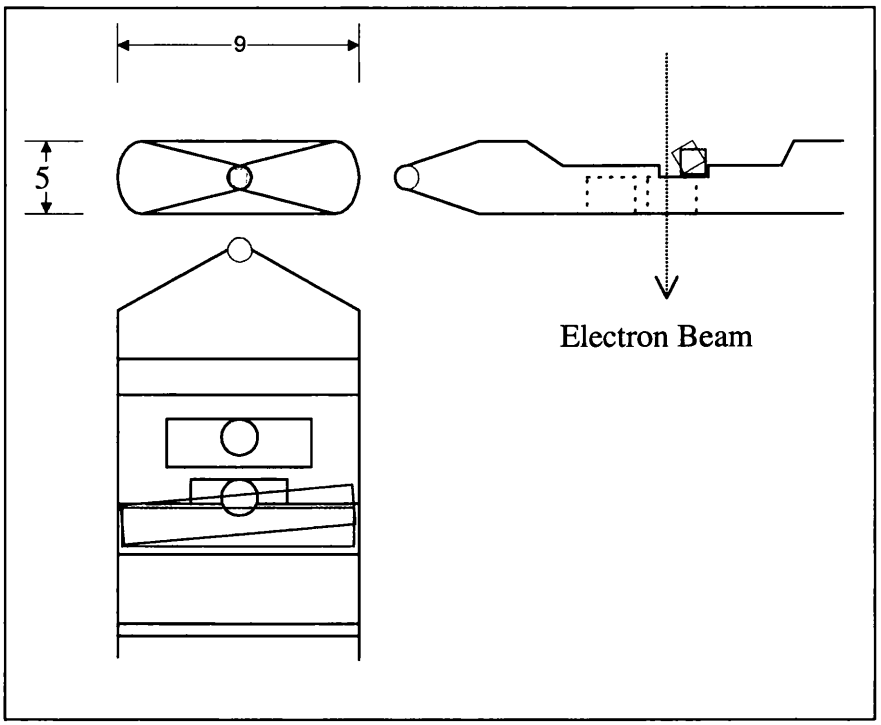

Fig.3.2.1.3 Diagram of the end section of the Sample rod used to hold the servo head during the (S)TEM experiments. The diagram is not to scale but the two most important dimensions (in mm) are given, as these determine the maximum width and height of sample that can be fitted into the microscope.

In the Fig. 3.2.1.3 the sample is drawn as a rectangular block and is shown in two positions. The red positions are the ideal situation (the normal to the polefaces is along the specimen rod rotation axis), and the blue positions represent two orthogonal extremes of misalignment with respect to the electron beam.

The initial study of the recording head was to determine if all the poles had similar stray field characteristics in projection. Thus for this experiment the sample was kept at zero goniometer tilt angle (i.e. zero rotation angle) and movement in the x and y direction was achieved by the sample stage

3.2.2 Experimental Considerations

The theoretical considerations of DPC image formation and data collection have been considered in an earlier chapter. What is now discussed are some of the more practical considerations when using this mode of Lorentz microscopy. The ultimate spatial

resolution is determined by the size of the focussed electron beam probe in the stray field region. However, at the low magnification needed to ensure that a minimum of one pole width is covered in any image, the effective resolution may be determined by the step length employed in the digital scanning mode. The precision of the data will be determined by the number of bits used in A/D conversion of the signal; 16-bit accuracy is generally employed.

To reduce the statistical error in the intensity data, the pixel dwell time of the electron beam and the number of image integrations must be adjusted; however, possible time variations in the incident electron beam current will set an effective upper limit on the total practical image acquisition time. In practice, for the JEOL 2000FX, after about one and half hours warming up with the filament switched on, the DPC signals become stable and the variations of the signals on the oscilloscopes are usually undetectable. However the signals on the oscilloscopes can show some signal variation due to changes in the descan conditions. Below in Fig.3.2.2.1 the time variation of the sum signal linescans over a period of 3days is shown. To allow us to monitor the stability of the electron beam a sum image was taken at the start of each session and at the end as well provided there was sufficient space on the hard disk; this disk was of limited data capacity due to the age of the acquisition system.

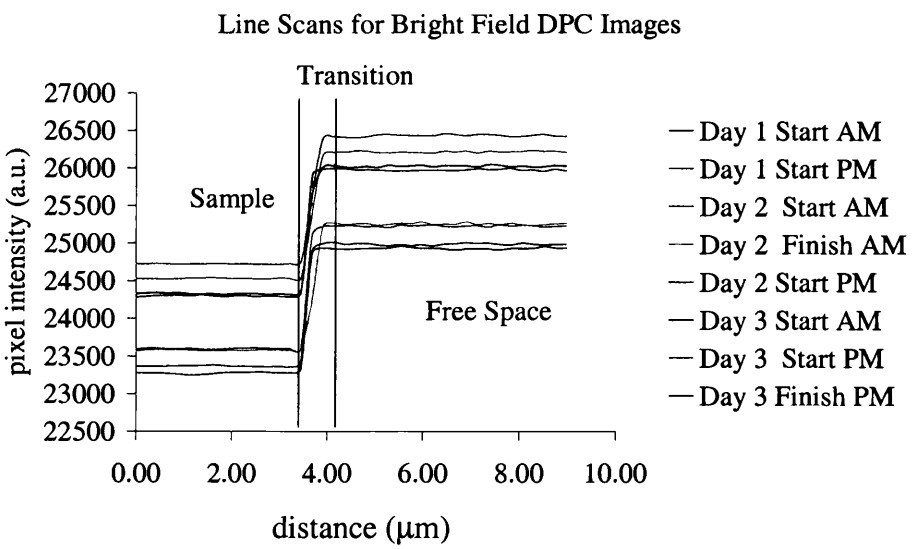

Fig.3.2.2.1 Line scans for DPC bright field images taken over a period of three days to check the stability of the electron beam.

In the experiments ideally we should focus the probe in the centre of the particular polegap under investigation; however given the specimen geometry, this is not feasible and instead the beam is focussed at the plane of the top surface irrespective of which sets of poles were under investigation. Given the depth of focus of the probe this does not impose a serious limitation on resolution. (A better approach would have been to do a follow up experiment with the electron spot under and over focused by a small amount to determine the effect of not scanning in the correct plane.) The initial microscope lens conditions used in these imaging studies are set out in Table 3.2.2.1

Table 3.2.2.1 JEOL 2000 FX DPC Initial Experimental conditions

Lens Currents								
COND1	COND2	CM	OBJ	OM	INT1	INT2	INT3	PROJ
6.91	4.85	.04	3.27	4.06	2.46	2.85	.02	7.12
Experimental Parameters								
Accelerating voltage				160KV				
Condenser Aperture size				70μm				
Spot Size				small				
Magnification Displayed				x6000				
Scan size				256 by 256 pixels				
Dwell Time				500μs				
Number of integrations				4				
ADC				16Bit/pixels				

In the experiments we studied a section of the head which covered 12 upper poles and 11 lower poles. A problem with DPC imaging of this type of sample is that there are no features to identify individual poles, since essentially we are looking at the edge of a solid specimen. Dirt particles can prove useful in locating a particular part of the head but normally we want to avoid this, because it interferes with extracting linescans from the image as close as possible to the TBS. Thus to fix a starting position for the experiments, backscattered electron imaging was used to map out the area to be studied. In Fig.3.2.2.2. are shown a typical backscattered electron image together with a schematic diagram to aid interpretation. The third image is a bright field DPC image, clearly showing that there are no features on the sample to identify precisely where on the sample the poles are located.

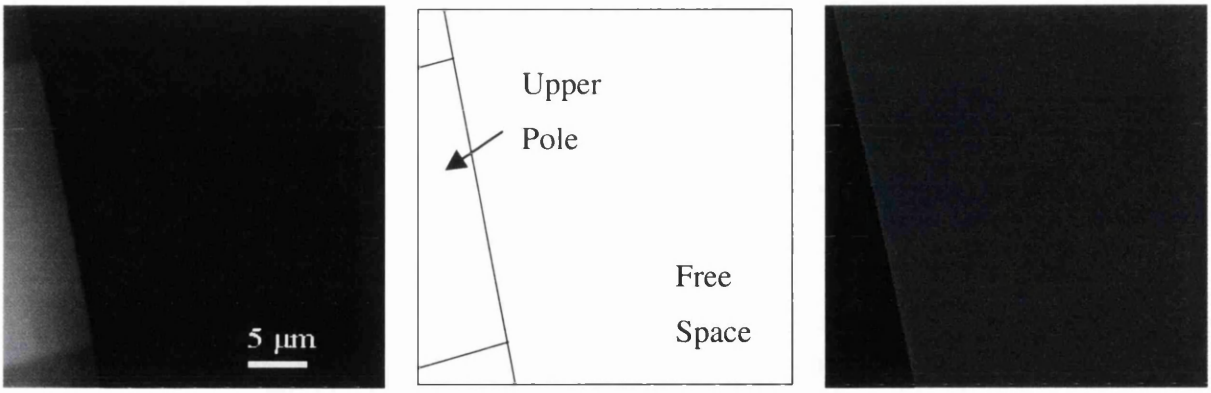

Fig.3.2.2.2 a) Backscattered electron image of an upper pole, b) schematic illustration, c) DPC bright field image of the same specimen area.

Before beginning DPC experiments on recording heads, which have a fixed orientation relative to the specimen rod axis, it is important to determine which signal combination (*A-C*) and (*B-D*) or ((A+B)-(C+D)) and ((A+D)-(C+B)) can be used to give orthogonal components of electron beam deflection parallel/normal to the TBS. Since the detector orientation is fixed in the column, the post specimen lens excitations have to be determined to produce the correct beam rotation and hence direction of differentiation with respect to the sample. Although it is not found that the lens settings vary significantly with time, nevertheless they should be checked occasionally. A convenient way of determining the correct effective detector alignment is to use a magnetic element with a flux closure structure as shown in Fig. 3.2.2.3. From experiments on this type of sample it was determined that the third intermediate lens should be employed to give the correct direction of differentiation.

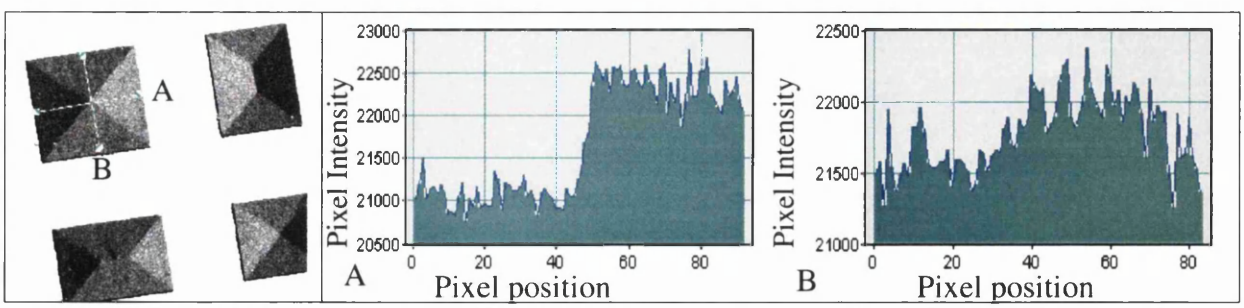

Fig.3.2.2.3 A DPC image of small patterned magnetic thin film element showing flux closure and the corresponding linescan. The blue lines represent the position from where the lines scans to the right of the image where extracted. Letter 'A' and 'B' below the graphs match up with the letters at the end of the linescans.

To help explain the process of alignment it is useful to consider an idealised square thin film element with a solenoidal magnetisation distribution as illustrated in Fig. 3.2.2.3a. If the detector alignment process has been carried out correctly and the orthogonal differentiation directions are set parallel to adjacent sides of the elements, then the linescan through the centre will show either maximum or zero contrast between domains.

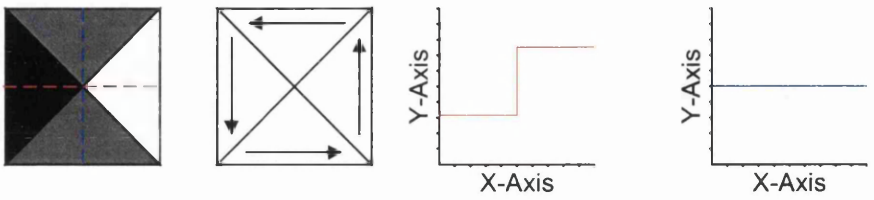

Fig.3.2.2.3a The idealised presentation of the data presented in fig.3.2.2.3.

The linescans on the right-hand side of the DPC image (Fig.3.2.2.3) shows that the direction of differentiation has been determined reasonably well. The first image shows a sharp step in the linescan which indicates a reversal in magnetic induction with respect to differentiation direction. In the second image there is a slight step in the linescan, if the direction of differentiation with respect to sample orientation was perfect then there should be no step. At the time this experiment was carried out, the direction of differentiation with respect to sample orientation was deemed satisfactory for the purpose of stray field investigation. For this case, signal pairs A-C and B-D give the magnetic mapping direction.

After the initial study of the Emboss head it was noticed that the linescans were skewed; this will be dealt with in more detail later. (The term skewed, as used here implies a deviation from symmetry of the linescans e.g. skewed to the right or left, a lack of balance in the profile of the graphs). One possible source of this was that the correct direction of differentiation had not been determined with sufficient accuracy. Hence the calibration of the differentiation direction was revisited. This time the signal combination that gave the best induction mapping was (A+B)-(C+D) and (A+C)-(B+D). As can be seen from Fig. 3.2.2.4, there is no "step" in the linescan contrast for one pair of domains. In all subsequent experiments this lens setting was adopted. It should be noted that detection of this null contrast condition is the more sensitive test for correct detector alignment.

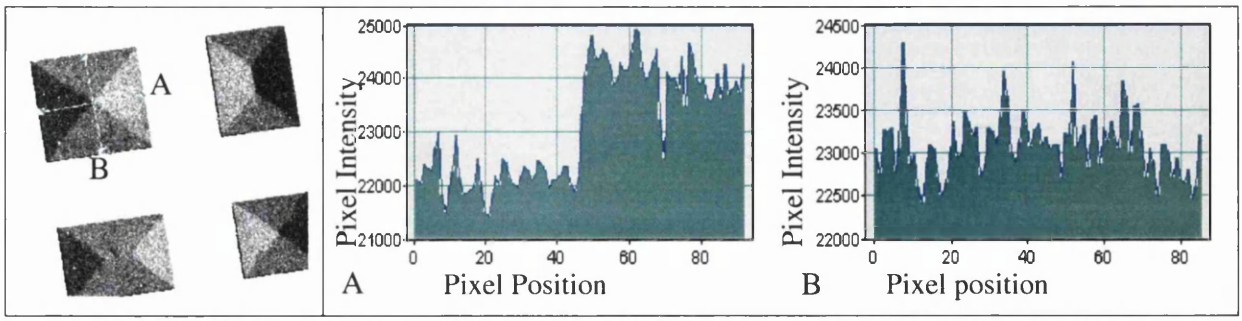

Fig.3.2.2.4 A DPC image of small patterned elements showing flux closure. The blue lines on the top left square represent the position from where the lines scans to the right of the image where extracted. Line 'A' is the position of the linescan for the first graph above. Note the improvement in detector alignment compared to the case in Fig. 3.2.2.3

Due to the low magnification values used in these experiments, it is not possible fully to correct for descan of the beam and additional (non magnetic) spatial contrast variation occurs across the image. This arises because there is usually a small amount of scan movement of what should be a stationary spot in the absence of beam deflections and in addition some electrostatic charging may also produce additional modulation to the phase of the electron wave. Since most of the noise is basically time independent, these effects can be removed by recording a pair of DPC images with the direction of the DC drive current reversed between image acquisitions. The magnetic contrast will be reversed in these images, but any other time-independent noise contrast will not and hence image subtraction provides a corrected image as show in Fig 3.2.2.5. The x, y and z- axes used to define the directions of magnetic induction are shown in the bottom right hand corner of the third image below. The top three images are for the in-plane integrated magnetic induction component, the double head arrow indicating the direction of contrast sensitivity to integrated magnetic induction. The bottom three images are the corresponding set for the orthogonal component. The descan contrast does not show up well in the above images but it is quite significant.

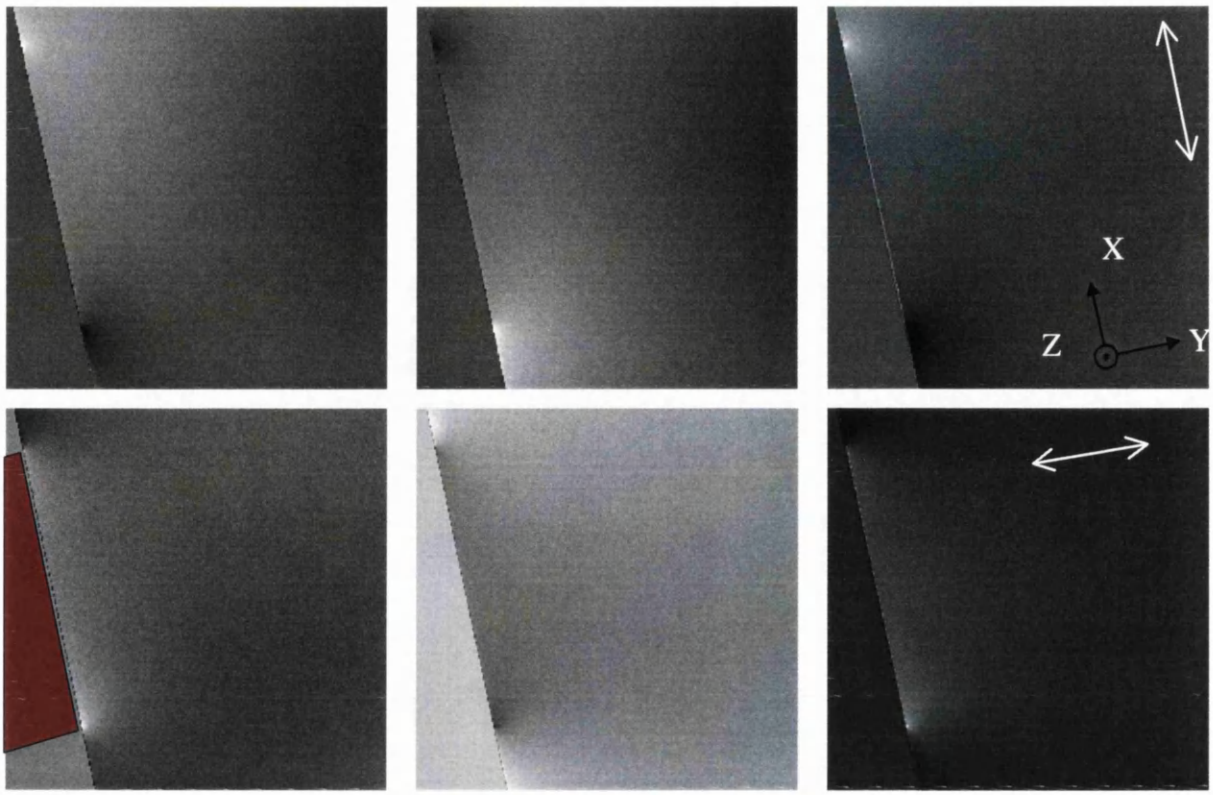

Drive current –400mA | Drive current +400mA | The final image after subtracting the previous two.

Fig. 3.2.2.5 The unprocessed DPC images with the corresponding drive current shown and the final subtracted images. There is additional contrast arising from failing to correct for descan present in left pair of images, but is absent in the subtracted images. The red shape indicates the position of the pole in the image.

From the final image, linescans are extracted. It is usual to take the linescans at a distance of one pixel from the tape bearing surface, see below, but in some cases dirt particles prevent us getting this close to the tape bearing surface (or we may have to interpolate the contrast in the vicinity of the particle). From the calibration of the field of view, one pixel was determined to be ~ 0.23 μm in linear dimension. In Fig. 3.2.2.7 typical linescans are shown.

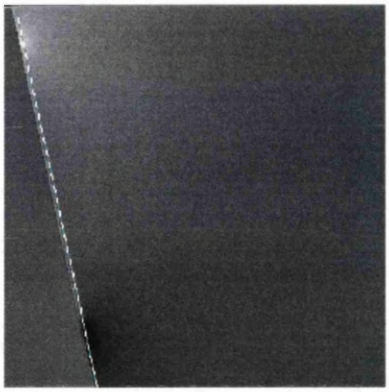

Fig.3.2.2.6 The extraction of linescans from the DPC images. The blue dotted line indicates the approximate position from which these are taken.

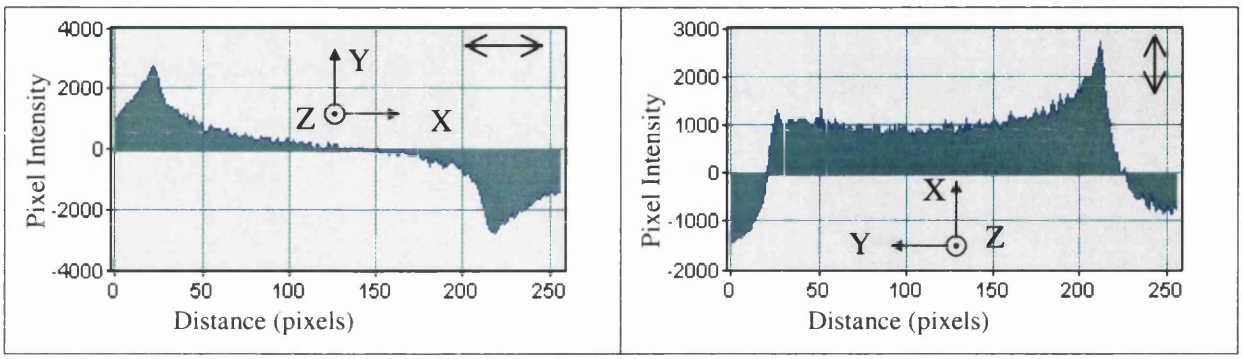

Fig.3.2.2.7 The lines scans were extracted from the final image pair shown in Figure 3.2.2.5, the first linescan is the y-component of the integrated magnetic field and the second is the x-component. The double head arrow indicates the direction of sensitivity to integrated magnetic induction

If we consider the first graph of Fig 3.2.2.7 then the direction of differentiation is along the TBS, which gives contrast sensitive to the out-of-plane component, (y-component), of magnetic induction. In the second graph the contrast is sensitive to induction in the plane of the TBS. The profile of the first graph is approximately antisymmetric about the centre of the pole and this is as expected; the other graph however shows unexpected asymmetry in its profile.

3.2.3 The results of the DPC Experiments

Initially we were interested in the magnetic field distribution along the head. Despite the large size of the head, we should nevertheless have been able to look at the central (~2mm)

of its length and this would have been sufficient to cover all the different sizes of poles in the structure. However, only two pole sizes were investigated due to difficulty in getting the largest pole in the scan frame.

By taking a set of images for every pole and space along the accessible section of the head and then extracting linescans followed by some image manipulation, we were able to build a complete "picture" of the projected stray field characteristics of the section of head studied. By taking an image for the driven poles and the adjacent spaces there is an overlap in the images. In the results presented below (Fig.3.2.3.1), the data was cut from individual linescans such as those shown above and then matched to the previous linescan in the sequence.

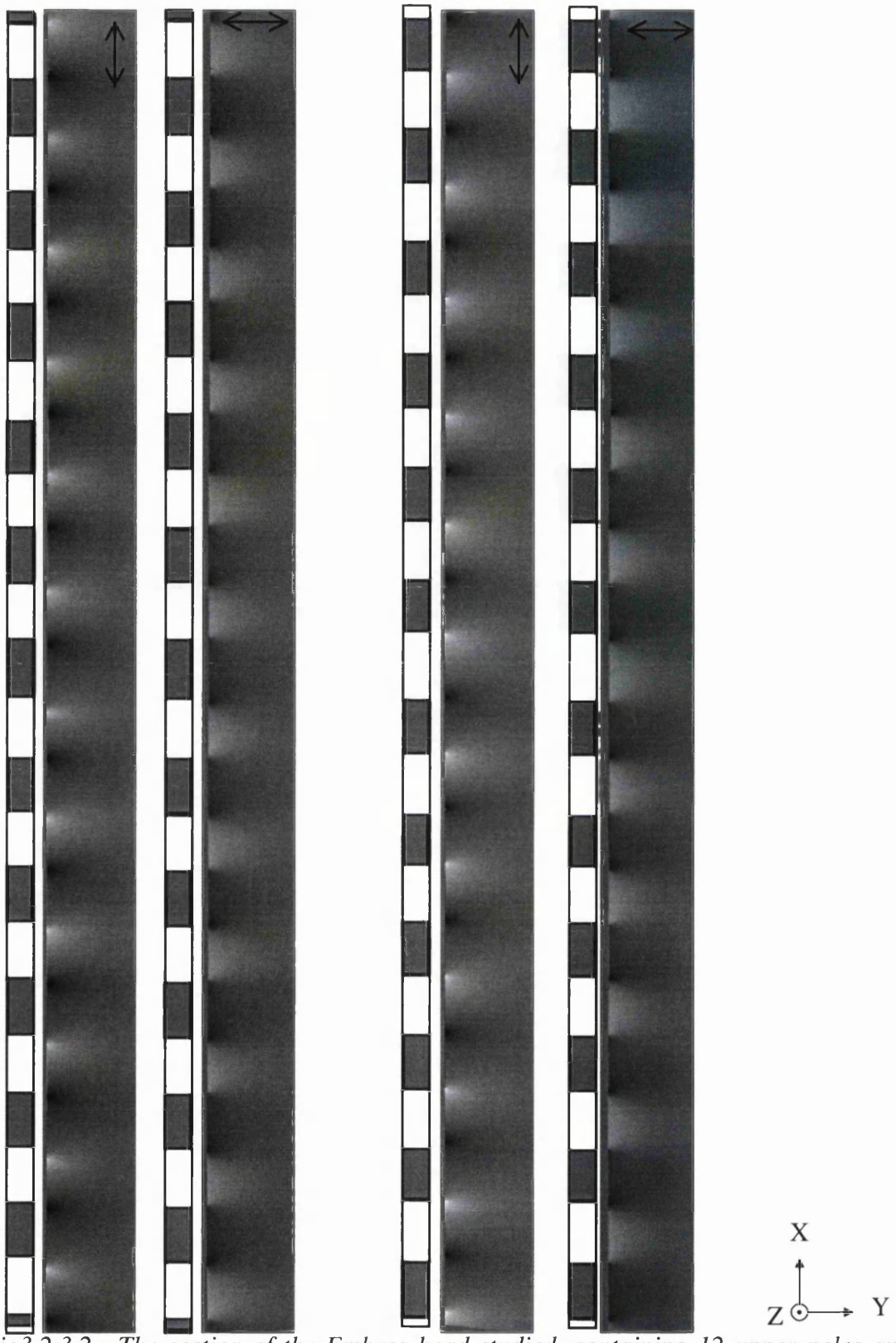

Fig3.2.3.2. The section of the Emboss head studied, containing 12 upper poles and eleven lower poles. The grey and white bar on the left-hand side of each image represents the position of the poles with respect to the contrast. grey being a pole and white representing a space. The left hand set of images is for the lower poles being driven and for the right hand pair the upper poles are driven. The double head arrows indicate the direction of contrast sensitivity to the magnetic induction.

In acquiring the data for Fig. 3.2.3.1 the sets of pole arrays were driven separately at 400mA d.c. during each experiment; for comparison it was hoped to drive both arrays simultaneously during an experiment, but this was never achieved. From the above images, linescans were extracted at a distance of one pixel from the perceived specimen edge and the resulting intensity maps are shown in Fig. 3.2.3.2. A crude form of filtering was used to remove the "noise" in these profiles due to dirt particles. The filter method consisted of interpolating "noise" peaks in the intensity distribution (as judged visually) in an Excel spreadsheet of the image intensity distribution. The grey blocks on the graphs below represent the driven poles and are included as a visual aid to help interpret the data.

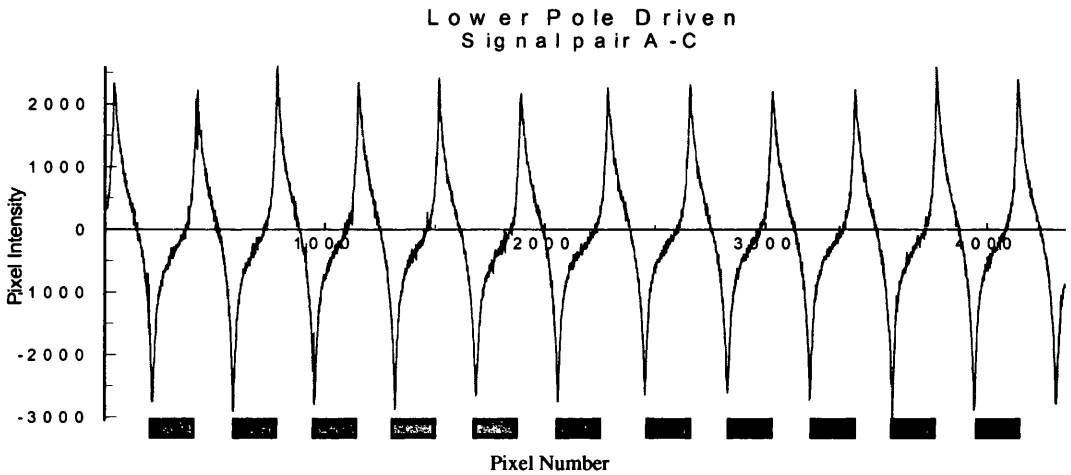

Y-component

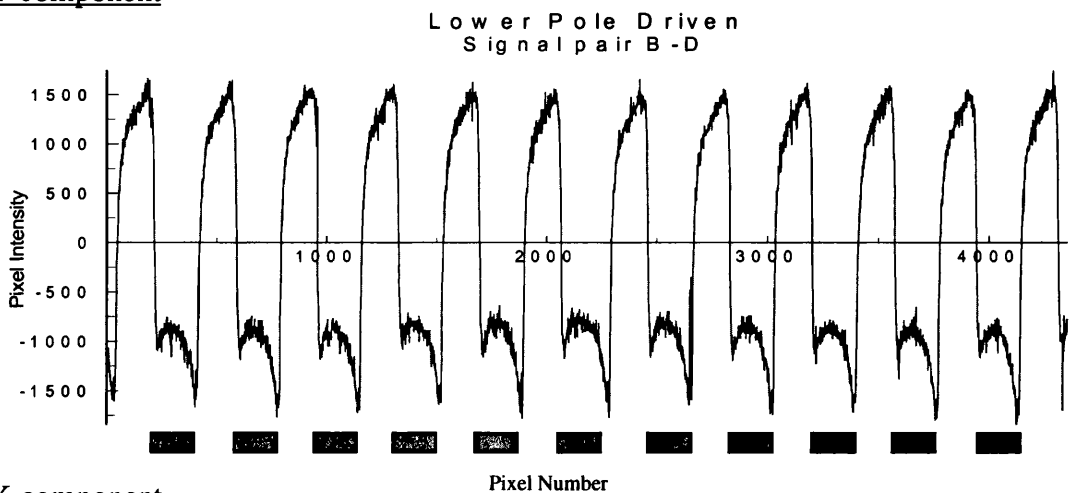

X-component

a. Line scans extracted from the first two images in fig.3.2.3.1

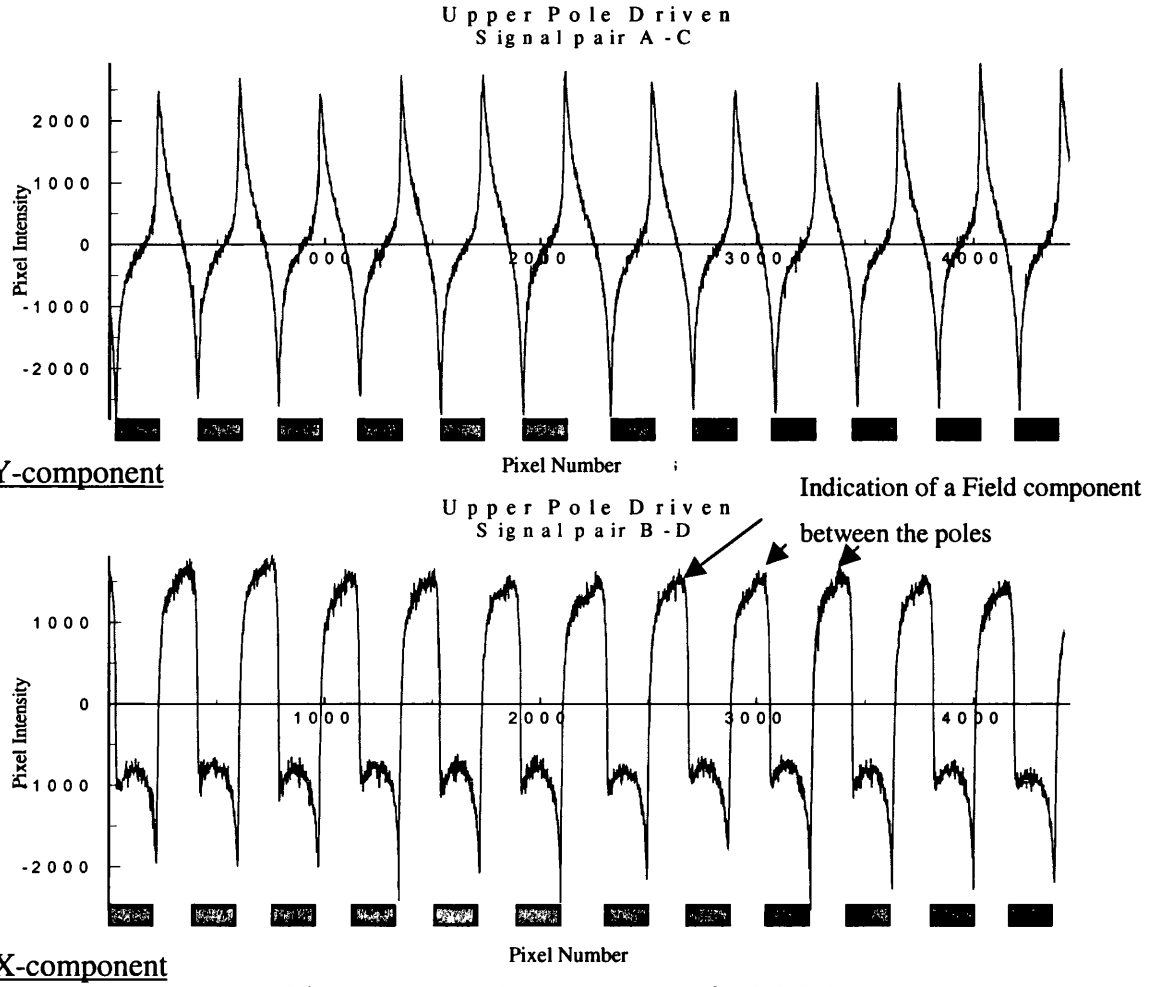

b. Line scans extracted from the second images pair in fig.3.2.3.1

Fig3.2.3.2.(a & b) These graphs were created from linescans extracted from the DPC images in Fig.3.2.3.1. The grey blocks represent the pole array that was driven in each study.

The top pair of graphs in Fig.3.2.3.2 represents respectively the y- and x-component of integrated magnetic induction for the lower pole array studied. From the magnitude of the electron beam deflection (pixel intensity), it may be noted that the field integral along the beam trajectory is relatively constant along this section of the head. This study was repeated for the upper pole array. The results are similar to those for the lower pole array, which was to be expected. Two main features of these graphs are worthy of comment. The first is the strange feature in the x-component of magnetic induction, which exhibits a relatively sharp peak to the right of the negative section of the linescan. This feature is slightly less prominent for the lower pole array compared to the upper pole array. It may be due to an artefact of the image/data processing, or it could be genuine. It could arise

from the fact that the point of focus is the same for both data sets i.e. the top surface of the TBS. However the 'points' of deflection are ~10μm apart; given that the length of the specimen is normal to the electron beam this is not very likely.

The second surprising feature of these graphs is that there appears to be a magnetic component from the region (in the projection) of the undriven pole (as shown in Fig. 3.2.3.2.b), which is approximately equal in magnitude, but opposite in sign to that from the driven pole. One interpretation of the results is that there is flux escaping from the undriven heads immediately below the gaps in the driven head array, this being essentially equal in magnitude, but opposite in sign to the adjacent (in projection) driven pole. This is not so apparent in the y-component as it is in the x-component of the integrated field. A possible source of this field could be a leakage between the common pole and the undriven poles in the other array. The line trace profiles for the x-components are very skewed to the right, one would have expected the field to be symmetrical along a given pole. A reason for this could be that the lens settings were not optimised with sufficient accuracy to setting the direction of differentiation with respect to specimen geometry.

In an attempt to investigate these stray field features further, we examined the DPC data for the larger 58μm wide pole. If the ratio of polegap width to pole length helps to determine the magnitude and nature of the side writing field, then changes may be evident for this wider pole, which has the same gap length adjacent to it as for all other poles. (Note that due to the limited area of the sample available to us in the (S)TEM, only one pair of these larger poles could be studied and the largest pole (387.2 μm) was not within the effective sample length. The results of the 58μm wide pole study are presented below in Fig. 3.2.3.3.

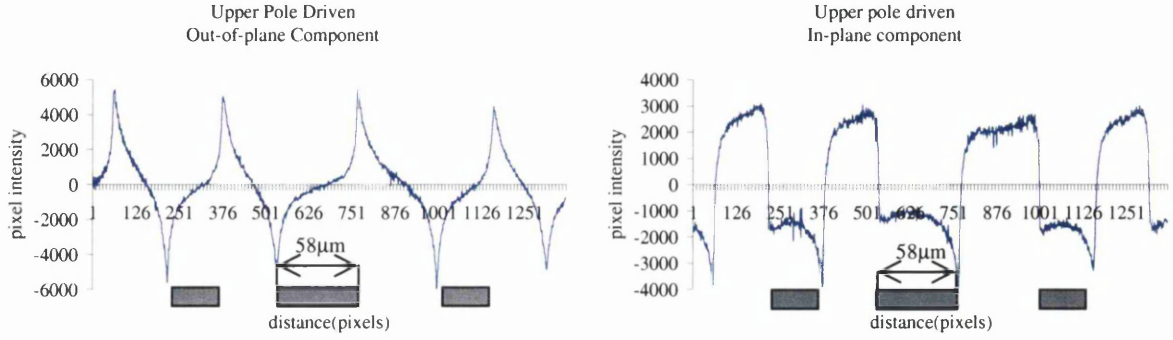

Fig3.2.3.3 Line scans from the larger pole (middle) and two smaller poles.

The linescans have the same characteristics as in the previous experiment and hence give us no additional information to help explain the integrated field profiles. The noticeable asymmetry in the profile of the linescan of the x-component was now reconsidered and it was decided to try to align the directions of differentiation in DPC more accurately parallel/normal to the line of the TBS (in projection). The results are shown below where we compare in Fig. 3.2.3.4/5 the line traces for a pair of poles taken with the original post specimen lens settings (see Table 3.2.3.1) and with the revised lens settings (see Table 3.2.3.2 below). The results are conclusive and show that the skewed line trace was entirely due to insufficient accuracy in setting the original DPC conditions; this should serve as a cautionary note to all future users of this technique.

Table 3.2.3.1 Original Lens Current Settings

COND1	COND2	CM	OBJ	OM	INT1	INT2	INT3	PROJ
6.91	4.85	.04	3.27	4.06	2.46	2.85	.02	7.12

Table 3.2.3.2 Final Lens Current Settings

COND1	COND2	CM	OBJ	OM	INT1	INT2	INT3	PROJ
6.91	4.85	.02	3.31	4.35	2.35	2.56	1.99	7.12

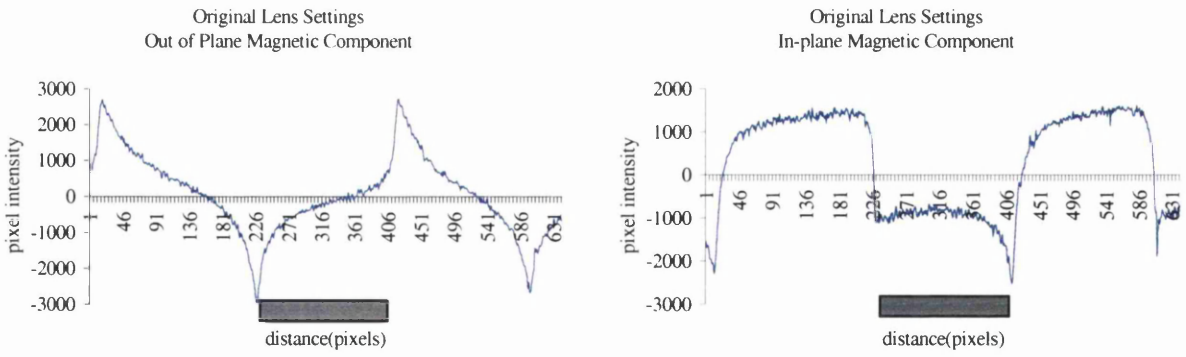

Fig3.2.3.4 Line scans extracted from a pair of DPC images taken with the original lens settings.

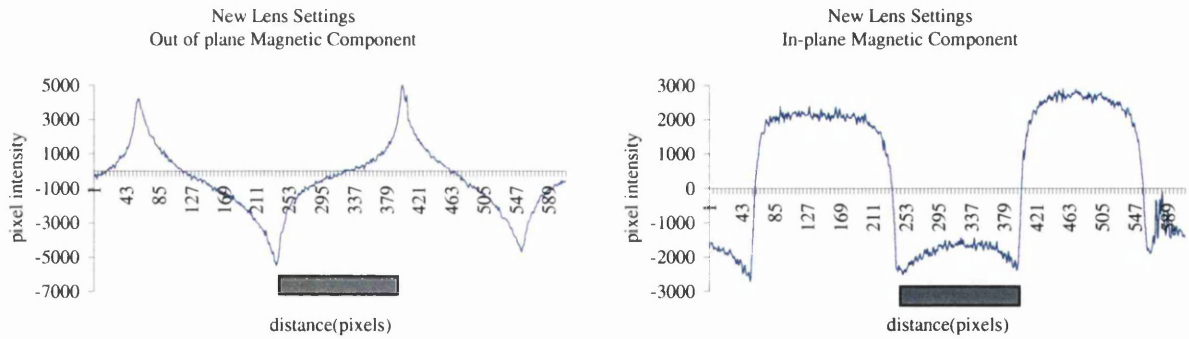

Fig3.2.3.5 Line scans extracted from a pair of DPC images taken with new lens settings.

We must still try to find an explanation for the apparent field coming from the gap region adjacent to the driven poles. It was decided to attempt to simulate the line scans extracted from the above images from a 'model' multi-pole Emboss head as shown in Fig. 3.2.4.1. This would be achieved by using magnetic field data for a model thin film recording head and this is discussed in the next section.

3.2.4 Simulation of DPC Line Scans for the Emboss Head

To test possible (very simple) models for the observed intensity distributions for the two components of magnetic induction integrated along the electron trajectory, we selected data from a finite element calculation performed using the Tosca™ program by David Heim at IBM San Jose [7]. The model thin film head had a writing pole of width 5.0μm, a gap of 0. 5μm and a leading pole width of 8.0μm. Three basic repeat units were then constructed as possible models to match the Emboss sample's pole layout; the first (a) had a pole width d (=5μm) plus a space of width d, the second (b) a pole width d plus a space of 0.8d and the third (c) a pole width d plus a space of 0.6d. The first and last of the proposed models are shown in Fig. 3.2.4.1. Only three of the six "multi- pole " heads have been drawn.

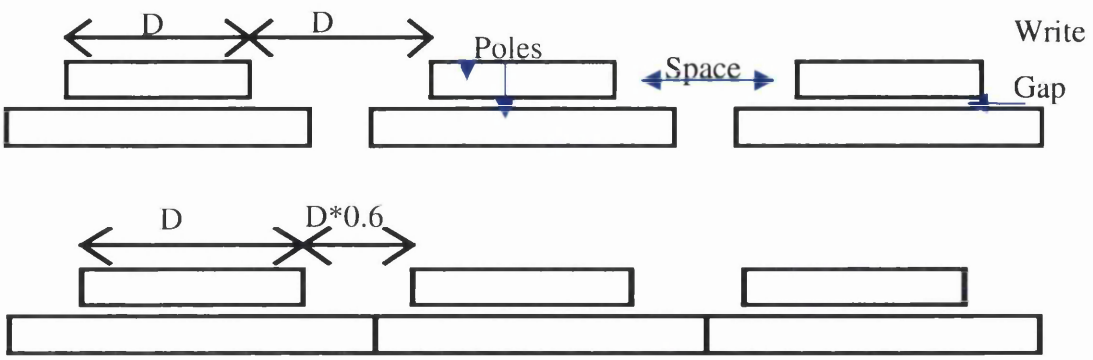

Fig3.2.4.1 Model of the "multi" pole Emboss recording head, showing two (a), (c) of the proposed pole layouts. (D = 5μm).

From these models field integrals were calculated thus simulating DPC imaging in the STEM. Line scans were extracted at a distance of 0.25 μm from the model "tape bearing surface" and the results are presented below.

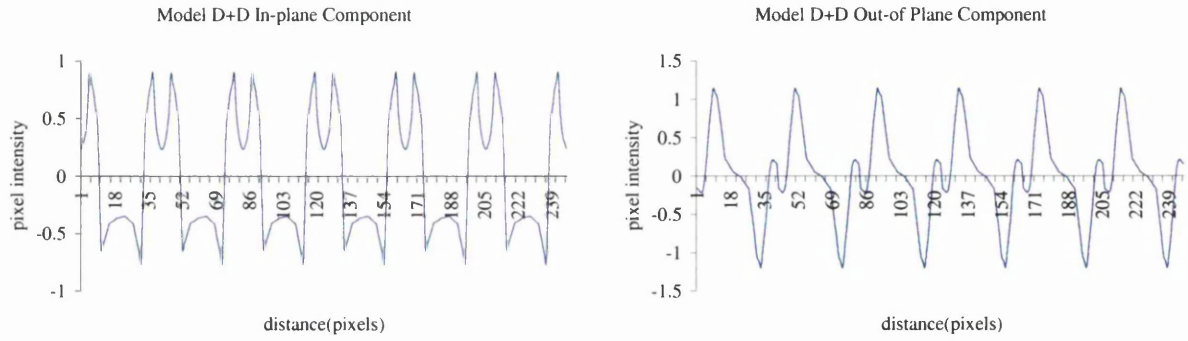

a.

b.

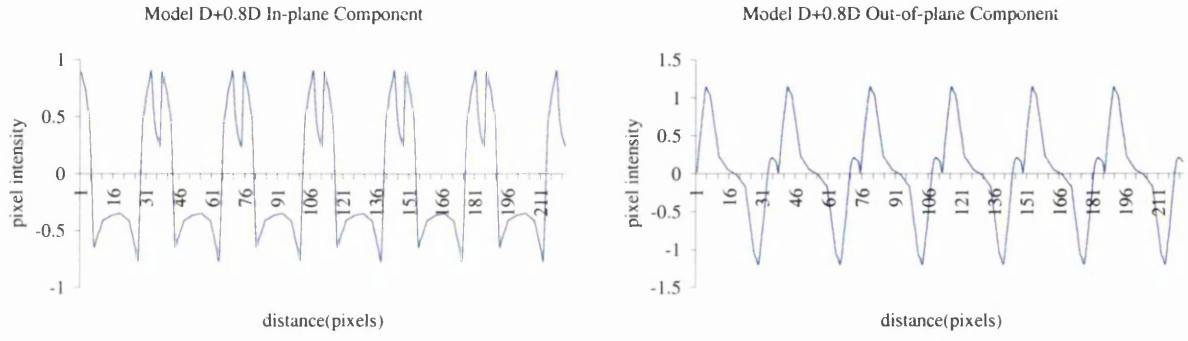

c.

d.

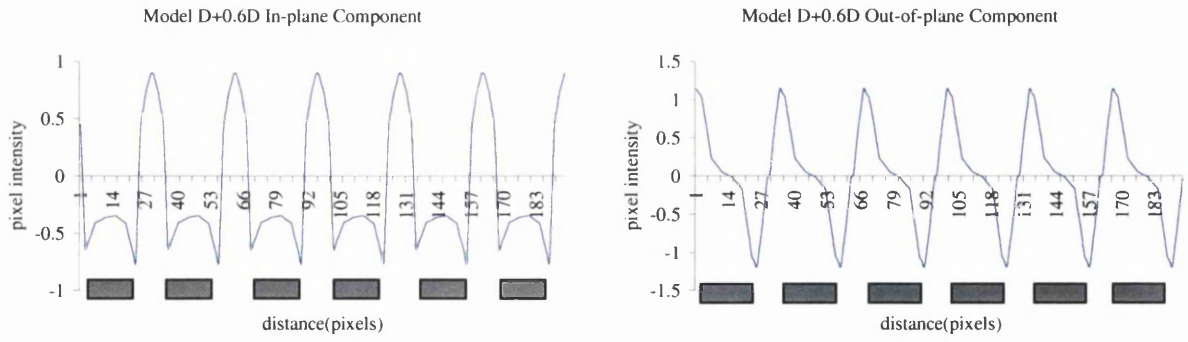

e.

f.

Fig3.2.4.2 Line scans from the model Emboss heads. The position of the "driven" head is given in the bottom two graphs.

The first model is closer to the real sample in terms of poles and spacing configuration. However it is the third model, in which the distance between the pole is only a fraction of

the pole width, that produces linescans, which are similar to those seen from the real sample. If we consider the first set of linescans, the one where the pole width and the space between them are the same. Then for this case the lower part of the linescans for the x-component is what one sees in the real data. In fact this is the same for all the model data. However the upper part of the linescan is like nothing seen in the real data. For the other component there is a small "shoulder" on the positive section of the linescan, again this is not observed for the real data. As the space between the poles is reduced then the "dip" in the x-component diminishes, as does the shoulder in the y-component. In the third model structure proposed there is agreement between the model data and the real data. However as has already been stated this least fits the real pole configuration. A possible explanation for this is that the gap/pole width ratio for the model thin film head, used to mimic the Emboss head pole configuration is 0.1, but for the real Emboss head it is ~0.125. It is this ratio that largely determines the extent of the side writing field.

This simple model suggests that the stay magnetic field between driven poles could be a side writing effect, and not flux leakage between the (undriven) lower pole and the common pole. It must also be noted that there will be a contribution to the stray field from the drive wire in the space between driven poles. Thus the most logical conclusion is that it is the side writing field. When these data were collected and analysed we had not yet obtained access to our own Magnetic Force Microscope (MFM). The results obtained using this different form of imaging the head stray field confirmed that the head field is restricted to the vicinity of the driven poles in the Emboss head, confirming the conclusions drawn above. This will be discussed in Chapter 4.

3.3 The DPC Study of a Data Head in the Philips CM20

In this section it was hoped to be able to use the EBT technique to study stray magnetic fields from recording heads, developed in the JEOL 2000 FX, but adapted for the Philips CM20. Then the data collected would be reconstructed using the Algebraic Reconstruction Program (ART) developed at Glasgow [7] and the Radon Transform Program (RTM).

These reconstruction techniques have been discussed in Chapter 2 so only the reconstructed fields will be discussed in the following sections.

3.3.1 Sample Preparation

The data head assembly has eight separate write and read heads. To carry out a full tomographic reconstruction of the field, a single write/read head had to isolated from the remainder. Fortunately the heads are wired individually to the output/input electronics, making it possible to isolate a single head electronically. Unfortunately the bias wire for the MR elements is common and was removed as part of the sample preparation. Thus, although it was possible to drive the MR element, it was not possible to bias it. One of the challenges was to remove seven poles and leave only one which was fully operational. This involved mechanically machining off the unwanted poles, a very difficult task, given the size and nature of the structure. Onstream were able to supply samples, which however, although nominally suitable for our purposes, were not sufficiently accurately aligned to enable us to extract quantitative information on the magnetic field characteristics.

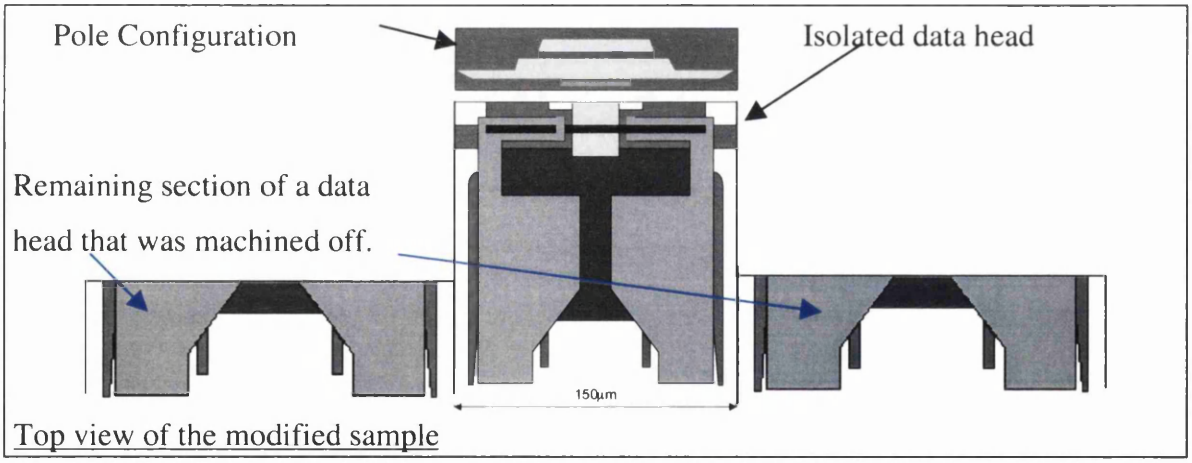

Fig.3.3.1.1 A Schematic of the top section of the data head, showing a single head, the other heads having been cut back. The pole configuration, which is located in the Tape Bearing Surface (not shown here), is also shown above the plan view.

One of the sample rods for the Philips CM20 was fitted with electrical contacts thus allowing the data head to be driven while in the microscope. To mount this sample in the rod, a new sample stub had to be designed to hold it. This was based on an earlier stubs designed for use in the JEOL 2000 FX and is shown in Fig 3.3.1.2. Onstream made the

stub and mounted the sample (as show in Fig.3.3.1.3) prior to being sent to Glasgow; in all two samples were supplied.

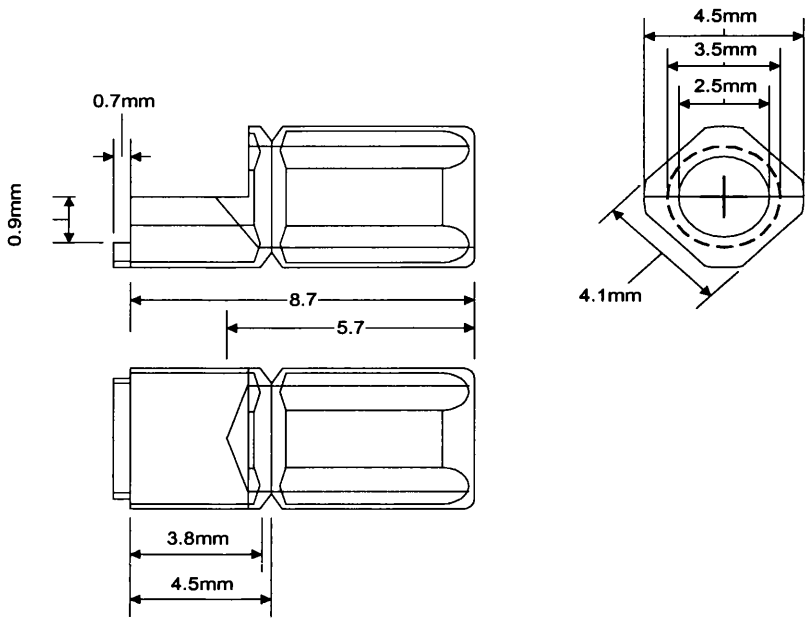

Fig3.3.1.2 The design of the sample stub used in the CM20's tomographic specimen rod. This is not a scale drawing but dimensions are given.

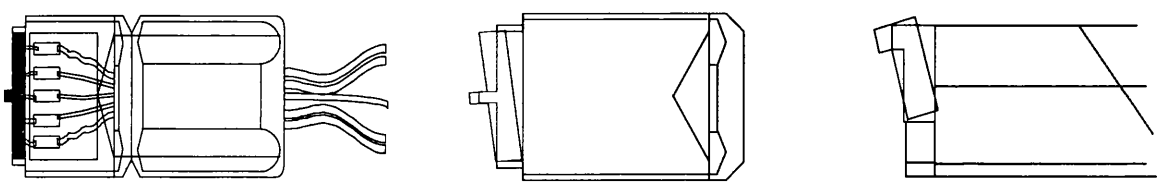

Fig3.3.1.3. The data head, show in grey, mounted on the sample stub and wired so that it can be driven. In the other two diagrams are shown the ideal sample position (red) plus two possible sample misalignment positions (blue) with respect to the stub's geometry.

During the first microscopy experiments on the samples it was discovered that the samples were not mounted on the stub correctly. The sample should have been fitted flush to the sample holder step (see fig 3.3.1.3) to reduce shadowing effects; the two supplied were not. It was decided to use the better aligned of the two samples, to see if it was possible to carry out EBT.

Another problem encountered in the first experiment was that the pole faces were heavily contaminated with dirt particles. This causes two problems, one is charging when in the sample is in the TEM. The second occurs when taking linescans, since it may be impossible to get very close to the sample's edge. This is important, since we wish to be able to evaluate the field as close to the TBS as possible. In the next set of figures, which are images taken in a Scanning Electron Microscope (SEM), the level of surface contamination can be seen clearly, as can the charging effect. The pole layout in these images is inverted from that shown in figure 3.3.1.1. A solution of "liquid plastic", normally used to replicate surfaces in electron microscopy, was used to clean the head and the results were reasonably satisfactory.

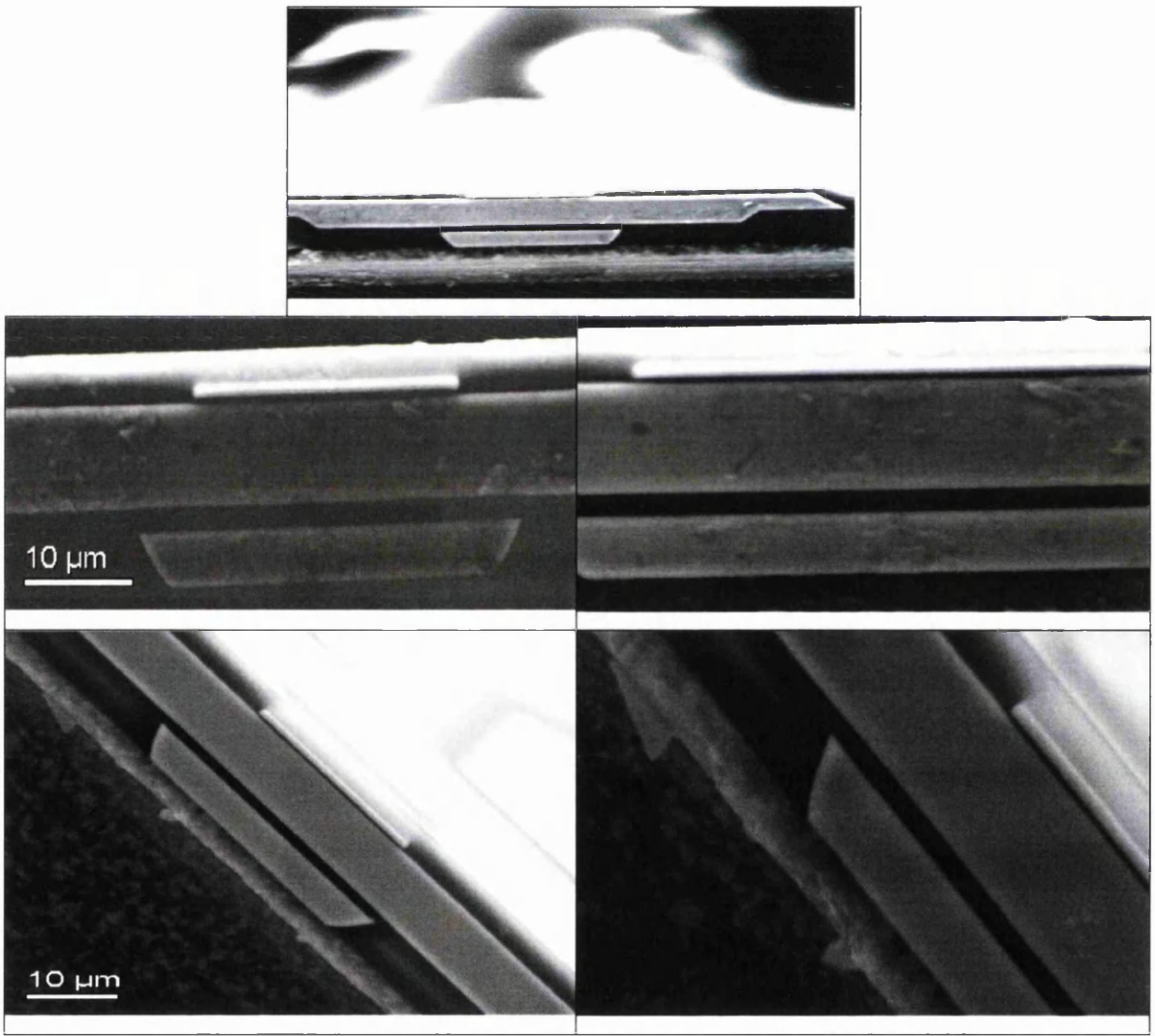

Fig3.3.1.4 A series of images taken in a SEM showing the pole faces before and after sample cleaning took place. The first image shows the effects of charging in an electron microscope and is included to show the possible consequences of using dirty samples.

The SEM images clearly show how dirty the sample was. Prior to the SEM study, optical inspection had failed to reveal the level of contamination on the pole face. Even after cleaning the sample there remained two particles on the pole faces that could not removed. There are also two large particles on the underside of the head, but these did not show up in the original investigation, and they could not be removed. Fortunately they did not cause any problems when the sample was studied in the Philips CM20.

3.3.2 Study of the Inductive Element

The section is split into four subsections that cover:- 1) the experimental set-up for the study of the data head in the Philips CM20, 2) the results from the study, 3) the reconstruction of the stray magnetic field and, 4) the investigation of magnetic saturation in the poles.

3.3.2.1 Experimental Considerations

This was the first time that Electron Beam Tomography had been carried out on recording heads in the Philips CM20. Therefore a new set of experimental parameters had to be determined for this microscope; the conditions/procedures determined for the JEOL 2000 FX could however be used to provide a checklist. Some of the experimental conditions to be determined are discussed below.

1. find the direction of differentiation with respect to specimen geometry,
2. find a suitable electron probe size to satisfy the Nyquist sampling theorem,
3. match the spot size to the detector size (there were eight segments in the CM-20 detector) - it was important to know which segments the spot was falling on,
4. determine a suitable camera length to match directions of differentiation to the sample orientation,
5. select a condenser aperture size so that the ratio of $\beta_L/\alpha < 0.5$ or <0.1, depending on the combination of detector segments used,
6. reduce/remove descan at very low magnification,
7. work out a suitable scan step in relation to acquisition time. If a very small scan step was chosen then the time taken to acquire the image was large,
8. choose a suitable dwell time to give acceptable statistical noise errors.

Unfortunately during our attempts to define a suitable experimental set-up in the microscope, the DPC detector failed and became unusable. The new detector was much smaller in size, but had the advantage of being capable of rotation about the optic axis. A benefit from this new detector was that it should be possible to use standard lens values for the experiments. It was discovered however that there were certain camera lengths in the middle of the full range of possible values that could not be used for DPC microscopy. Within this region it was impossible to align the microscope for DPC. Hence a shorter than ideal camera length had to be selected to centre the disc on the detector. Short camera lengths result in a small disc being formed on the detector, and hence the "dead" zones on the detector assumes more significance (these "dead" zones are inherent to the quadrant detector and mark the physical boundary of the individual sectors)

Another problem encountered and as yet unresolved was the magnitude of descan, which becomes harder to correct the lower the magnification used (descan:- the contrast due to the disc not being stationary on the detector when no external field is present). The sample was approximately 150μm in length, so in order to keep the stray magnetic field within the field of view and aid subsequent alignment of the linescans from the image rotation set, a magnification of only x150 was required. Note this was the displayed value and not the actual magnification value. At this magnification it was very difficult to get the spot to be stationary on the detector during scanning. If the magnitude of the descan effect is not too large then, as discussed previously, its influence can be removed by recording pairs of images with opposite drive current and subtracting them. However in this case given the scale of the spot movement on the detector, the results have to be treated carefully. To achieve a linear DPC image, the ratio of the deflection angle to the probe angle must be ≤ 0.1, a condition easily realised for normal DPC imaging. In this initial case, given the magnitude of the problems associated with descan discussed above, there must be questions raised regarding the linearity of the imaging and hence the results can only be regarded as a qualitative investigation of the head field.

In the first series of investigations of the inductive element of the head, there were two areas of interest. The first was to assess if it would be possible to carry out a tomographic reconstruction of the field and the second to determine if there were any saturation effects visible in the head field images at high drive currents.

Table 3.3.2.1.1 below gives the parameters used to collect the data shown later. One parameter, which was not selected correctly, was the spot size. The spot size should be of the same order of magnitude as the pixel size, which is determined by the scan step size. In the conditions used for the experiment, the pixel size is ~400nm, but the spot size was set in error at ~18nm. This resulted in under sampling by a factor of ~20. By selecting either a larger spot size or a smaller scan step the experimental parameters would have been improved. Unfortunately before these incorrect settings had been discovered, the head had been accidentally damaged and no further studies could be conducted.

Table3.3.2.1.1 Philips CM20 DPC Experimental Conditions

Accelerating voltage	200KV
Magnification as displayed	X150 to x550
Spot size 9	nominal size 18 nm
Condenser Aperture no.2	200 μm
ADC	16 bits/pixels
Dwell time	842.3 μs
Scan size	256 by 128 pixels
Inner detector	Splits combination
Camera length	6.6m
Standard Lens settings	Low Magnification Scanning Mode
Detector rotational position	12.5

3.3.2.2 Results from the initial EBT studies of the Inductive Element

In the initial investigation of tomographic reconstruction of the inductive write head field, it was decided to collect the set of DPC images at 10° angular rotation intervals (in a full quantitative experiment, data would have been collected at a maximum of 5° angular intervals). The results, although obtained under non-ideal experimental conditions, do serve to prove the viability of the method in the CM-20. A selection of images from the full data set are shown in Fig. 3.3.2.2.1a below. The images are displayed using a "temperature" colour scale, which is shown in Fig. 3.3.2.2.1b.

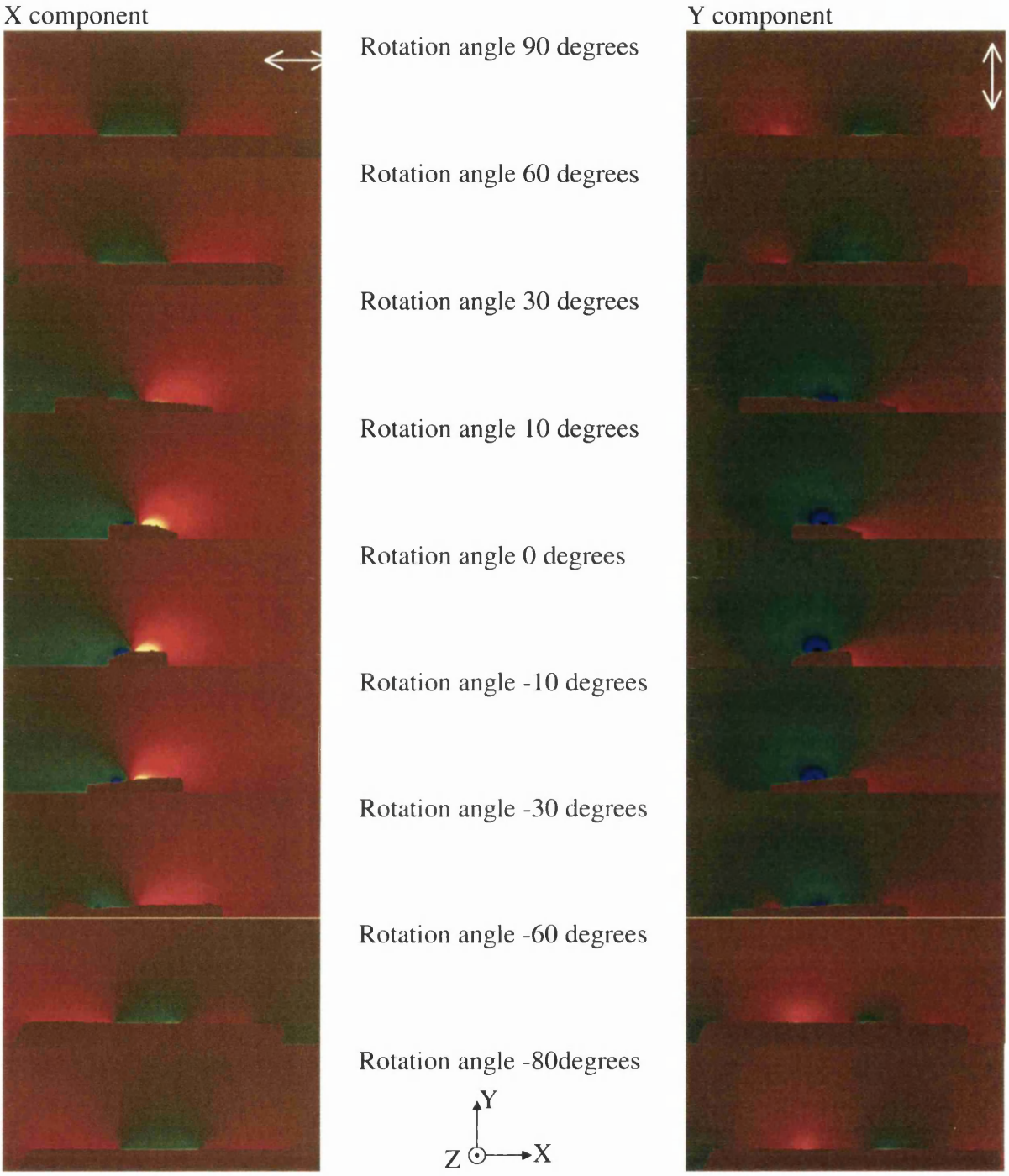

Fig.3.3.2.2.1a Subtracted DPC image pairs collected from the inductive write head as a function of rotation angle. The arrows give the direction of the magnetic induction to which the contrast is sensitive. The drive current in the head for the initial images was ±10mA.

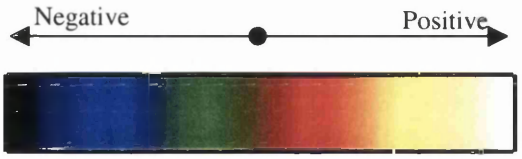

Fig. 3.3.2.2.1b The colour scale which, is used to display the DPC images presented in Fig. 3.3.2.2.1a

In collecting the data the drive currents used in the head were ±10mA, but it should be noted that in the tape file the drive currents are higher viz. ±30mA. As the sample was rotated in the microscope there was a small tendency for the stub to move slightly within the sample rod; this adds to the inaccuracy of the data. It should also be noted that at zero degrees of tilt the polegap of the head is off by a small angle from being normal to the optic axis. This effect is apparent in the slight differences visible between, for example, the images at +10° rotation and -10° rotation and also shows up in the tomographic reconstructions to be discussed below. As stated earlier, the mounting of the head in the stub was imperfect being off by several degrees from the TBS being normal to the rotation axis; this leads to an unquantifiable, but significant, variation in the effective distance of the linescans from the actual centre of the polegap. Because of this we can anticipate only a relatively crude field reconstruction.

From the DPC image rotation set, linescans were extracted at a distance of one pixel from the edge of the head in projection. The size of one pixel was determined to be ~ 400nm. Once the linescans are obtained they must then be aligned relative to one another. The deflection data sets from the model head described in section 3.2.3 were used as a visual guide to assist in this task (the data sets chosen were at distances of 1 and 1.5μm from the ABS). The starting point for the alignment of the linescans was to centre the 90° rotation scan with respect to the 0° rotation scan for one of the orthogonal components of induction and then to apply the same 'pixel shift' to the linescans of the orthogonal component. The intermediate rotation data sets were then aligned using the model data as a guide, although this is approximate given the dissimilarity between the practical and model head forms

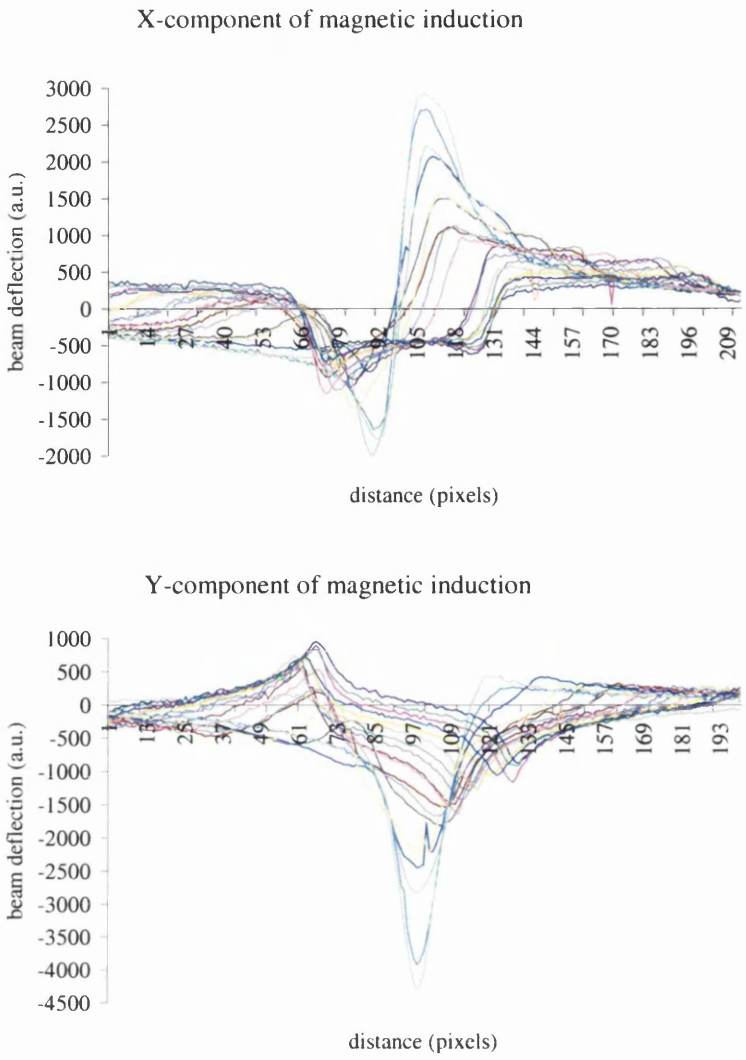

Fig.3.3.2.2.3 The linescans representing the integral of the magnetic induction along the electron trajectory extracted from the DPC images and aligned visually.

The aligned linescans extracted from the DPC images are shown above in Fig.3.3.2.2.3. It should be noted that the integrated stray field falls away at the edges of the images and this is a requirement for a faithful tomographic reconstruction. The peak profile in the second graph is somewhat rounded, indicating that these linescans refer to a plane at some distance from the TBS and certainly greater than the pixel size of 400nm (to be meaningful the reconstruction should ideally refer to a plane distanced only a few nanometres from the TBS, since, with this type of head, we are dealing with contact recording). There is also spurious "noise" in the linescans due to a dirt particle on the sample and no attempt was made to interpolate the intensity distribution. In the case of the in-plane component no

reason can be supplied for the relatively large spread in values for the linescans on the left hand side of the graph.

3.3.2.3 Qualitative Reconstruction of the Stray Magnetic field.

The above data set was used as the input to an ART reconstruction of the head field and the grey scale images of the reconstructed field components are shown below in Fig. 3.3.2.3.1

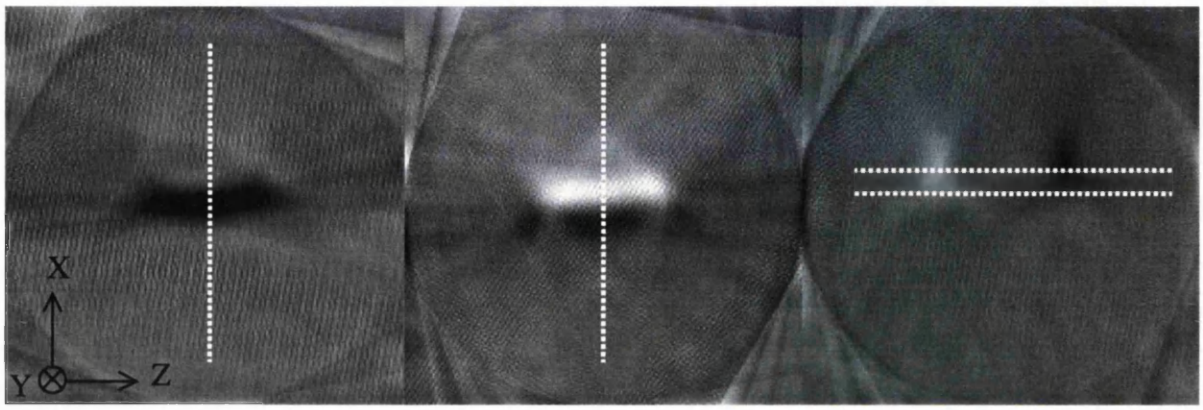

Fig.3.3.2.3.1 The 2d grey scale images of the x-, y- and z-components of the reconstructed fields using the 10° rotation data set (see Fig.2.3.1 for the definition of cartesian co-ordinate systems for this case). The dotted lines indicate the position from which the linscans in Fig. 3.3.2.5 were extracted.

Two of the three magnetic field components reconstruct moderately well from the data set and linescans extracted from the images are shown in Fig. 3.3.2.3.2 (to suppress some of the noise, these were from the average over a region 15 pixels wide). However some of the finer details seen in the reconstructed fields of thin film heads are not present and this is most apparent for the z-component. In particular the lower of the two line traces - Fig.3.3.2.3.3d – shows opposite contrast to that expected for the side-writing profile of such head; the reconstruction may be compared to the reconstructed z-component contrast for the model head shown in Fig. 3.3.2.3.4. This indicates that the input data set for the experimental head is rather poor and almost certainly contains significant artefacts. (Although the head structure of the write head is rather different from that of the model – in particular the trailing pole is a great deal longer than the writing pole - it is not expected that this would produce major changes in the shape of the side writing field).

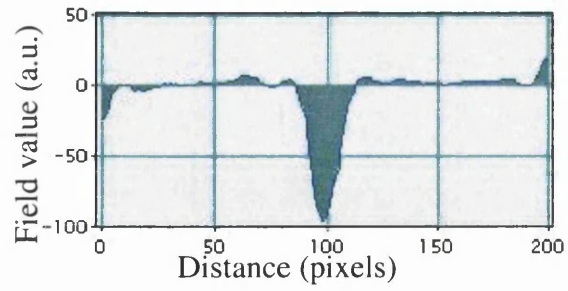

a) Y-component of the field.

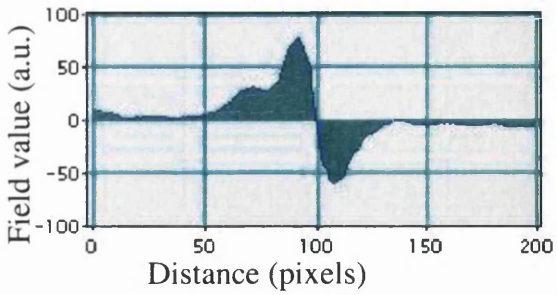

b) X-component of the field.

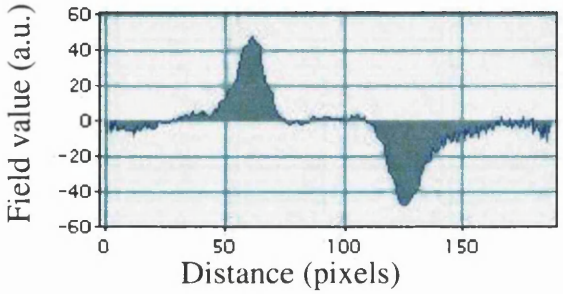

c) Lower part of the z-component of the field.

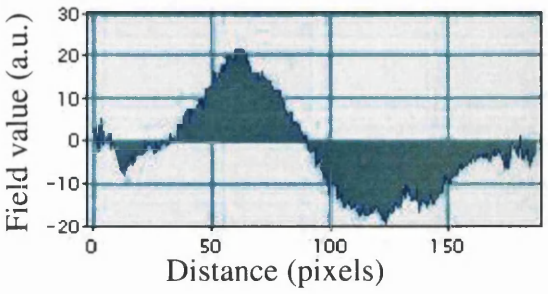

d) Upper part of the z-component of the field

Fig.3.3.2.3.3. Linescans extracted from the 2D grey scale images in Fig.3.3.2.3, these have been integrated over a width of 15 pixels.

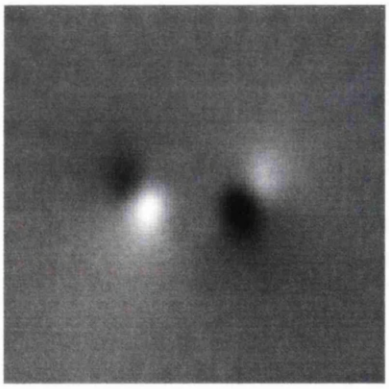

Fig.3.3.2.3.4. The 2d grey scale image of the z-component for the model thin film head. The data set chosen was at a distance of 500nm from the ABS.

The original DPC data was taken at 10° rotation angular intervals compared to previous work on heads, which used 5° rotation intervals [7]. By image processing the DPC linescan information can be interpolated to give 36 lines of data equivalent to 5° rotation intervals. However this does not improve the accuracy, since there is no new data present (it may however change slightly the fringing effects, which arise from the equivalent of series termination errors in Fourier analysis). Despite the argument above, a 5° data set was

prepared for RTM reconstruction and the line traces are shown in Fig. 3.3.2.3.5. The RTM program can reconstruct the full 3-D magnetic field of the head from each of the orthogonal DPC data sets, whereas the ART method requires both data sets for a single determination. To aid comparison the same '5°' data sets were used for both methods and the reconstructed fields are shown in Fig. 3.3.2.3.6a in the form of 2D grey scale intensity distributions.

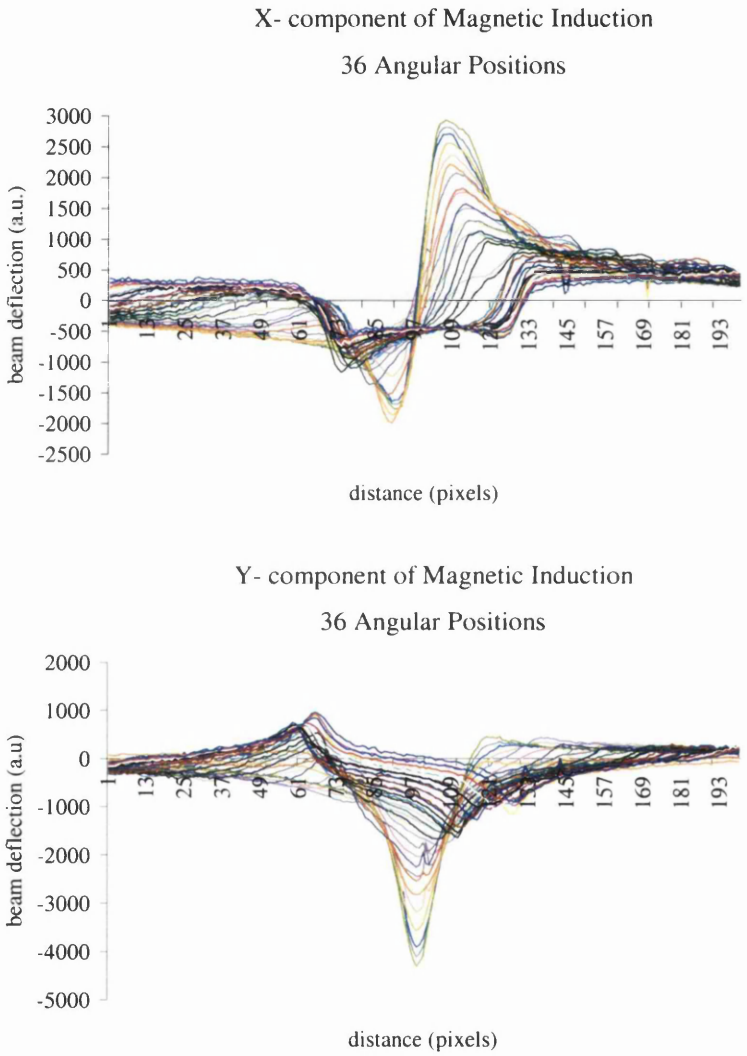

Fig.3.3.2.3.5. The interpolated DPC data sets. These have 36 angular positions instead of the original 18.

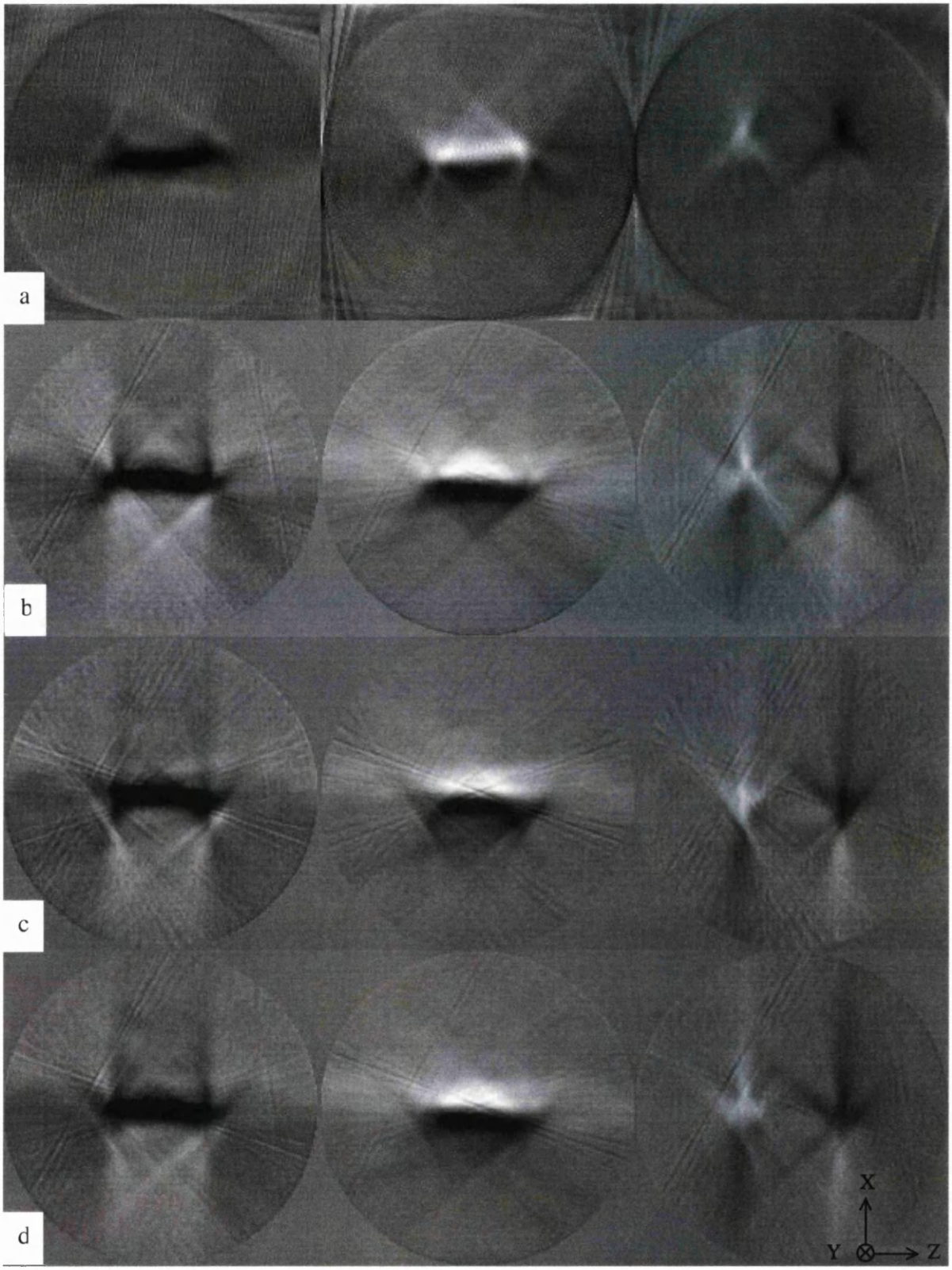

Fig.3.3.2.3.6a. 2D grey scale images for the tomographic reconstruction using the interpolated 5° rotation DPC data:- a) the ART reconstruction, b) the RTM reconstruction using the in-plane deflection component, and c) the RTM construction using the out-of-plane deflection component, d) the average field from the two RTM results.

The comparison of the reconstructed fields is shown in Fig. 3.3.2.6a, where the result of ART is presented in a), and the two RTM reconstructions and their average are shown in b), c), d) respectively. Whilst qualitatively the intensity distributions appear very similar (as they should!), closer inspection shows that the z-component is significantly closer to the anticipated form for the RTM method and in particular in the averaged field intensity in d) (see fig3.3.2.3.6b). We should not be totally surprised by this since the bases of the reconstruction methods are quite different and their performance with relatively poor initial input data could be expected to vary

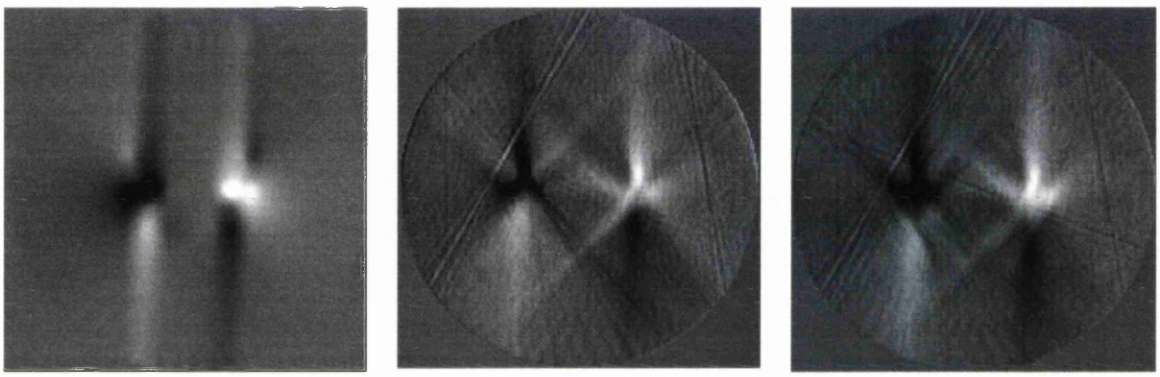

a) b) c)

Fig.3.3.2.3.6b A comparison of the reconstructed z-components. The first image is the z-component from the model data set discussed earlier. Image 'b' is a RTM reconstructed field from the data collected in the Philips CM20 and image 'c' is z-component from image d in fig.3.3.2.7.a i.e. the average RTM reconstruction.

In a series of graphs below Fig. 3.3.2.3.7 – Fig. 3.3.2.3.9 below, we carry out a comparison of linescans of the reconstructed fields from the write head. In Fig. 3.3.2.3.7 we compare the line profiles for the x- and y- components for the 18-line and 36-line input data sets reconstructed by ART. It is clear that no new information has been gained by interpolating the original data from 10° rotation intervals to 5° intervals.

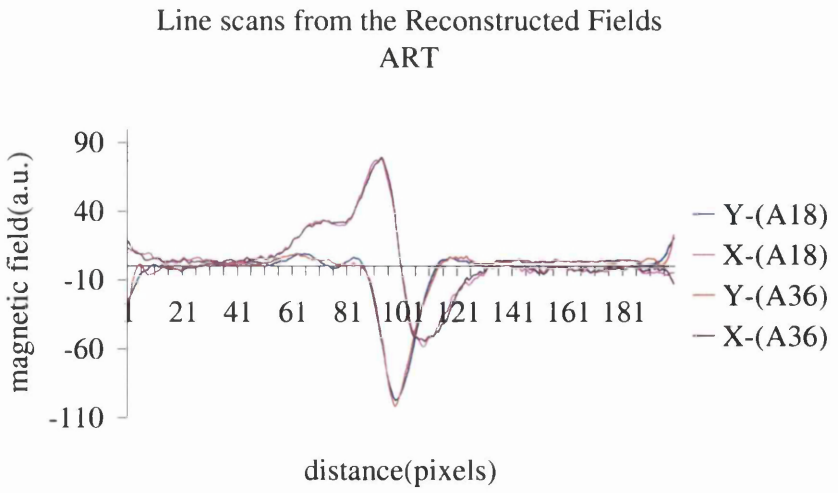

Fig.3.3.2.3.7. Comparison of the x- and y- field components for the two angular steps used, 10° and 5° in ART reconstruction.

The Z-component is not shown, the line traces are too noisy, and don't reveal much detail on the side writing field. There is a scaling difference in the reconstructed fields between the ART and RTM programs, the maxima and minima in the RTM linescans are 100 times smaller than for ART.

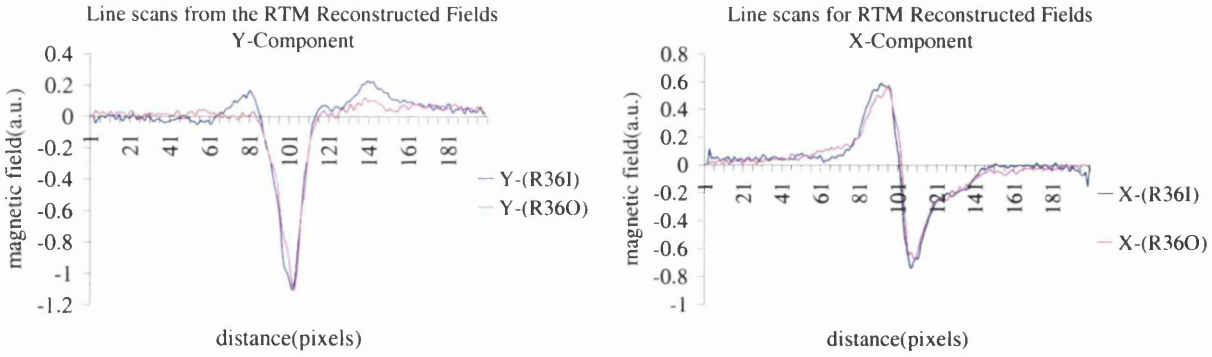

Fig.3.3.2.3.8 Linescans extracted from the RTM 2D grey scale images. 'I' indicates that this component was reconstructed from the in-plane deflection component and 'O' the other component.

There are slight differences in the profiles of the linescans, in the second of the two graphs the x components have a small dip in the peak value. This is probably due to poor alignment of the input linescans or the poor quality of the data. It may be a reconstruction artefact but this is unlikely. To get a direct comparison between the two programs used to

reconstruct the fields, the RTM linescans were scaled up, then both the X and Y components graphed.

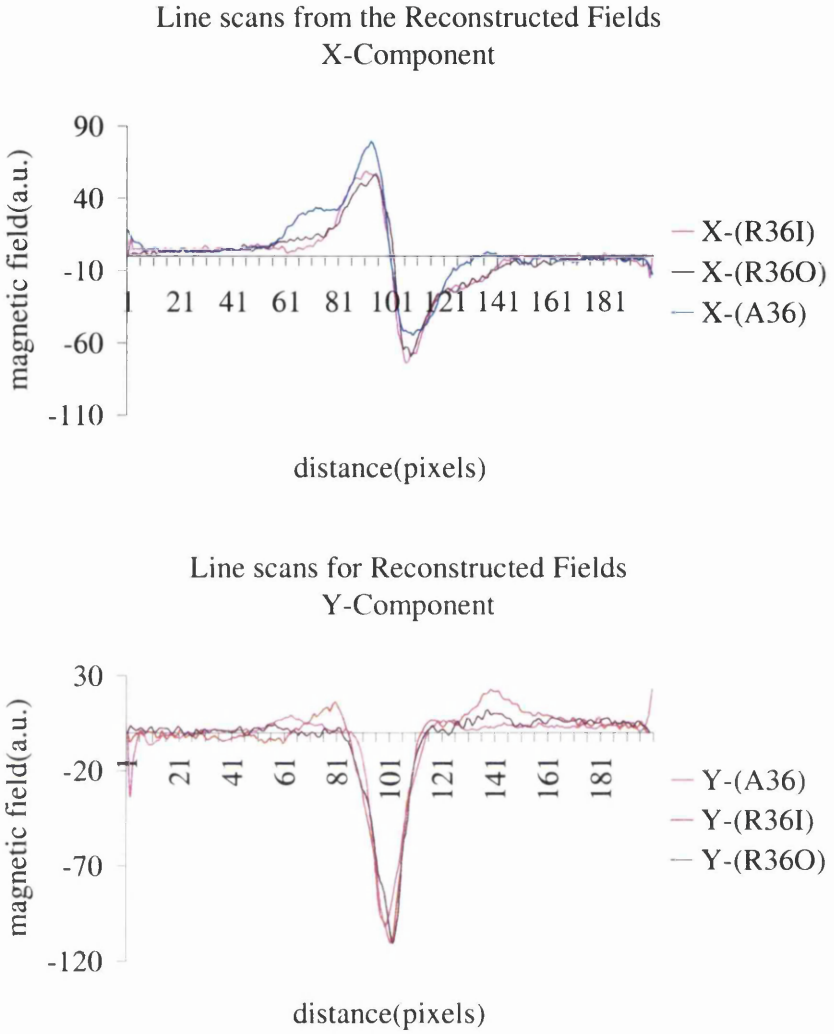

Fig.3.3.2.3.9 A comparison of output from the RTM and ART programs. Only the x and y components are shown. 'A' and 'R' differentiates between the two programs, ie 'A' is the reconstruction using the ART program.

Both programs produce similar reconstructions of the field, but for RTM the peak value for the y-component is higher than the equivalent ART field output. In summary of the reconstructed fields:

1) no new information on the field characteristics arise from the 36-line input cf. the 18-line input data,
2) the z-component is better defined by the RTM method,

3) there is not much difference between the methods for the x- and y- components.

Given the poor experimental conditions, it is perhaps surprising that the reconstructions are as good as they are. If the experimental conditions were improved, the sample mounting problem solved and the contrast calibrated, then quantitative field reconstruction should be achieved. Unfortunately the two samples were damaged while attempting to clean them and no further samples were made available by Onstream due to pressure of commercial work.

3.3.2.4 Investigation of Saturation Effects in the Writing Head

The second aspect of write head behaviour, which I investigated was the field saturation behaviour as the head drive current increased; once again DPC imaging was used. The head position was chosen so that the electron beam passed across the pole gap, i.e. from one pole to another, as opposed to along it, i.e. 'in-between' them. The latter position would have given a much larger electron beam deflection and non linearity of detector response would have been experienced at much lower drive currents. A series of DPC image pairs were collected with the head drive current varied over the range 10mA to 80mA d.c. The head is normally driven at 30mA. Linescans were extracted from the images immediately in front of the TBS and they are shown plotted in Fig. 3.3.2.4.1

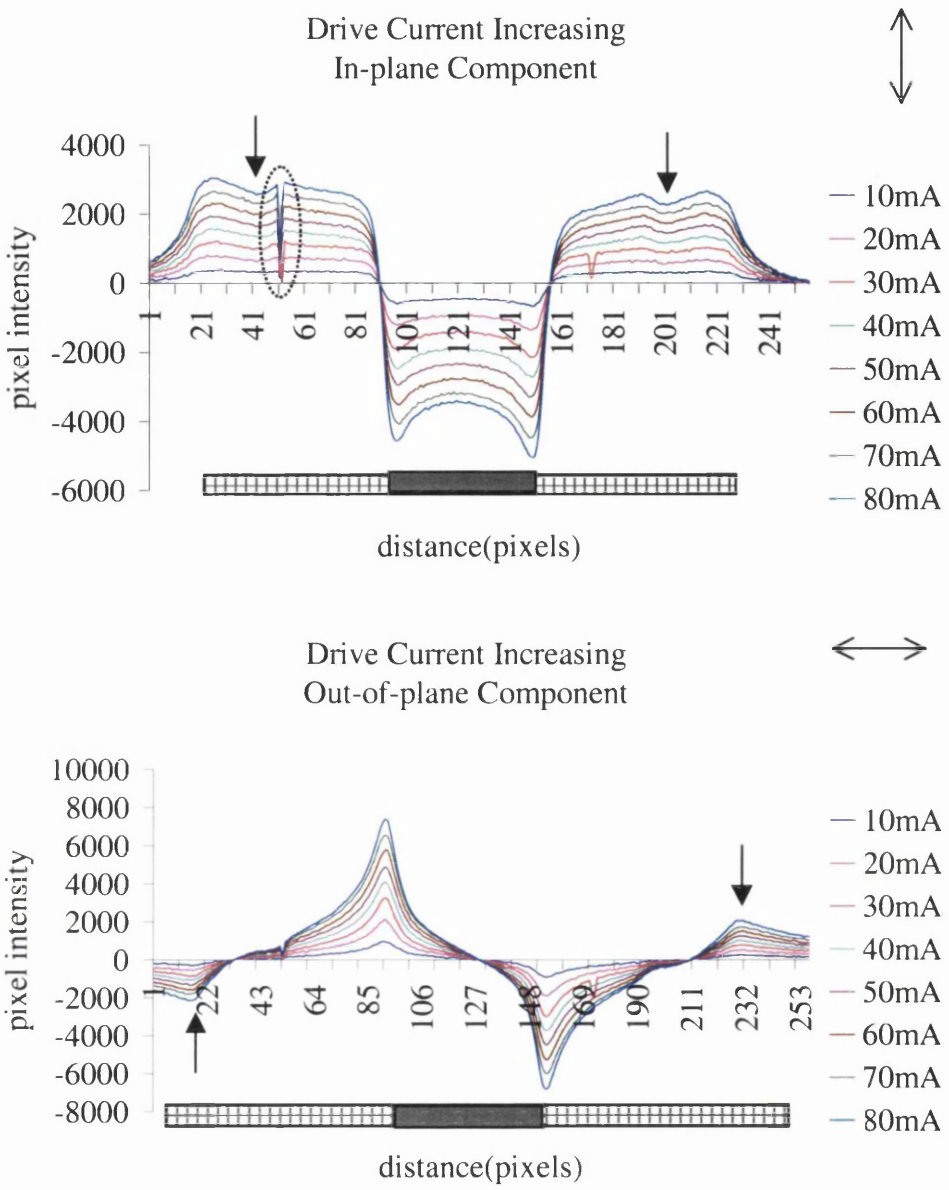

Fig.3.3.2.4.1 Equivalent linescans from the in-plane and out-of plane deflection data sets as a function of drive current. The double-headed arrows indicate the direction of sensitivity of the contrast to magnetic induction. The single arrows indicate the small deflections that occur on either side of the writer pole. In the graphs the position of the writing pole (grey rectangle) and the common pole (checked rectangle) are given approximately.

There are a number of interesting features in the above graphs. Obviously as the current increases there is an increase in the magnitude of the beam deflection for the orthogonal components. The dotted ellipse in the top graph highlights an anomaly in the extracted

linescans. It is probable a dirt particle on the head; as to why the minimum increased as the drive current was increased is strange as the head was not moved during the experiment. There may have been some movement of the head due to heating effects but these were not observed at this magnification. Even "magnifying" this area digitally did not reveal the source of this anomaly.

Another feature in this graph is indicated by the single arrows is the dip in the linescans on either side of the writing pole. This minima increased with each increase in the applied drive current. If one refers back to the schematic (fig.3.3.1.1) a possible explanation for this "dip" is that it occurs where the common pole narrows toward the outer edges, (see argument below), and hence one is observing a reduction in the integrated component of magnetic induction (in projection).

In the second of the two graphs one feature should be pointed out and that is at the ~20 μm from each end of the common pole there appears to be a magnetic component which is opposite in sign to the one on the writing pole nearest it. These coincide with the section of the common pole that drops in width by a factor of ~0.5 and some flux leakage would be expected there. The writing pole width is ~36 μm with the distance between the "thick" section of the common pole being ~84 μm. From the graph the distance between the two main peaks is ~ 26 μm and between the two minor peaks its ~85 μm. Despite the difference in measured widths for the writing pole we still believe that these smaller peaks occur due to flux leakage when the common pole gets thinner.

It is not immediately obvious from the above graphs if there are any saturation effects visible in the pole. Hence values at a particular position were extracted and plotted as a function of drive current in Fig. 3.3.2.4.2. For the in-plane component the middle section of the pole region was sampled and for the out-of-plane component the maxima and minima values were selected with the modulus of the minima plotted.

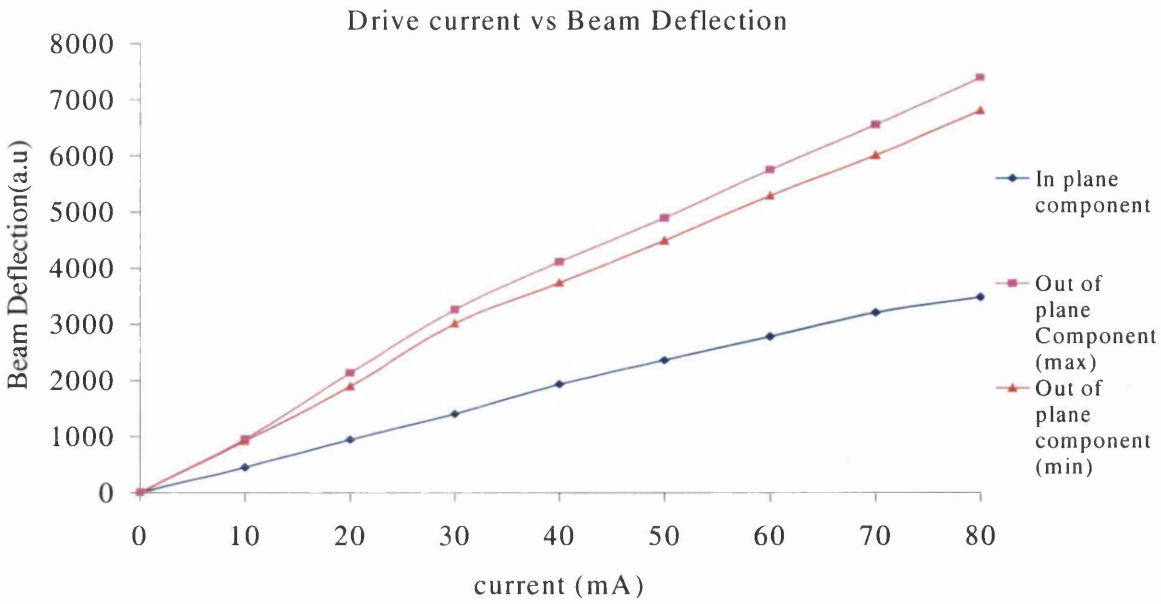

Fig.3.3.2.4.2. The beam deflection as a function of drive current (see text for explanation).

In graph there is a deviation from the linear plot at ~30mA for the data arising from the magnetic component normal to the tape bearing surface. However for the other component (parallel to the TBS) it is not until ~70mA that this deviation is really significant but there is a small deviation at ~30mA as well. From this graph the indication is that saturation effects begin to appear around 30mA drive current, which is the value used in the tape file. Thereafter the deflection increases at a progressively slower rate. It was expected to see a noticeable plateau appearing in the above graph at drive currents higher than 30mA. However, it would appear that the head design is such that significant saturation effects do not occur over the range of drive currents that were applied to the head during this study.

In the next section the second component of the head viz. the 'read' function of the head was studied.

3.3.3 Study of the MR Element

The latest generation of hard disk and tape drive heads all incorporate an MR element as the readback transducer. In this investigation it was hoped to be able to carry out electron beam tomography on the stray field, which should be present at the flux guide gap when the MR element is excited by a d.c. current. Reciprocity theory should then permit us to

comment on the effectiveness of the MR element for the read process. In normal operation in the tape drive unit, the MR element is electrically biased but, as explained earlier, this provision was removed during the sample preparation to isolate a single read/write head for our examination by electron microscopy.

When we first investigated the head by DPC imaging with neither the write head nor the MR element being driven, we observed contrast, which we ascribed to electrostatic charging and this is shown in Fig. 3.3.3.1. We expected that any observable DPC signal from the MR element would be small and hence might be swamped by the unwanted contrast, if this was too large. Also, if the contrast was time varying, we would not be able to use the standard subtraction method to get rid of it. With no drive currents present, DPC image pairs were taken with an interval of a few minutes between them and these are shown in Fig. 3.3.3.1. The images appear very similar and linecans extracted from equivalent positions in the images show (Fig. 3.3.3.2) that they are closely matched. Further proof is obtained by subtracting the two sets of linescans (see Fig. 3.3.3.3) and generally the contrast is very small in comparison to the original signal. Once we had recorded DPC images with the MR element driven at 10mA (Fig. 3.3.3.4) we established that the magnetic contrast was comparable in magnitude to the raw electrostatic contrast; hence the image subtraction method should give a reasonably faithful representation of the influence of the magnetic field present.

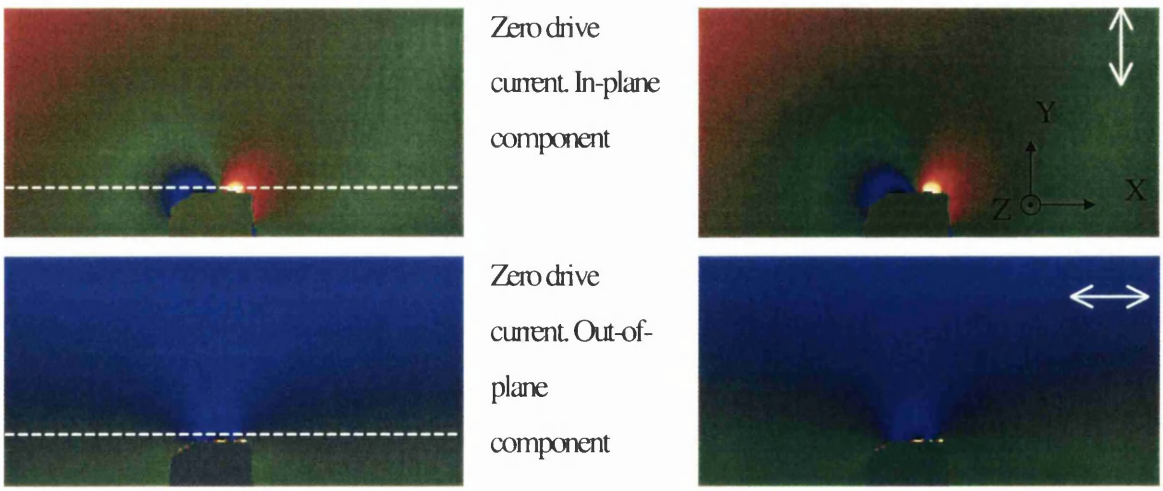

Fig.3.3.3.1. Images of the electrostatic field; the arrows indicate the mapping direction if the field is magnetic. Two pairs of images are shown and these were taken a few minutes apart.

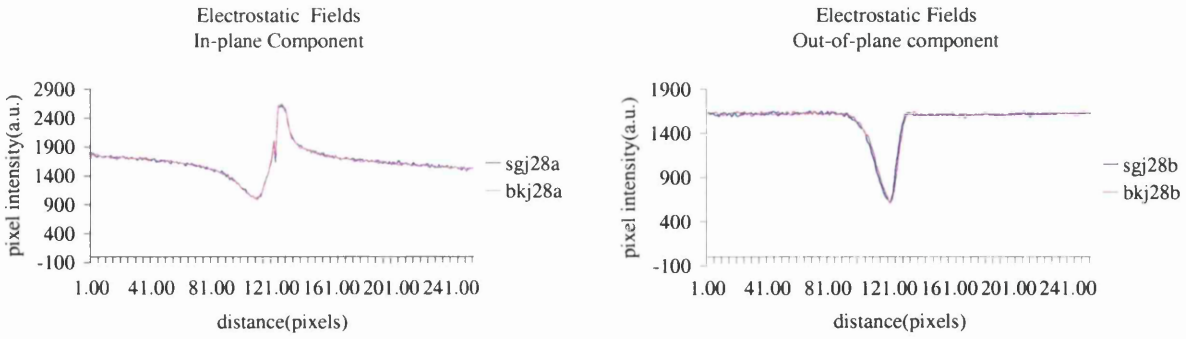

Fig. 3.3.3.2. Line scans extracted from the positions indicated by the white dashed lines in images in Fig. 3.3.3.1. The pink and blue linescans represent data separated in time by a few minutes

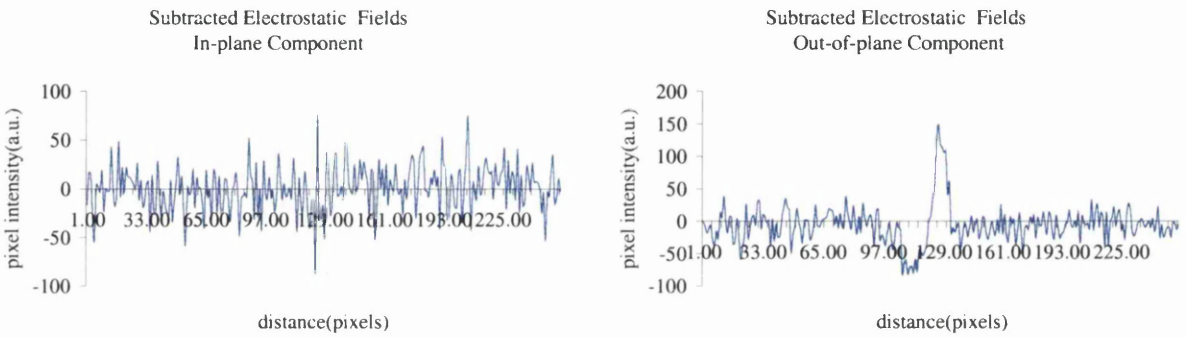

Fig.3.3.3.3. The results of subtracting the pairs of linescans in Fig. 3.3.3.2.

Pairs of images were taken at ±X mA and then subtracted to form the individual images in Fig.3.3.3.4. The first thing that is clear is that the expected form of the field at the gap is not visible and secondly that there is substantial magnetic flux emanating from the side of the head where the MR element is located.

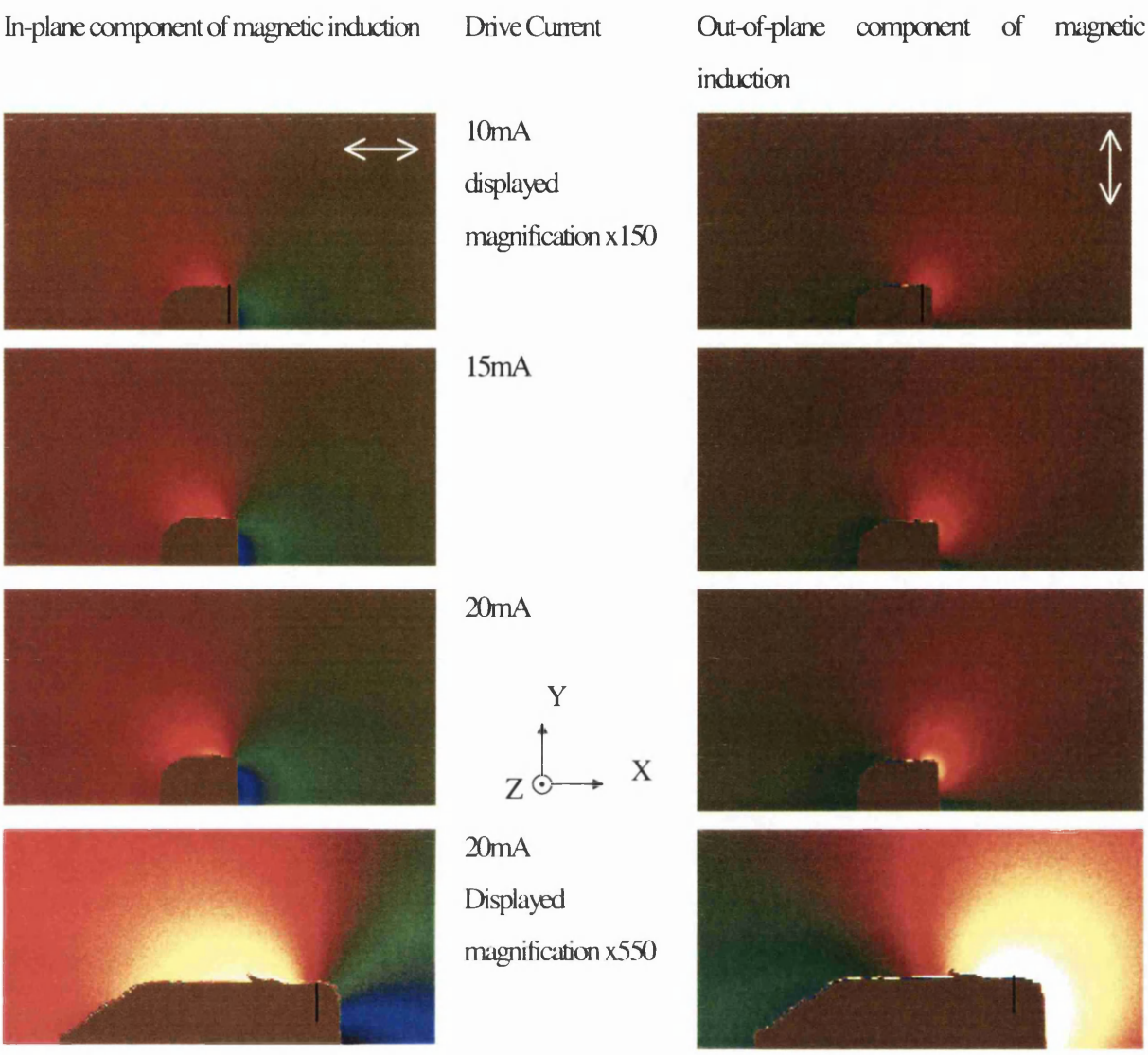

Fig. 3.3.3.4DPC images obtained with the MR element driven at various drive currents. The vertical black line in the top and bottom images indicates the approximate position of the MR gap.

To see if there was a field from the read gap, an image was taken at a higher magnification of X550, however there is no obvious contrast of the expected form from the gap region, although the flux leakage round the side of the structure is very evident. Even from the final image in the above sequence there is no obvious field from the read gap. Late in these studies Onstream started to use the finite element TOSCA program to evaluate theoretically head performance for their tape file. One of the first tests was a 2-D (as opposed to the more desirable 3-D evaluation) of the read/write head supplied to us. The

field characteristic calculated for the vicinity of the MR element are shown in Fig 3.3.3.5 below.

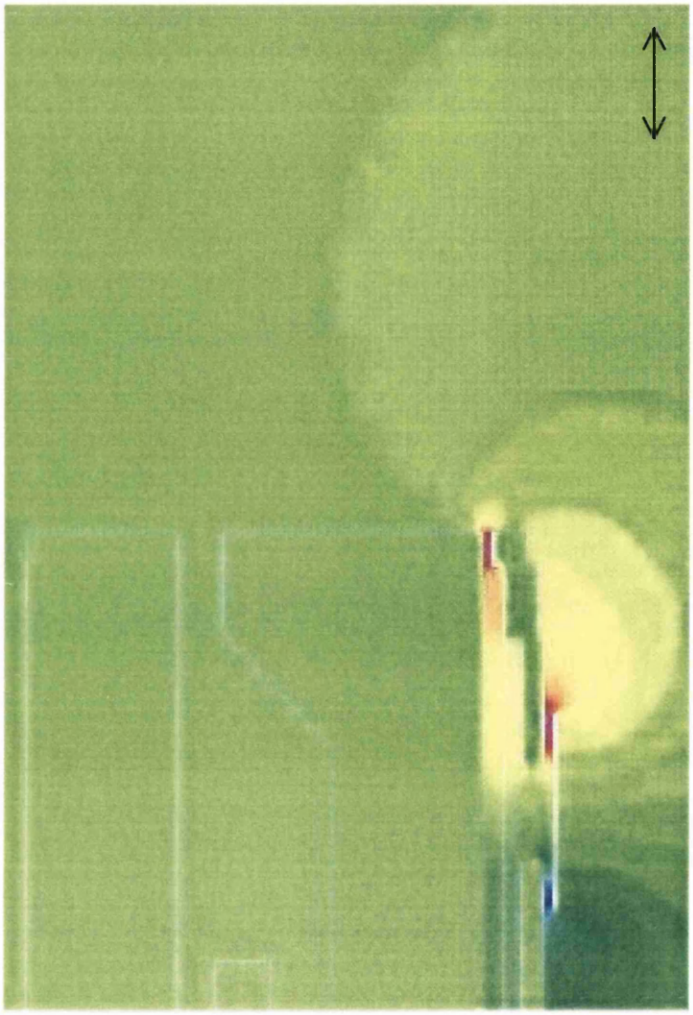

Fig.3.3.3.5 Result from the static analysis of the field with the MR element driven at 10mA. The arrow shows the direction of the field component to which contrast is sensitive.

It must be remembered that in the DPC images of Fig. 3.3.3.4 we are concerned with the field component integrated along the electron trajectory, whereas the theoretical determination is of the field itself, albeit in a 2D calculation. Nevertheless we would expect these to qualitatively similar in spatial distribution and, apart from the immediate vicinity of the flux gap, this is confirmed by comparison of the two images. However, we know that there was substantial misalignment of the head on the specimen stub and this could result in marked shadowing effects. These will be relatively more severe for the MR element, given that the flux gap width is small 0.25μm; we expect the field will be close to its maximum value only over a similar distance from the TBS. Hence we may well not see

its effect in the DPC images. We could extract linescans from the figures, but the comparison would be of dubious validity. However this is the first time to our knowledge that magnetic flux associated with an MR element in a production head has been viewed in DPC imaging. We should therefore take substantial encouragement that when we have the specimen alignment problems sorted out we will be able to assess the performance of the MR readback element.

3.4 Discussion of the Results

3.4.1 Emboss Head

The major problem with the Emboss head study was its large size as it was only just narrower than the specimen rod width. It was also impossible to isolate a single head from the multi-head array for study by tomography. In principle, we had the option of collecting a restricted DPC data set for tomography, but this would have been limited to only ±45° of tilt about the specimen rod axis, beyond this there would have been substantial interference from the heads immediately adjacent. In addition, the symmetry position for such a data set, with the electron beam direction normal to the polegap length, would have given us little information on the writing field [7], although information on the side writing field characteristics would have been obtained [8]. There was also substantial DPC image contrast from the gap between the heads even at zero tilt angle and this would also have influenced the accuracy of any reconstruction. The source of this additional DPC contrast was considered and one possibility was that it arose from magnetic flux established between the common pole and the undriven poles. A modelling exercise, based on the field of a thin film hard disk read/write head calculated using a finite element program, indicated however that the most likely source was the side-writing field from the drive head. The fact that the model head was only a moderate match to the practical sample and also the presence of the continuous drive current through the wire could easily account for the discrepancies between the contrast of the experimental linescans and those based on the model. MFM imaging carried out at the end of the thesis studies confirmed that there was little or no magnetic flux escaping to the undriven poles.

The DPC imaging studies, which were performed on the Emboss head, did however provide useful information to the head designers. It was confirmed that there was substantial reproducibility between the DPC contrast profiles of the elements comprising the accessible region of the multi-pole array (only the element of largest linear dimension was not studied). It should be noted that the initial work on these heads using the DPC mode of Lorentz microscopy suggested that there was asymmetry in the writing field, but this was later explained by the fact that the differentiation directions of the detector had not been sufficiently closely aligned relative to the specimen geometry.

3.4.2 The Data Head

It was originally intended that the stray magnetic fields from both the write part of the head and also from the gap associated with the MR element (in this case the MR element was driven by a d.c. current) should be studied by DPC imaging and if possible quantitative field data should be extracted from tomographic reconstruction. The first hurdle to be overcome was the isolation of a single head unit from the 8-head array, which comprises of a parallel write/read transducer. Personnel in Onstream model workshop achieved this difficult task. However a major problem arose in mounting the specimen on the special stub used in conjunction with the CM-20 specimen rod; it was required that, under rotation about the rod axis, the specimen face containing the poles should be maintained parallel to the optic axis to an accuracy of better than 0.5°. The two samples supplied to us were misaligned by several degrees. This, and the fact that it proved extremely difficult to clean the samples and remove all debris arising from the machining, severely curtailed the useful information, which could be extracted from the DPC imaging studies. A crude tomographic reconstruction of the write field was achieved, but the plane to which it refers was imprecisely defined and probably on average at least 1μm from the TBS. DPC contrast can of course be put on an absolute basis using a thin wire specimen driven by a d.c. current [9], but in this case the DPC data from the head was not considered good enough to warrant quantitation. There is however no reason why future studies cannot yield quantitative field reconstruction. However, even if the specimen geometry is optimised, it will be difficult to get closer than 0.25 – 0.35μm to the TBS – ideally of course we would want to be much closer since we are concerned with contact recording.

The experimental study of the write field saturation characteristic did produce useful data and it was established that at a drive current of 30mA, which is used in the tape file, field saturation is starting.

The study of the magnetic field from the flux gap associated with the MR element proved difficult due to the presence of DPC contrast when no drive current was applied to either the MR element or the write head. However this contrast, which we ascribed to charging effects, appeared to be time invariant and could therefore be removed by subtracting images taken with opposite sense drive currents in the MR element. Given the known misalignment of the head in the specimen stub, the absence of DPC contrast, which could be identified with the flux gap, was not surprising., We would expect the gap field to be of significant magnitude only over a distance comparable to the gap width (0.25 μm) and this region was probably inaccessible due to shadowing effects arising from the specimen misalignment. The larger scale DPC contrast observed in the vicinity of the MR element is of significance and the indicated field integral qualitatively matches a finite element field calculation for a model of the field from the MR part of the head. In the future, such studies performed on a better aligned head, comparison of experiment with modelling could provide useful information on the efficiency of the MR transducer.

3.5 Conclusion

The DPC study of the Emboss head was only partially successful in trying to study the stray magnetic field. There were a number of problems with the microscope, the main one being the instability in the HT tank and this hampered the study of the heads. A number of outstanding issues still remain, such as the rotation experiments and the magnetic field reconstruction from data collected from such experiments. The most significant problem with trying to characterise this type of sample further, is its size. This sample was a production head and it would have been more useful if our collaboration with Onstream had started at the development stage of the head. Then it may have been possible to obtained a miniature version of the head with a smaller number of poles. An experimental Emboss head was supplied for the MFM studies but it was also full size, which was not a problem in the MFM.

For the data head the outcome of the studies was more positive, we have shown the potential of the Philips CM20 to carry out DPC studies on tape heads. If the samples had not been damaged then some the experimental parameters would have been refined and further characterisation experiments carried out. The one remaining task with the studying this sample is to align the sample such that it is flush to the sample stubs geometry in order to achieve correct alignment with respect to the optic axis of the (S)TEM.

Both of the above types of Tape head were studied in a Digital Instruments MFM. This technique is viewed as being a complementary method to the DPC mode of Lorentz microscopy in that the magnetic field component normal to the TBS can be studied by both techniques.

3.6 References

1. Philips Research, Press & Media, Press Release, Archive number: Demo2/June 1997
2. Barrett R.C., Klaassen E.H., Albrecht T.R., Jaquette, G.A. and Eaton J.H., (1998) *IEEE Trans. Mag.*, **34** 1872
3. Ruigork J.J.M., Van Kesteren H.W., Cumpson S.R., Adelerholf D.J. and Luitjens S.B., *IEEE Trans. Mag.*, **34**, 2983
4. Ruigork J.J.M., Draaisma E.A. and Van Kesteren H.W., (1998) *Phillips Journal of Research,* **51**, 21-56
5. Ferrier R.P., Liu Y., Martin J.L. and Arnoldussen T.C. (1995) J. Magn. Mag. Matls., **149**, 387-397
6. Petri I., Zimmermann T., Zweck J., Hoffmann H., Liu Y., Ferrier R.P., and Nichtl-Pecher W., (1996), *IEEE Trans. Mag.*, **32,** 4141-4143
7. Liu Y. (1996), 'Electron beam tomography of recording head fields', Ph.D Thesis, Univ. of Glasgow
8. Ferrier R.P.,(2000) private communication
9. McVitie, S., Ferrier, R.P. and Nicholson, W.A.P, (1997) Inst. Phys. Conf. Ser. **No.153,**.201-204

Chapter 4

4 Magnetic Force Microscopy of Magnetic Recording Heads

4.1 Introduction

DPC electron microscopy and electron beam tomography of the Onstream Emboss and read/write tape heads were only partially successful in characterising their stray magnetic fields. Fortunately late in the thesis programme another type of microscope became available, a Digital Instruments 3100 Magnetic Force Microscope (MFM); in this chapter the results from studies using this technique will be presented. The first head to be discussed will be the Emboss head previously studied in the JEOL 2000 FX and then we will discuss results obtained with a newer version of this form of head. The final sample studied was a standard production data head supplied by Onstream. For the last two types of head studied, no special sample preparation was necessary, one of the advantages of using MFM. However the samples do have to be thoroughly clean or else the tip becomes prone to damage; if this happens then the results may be inconsistent and/or uninterpretable.

In Chapter 2, the basic theory and general instrumentation requirements for MFM were discussed. In the study of the stray magnetic fields from recording heads, it is not the direct force arising from the sample/tip interaction that is measured, but the force gradient since the tip is vibrated along its axis while scanned over the sample. This is not a direct method of studying the stray magnetic field as it is the tip interaction with the field that is observed/recorded. Using this technique on a recording head, it is generally the gradient, with respect to the normal to the TBS, of the out-of-plane component of magnetic induction that is studied. The method can be considered as complementary to the DPC mode of Lorentz microscopy. To be able to derive quantitative information on the head field from MFM studies, extensive modeling of the tip interaction with the head field is

required and this is being pursued in a number of laboratories; it is part of the general goal of developing quantitative MFM.

4.2 Practical MFM imaging and data interpretation considerations

Before describing the results from the MFM studies on the heads, some of the experimental details are discussed. The Tapping Mode™ of the DI instrument was used for imaging the head samples. In this mode for each linescan of the selected image raster, two passes are made by the tip across the specimen. In the first, the presence of the surface is sensed and then in the second the signal is recorded with the tip withdrawn a specified vertical distance from the specimen; in all cases of imaging in this study this offset distance was 100nm. The first pass provides height information on the specimen. The tip position is determined for each point on the scan and then the data is then analysed to detect the presence of any specimen tilt. The phase signal, which contains the information on the magnetic interaction of the tip with the sample, is obtained on the second pass of the tip across the specimen. It should be noted that if the tip encounters a high feature on the sample e.g. a small piece of dirt, its height is of course added to the lift height. Hence in some cases topographic information may "appear" in the phase data

The maximum area of a scan in our DI instrument is $90\mu m^2$. For most samples studied by MFM, this is not a limiting feature, but for the Emboss head samples, this restricts us to an image covering at most two poles from the multi-pole array; it would have been useful to have been able to study more poles in one scan. It should be noted that a large scan area has an effect on the tip, as it reduces its operational life. Prolonged scanning of large areas can also reduce the life of the piezoelectric material used for the scanning stage. The number of pixels in a given linescan will determine the spatial resolution of the information. Generally, due to the relatively large size of the poles, a raster of 256 by 128 pixels was selected; the pixels were square and a 2:1 ratio of image length/height was the best fit to the useful scan area. The ultimate spatial resolution of MFM imaging is generally set by the tip shape and is typically ~50nm, but in our case this is irrelevant since the pixel spacing greatly exceeds this value.

There are several different commercial standard MFM tips available and a much larger number of experimental ones. The selection of a tip for the study of stray magnetic fields requires some thought. If magnetic tracks or patterned magnetic elements are under investigation, then the choice of the tip will be determined by the coercivity of the sample, since we do not want to influence its magnetic structure by the tip field. Equally if the sample stray field is large, as will be the case for magnetic recording heads, particularly at high drive currents, then the magnetisation of the MFM tip can be altered and the phase signal will not necessarily correctly reflect the magnitude of the head field. In the investigations which follow, we have explored the use of several different types of MFM tip, both hard and soft magnetically, with the hope of being able to assess their relative usefulness for recording head studies.

Before the actual data is presented, the basic forms of the images which we expect are discussed. In the schematic phase images of an Emboss head, shown in Fig. 4.2.1, there are two upper poles, a section of the common pole and a lower pole. This layout is similar for all the images of the heads. The two possible scan directions are shown; for the scan up direction, the tip starts at the bottom of the image and finishes at the top and vice versa for the scan down case. It has been observed that in some cases, image contrast can be slightly different for the two directions of scan, even when all other parameters are held constant. There is not a significant difference between such images as shown in fig. 4.2.2 But the scan direction is recorded as an aid for data interpretation. In the case presented below the peak values can differ by ~1 degree. Prior to using a tip it is 'magnetised' parallel to its axis. This should make the tip sensitive to the y component of magnetisation of the sample under study.

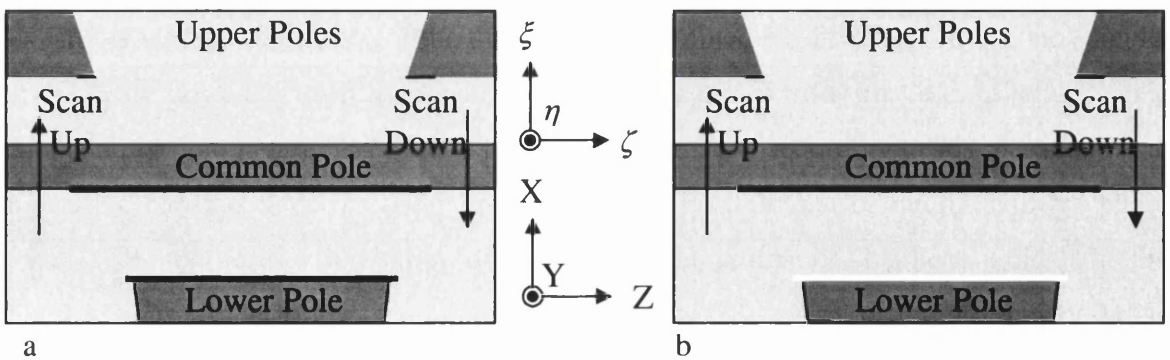

Fig.4.2.1. Schematic of a typical MFM phase image, including an idealised MFM tip to show the magnetising directions. (a) represent the image obtained using a soft magnetic tip

and (b) that with a hard magnetic tip. The top co-ordinate system (ξ, ζ, and η) is tied to the MFM scanning directions. The lower co-ordinate system shown gives the field directions for the sample and the particular direction of interest is 'y' which is either in or out of the page.

In Fig 4.2.1a we show the expected form of the contrast for a soft magnetic tip when a current is applied to the head. In this case the phase shift is always negative [1] and for a driven lower pole we get black contrast at the lower edge of the common pole and at the upper edge of the lower pole. In reality this does not stop as sharply as shown in Fig.4.2.1a, this is an idealised diagram. Precisely the extent of this contrast will depend on the field configuration of the head. It will be noted that black contrast is also shown at the edge of the upper pole and this indicates the (possible) presence of stray magnetic flux from this vicinity; we wish to establish if this stray field is in fact present in these heads. In Fig. 4.2.1b the situation for imaging with a hard magnetic tip is presented with an applied current. In this case the tip oscillation frequency will experience a positive phase shift on one pole edge and a negative phase shift on the other leading to separate black and white contrast regions; which edge is black and which white will depend on the direction of the drive current in the head. Contrast also arises when no drive current is applied to the head. For this case the contrast is uniform over the image with one level for the pole faces and another level for the non-magnetic areas of the head. This is only observed with the magnetically hard tips, the contrast from the soft tips is not nearly as sharp and well defined.

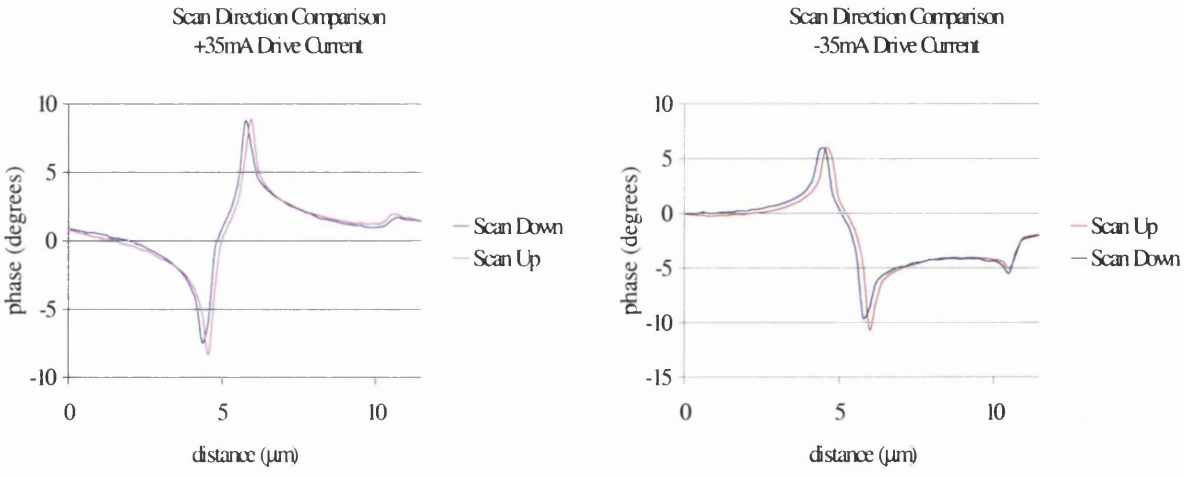

Fig. 4.2.2 The comparison between the scan up and scan down directions on a sample.

The co-ordinate system used in this chapter to discuss the head field is also shown in Fig. 4.2.1; however the only direction in which we will get information on the field is along –y i.e. normal to the TBS. However, there is another co-ordinate system tied to the MFM and that is the scanning directions of the MFM tip. These are defined as ζ', ξ, η (the second axis in fig. Fig.4.2.1), for the purpose of our discussions. The ζ -direction is the horizontal scan direction and is parallel to the edges of the poles in the above diagrams. ξ' is the vertical scan direction and is normal to the edges of the poles in the above diagram. The other direction plays no part in the scanning as when the tip is moved in this direction it has been physically removed from the surface off the sample.

One other issue needs to be addressed before the results are presented. On careful examination of the phase data it was noticed that it is superimposed on a phase contrast gradient. The linescans in particular, but also the other graphical data suffered from this anomaly. The best way to describe this problem is to show it and this is done on the left side in Fig. 4.2.3

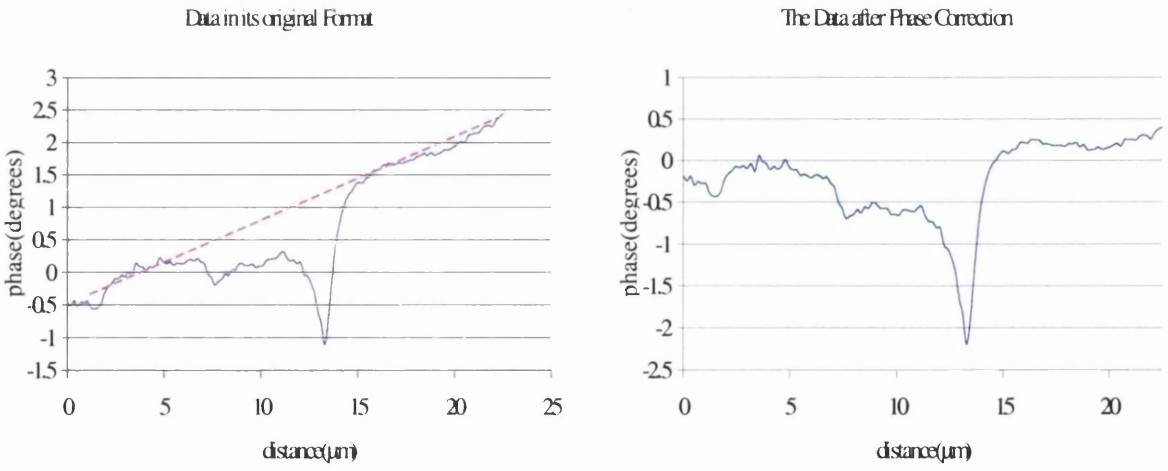

Fig.4.2.3. The removal of the phase gradient from the data collected using the MFM. The pink dotted line highlights the gradient in the data.

In the graph on the left-hand side this phase gradient can clearly be seen. From a starting point of ~-0.5^0, the phase constantly increases up to 2.5^0. For the second graph it has been "removed". This phase gradient is an imaging artefact and we are not sure why it occurs. It has only been observed in the data from the tape heads and was not observed in data

collected from the tip characterisation studies. One possible explanation is that the tape heads are not flat but slightly bevelled across the poles.

Two methods were proposed to "phase" correct the data; (i), use a plane fitting option in the Nanoscope™ software or (ii), visually correcting the data in Excel using the formula

$$y = mx+c \, . \tag{4.1}$$

Option one was tried and the results studied but other problems arose using this method. The images were not square but rectangular and this caused a problem with the plane fitting software. Another problem with the software correction method was it assumed the surface of the sample under investigation was flat, and in this case it was not.

So option two was chosen to correct the data. Excel was used to determine the base equation and then the data was corrected visually as shown in Fig. 4.2.3. This was not extended to the images presented in this chapter, these are for visual representation and one can not visually see the phase gradient in the images, it only manifests itself in the extracted numerical data.

4.3 The MFM study of the Emboss head used for the DPC experiments

Due to the sample preparation method for DPC imaging (see Chapter 3), imaging this sample was very difficult. The poles being in a small section of the TBS, which was prominent from the remainder of the sample (see fig. 4.3.1), meant that if the tip was scanned too high or low in the $-\xi$ direction, it could drop off the sample. This is highly undesirable as it could result in the tip being damaged. Four different forms of MFM tip were used to study the head and the results are presented in the following sections.

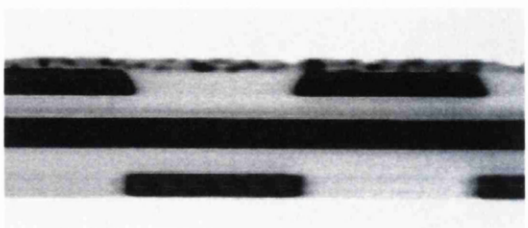

Fig.4.3.1 An optical image of a section of the Emboss head studied with the MFM.

4.3.1 The Metglas tip study

Firstly the phase images are presented together with the linescans from selected regions of the image; at the end of the section the data is presented in the form of contour and 3D plots. The data had to be extracted from the Nanoscope™ file structure by importing the image files into the Digital Micrograph™ program and eventually into other analytical software packages such as AXUM™. The original analytical software supplied by DI was good for on-the-spot analysis, but when the data was wanted in a friendlier format it had to be imported into the above packages. All images were taken at a lift height value of 100nm. The three values of drive current used for this study were 200mA, 300mA and 400mA d.c. The nominal operating drive current for the head in the tape file is 400mA in each half of the head, the polarity being reversed in the two halves. In this series of experiments the lower array of poles was driven.

The particular metglas tip used in this study had a coating 50nm in thickness – DPC and electron tomography studies [2] indicate that the coercivity of the coating should be low, although it does exhibit an easy axis along the tip direction when magnetised axially. We would expect the tip interaction with the head field to be predominately attractive in form and this is confirmed by the images in Fig. 4.3.1.1. We note first the strong contrast at the top edge of the lower pole (and also at the sides) and on the opposite lower face of the common pole; this is expected since it is this pole, which is being driven. There is also dark contrast visible at the lower edge of the upper pole indicating the possible presence of stray flux from this undriven pole; there is no strong indication of significant flux leakage from the upper surface of the common pole. There is a feature on the lower pole, a straight line just up from the bottom of the image; this is most likely not a magnetic feature but rather a topographic artefact.

The linescans shown to the right of each image were extracted from positions indicated by the corresponding coloured lines in the first image. There are four distinct peaks in these graphs, their magnitude being related to the head field strength. It is obvious from the images where the peaks will occur along a linescan. The first peak occurs when the tip passes over the edge of an upper pole, the second and third when it crosses over the upper and lower edge respectively of the common pole and finally the fourth peak when it crosses over the upper edge of the lower pole.

metglas Tip #1955 (metglas thickness 50nm), Lower pole driven @ +200mA D.C, scan direction up

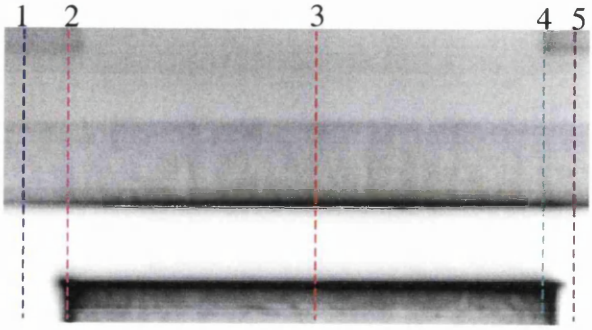

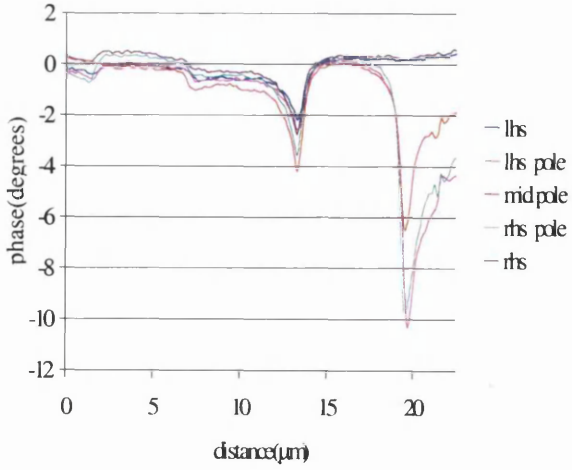

Metals Tip #1955, Lower pole driven @+300mA DC, scan direction down

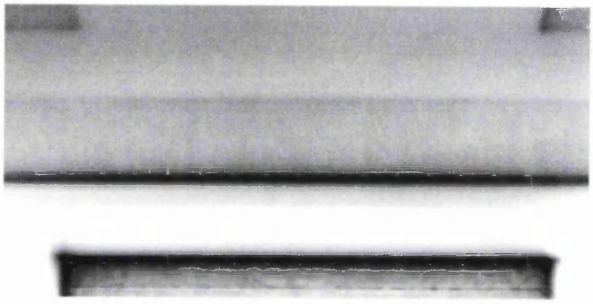

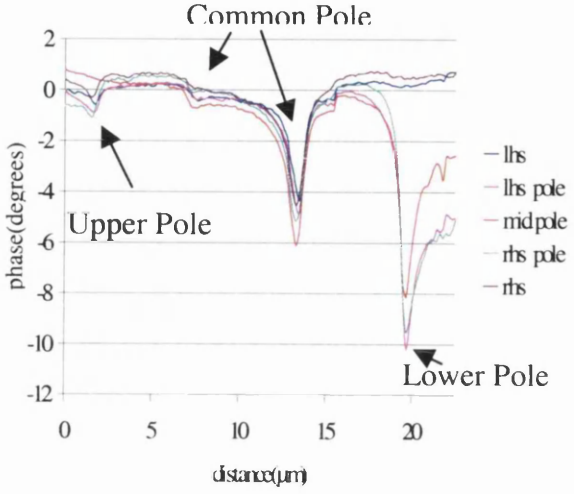

Metals Tip #1955, Lower pole driven @+400mA DC, scan direction down

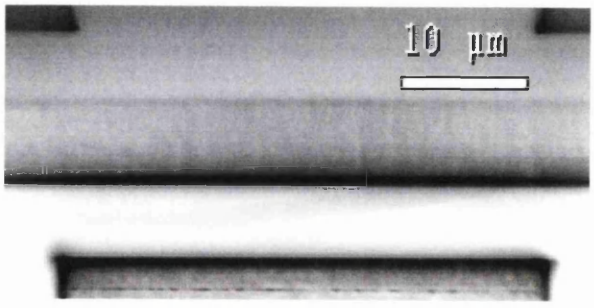

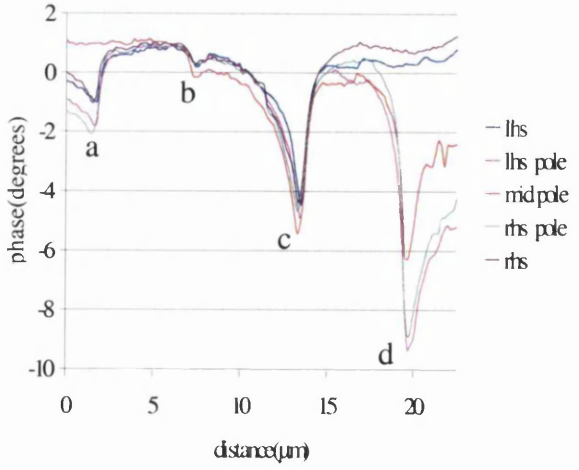

Fig.4.3.1.1 Phase images of the Emboss head taken using a metglas tip, and the linescans extracted at the positions indicated by the corresponding coloured lines in the first image. Key for the graph legend is as follows: 1 on the image corresponds to lhs, 2 - lhs pole, 3- midpole, 4 - rhs pole, 5 - rhs

Due to the layout of the poles, the linescans only ever cross over four pole edges in two positions. Only three peaks are interesting, viz. a, c and d; peak b does not change significantly in magnitude over the range of applied drive current. These peaks have different values depending on where on the image they have been taken. The highest peak profiles occur at the corners of the lower pole, their values remaining approximately the same even when the drive current was increased. In the middle of the lower pole (the red line in the above graphs), the signal magnitude is greater at the lower pole edge than at the common pole. However each scales approximately with drive current magnitude at least for 200mA and 300mA drive currents, but not for the 400mA drive current. A possible explanation for this is specimen heating. In Fig. 4.3.1.2 the height data image obtained for the 400mA drive current case is shown. The white contrast at the pole edges (corresponding to the positions of the magnetic peaks under discussion) indicates that the specimen was changing its vertical position during the scan; in these circumstances reliable phase data will not be available.

Metglas Tip #1955 (metglas thickness 50nm), Lower pole driven @ +200mA D.C, scan direction up

Metglas tip #1955 Lower pole driven @+400mA d.c.; scan direction down.

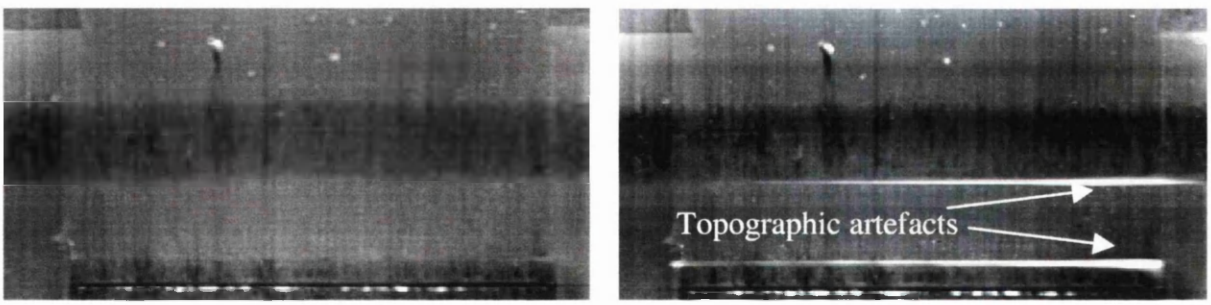

Fig.4.3.1.2 Topographic image taken simultaneously with a phase image. In the right hand image there are clear signs of a change in the topographic information when the drive current was increased and this may have been due to heating effects on the common and lower pole.

When this sample was observed using DPC imaging in the electron microscope, it was thought that there may have been a stray magnetic field component in the region between the driven poles, of approximately equal magnitude but of opposite polarity to the field

from the driven pole. It was concluded however that, on balance, the observed signal probably arose due to a side writing effect at the driven pole. Thus it is interesting to examine carefully the parts of the images where the upper pole edges are visible. From the images in Fig. 4.3.1.1, the linescans extracted at positions '1' and '5' for the three drive currents are re-plotted in Fig. 4.3.1.3 below. At the upper pole edge there is a contrast peak, which increases approximately linearly with drive current; there is however no clear indication of a corresponding change at the top of the common pole. Nevertheless the presence of a small amount of stray magnetic flux in the vicinity of the upper pole edge is indicated.

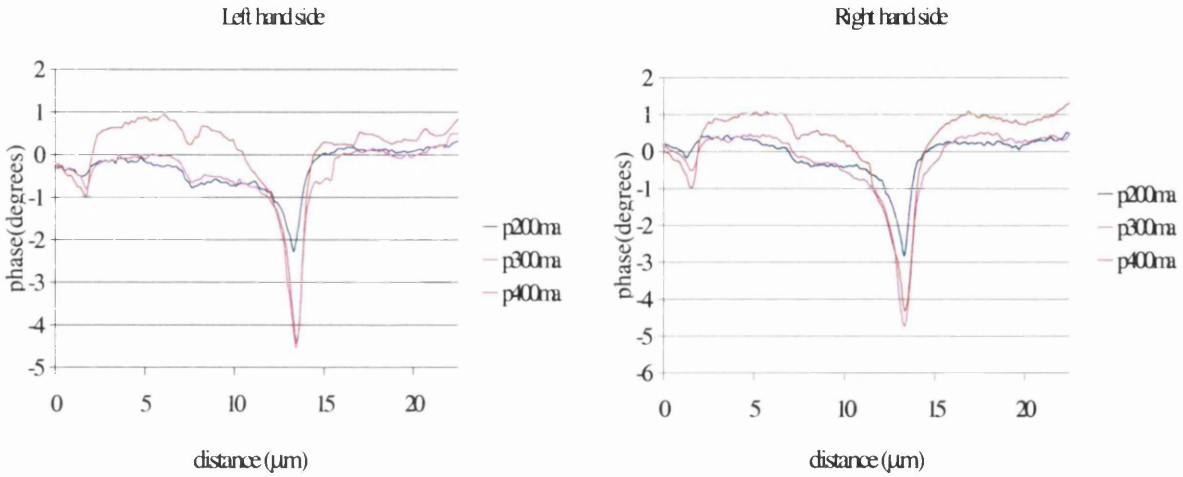

Fig.4.3.1.3 A compilation of line scans taken from the left (position 1) and right (position 5) hand side of the above images in Fig. 4.3.1.1. at the three applied drive currents.

So far we have presented our MFM data as intensity images or as linescans extracted therefrom. Two other forms of presentation are also sometimes useful in visualising the data. The first is to present the data in the form of contour plots of signal level and these are illustrated in Fig. 4.3.1.4. The contour lines around the lower pole and opposite on the common pole edge are very close together indicating that the differential force gradients are very large in these regions. This is to be expected since this pole is being driven.

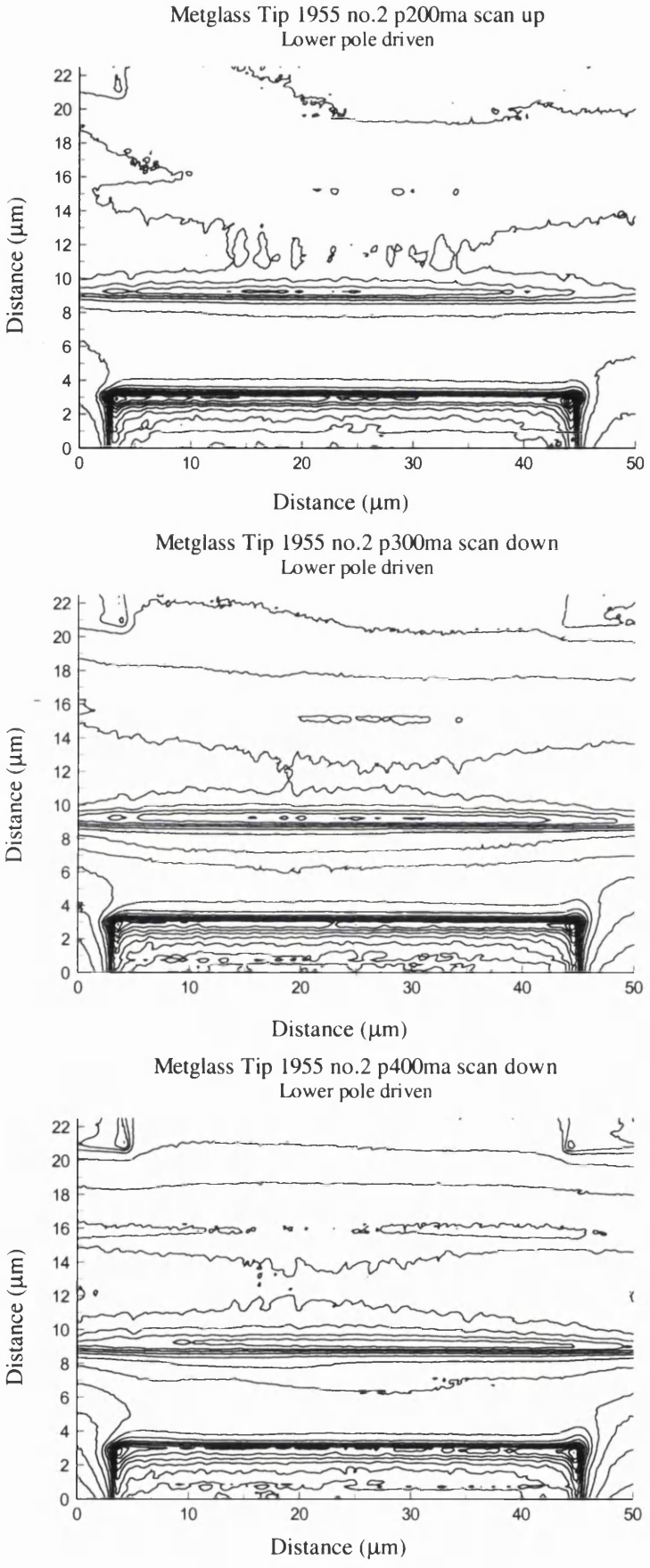

Fig.4.3.1.4 Contour data plots of the Metglas tips response to the magnetic field while being scanned over the area shown in Fig.4.3.1.1.

The contour lines in the top corners of the graph, the position of the upper pole edges, develop as the drive current increases, indicating the presence of stray flux. Ideally we should have extended our imaging to cover the region in the middle between two driven poles to explore this question of stray flux further, but that was not done this time. Another form of data presentation is to show the signal in the form of vertical offset as the raster is scanned down – in SEM imaging this is known as y-modulation imaging. The results are presented below in Fig. 4.3.1.5

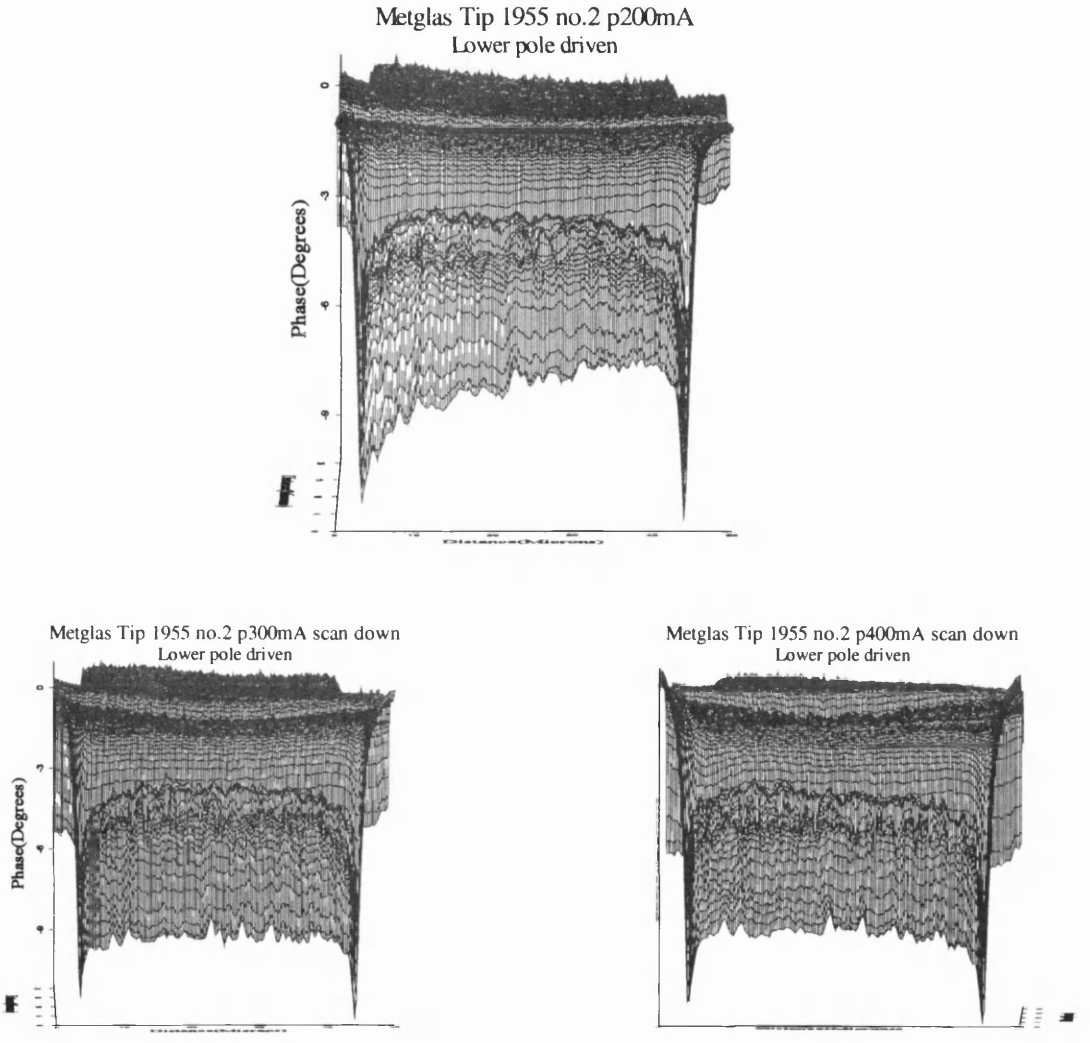

Fig.4.3.1.5 '3D' data plots (y-modulation) of the tip response to the magnetic field while being scanned over the sample area shown in Fig.4.2.1.1. This view was chosen to show the profile of the response over the lower pole.

It is not apparent from the way the data was presented earlier, what is the form of the horizontal variation of the MFM signal along the pole edges. The '3D' plots help us to visualise this, although the overlap between the data for the lower pole edge and from the opposite common pole edge does give rise to some confusion. We therefore separate the data for these two regions and plot them in Fig. 4.3.1.6. It is clear that the MFM signal, particularly at the lower drive currents, is peaked towards the edges of the lower pole, but is the inverse of this at the common pole edge. Given that there is a substantially greater poleface area on the common pole, this is not surprising. Similar field profiles have been seen in fields calculated by finite element methods for model thin film recording heads [3]. We must however stress that the MFM signal is related to the differential of the vertical component of field with respect to the surface normal and we should not assume that the spatial variation is the same as for the field itself.

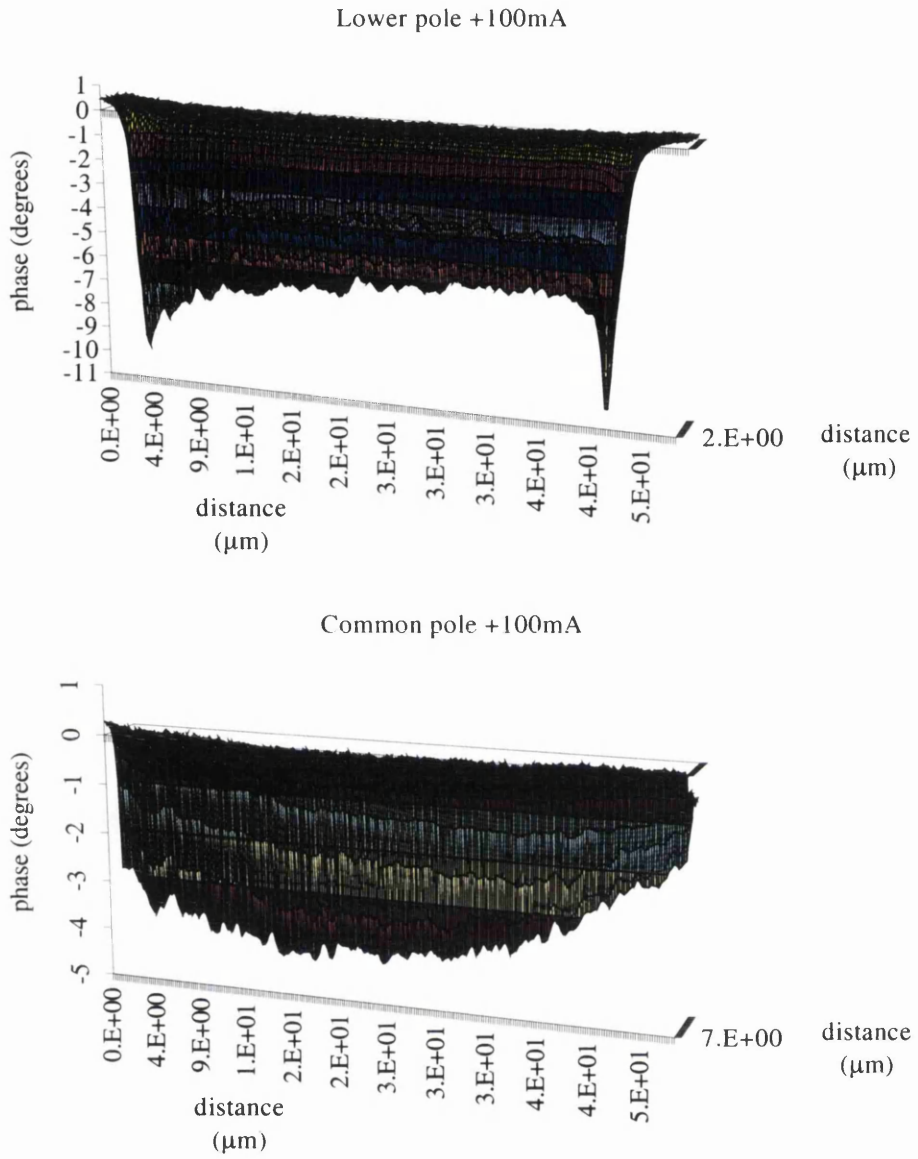

Fig 4.3.1.6 y-modulation images showing the profile of the signal at the two polgap edges for a drive current of 100mA d.c.

The results for the metglas tips may be summarised as follows. The tips are magnetically soft and we get an attractive force signal at both the driven pole edges, that on the lower pole being larger than on the common pole. For the lower drive currents the signals scale in magnitude with the current, but at 400mA heating suggests that the normal derivative of the field there is larger than at the common pole; we will use this fact later to explain the features of the images of the head using hard magnetic MFM tips.

4.3.2 The metal evaporated standard probe (MESP) tip study

The second MFM tip, which we studied in conjunction with the Emboss head, was the DI MESP tip. This is DI's standard/general purpose tip with a CoCr alloy coating; it is a relatively hard tip having a high coercivity. The experimental conditions and the range of drive currents were the same as in the previous study. This time however the polarity of the current was reversed for the images at 200mA and 300mA drive currents so there are "plus" and "minus" images available. For the 400mA drive current only one image was collected, because when the polarity was reversed the 'Z' limit of the piezo was reached due to a large sample/tip interaction. Failure to withdraw the tip from the sample's surface could have resulted in damage to the scanning stage. Once again the lower pole array was driven.

It was mentioned in Section 4.2 that there is a tip/sample interaction even if no drive current is applied and this is illustrated in Fig. 4.3.2.1. The low coercivity of the polepiece material leads to a relatively strong magnetic interaction and the poles are clearly differentiated from the SiO_2 interlayers. It should be noted that there is an equally strong signal from all pole regions including the upper pole.

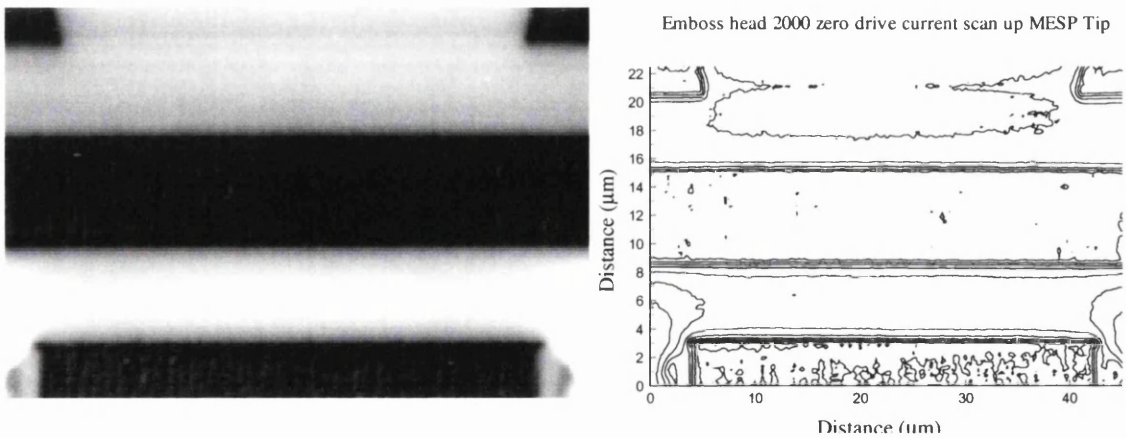

Fig.4.3.2.1 The phase image of the Emboss head with no drive current applied and the corresponding phase contour plot.

In the above image the force gradient is large around all corners of the upper and lower poles, so it is possible that our conclusion that, under drive conditions, there is stray flux emanating from the undriven pole is incorrect. One potential method to resolve this issue

would be to subtract the zero drive current image from that obtained under a particular drive condition; we will explore this possibility in a later section.

We now present the results from the drive current experiments with the MESP tip and the images/linescans are shown in Fig. 4.3.2.2. There are a number of features of these data that must be discussed. The first is the asymmetry in the form of the contrast at the pole edges of the driven head. The results of the metglas tip imaging would have led us to expect to observe, for the hard MESP tip, two peaks of opposite contrast corresponding to the tip experiencing an attractive force on one side of the gap and an repulsive force on the other. We are using the term's attractive and repulsive force for the purpose of describing the results but this relates to positive and negative force gradient respectively. The peak corresponding to the attractive force is well defined, but that for the repulsive force (white contrast) is not; this holds true for both +ve and –ve drive currents.

At a drive current of +300mA another feature begins to appear at the lower pole edge and that is a fine dark line, indicated by the 'tip switched' label; this phenomenon is even more pronounced for the +400mA case. The reason for this effect is 'tip switching', where the magnetisation of the tip, which should be aligned along the tip axis direction, is switched in whole or in part by the strength of the (opposite sense) field from the head. This would be expected to occur only for the attractive force case and that is borne out by these data. We cannot however rule out that some form of change in the magnetisation did not occur at lower drive currents for regions where the force is repulsive. This could explain the unexpected form for the 'white' contrast peak discussed earlier, particularly if the supposition that the head field gradient normal to the TBS is larger at the lower pole than the common pole is correct. In these circumstances it is not possible to draw any conclusions on the magnitude of the observed contrast and the reasons for it. We can however note that there is again evidence for a small amount of stray magnetic flux at the undriven upper pole edge.

Another feature of the images in Fig. 4.3.2.2 is the contrast banding across the images. There are three possible explanations for this. The first is that it is caused by the tip-switching discussed above. The second is that the contrast arises from new topographic features, which are evolving as the tip is continuously scanned across the specimen and

finally that the tip has picked up some debris from the specimen altering its imaging behaviour.

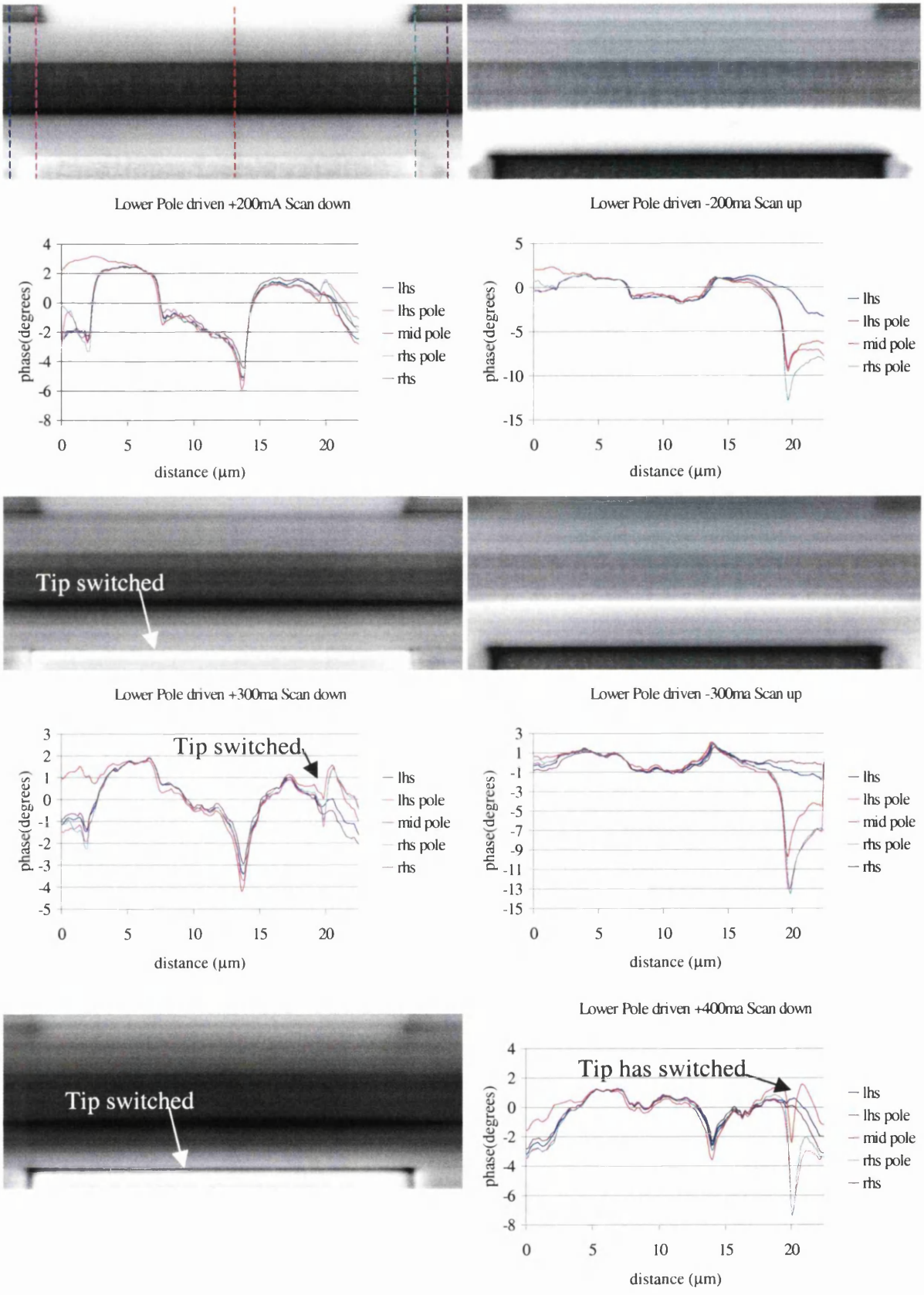

Fig.4.3.2.2. The images acquired with the MESP tip and their corresponding peak profile linescans. For the first two drive currents the linescans are immediately below the image, for the 400mA case they are to the right.

Before the start of the imaging studies with the MESP tip, a reference image of recorded tracks on a hard disk specimen was obtained and this is shown in Fig 4.3.2.3a below.

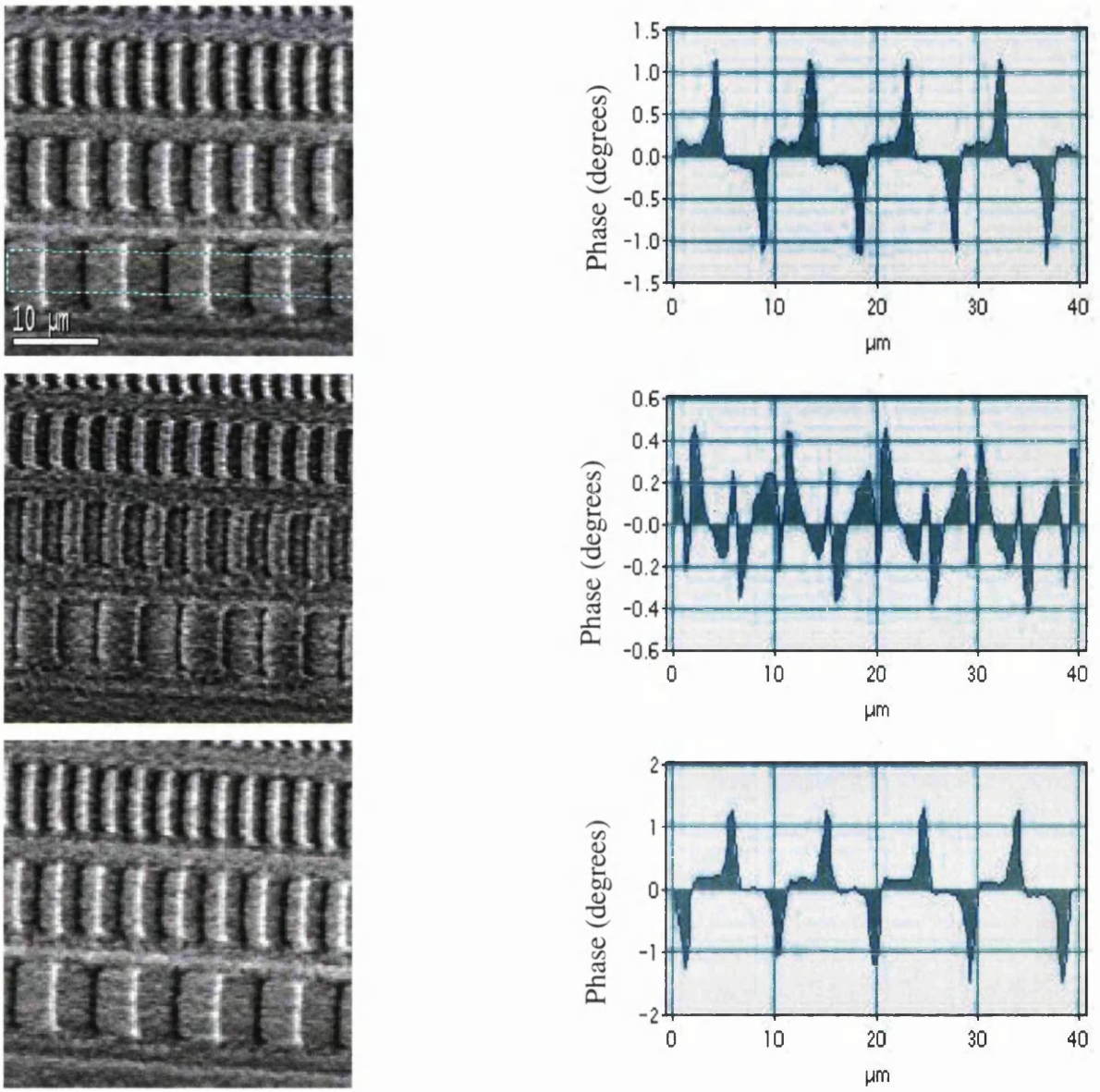

Fig 4.3.2.3 Images of a hard disk sample used characterise the MESP tip. The first image was taken at the start of the experiment, the second at the end and the third after the tip had been re-magnetised and returned to its "normal" state. There is no obvious loss of resolution in the last image due to a "dirty" tip.

The image of the same hard disk specimen taken after the experimental study of the Emboss head is shown in Fig. 4.3.2.3b and it is clear that the contrast features of the written bits have changed dramatically, indicating that the magnetic state of the tip has

altered significantly. In fact the observed contrast does indicate that there is now a component of tip magnetisation normal to the tip axis. Confirmation that the imaging resolution of the tip had not changed is given by the image of the hard disk tracks shown in Fig. 4.3.2.3c, which was taken after the tip had been re-magnetised along its axis in a field of 0.75T. There is no dramatic difference between the initial and final track images indicating that the changes in tip magnetisation, induced by the Emboss head field, are not irreversible provided the aligning field is strong enough.

The conclusions, which we can draw from our imaging studies with the MESP tip, are threefold. Firstly, although the tip is classed as magnetically hard, it is not hard enough to remain unchanged when imaging the Emboss head with drive currents as low as 200mA. Secondly, when specimen/tip interactions are strong, interpretation of MFM images is at best difficult and certainly there is no hope of extracting quantitative data on the nature of the head field under investigation. Lastly, the changes in the tip imaging characteristics could lead to contrast features, which are misinterpreted as arising from changes in topography. Finally we could in our imaging studies have raised the lift height in the Tapping Mode – inevitably this would have reduced the adverse effects of the tip/specimen interaction. However the Onstream tape file is a contact recording system so we must aim to characterise the head field as close as possible to the TBS.

4.3.3 The Cobalt Tip Study

A cobalt-coated tip prepared in the Department was studied next; the cobalt was evaporated on to the bare silicon tip structure, the estimated film thickness being 50nm. The tip was expected to be comparable in hardness to the DI MESP tip and this was confirmed experimentally. In particular, similar tip magnetisation switching effects were observed when the head drive current was 300mA and these are illustrated in Fig. 4.3.3.1 (this was the highest drive current used since the tip imaging characteristics altered substantially at this point and the tip appeared to have suffered damage).

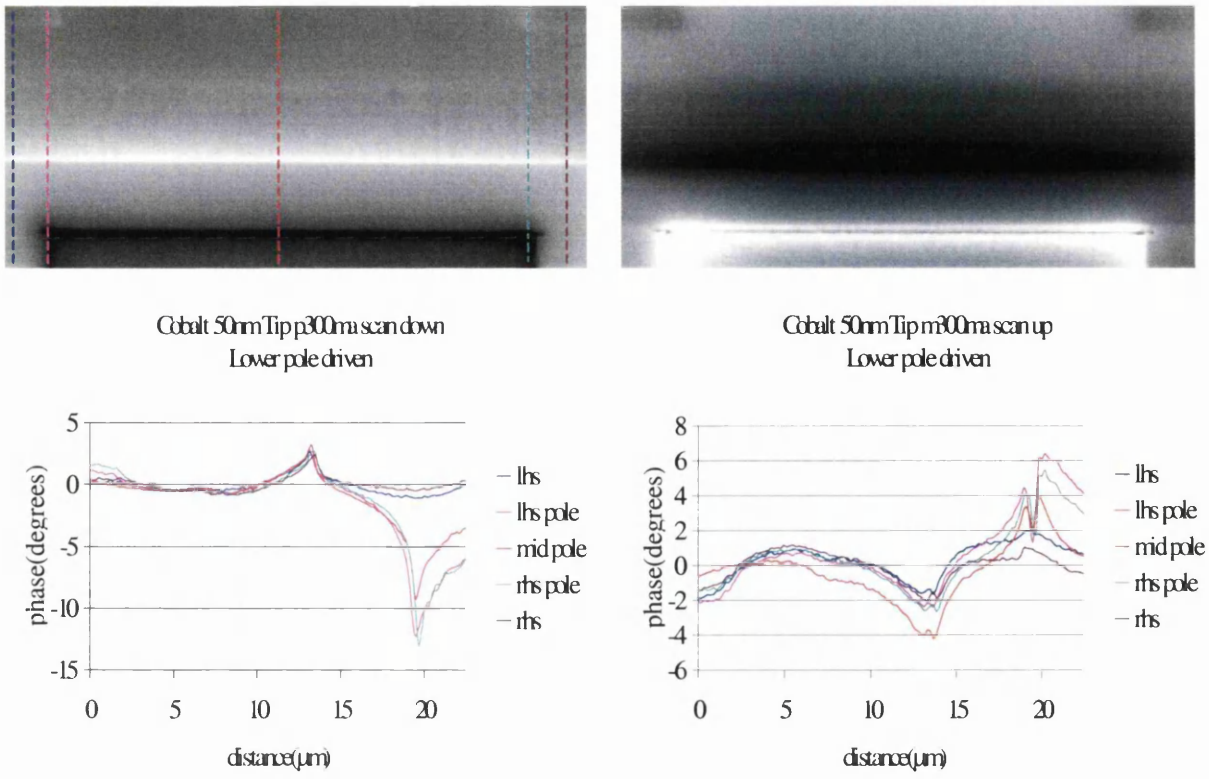

Fig.4.3.3.1 The images and linscans obtained using the cobalt coated tip.

In this pair of images the lower pole array was again driven. For the +300mA case, unlike the MESP tip images, the bright contrast at the lower edge of the common pole is quite sharply peaked i.e. the form we would anticipate. The contrast at the edge of the lower pole is similarly sharp and greater in magnitude; this is consistent with previous observations. When the drive current was changed to –300mA, significant tip switching occurs at the lower pole edge, where the force is attractive. The fact that tip switching is not obviously apparent in the image for the +300mA, does indicate that the field gradient normal to the TBS is smaller at the common pole than at the lower pole as suggested previously. These results indicate that the coercivity of this tip is probably somewhat harder than for the MESP one. It should also be noted that there are no contrast banding effects visible in these images suggesting that the contrast seen in the MESP case was an artefact.

4.3.4 The low coercivity tip study

The final MFM tip studied in this sequence was a low coercivity type supplied by DI; in this case the magnetic coating was permalloy of unknown thickness, but anticipated to be very soft magnetically. To prolong the tip's operating lifetime, a relatively low drive current was used in this investigation. In separate experiments both the upper and lower pole arrays were driven, to see which if any caused stray flux leakage at the corresponding undriven pole. The images were taken at ±200mA. Both images are presented to show that the shape of the pole affects the magnitude of the contrast and to try to establish the influence of drive current direction on stray flux leakage at the undriven pole.

One possible way to confirm the presence of a stray field at the undriven pole would be to take an image with zero drive current and compare the magnitudes of the signals to those taken from images when the head was driven. Unfortunately when no drive current was applied to the head and an image acquired, the quality was very poor, but did indicate a phase jump at the lower pole edge of ~0.2 in phase magnitude and we will use this value later in our analysis.

First the results for the upper pole array being driven are presented in Fig. 4.3.4.1. The letters in the top left-hand image indicate the point where the tip passes over a pole and the letters 'A', 'B', 'C' and 'D' correspond to the letters on the graph below e.g. the point 'A' is on the bottom edge off the upper pole and corresponds to point 'A' on the graph blow. The 'X' is to highlight the overlap of scan area between the separate images centered on the middle of the upper and lower poles

The results obtained are interesting. The first thing to note is that the tip/field interaction should always be attractive. At -200mA the magnitude of the minimum signal at the middle of the upper pole edge is slightly greater than at the corresponding minimum at the common pole edge. The situation is similar when +ve drive current is applied, although in this case the difference between the two minima is larger. If our supposition that the field gradient normal to the TBS is somewhat greater for the lower pole, then this would imply that we may still have a degree of magnetic hardness in the tip coating and we are seeing the influence of partial tip switching.

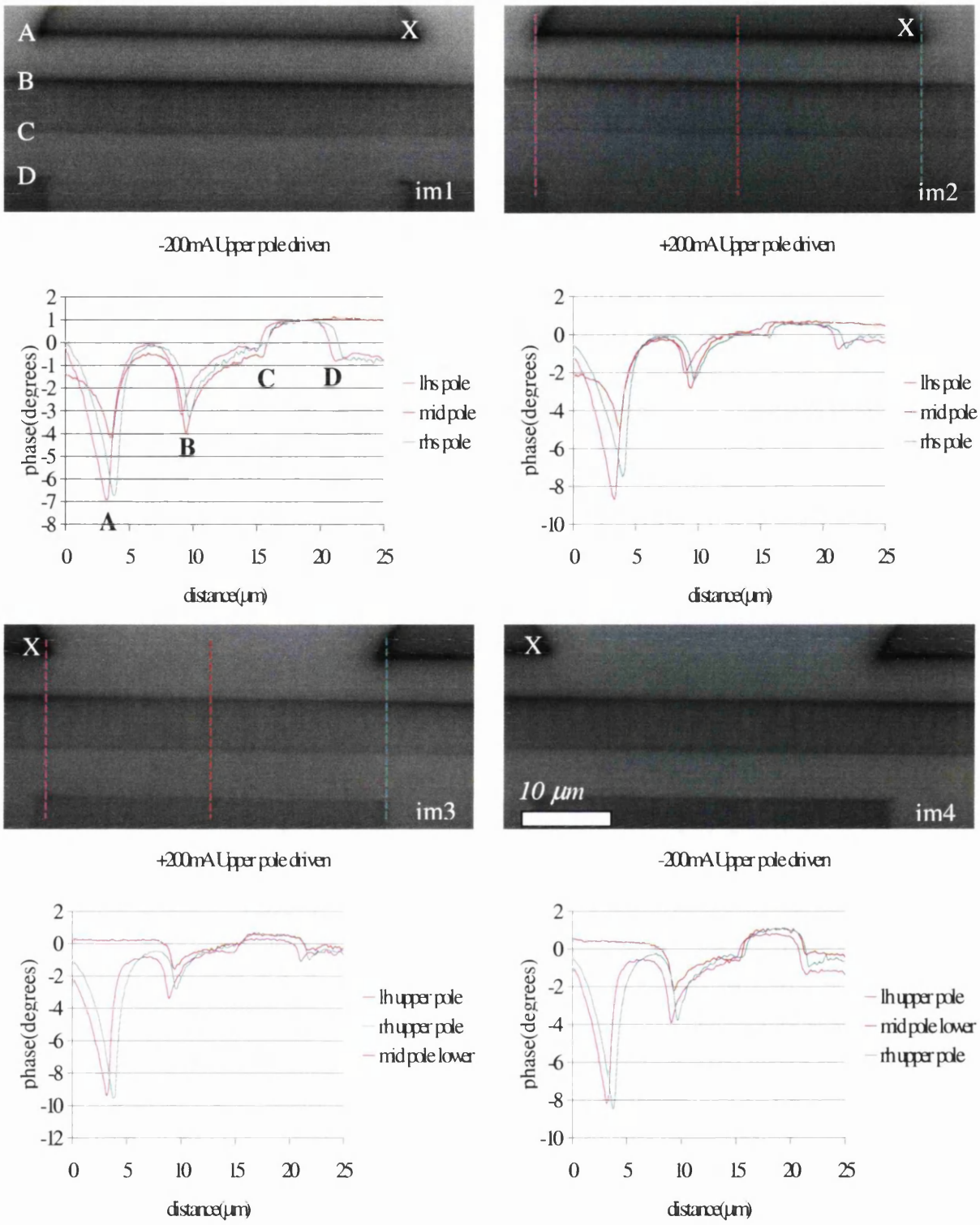

Fig.4.3.4.1. Images and linscans for the case where the upper pole is driven. For the top image pair the area is centred horizontally on the middle of the driven pole and for the bottom pair it is centred horizontally on the middle of an adjacent lower pole.

When the bottom pair of images are analysed it is clear that there is a local contrast minimum along the whole of the top edge of the common pole and hence there is stray field present. This is perhaps clearer in Fig. 4.3.4.3, which is a compilation of relevant linescans from the full image set. Fig. 4.3.4.2 indicates the positions from which the linescans were taken. The legend of the graphs below indicates the image and position from which a linescan was extracted e.g. im1 p1 corresponds to im1 in Fig. 4.3.4.1. and p1 is as indicated in Fig. 4.3.4.2. There is no evidence for any significant contrast dip at the bottom edge of the common pole (position C) and hence any field component will be at best very weak. If the linescans at the edge of the undriven pole (position D) are considered there is an indication of a small dip indicating a small stray field is present. It should be noted that peak value of contrast at the lower pole edge with zero drive current was ~-0.2 and for corresponding positions in these images the values are around –0.8.

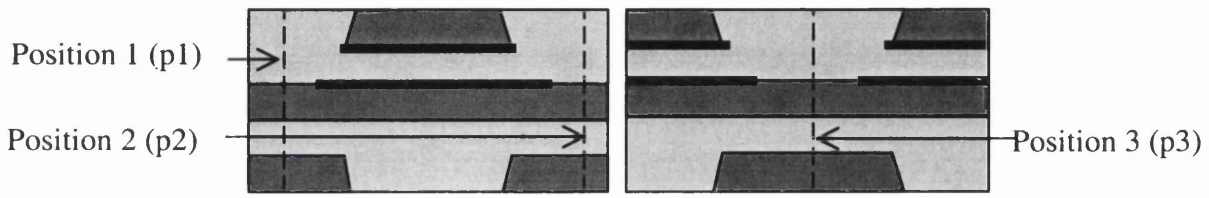

Fig.4.3.4.2 Schematic showing the positions from where the linescans were extracted for the graphs in fig. 4.3.4.3. The "field" shown as thick black lines in the above schematic does not fall to zero in the actual image.

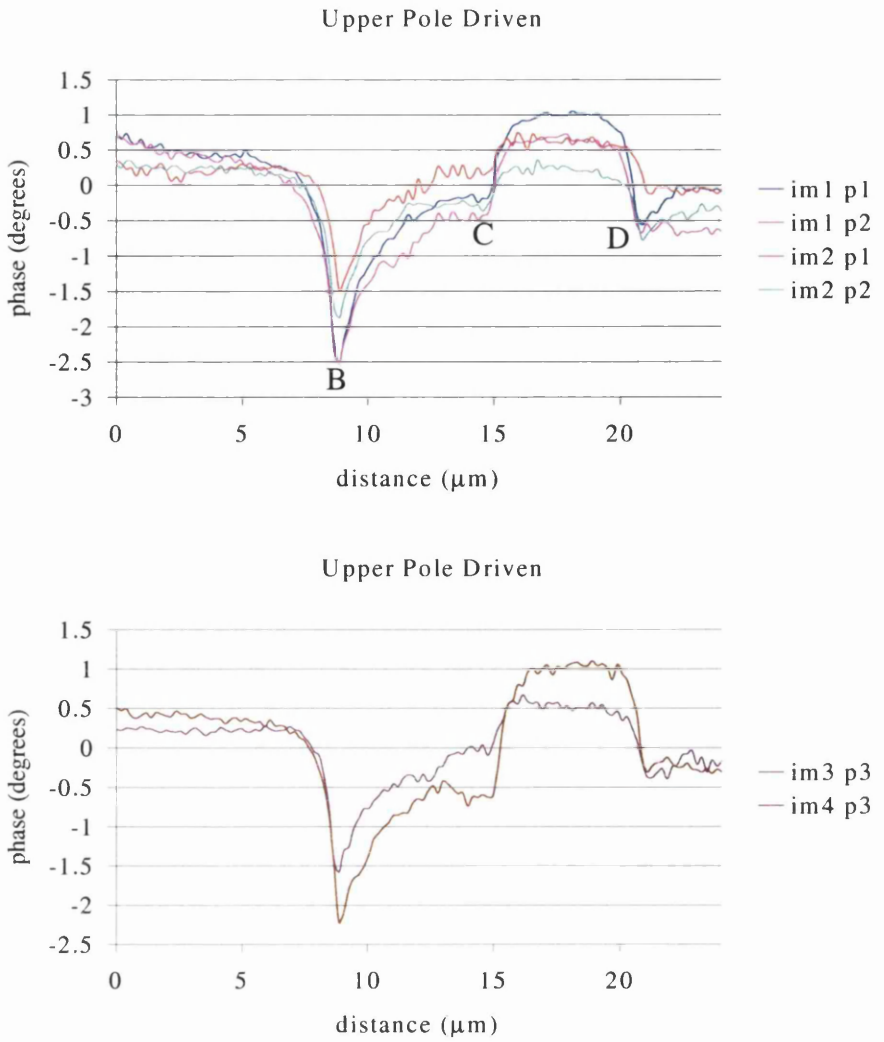

Fig. 4.3.4.3. The linescans from all the graphs extracted at positions where the driven pole has least influence on the tip. These linescans never pass through the driven upper pole. 'B' is on the common pole on the side of the driven pole etc.

Next the results for the second case, where the lower pole array is driven, are presented. The images and linescan data are shown in Fig. 4.3.4.4; in this case there was no initial zero current image, although it would have been expected to be the same as at the beginning of the study. The letters on the diagrams have the same meaning as before.

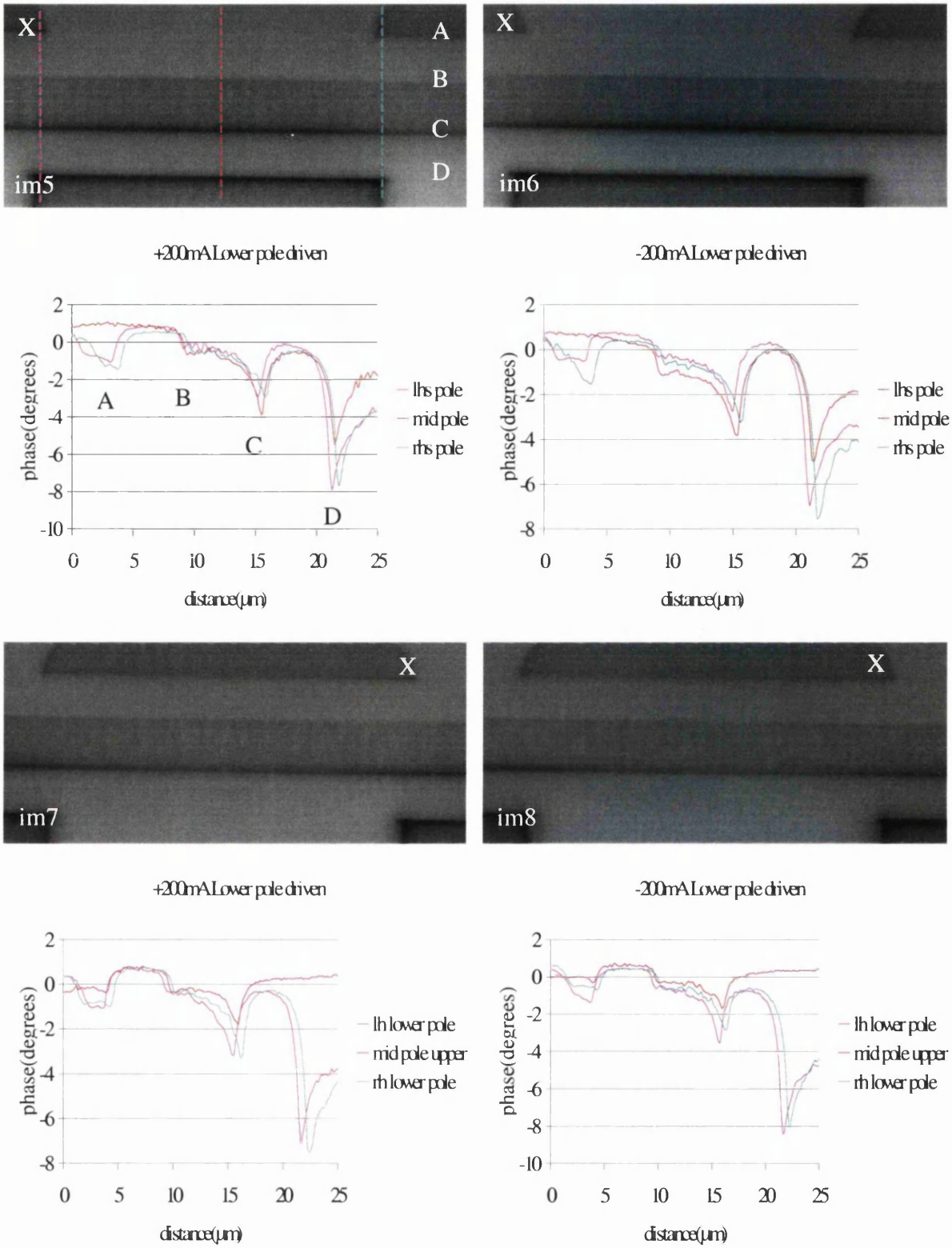

Fig. 4.3.4.4. Images and linescans for the case where the lower pole was driven.

It is noticeable that in the top image pair the ratio of the two contrast minima at opposite edges of the gap for the driven head are approximately the same for both +ve and –ve drive

currents. This is unlike the case where the upper poles were driven and supports the proposal that the field gradient is greater on the separate pole than on the common pole. It also suggests that in this case the tip is not exhibiting any hard magnetic chracteristics. However the geometries of the upper and lower poles are not the same and hence the forms of the respective magnetic fields may differ; we would need a much more extensive study to settle the issue. It should also be noted that there is a local minimum along the whole of the bottom edge of the common pole, indicating that the stray field there never falls to zero. The question of stray flux from the region of the undriven pole gap is again examined by plotting in Fig. 4.3.4.5 the linescans from positions where the field from the driven pole should have least influence on the tip.

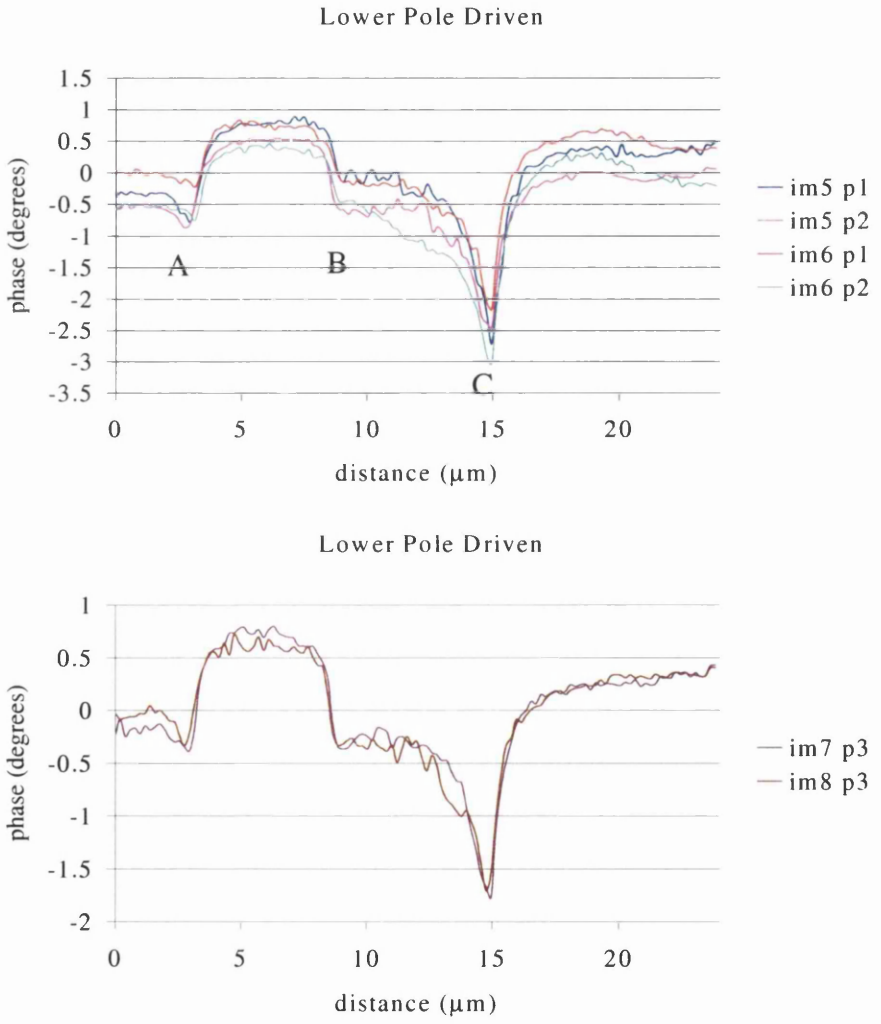

Fig. 4.3.4.5 The linescans extracted at positions where the driven pole has least influence on the tip. In the first two images Fig. 4.3.4.1, p1, p2 correspond to the extreme left and right hand side of the images respectively. In the last two images (im7, im8) the linescans were extracted midway between the two driven poles.

For the above case it is not so obvious what is happening in the areas outwith the immediate vicinity of the driven poles. In the middle of the undriven pole the signal - the bottom graph above - the signal strength from the undriven pole is comparable with the value of –0.2 obtained with zero drive current. Once again there is evidence of some stray flux at the corners of the undriven poles.

Contour maps of the MFM signal for a drive current of –200mA are shown in Fig. 4.3.4.6a,b for the head regions under investigation. The strong tip/field interaction in the vicinity of driven pole is clear, the contour lines being closely packed. On the other edge of the common pole the contour lines are not close together and are not as curved. This suggests that there is either no field or only a very small field in this region of the head. In the second graph in both figures, the two red circles highlight a region where the contour lines due to the field decrease in density. This suggests that there is only a relatively small field in this region of the head structure. In the last chapter it was suggested that the field from any given pole would retain a significant magnitude only up to a distance from the pole edge approximately equal to the pole gap. For this sample the gap is ~5μm and the centres of the two red circles are at this distance from the driven poles. In both cases the undriven pole has very few contour lines around it and they are not closely spaced; this suggests either very low or no field present and the contrast which is visible arises largely from the pole material coercivity.

The type of head we have just discussed was a first generation design and no longer in production. The basic design principles however remain for the heads now in production. The main reason for the study was to solve the mystery of the stray field observed in the DPC studies of the head; the mystery can now be regarded as solved to a high level of probability i.e. the observed DPC contrast in the space between adjacent write poles is a side-writing effect.

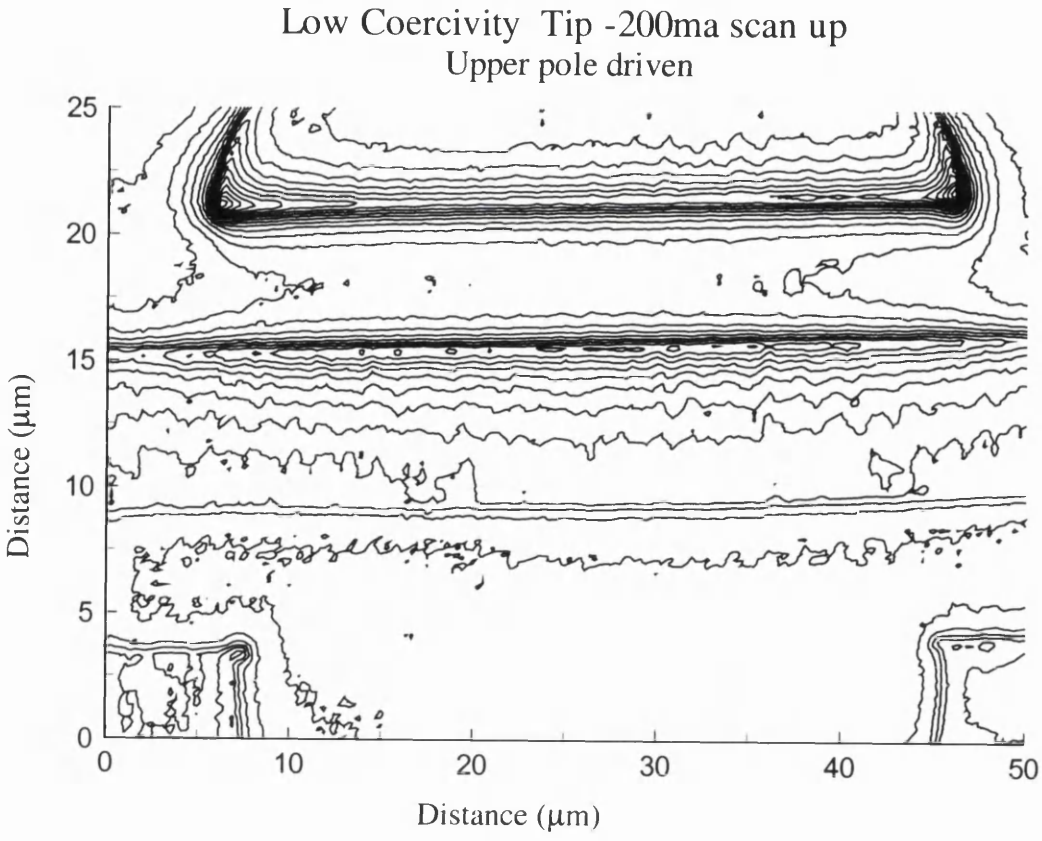

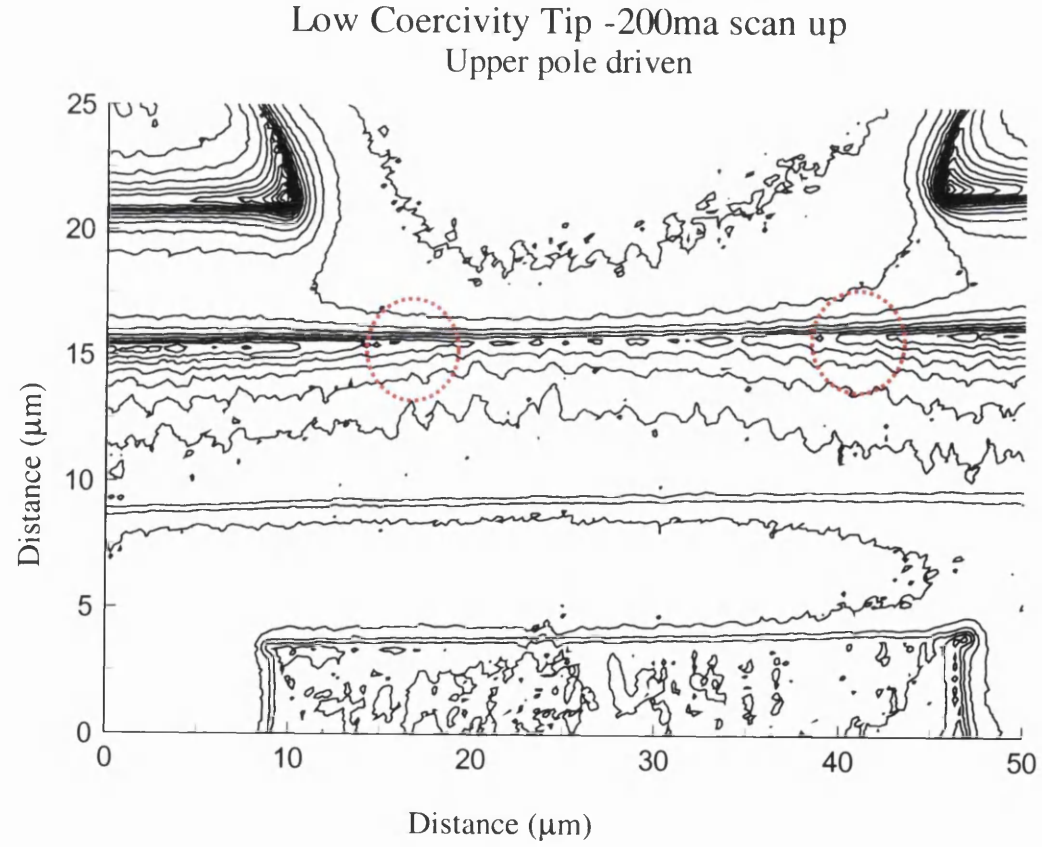

Fig.4.3.4.6a Contour plots for the upper pole driven at –200mA d.c..

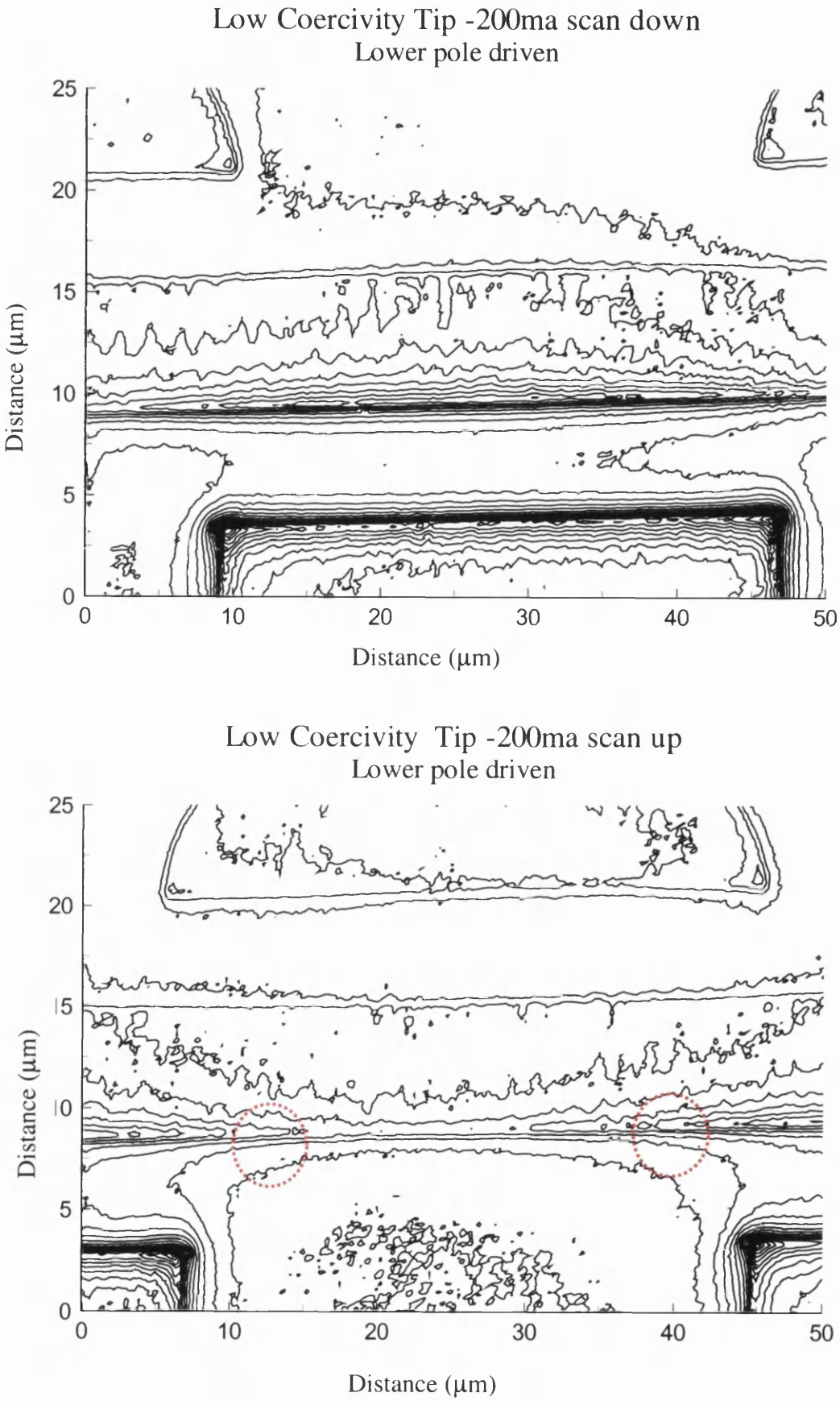

Fig.4.3.4.6b Contour Plots for the lower pole driven at –200mA D.C.

4.4 An MFM study of a prototype Emboss head

The second sample studied by MFM was a prototype Emboss head supplied by Onstream. In the relevant tape file the operating current range was similar to the previous sample viz. 400mA. Due to the problems encountered in the previous investigation with tip switching effects at high drive currents, it was decided to start this investigation at much lower head drive currents and then gradually increase the current up to the maximum value. This would enable the sample/tip interaction to be studied more closely and to build up a clearer picture of the tip's behavior.

Once again a number of different types of tip were used to enable a comparison of their usefulness for the study of this new tape head. Also considered in this section is the effectiveness of subtracting images to remove the "background" noise from the undriven parts of the head and hopefully to isolate from the contrast the contribution of the stray magnetic field to the signal. In addition a larger area of the head was studied to allow us to comment on the reproducibility of the field characteristics of neighbouring heads. The first optical image (Fig. 4.4.1) shows the region of the head studied and the Cartesian coordinate system used in the description of the head field. The dimensions of the poles and pole gaps are given in Table 4.4.1.

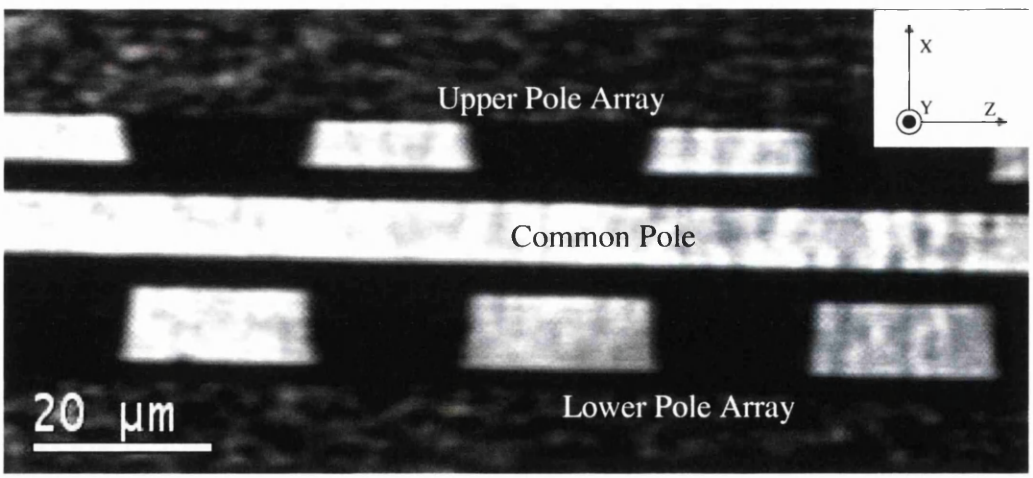

Fig 4.4.1 An optical image of the section of the Emboss head under investigation.

Table 4.4.1 Pole Dimensions

	Length (μm)	Width (μm)
Upper Pole	17.8	5.1
Upper Space	19.3	
Upper Gap		3.5
Common Pole		6.8
Lower Pole	20.1	8.1
Lower Space	18.1	
Lower Gap		3.5

4.4.1 The drive current experiments with the standard DI MESP MFM tips

Instead of driving the head at its higher operating current range immediately and getting tip switching problems, it was decided to start at a much lower value and gradually increase the current value. We anticipated this would give a meaningful insight into the tip sample interaction and aid in the interpretation of images taken at higher applied currents. The current direction was reversed for each current value selected, so in all cases there is a 'positive and 'negative'; image. Only the lower pole array was driven for this experiment and a single pole was selected within a scan area of $40\mu m^2$. The lift height was again 100nm as this had been used in the previous experiments. The drive current was to be increased in 50mA increments from a starting value of 50mA. Due to the large number of images in this section, they will be discussed in groups of four, with a summary of the findings presented at the end of the section.

A zero drive current image was taken to give us a benchmark with which to compare the magnitude of the signals under drive conditions and this is shown in Fig. 4.4.1.1. The image will be used in the next section in the investigation of image subtraction to remove the background due to the tip's interaction with an undriven pole. It is clear from this image that there is a strong tip/sample interaction in the pole regions due to the permeability of the head magnetic material, the tip/specimen force being attractive. There is an apparent difference in signal level between the common pole and the lower pole but this arises because of the general phase gradient down the image, which we have discussed earlier. When this is taken into account there is probably no problem.

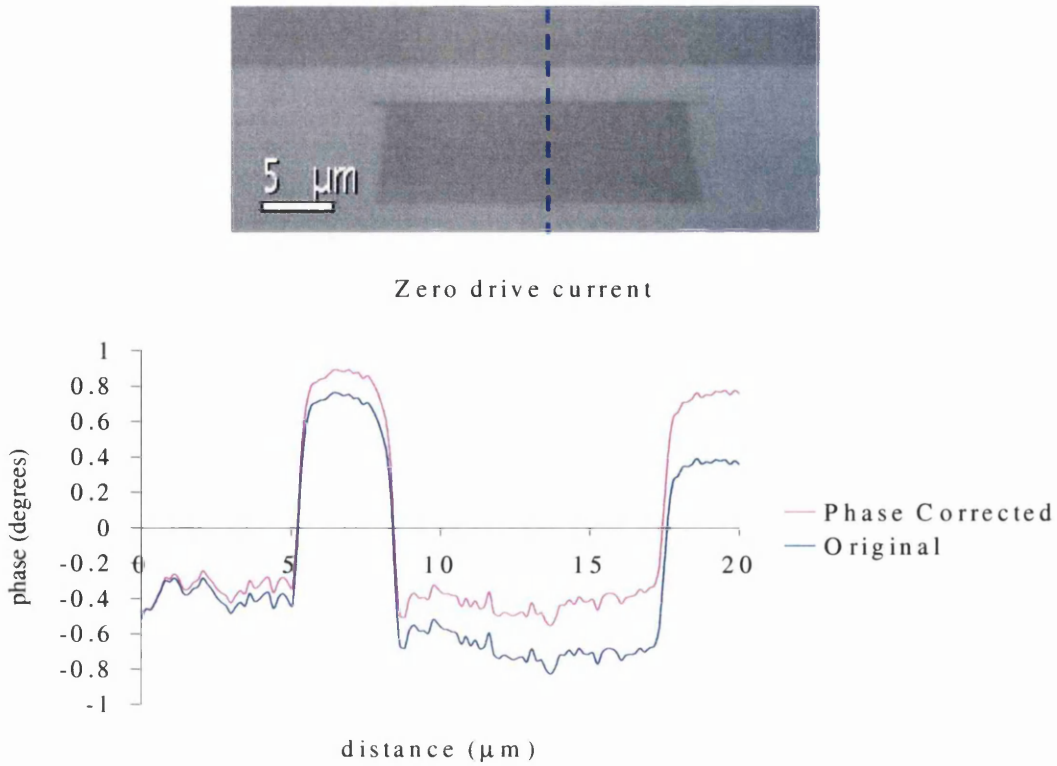

Fig 4.4.1.1 A phase image of an undriven pole and the corresponding linescan extracted from the position indicated in the image. Even with no applied current there is a phase signal of ~0.5 degrees from the poles. The "pink" linescan has had the phase gradient removed.

The images and graphs for cases where the lower pole is driven are presented in Fig. 4.4.1.2a, b, c. There are images for both positive and negative currents and the graph immediately below an image refers to that image.

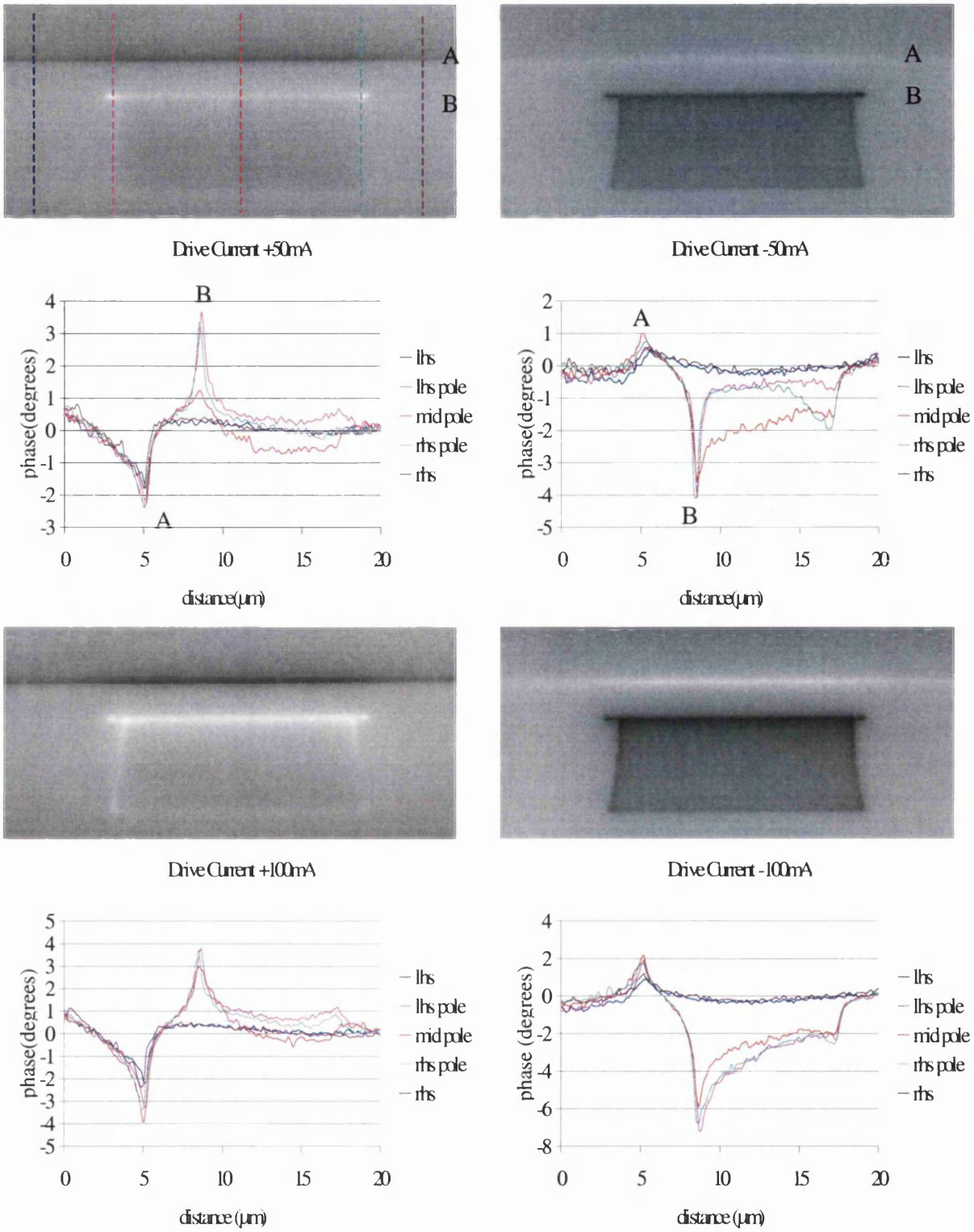

Fig 4.4.1.2a Images and corresponding graphs from the lower pole taken at ±50 and ±100mA D.C. The coloured lines in the first image indicate the position of the corresponding linescans in the graphs. 'A' and 'B' indicate the horizontal pole edge on the images and match up the peaks in the graphs to the image.

The profiles of the linescans for a positive drive current are as one would expect, dropping from approximately zero phase to a peak, rising sharply to zero, then reversing in polarity to a peak of approximately equal magnitude then falling rapidly to zero. For the negative drive current images the peaks at the pole edges are of differing magnitudes; that for the common pole being significantly smaller than at the lower pole. A similar effect was observed at the higher drive currents in the previous study. When the head is driven at +50mA, there is a very considerable asymmetry in the signal along the lower pole edge. It is approximately three times larger in the immediate vicinity of the corners than over the remainder of the pole and twice as large in magnitude as the minimum on the common pole; this asymmetry is largely absent when the drive polarity is reversed, (see fig 4.4.1.3).

In the next two images, the applied drive current is 100mA and the signal strength from the head would be expected to double. However it is the tip interaction with the sample that is recorded and the relevant parameter is the field gradient normal to the surface; hence we cannot just assume that the phase magnitude will scale linearly with field strength.

At +100mA the negative peaks are indeed approximately twice as large as those at +50mA. For –100mA drive current the maxima and minima are approximately twice their value at -50mA drive and the large difference in magnitude in peak size scales approximately linearly.

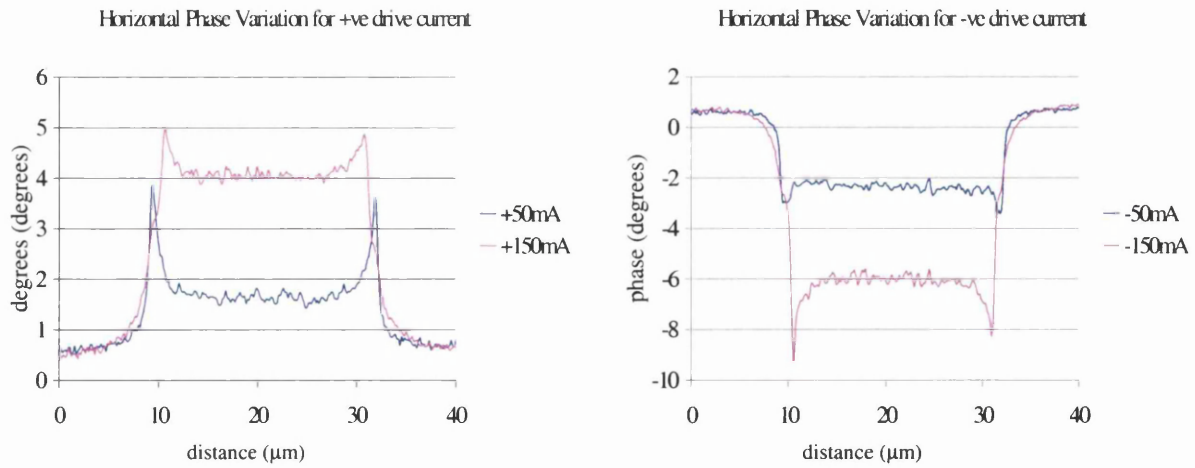

Fig.4.4.1.3 Line scan profile along the upper edge of the lower pole.

The next set of images are at higher drive currents of 150 and 200mA; the images/graphs are shown in Fig. 4.4.1.2b. With the drive current increased to 150mA, we begin to observe changes in the profiles of the linescans.

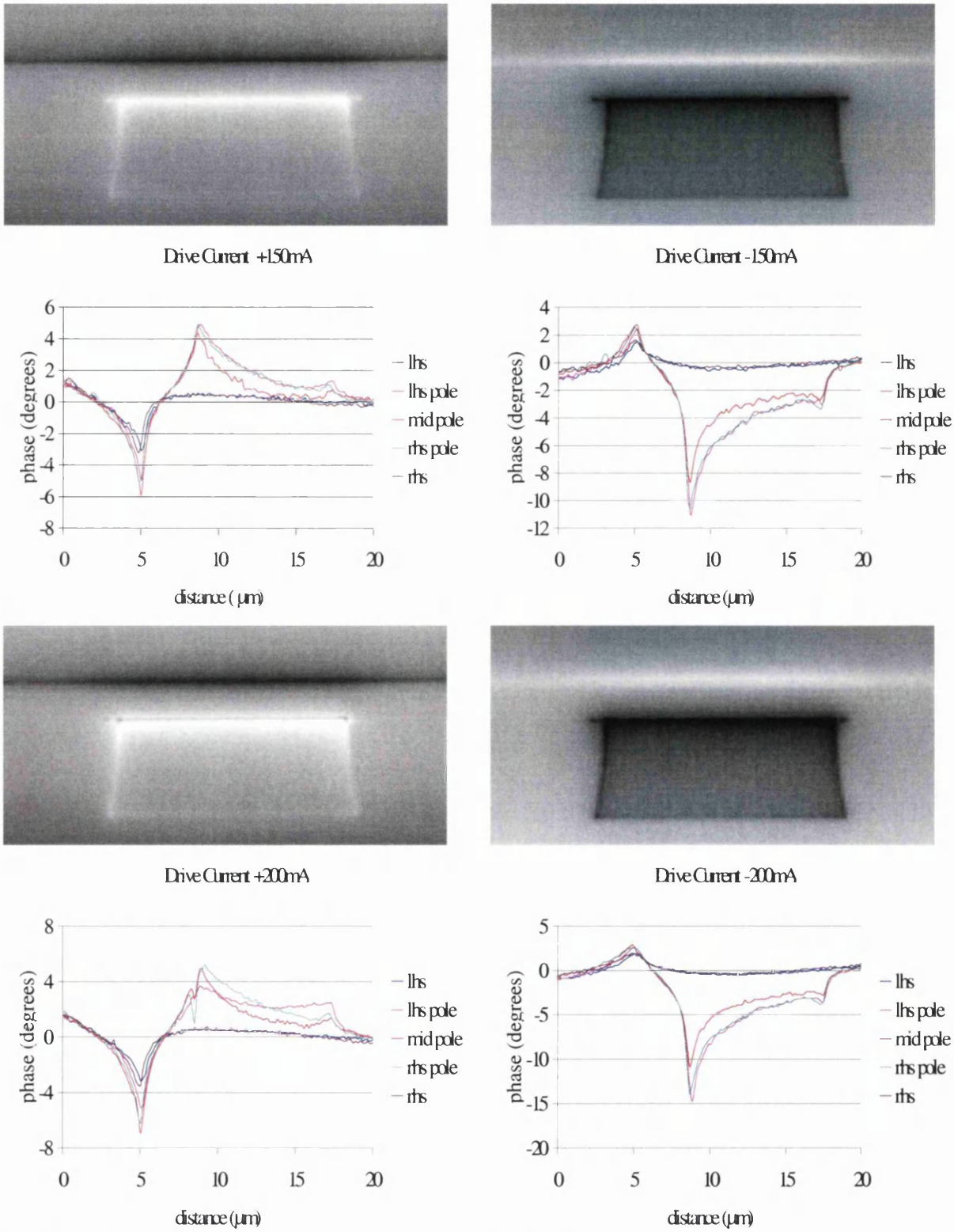

Fig 4.4.1.2b Images and corresponding graphs from the lower pole taken at 150 and 200mA d.c.

At +150mA, the magnitude of the negative peak is slightly larger than the positive peak. At the centre of the pole the magnitude of the negative peak is approximately three times as large as the same peak in the first graph for +50mA; the same is true for the positive peak. At the pole corners however the signal is now approximately the same as at +50mA and along the lower pole edge the contrast is now much more uniform. At –150mA drive current the linescans are similar in form to those at –50mA, but the increase in magnitude is less than a factor of three. In the pair of images taken at ±200mA there is clear evidence that the stray magnetic field from the head is switching the magnetisation of the tip. This occurs first for the +200mA drive and at the lower pole. The characteristic thin dark line in the middle of the white contrast indicates a change locally to a smaller repulsive force and in the linescan a dip in signal magnitude is evident. There is no obvious sign that tip switching is occurring for the negative drive case, i.e. there is no indication that the field from the head is changing the tip's response.

The final image/graph set is for the drive currents of ±250mA and ±275mA and these are shown in Fig. 4.4.1.2c

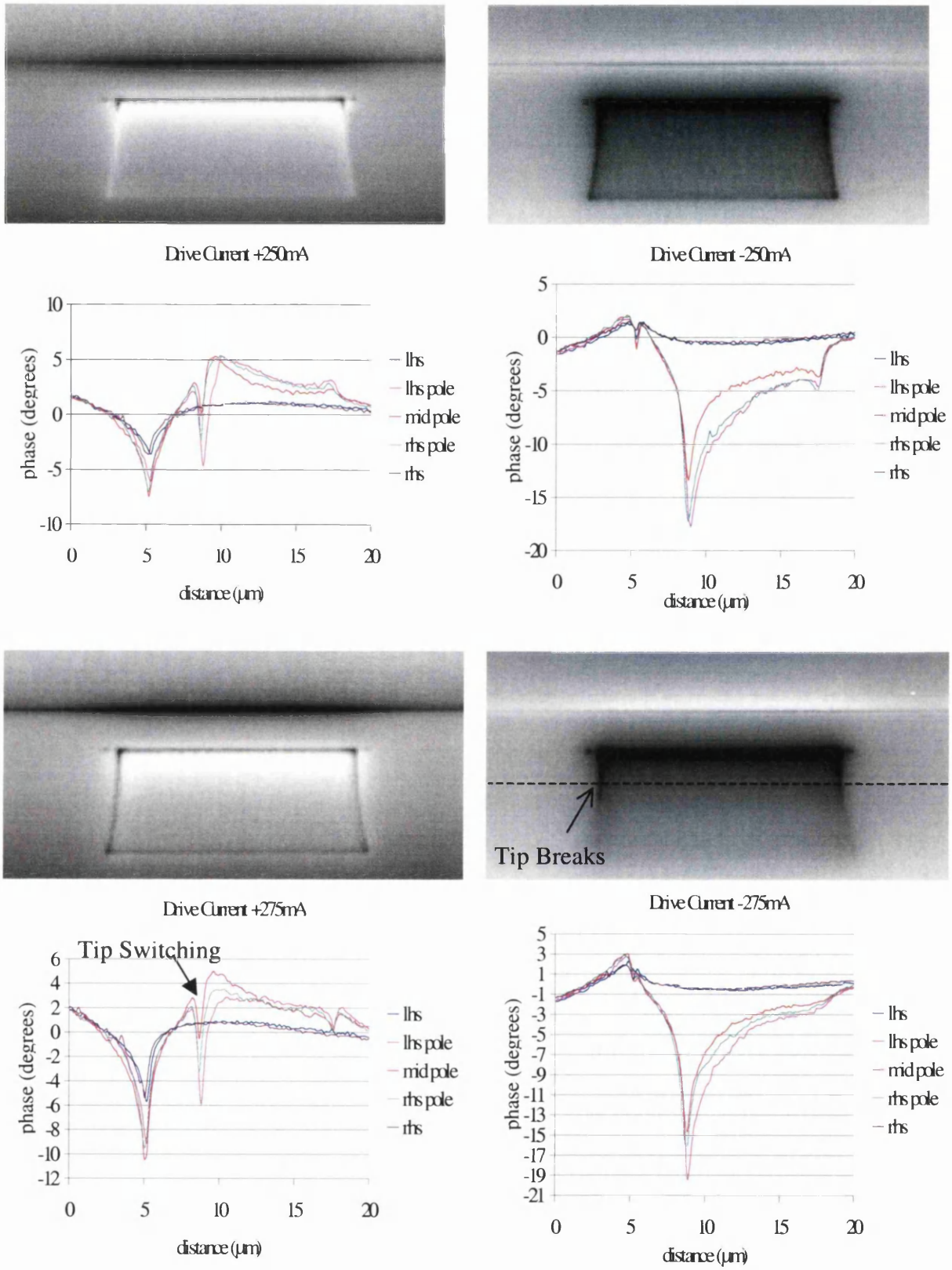

Fig 4.4.1.2c Images and corresponding linescan graphs 250mA and 275mA d.c. The single headed arrows in two of the images and graphs on this page highlight the position where the tip is switching.

When the drive current was increased to 250mA the tip was switching at the lower pole for positive current and at the common pole for negative current. In fact for the negative drive case the positive peak of the linescan extracted vertically from the middle of the lower pole has become slightly negative. There is also evidence that stray flux is now more prominent at the vertical edges of the lower pole. In the final pair of images for 275mA drive current the tip is switching at all the edges of the lower pole, which is now outlined in dark contrast. Whilst the last image at –275mA was being taken the tip was broken and this is indicated on the image. Tip switching at the common pole edge is however visible. This means that the tip's direction of magnetisation may be changing. Thus indicating that the field from the head is changing the tip's response characteristics, which is not desirable. Ideally the tip's response should be unaffected by field from the head.

The results of this study were analysed by plotting in Fig. 4.4.1.4 the maxima and minima for each of the linescans through the centre of the lower pole (the red line in each of the previous set of graphs). To aid comparison of the behaviour, we plot the modulus of the phase value and hence we can compare data using a single graph. Where obvious tip switching was present, we have interpolated the values by adding the half magnitude of the negative going part to that before the change in slope; these points are marked by a square of the same colour as the line. By 'removing' the deviations from the expected tip response it was hoped would give a truer insight into the tip's response to the field from head as a function of applied drive current.

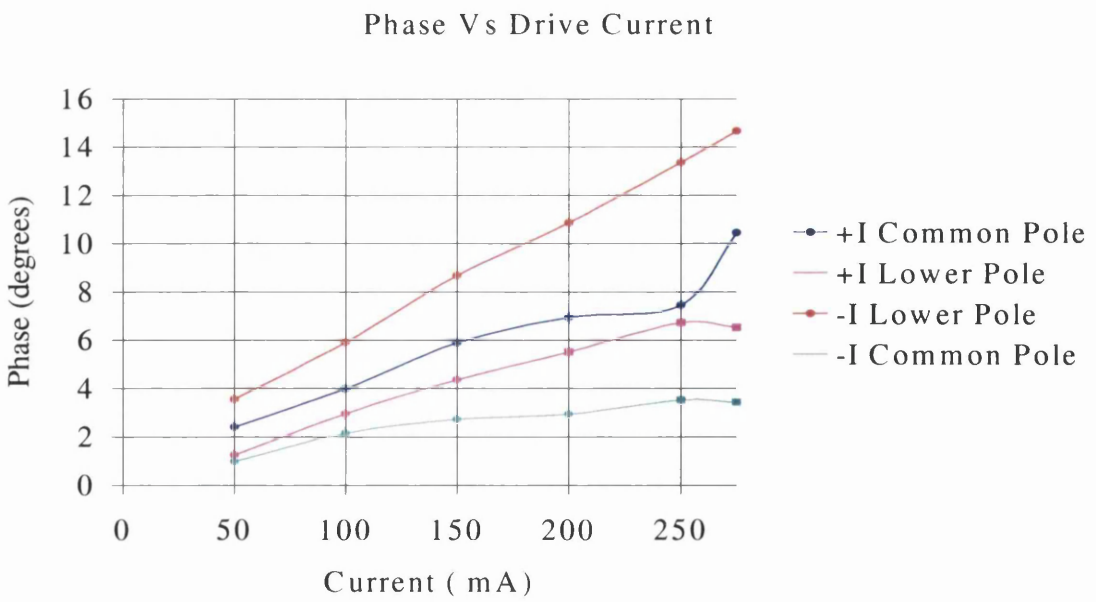

Fig.4.4.1.4 A comparison of applied current versus phase.

A number of observations can be made on the form of these graphs.

1) Apart from the values for the minima at positive drive currents of 200mA and 250mA, which must be regarded as anomalous, the phase values of the maxima/minima show a similar trend as a function of drive current. There is an initial linear increase in amplitude up to ~150mA and then a relatively slow fall off in gradient thereafter. It should also be noted that two of the curves projects back to a value ~-1.0 in phase at the origin (the contrast measured at zero current), the other two appear to extrapolate to a value of zero phase.
2) For negative drive currents, the minimum signal is on the lower pole and is significantly greater in magnitude than the corresponding maximum on the common pole edge.
3) For positive drive currents, the differences between the corresponding maxima and minima are much less pronounced than was the case for negative currents. At any particular drive current, the larger phase signal, in absolute terms, is again at a minimum, which is on the single pole's edge.

To attempt an explanation for the observed behaviour, we must note that the larger phase signal amplitude occurs where the force between the tip and the field is attractive. Previously we wrote (equation 2.9) the force gradient on the tip as a convolution between the magnetisation of the tip and the second derivative of the head field with respect to the normal to the TBS. Given the geometry of the head, the magnetic flux will be more spatially concentrated on the lower pole than on the common pole. We therefore postulate that the relevant second derivative of field will be greater in magnitude at the lower pole edge than at the common pole edge. Hence, in the absence of any asymmetrical tip/field interaction, the magnitude of the mfm signal would be larger at the lower pole edge than at the corresponding point on the common pole edge. We also note that the polegap for this head is relatively large and hence the tip will experience quite high field for several microns along its length. If we postulate that the effective coercivity, associated with the magnetisation of the tip coating at distances in excess of 0.5 – 1.0μm from the tip end, is significantly less than at the geometric tip, then the magnetisation there could switch direction in an opposing field. This would have the effect of lowering the force experienced by the tip when the tip field interaction is repulsive. In combination with the

assumption about the head field second derivative, This would give the observed trends in phase maxima/minima behaviour.

4.4.2 The investigation of images subtraction to remove "Background" Effects

From earlier studies on the Emboss tape head supplied by Onstream it was observed that there was a relatively strong signal from the recording head even in the absence of a drive current. This raised the question of what effect this had on the image contrast when the head was driven and there was stray field emanating from the poles; in particular did this distort the field gradient profiles extracted from the MFM images. It was concluded that image processing might supply the answer. However a known problem with adding or subtracting images in MFM is that the scan areas are not always precisely reproducible, the result being that spurious contrast features could be introduced in image subtraction. Another potential problem is that forces exerted on the tip by the magnetic field could cause small variations in scan position and be drive polarity sensitive. To monitor and to check how significant these problems are, the topographic data collected simultaneously with the phase data must be examined. This should remain constant throughout an experiment provided the tip does not modify the surface being studied. The phase data selected for subtraction was visually aligned in Digital Micrograph using the topographic detail as a guide. The topographic data was subtracted from its 'twin' image and was deemed to match when there was minimal variation in contrast in the final image. The topographic section details were recorded to enable the same sections of phase data to be subtracted. In Fig. 4.4.2.1 are a set of topographic images collected under differing conditions for the head.

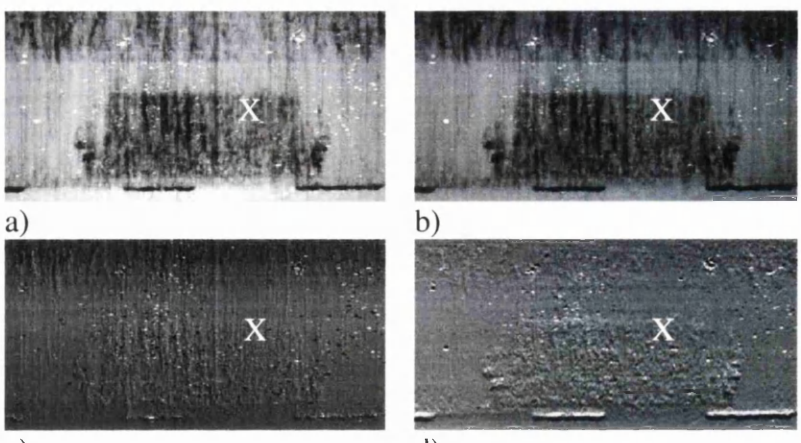

Fig.4.4.2.1. Topographic images of the pole region. The images are, a) no drive current applied, b) drive current +50mA, c) image (a) – image (b) and d) the subtraction from image (b) of an image (not shown) taken with a drive current of –50mA

The first image in the above series was taken with no drive current applied. The white flecks are topographic features that are near or just exceed the limit of the height scale range, which is 100nm in this case. If this image is compared to that denoted (b), taken with a drive current of +50mA, there are no obvious differences, apart from a scan fault at the bottom of (a). This is confirmed by the third image (c), which is the subtraction of (a) and (b). Clearly if the individual images, (a) and (b) are identical then there should be no contrast in the subtracted image (c). This of course is not true although the residual contrast is at a low level and can be in part accounted for by statistical noise in the original images. The final image (d) was obtained by subtracting images taken with opposite polarity of drive current ±50mA. In this image, no polishing marks can be seen (the 'x' marked on the images in Fig. 4.4.2.2), but there is evidence for a small vertical shift between images leading to the linear black/white features at the bottom of the image. However these results suggest that image subtraction may be useful when applied to phase images, which contain contrast related to the permeability of the head's magnetic material.

The corresponding phase images to those in Fig. 4.4.2.1 are shown in Fig. 4.4.2.2. The MESP tip was used for these experiments and this experiences an attractive force on one pole and a repulsive force on the other.

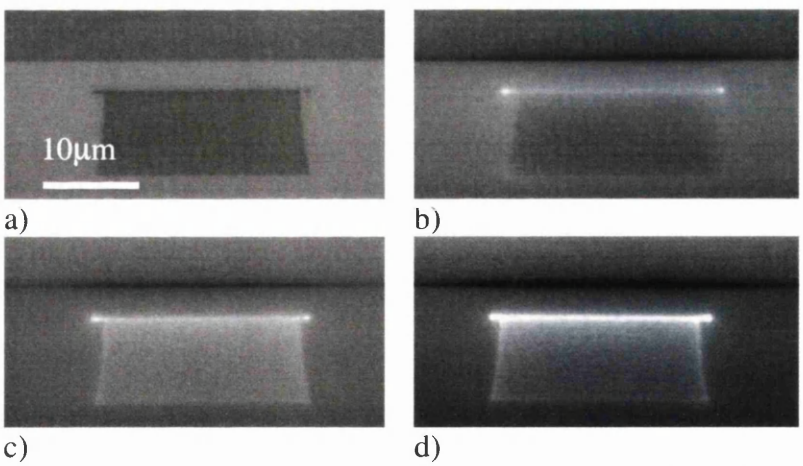

Fig.4.4.2.2. Phase images corresponding the image set in Fig. 4.4.2.1. These are a) no drive current, b) +50mA drive current, c) image (a) – image (b) and d) the subtraction from image (b) of an image (not shown) taken with –50mA drive current; to aid comparison the phase magnitude in image (d) has been divided by 2.

The success of the subtraction process may be assessed by comparing linescans extracted at corresponding positions in the image series. It was noted however in section 4.2 that for many phase images there is a problem with a phase gradient across the image; this requires correction if a meaningful comparison is to be made between linescans from different images. In the correction procedure a number of assumptions were made. Firstly, it was assumed that at the top of the common pole, i.e. at the top of an image, there was no stray magnetic field present. The magnitudes of the first row of pixels were then scaled such that their average value equalled the average in the corresponding row of the image of the undriven head. Secondly, the signal from the non-magnetic part of the head near the edges of an image, in a position which corresponded to midway between two driven poles, was assumed be the same for all images. These two baselines were then used to phase correct the original date. The result was not however totally successful, but it was sufficiently good to allow the subtraction method to be assessed with confidence. The first set of linescans is shown in Fig 4.4.2.3 and the second set in Fig. 4.4.2.4. Only at the start of this experiment was an image taken with no drive current applied, this is the first image in the above sequence in Fig. 4.4.2.2.

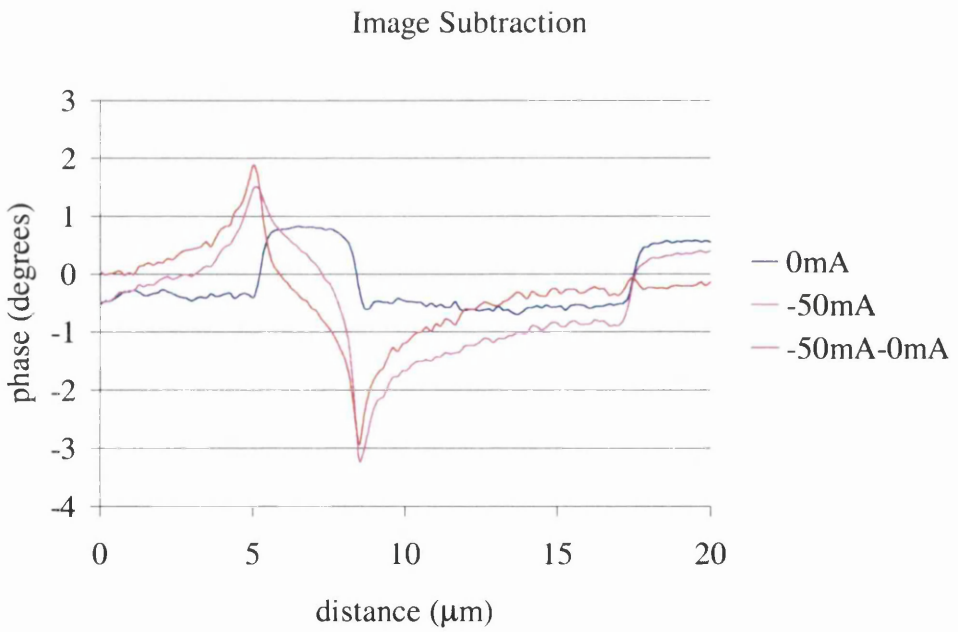

Fig.4.4.2.3 Linescans extracted for the images in Fig.4.4.2.2 and the linescan extracted from the –50mA image (not presented in this section).

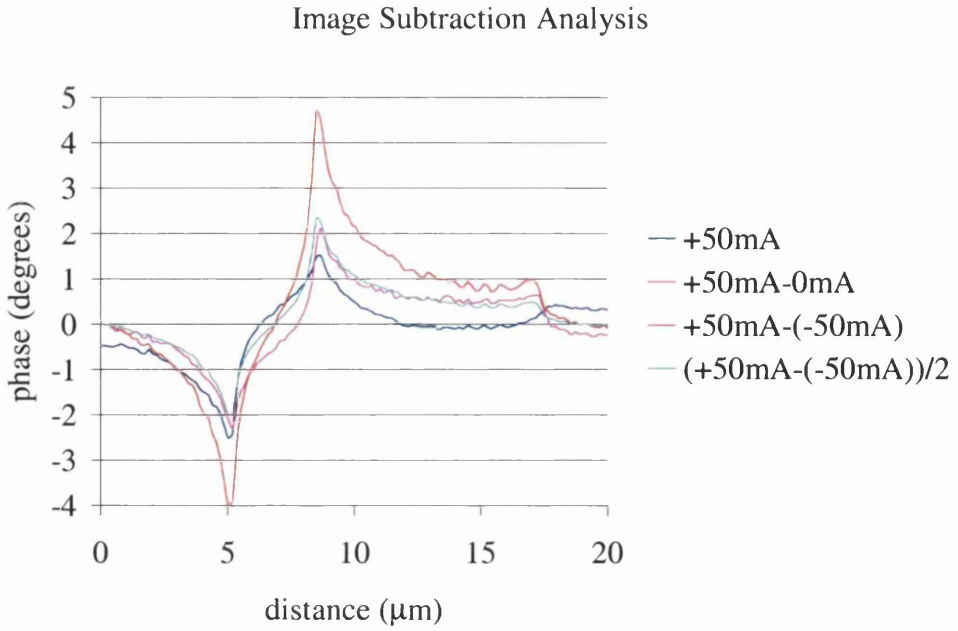

Fig.4.4.2.4 Comparison between the linescan extracted from the +50mA image and the two processed linescans.

The linescans were extracted from the middle of each image and integrated over 20 pixels in the horizontal direction. The first point to note in comparing the linescans is that magnitudes of the maximum and minimum signals at the pole edges have been influenced very little. This is despite the fact that the phase excursion at the lower pole in the undriven state is almost half that of the peak magnitude when driven at –50mA. The second point is that the maxima/minima are much sharper in the subtracted image. These are consistent with the assumption that we have removed the influence of the pole material by the subtraction procedure. The second set of linescans (Fig. 4.4.2.4) taken under the same conditions exhibit features, which are consistent with those just discussed. A similar analysis was performed with the head driven at ±150mA and the results are generally in agreement with those above.

A corollary to the argument regarding the result of subtracting pairs of images is that if we now add a pair of images taken with equal and opposite drive currents we should reproduce the original image of the undriven head, but of course with twice the signal magnitude. We tested this by adding the image pairs for the ±50mA and ±150mA drive current conditions and the results are shown in Fig. 4.4.2.5. Overall the images are

generally very similar in appearance to that of Fig. 4.4.2.1(a). In fact the only significant discrepancy is along the pole edges, where there are darker lines particularly for the case of the higher drive current. This is confirmed by examining the vertical linescans, shown in Fig. 4.4.2.6, from the middle region of the single pole. In the case of the lower drive current the dip in contrast is significant only at the single pole edge. For the higher drive current case there are dips at both pole edges, but again the larger effect is at the single pole edge. These observations are however consistent with our previous analysis, the main points being that i) for the same pole edge the attractive force signal magnitude is always greater than the repulsive force case, and ii) the signal at the single pole is somewhat larger than at the shared pole edge. The sharpness of the contrast dips observed at the pole edges must be related to the field gradient profile and this method of image addition may present an alternative method to study the field characteristics. Unfortunately time did not permit a more complete assessment of this possibility.

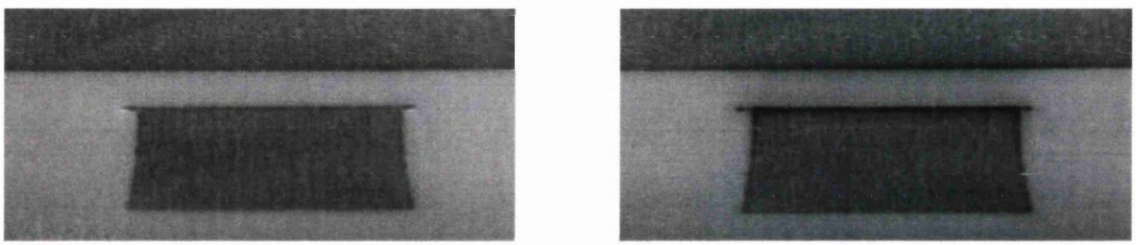

a) b)

Fig.4.4.2.5.Images formed by the addition of images taken with opposite polarity drive currents: a) for ±50mA, b) ±150mA.

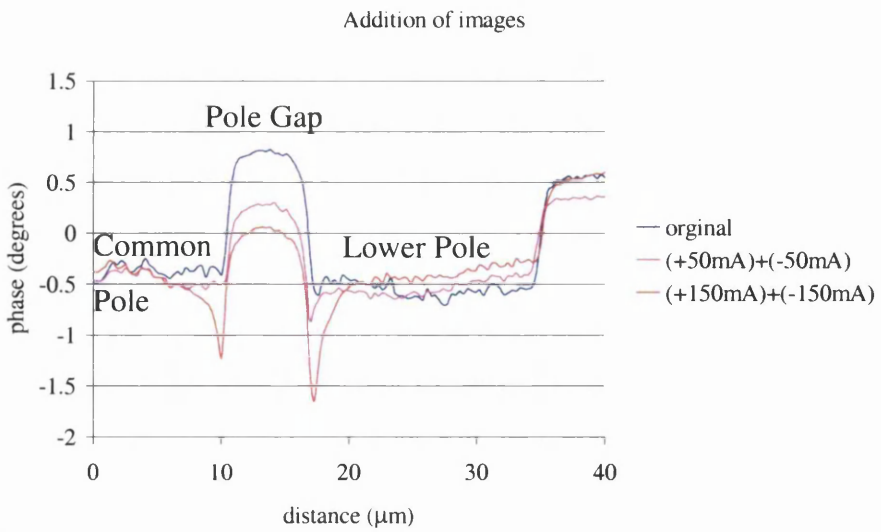

Fig.4.4.2.6. A graph of the linescans extracted from the two images above and one from the image taken at the start of the experiment with no current applied.

4.4.3 Stray field investigation along the Head Using the MESP Tip

Up until this point in the study of the Onstream Emboss heads, only a single pole at a time had been studied. This was due to the limit placed on the scan area due to geometry of the sample in relation to the pole size. The experimental Emboss head had smaller pole widths and hence we could investigate more than one pole in the same image and hence investigate the reproducibility of the field form. The maximum scan area for the MFM is a nominal 90 μm^2 and is determined by the piezoelectric material used for the scanning stage. However, the manufacturer does not recommend scanning at this maximum value for long periods. Hence although it would have been possible to image three poles simultaneously, we restricted the scan to 65μm in width giving two poles in the field of view.

To determine if the MESP tip had a similar response function, when scanned over different poles, several upper and lower poles driven at ±150mA. were scanned Again, to keep the experimental parameters consistent, the lift height was 100nm. The reason for reversing the polarity of the drive current between images was to observe the tip's behavior for a given current direction. Only one image Fig. 4.4.3.1 is presented here to indicate the size and position of the poles in an MFM image frame.

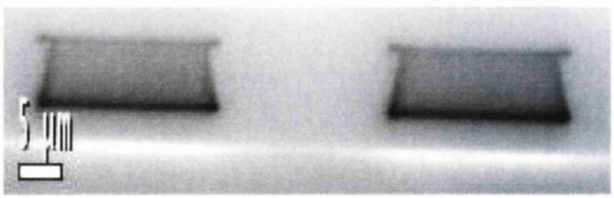

Fig.4.4.3.1. Two upper poles driven at 150mA, the scan length of 65μm.

In total six poles were studied and from each one, a linescan integrated over 16 pixels was extracted from the middle section of the pole. The results for the two scan current directions are shown in Fig. 4.4.3.2 below. Prior to extraction of the linscans the images were corrected for the phase gradient effect discussed previously

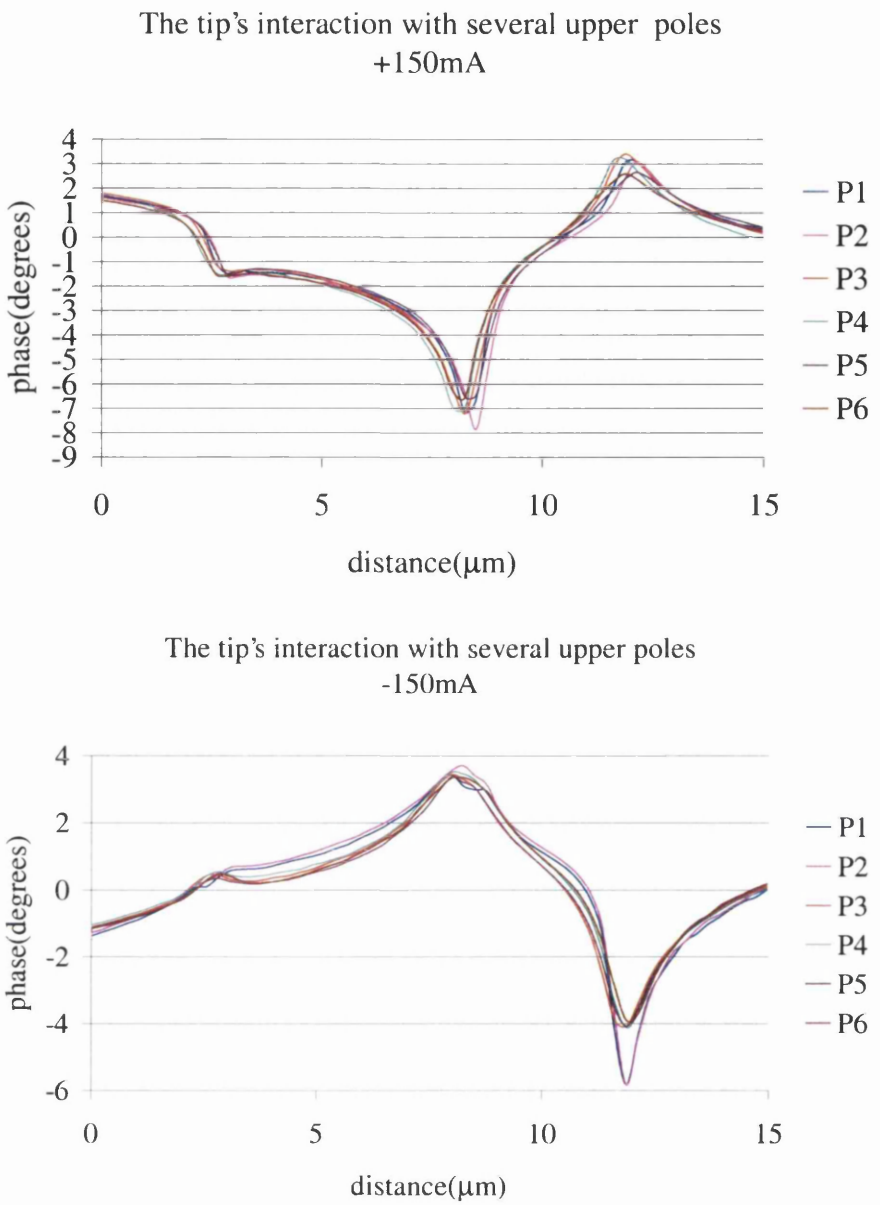

Fig.4.4.3.2 Lines scans extracted from the middle of each of the six upper poles studied. Both drive current directions are shown.

In the first of the graphs for +150mA drive current, the field gradient profiles are very similar except for one where the deviation from the average is ~1 degree in phase. The results for the –150mA drive current are however different and show a greater spread in peak values, the differences from the average ranging up to 2 degrees. There is an indication that the tip was switching as it scanned over the upper pole, as indicated by the rounding of the field profiles there. Since the two profiles which gave the largest peaks at

the pole edges were from the first two scans performed, it is possible that the remainder were influenced by a change in the tip properties.

The experiment was repeated for the lower pole array, but this time only four lower poles were studied due to a tip breakage. Scanning large areas of this sample was very demanding on the tip and several could be used before collecting a reasonable data set. Again, both current directions are presented, however during the last image a scan fault occurred resulting in the data from this image being partially rejected. The image in Fig. 4.4.3.3 shows a typical scan area selected for the study of the lower pole array and it should be noted that the undriven upper poles are also visible. This allowed us to check that there was no significant change of contrast from the edges of these poles and the adjacent edge of the common pole, when the lower poles were driven.

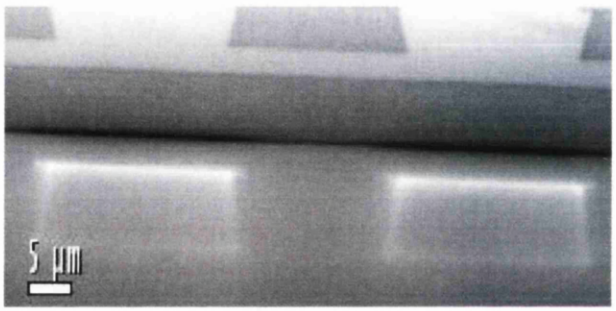

Fig.4.4.3.3. Two lower poles driven at 150mA and a scan length of 65µm.

The linscans integrated over 15 pixels near the centre of the poles are shown in Fig. 4.4.3.4. for the two directions of drive current. It should be noted that the linescans are only over 15µm, rather than the full height of the image and as a consequence the phase never goes to zero at the extremities. The response from the poles as determined by the contrast profile is reasonably uniform particularly for the negative current direction

The results have not revealed any dramatic discrepancies in the field behaviour of nominally identical poles.

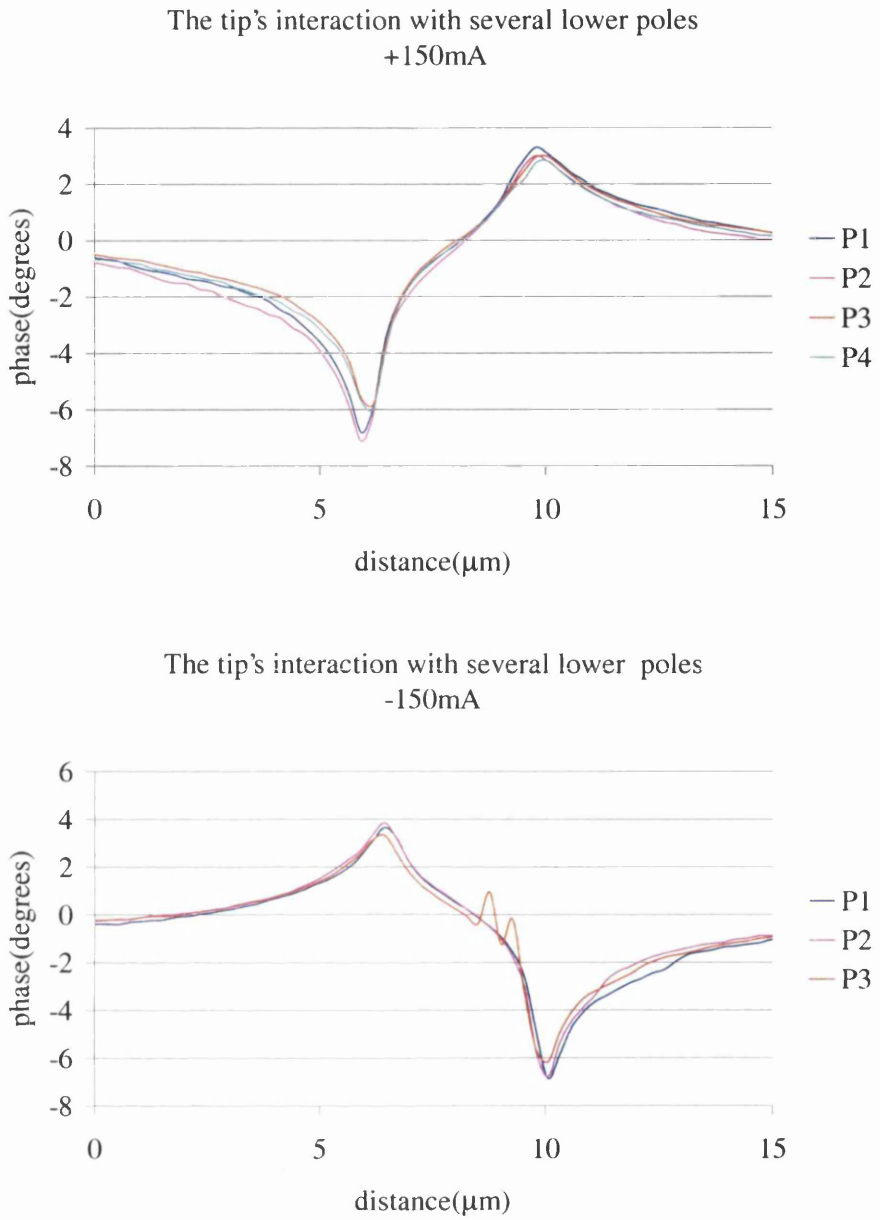

Fig.4.4.3.4. Linescans extracted from the middle of each the upper poles studied. Both drive current directions are shown. There is only three linescans for the –150mA current due to a scan fault on the fourth pole. Signs of which appear on P3.

4.4.4 Studying various Tips to determine their suitability for MFM of Heads

Three other types of tip were used on this sample to determine if they were suitable for the study of this type of sample at its operating current of ~400mA. Two tips were magnetically soft and the third was a CoPt coated tip obtained from Professor Liow at Nebraska. The latter tip was successful in retaining its magnetic stability at the maximum

drive current. Only the results from the hard tip and the low moment (LM) tip will be presented here. These tips were not previously used in our studies of the heads.

4.4.4.1 The Low Moment Tip

The reason for selecting the low moment (high coercivity) tip was there would be reduced tip/sample interaction with the outcome that one could reduce the number of mfm tips destroyed during these studies. It was partially successful in that the phase shift was reduced in magnitude but with this tip it was difficult to collect images. The highest drive current applied to the head while scanning with this tip was 150mA, the results of which are shown below

.

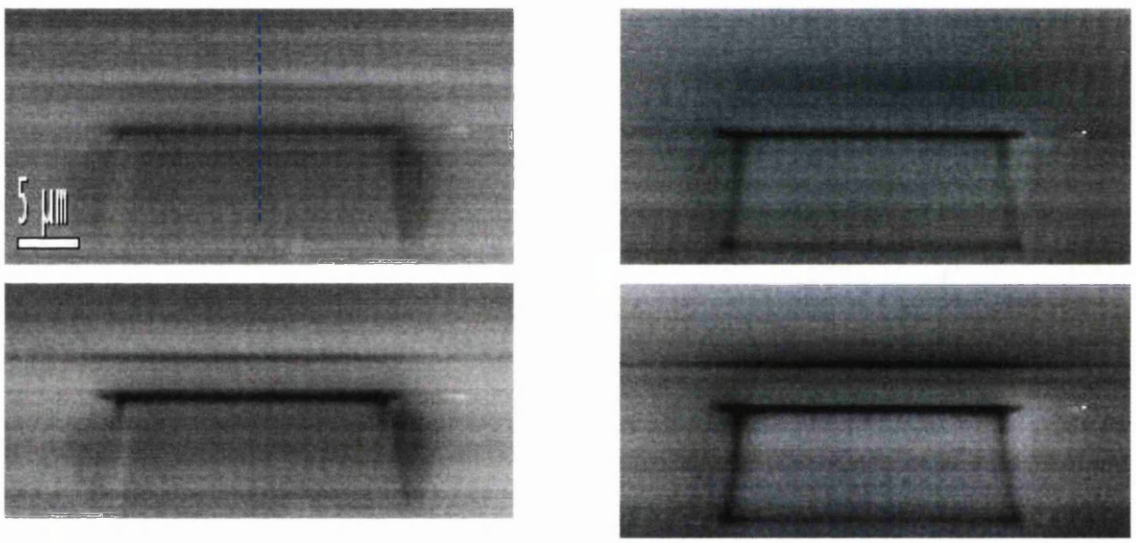

Fig.4.4.4.1 Phase images of the lower pole taken with a low magnetic moment tip, in the top image pair the head was driven at +100mA, -100mA from left to right. For the lower image pair the head was driven at +150mA and –150mA from left to right.

These were some of the poorest images seen using the MFM technique. Faint vertical lines occur at regular intervals across the image and the frequency of this spurious signal is ~50Hz. The most likely source of noise is from the electrical mains. From the above images linescans were extracted from the middle of the lower pole.

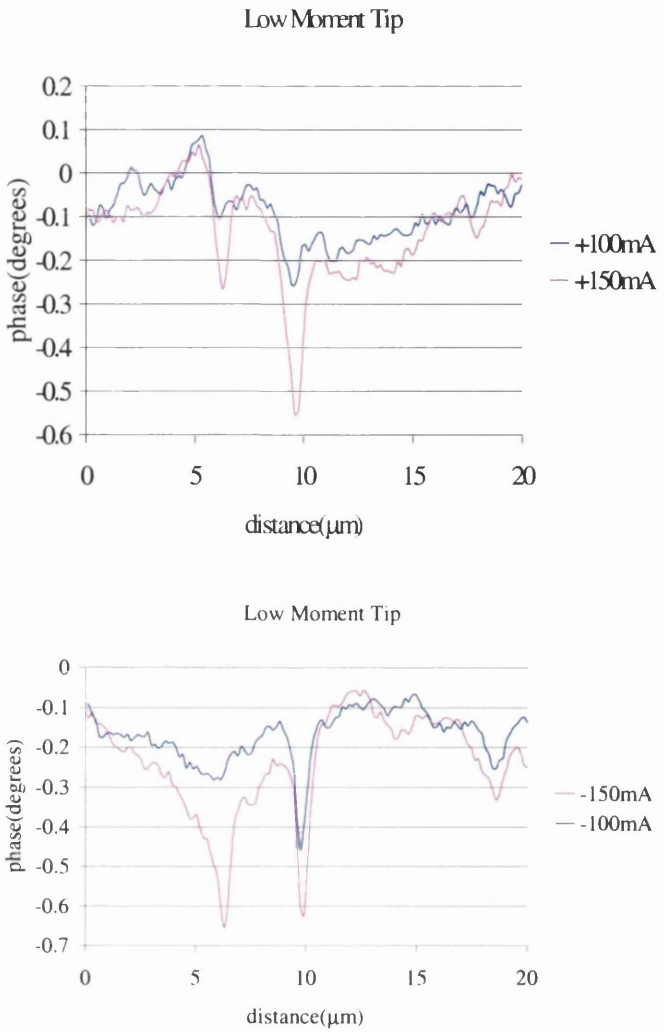

Fig.4.4.4.2 Lines scans extracted from the middle of the upper poles, both current directions are presented.

The first thing to note is the magnitude of the minima. At -150mA the largest minimum is less than 0.7 degrees; a very small signal compared to those recorded for the other tips. One major concern about using this tip was that it was found that characterisation using the standard sample was difficult. This LM tip may have been suitable for the study of the head at high drive currents, but the experiments were not performed.

4.4.4.2 The CoPt Coated Tip

The CoPt tip discussed previously, which is very hard magnetically, was successful in imaging the head at the full drive current of 400mA. Three representative images from a

negative drive current sequence are shown in Fig. 4.4.4.3 and the linescans, extracted from the middle of the driven single pole, are shown in Fig. 4.4.4.4. Also included in Fig 4.4.4.4 are the linescans extracted from the positive drive current images, none of which are presented here.

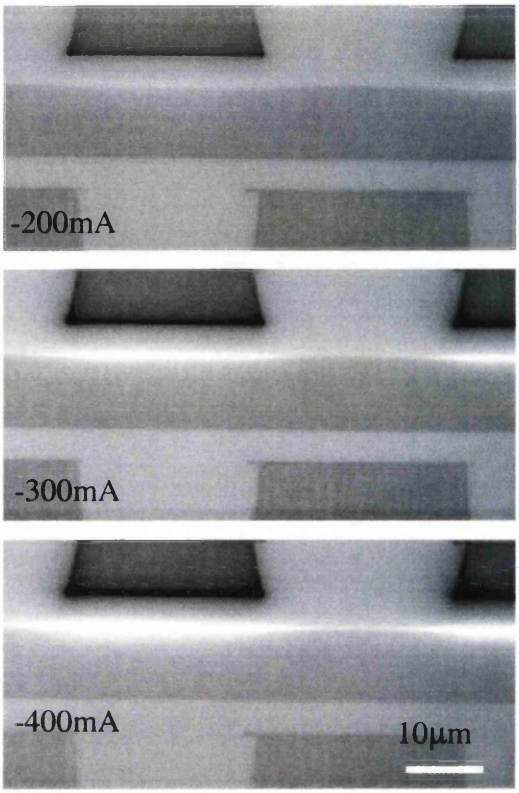

Fig.4.4.4.3 Images taken with the CoPt coated tip - the drive current is indicated in the bottom left hand side of an image.

The first point to note is that, even at the full drive current of -400mA, there is no sign of contrast changes arising from tip switching. This was also true for an image taken with an applied drive current of +400mA. However, when reviewing the topographic image, taken simultaneously with the phase image, it was decided not included it in the subsequent detailed analysis of the phase contrast due to anomalies in the height data. This topographic image did not compare favourably with similar images taken at lower applied drive currents, which it should have done. The contrast maxima and minima at the pole edges generally increase with drive current and for the negative drive currents the magnitude of the attractive signal minimum on the single pole edge is always greater than the corresponding maximum at the common pole edge. The positive drive current images behaved in a similar general manner. However for both the 100mA and the 300mA drive

currents, the magnitude of the signal level at the common pole is larger than at the single pole. This was only the second time this effect had been observed (the first was with the MESP tip at a head drive current of +150mA; see section 4.4.3) and is contrary to the model of the head imaging, which we have proposed.

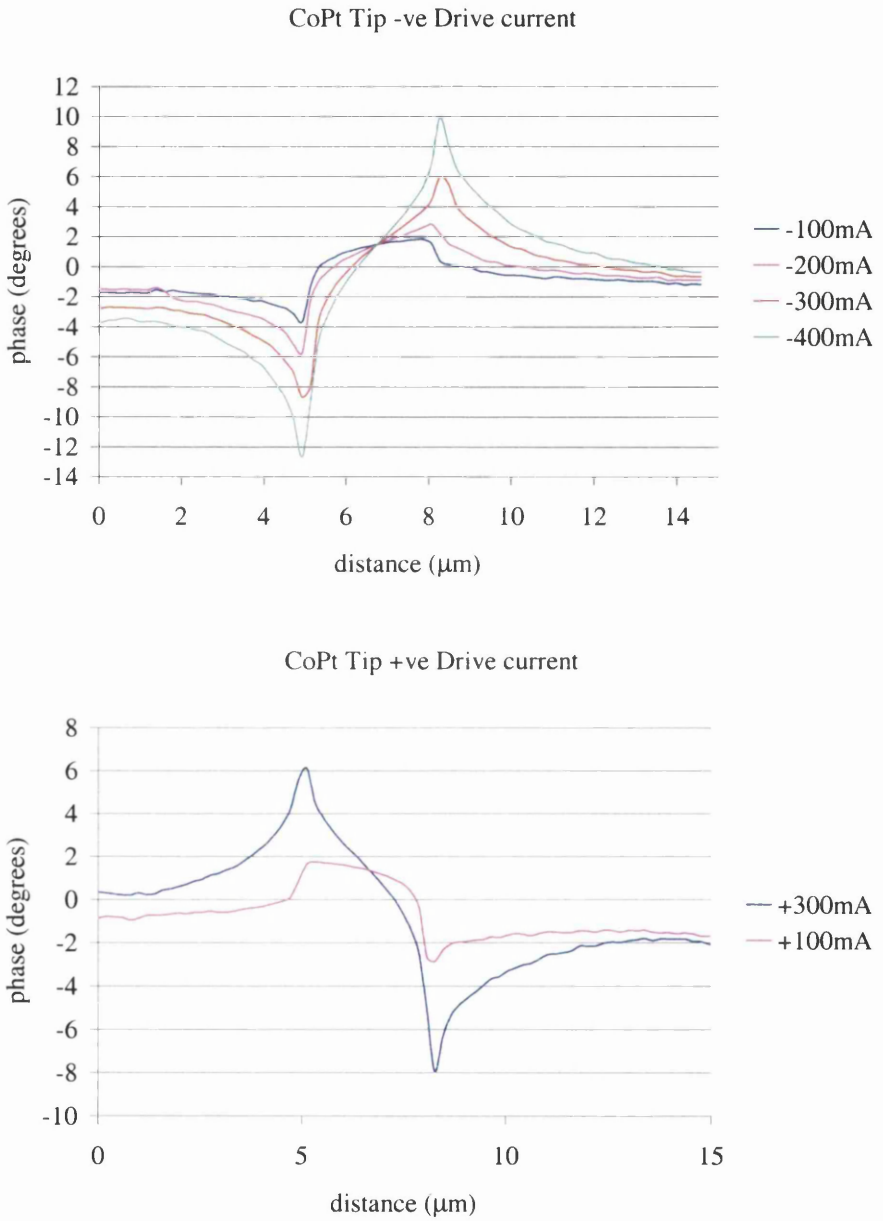

Fig.4.4.4.4 The linescans extracted from the images obtained with the CoPt tip.

To analyse this data further, the magnitudes of the pole edge maxima and minima were extracted from the linescan data of the negative drive sequence and were plotted as a

function of drive current in Fig. 4.4.4.5. The signals, which are in white contrast (repulsive force), are shown in blue and those in black contrast (attractive force) are shown in pink.

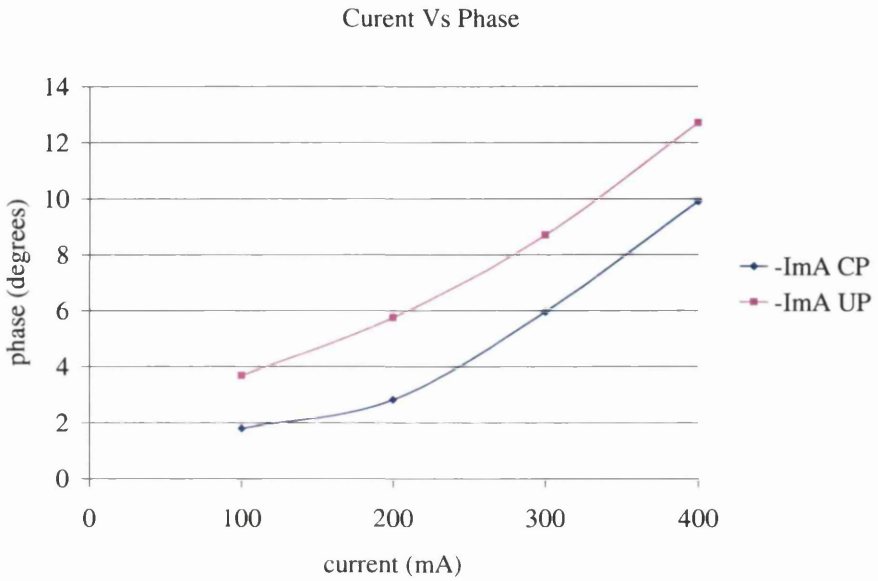

Fig. 4.4.4.5 Peak phase magnitudes at the pole edges for the negative drive current sequence. The key to the legend on the graph is as follows:- CP – Common pole; UP – Upper pole;

The general trend of increasing maxima and minima as a function of drive current is established, but for both curves a fit to a simple linear slope passing through the origin would not be feasible.

The intensity distribution in the images is clearly influenced by the presence of the contrast arising from the permeability of the head's magnetic material. Hence it was decided that the application of the image subtraction method, which was discussed earlier, should be attempted to try to understand the behaviour of the peak intensities. The image subtraction method requires, as the reference, an image taken with no drive current present. Unfortunately no such image was taken with the CoPt tip. However, it was noted in section 4.2.2 that the addition of two images taken with equal and opposite drive currents, produced an "image" of the undriven pole (the image intensity had of course to be divided by 2 to correspond to what would have been expected). This worked best for images taken at low applied drive currents. In our image set, we had images taken at ±100mA and so

these were added to give our reference image, which is shown in Fig. 4.4.4.6. The linescan extracted from the indicated position shows that the method is successful, any peaks near the pole edges being very small (< ~0.1) in phase magnitude. From the linescan, the average phase signal from the poles is ~1.25 degrees. This image was then subtracted from each of the original images; a representative set of these processed images is shown in Fig. 4.4.4.7.

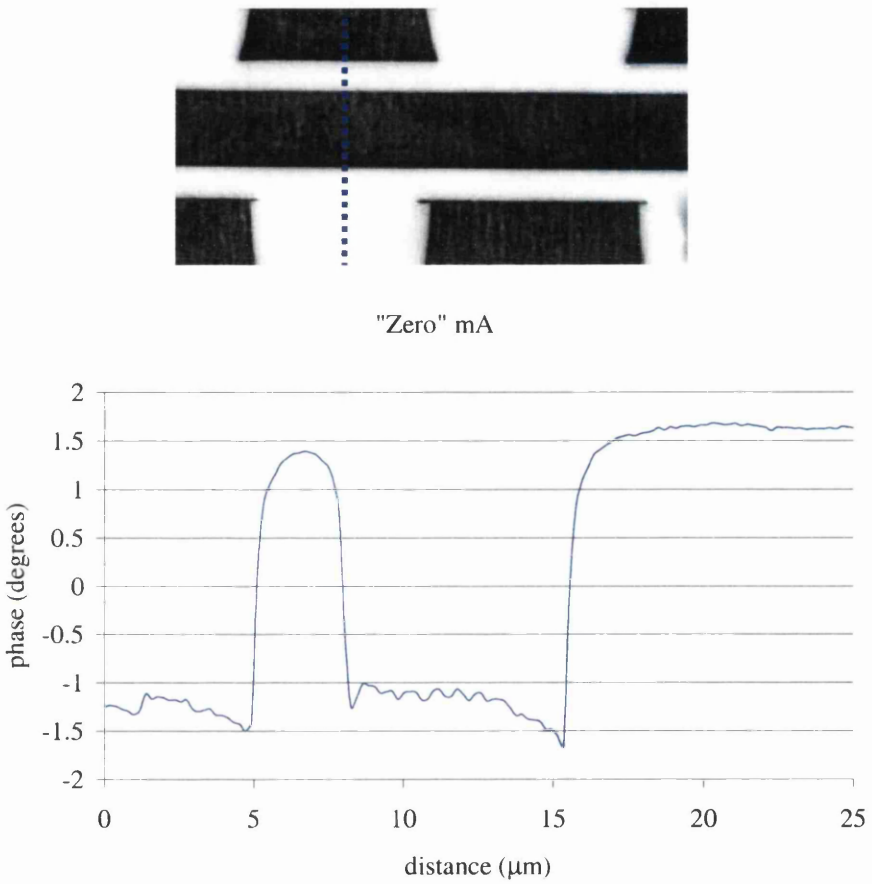

Fig.4.4.4.6 The "model" image of the head formed by adding the image pair for ±100mA drive currents and then dividing the signal by a factor 2. The linescan extracted from the position indicated in the image is also shown.

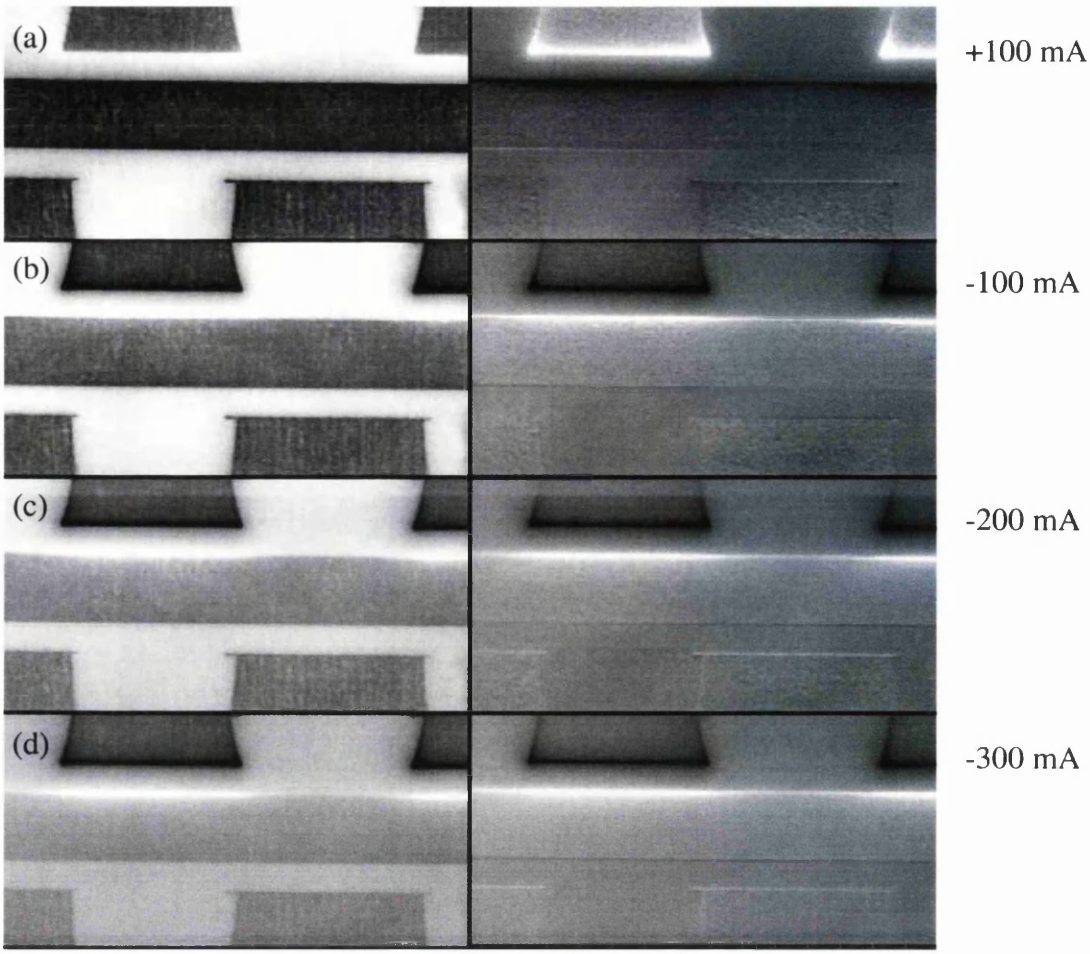

Fig. 4.4.4.7 The original images (left) taken with different drive currents compared to those (right) obtained as a result of subtracting the 'model' zero drive current image. Drive currents are: a) +100mA, b) –100mA, c) –200mA and d) -300mA

The success of the subtraction method is particularly striking for the image pair at ±100mA and is further illustrated by the linescan data shown in Fig. 4.4.4.8. It should be noted that in some cases there is a small degree of residual contrast at the bottom edge of the common pole and the top edge of the lower undriven single poles. In some cases it was found necessary to displace vertically one of the images in a pair by one or at maximum two pixels prior to subtraction to take into account relative image movement in the vertical direction. The noted residual edge contrast indicates that the relative image movement was probably non integer in terms of the number of pixels of image shift, but we made no attempt to refine the procedure further.

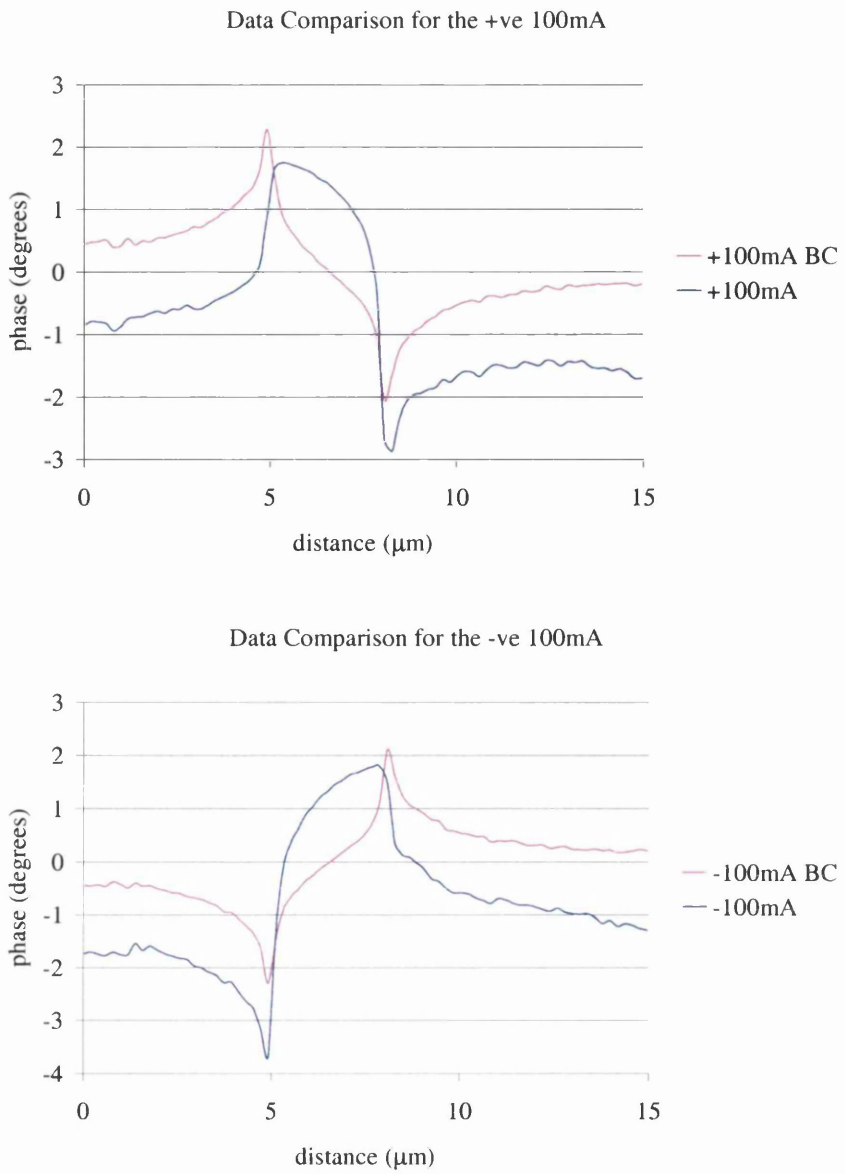

Fig.4.4.4.8 These linescans were extracted from the original ±100mA image and to show the effect of subtracting the 'zero' mA image from this data the linescans from the processed images are also presented. (The BC indicates that the data has been 'background' corrected)

The linescans (averaged over a width of 20 pixels) extracted from the middle of the driven pole are shown separately in Figure 4.4.4.9 for the negative and the positive drive currents. In all cases the maxima/minima at the driven pole edges are much more symmetric than in the raw images and the difference in their magnitude is reduced. The previous observation that, compared to the common pole edge, the contrast for the negative drive sequence is

greater in magnitude on the single pole edge is maintained. Of much more importance is the observation that this behaviour is also now observed for the two positive drive current images. However for this latter case the difference in magnitude between the maxima/minima is less than for the negative drive set, but this is consistent with the tip-specimen force being somewhat greater for the same field when the force is attractive rather than repulsive.

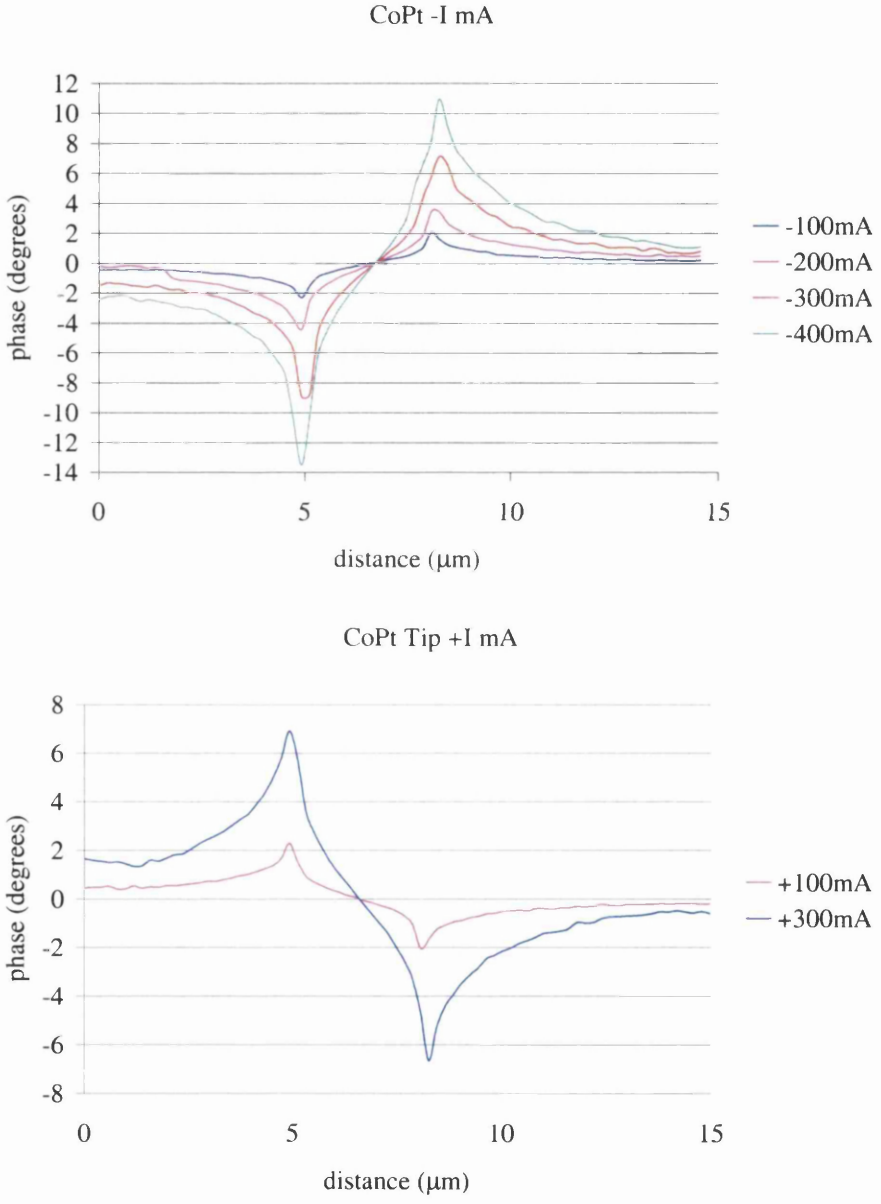

Fig.4.4.4.9 Linescans extracted from the images corrected for the effect of background contrast.

The graph corresponding to Fig. 4.4.4.5 for magnitudes of the maxima/minima as a function of drive current is shown in Fig. 4.4.4.10 for the negative drive current case. Although there is still a tendency for the slope to increase with drive current, the best-fit line would come close to passing through the point –1.2 (the value of the signal with no applied drive current) for each of the cases, particularly if the values at 200mA are for anomolous. The reason(s) for the departure from a linear fit are not known, but one possibility is that the relatively crude image subtraction method is not properly taking into account the influence of the material coercivity for higher drive currents.

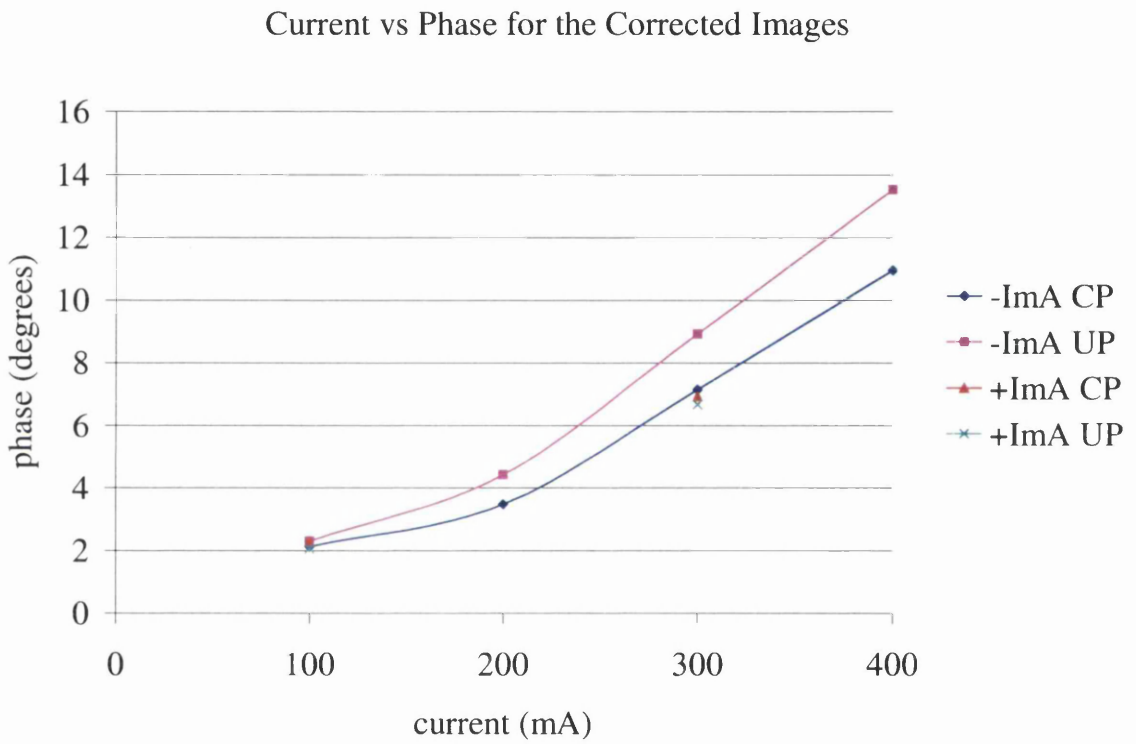

Fig 4.4.4.10 Peak phase magnitudes at the pole edges for the background corrected drive current sequence.

The results discussed above for the CoPt tip indicate that it is the most promising type of tip for recording head studies where we wish to determine the performance with the head driven at the current level appropriate to the commercial drive. The raw data for the maxima/minima contrast exhibited at the head gap showed anomalies and it was thought that the contrast due to the coercivity of the head material could be at least in part responsible. The application of the image subtraction method was thus indicated.

However the absence of a zero drive current image was potentially a major deficiency; but we have proved that the addition of two images taken at low drive currents of opposite polarity can provide a satisfactory substitute. The results of image subtraction were excellent, but more work is needed to refine the technique and to establish its limitations. Regrettably the fact that we only had one of these CoPt tips, which was suitable for imaging, meant that the investigation could not be pursued further by the author.

4.5 The MFM Study of the Data head and the MR Element

The data heads supplied by Onstream for these studies were production heads. The difference between these and those supplied earlier is that in the former the MR element is "buried" within the head assembly. So only the read gap is visible and it was hoped that when the MR element was driven one would "see" some stray magnetic field with the MFM. In the optical image below (fig. 4.5.1) one of the eight heads is shown. The second image (Fig. 4.5.2), taken in the SEM, highlights a typical area scanned with the MFM in the experiments to follow.

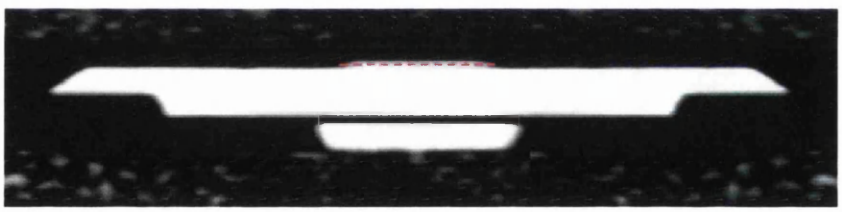

Fig.4.5.1 An optical overview of a read/write pole width in the data head. The read gap is not resolved in this image. The red dashed line indicated the position of the read gap.

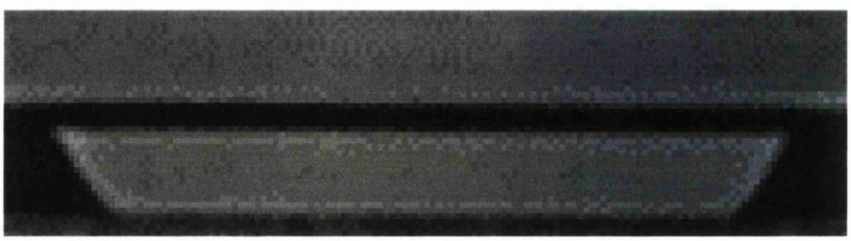

Fig.4.5.2 A SEM image showing a typical scan area of the pole faces studied using the MFM. The writing gap "enclosed" by the lower and common poles is the view presented in the above image.

In the tape drive unit the operating current for the data head is ~35mA and it was hoped to be able drive it at this current to study stray magnetic field from a single head. In this sample all the drive electronics were complete, unlike the earlier data head studied in the (S)TEM, so the MR element could be biased and studied as a fully functional element. From the earlier studies on the Emboss heads with the MFM, it was expected that finding a suitable tip would prove to be the one of the more challenging issues in studying this type of tape head

4.5.1 The study of the Data Head using various Tips

4.5.1.1 The CoPt coated Tip

For the initial investigation of an individual write head the magnetically hard tip coated with CoPt was chosen; this had been used briefly in the study of the experimental Emboss head at the maximum drive current. This tip appeared to have suitable magnetic characteristic for the study of the heads. It retained its sensitivity to the magnetic component normal to the TBS at large drive current values. In the following experiment the head was driven initially at ±20mA to test the tip's performance with this new sample. After a short period of time the drive current was increased to (±)35mA. As per the previous experiments the lift height selected was 100 nm. It was observed during the experiments on the emboss heads that the direction of the current influenced the tip's behavior, hence both current directions are presented below.

A short note about the current directions, they are quoted as shown on the current supply and care was taken to ensure that when connecting the heads to the power supply that the same connections were maintained, thus ensuring that all the current directions should be consistent for all the images presented.

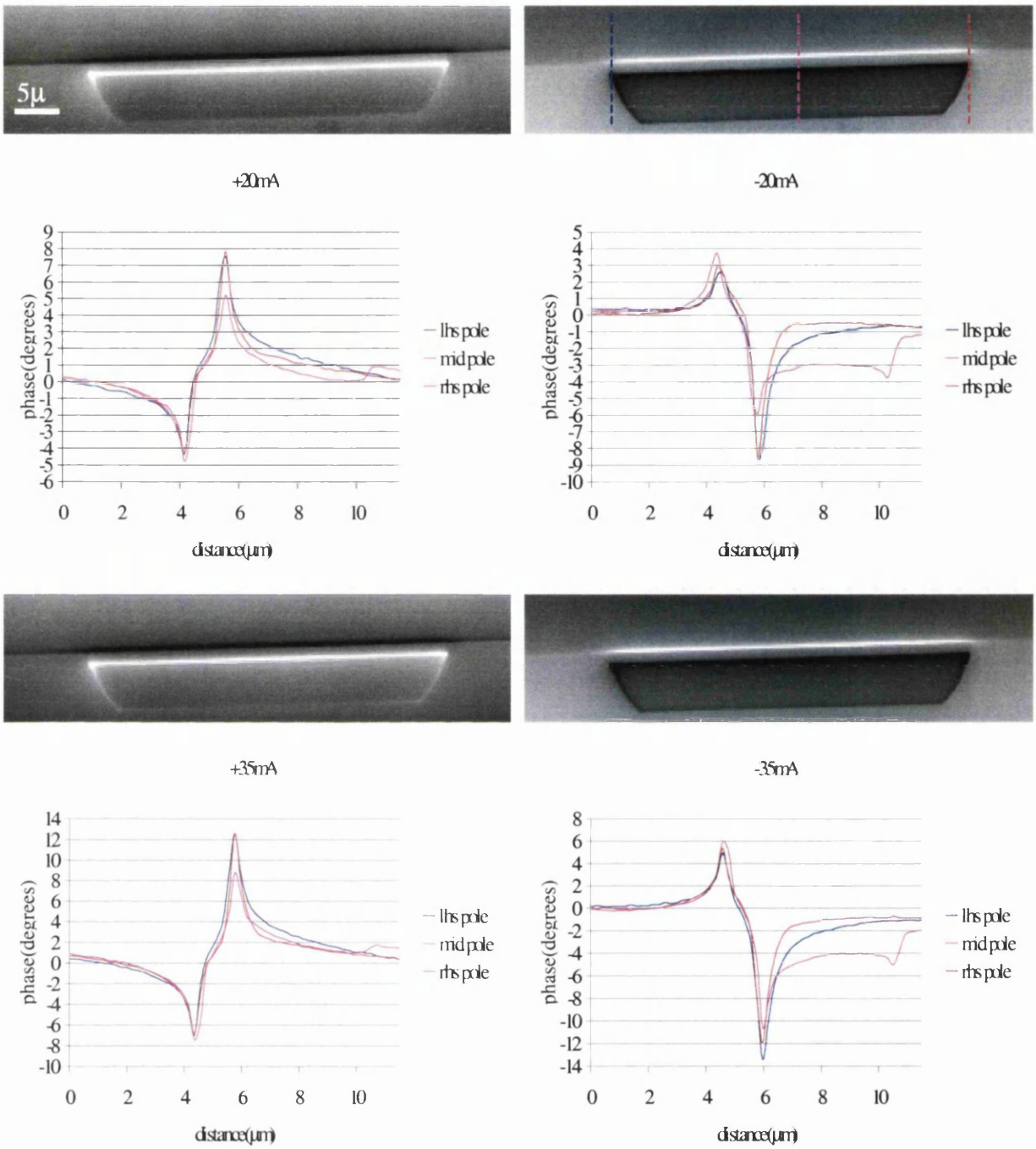

Fig 4.5.1.1 Phase images taken with the hard magnetic tip and the corresponding graphs of the linescans extracted from the images. The coloured lines in the top right hand image indicate the positions from which the linescans were extracted.

The images show relatively sharp maxima and minima and along the single pole edge there is the same overall asymmetry observed previously i.e. the maximum (minimum) is of greater magnitude near the ends than at the centre of the pole. It is also observed that for equivalent positions along the pole in each image, e.g. at the centre, the magnitude of the

signal on the separate pole is always greater than on the common (longer) pole. This would be consistent with a higher field gradient at the writing pole edge. The asymmetry is also greater for the negative drive current case when the force at the single pole is attractive, showing that there are two contributions to the effect. In relation to previous studies it should be noted that there are no indications of tip switching in these images and hence potentially this type of tip is suitable for more extensive studies of recording head fields.

A careful study of the images in Fig. 4.5.1.1 also reveals that there is an additional contrast 'ripple' modulation along the pole edges and this is more clearly distinguished in the contour plot in Fig. 4.5.1.2, which is a contour map of the data and in the y-modulation images of Fig. 4.5.1.3.

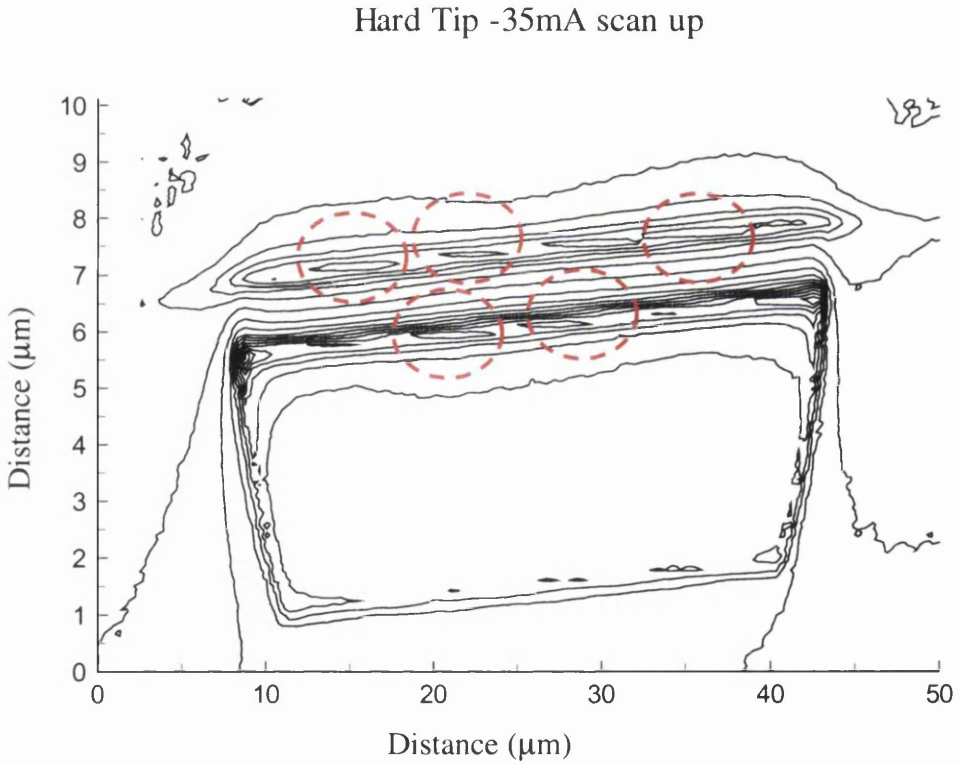

Fig.4.5.1.2 A contour plot of one of the above images. The red dashed circles highlight the anomalies in the data.

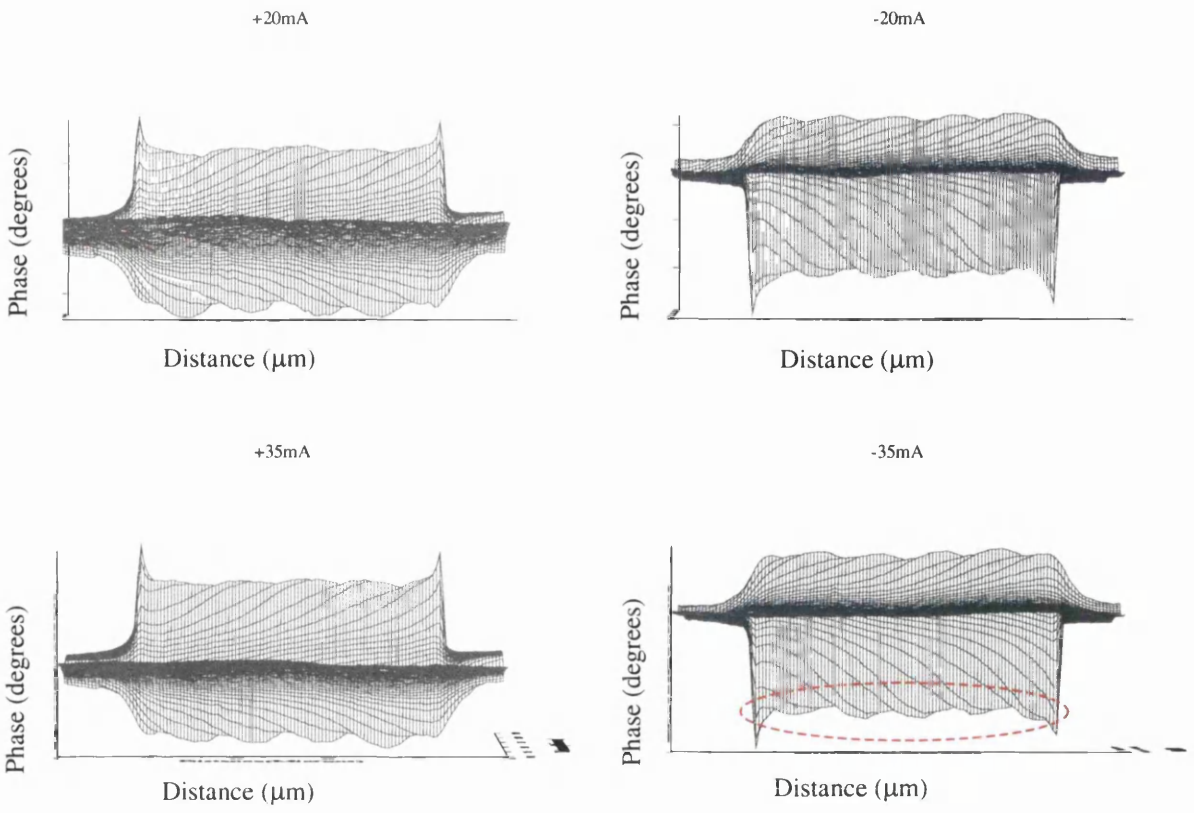

Fig.4.5.1.3. The y-modulation form of the images in Fig 4.1.51 showing the contrast ripple along the pole edges. The red dotted line highlights this feature in the bottom right hand graph.

The head was not parallel to the horizontal scan direction (X'), it was at an angle of ~1.6 degrees. In the previous experiments, the pole gap was parallel to the horizontal scan direction.

If we compare that above data to that taken from the experimental Emboss head with the same tip (fig. 4.5.1.4) then we note that there is no obvious 'ripple' in the phase data. The negative section of the graph does show that the phase shift is not symmetrical along the common pole in the section opposite the upper pole. If there was a tip hysteretic effect then it would be expected to show up in this data set as well. The angle between the pole edge and the horizontal is the determining factor for the ripple period.

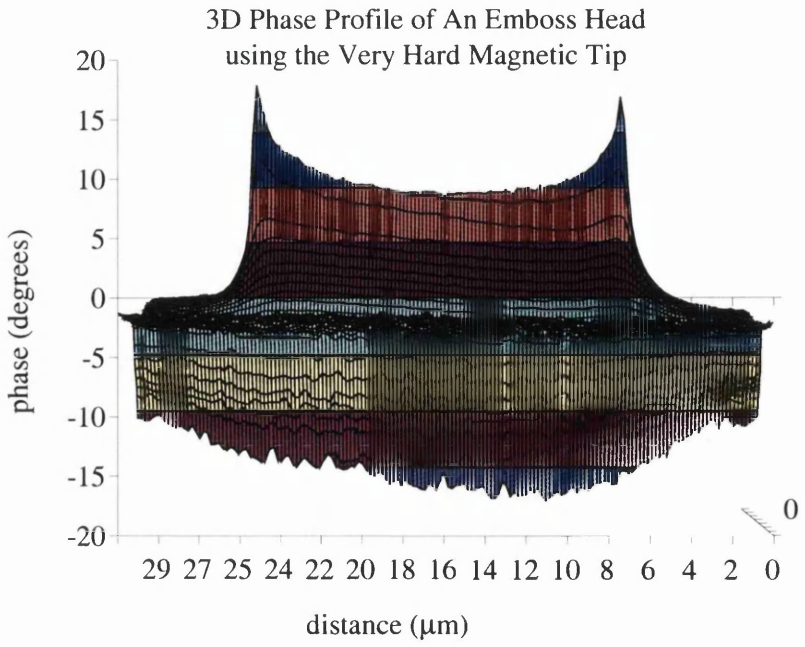

Fig.4.5.1.4 3D profile of the phase shift recorded on the Emboss head using the CoPt tip in which there is no signs of the ripple that appears in the data for the data head.

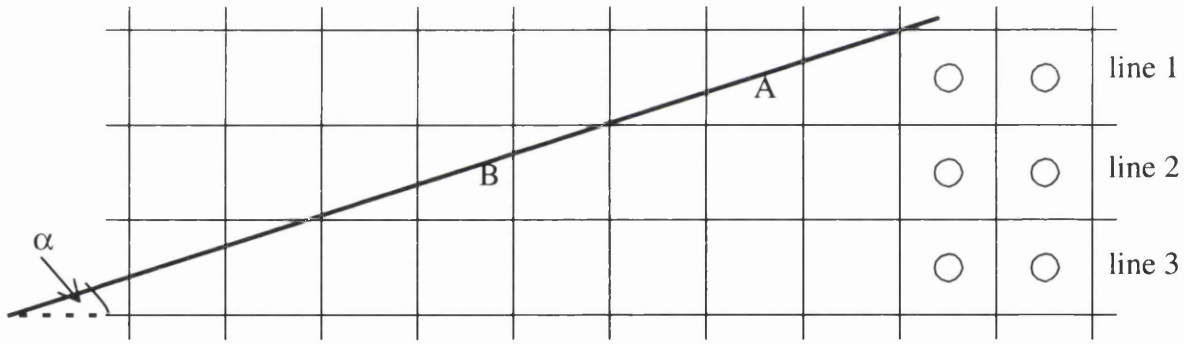

Fig.4.5.1.5. Diagram to aid explanation of the pixelation effect. The centre of each square represents the probe position. The sharp line feature in contrast is at an angle α to the horizontal linescan.

Consider a sharp line feature crossing the scan lines at a small angle α to the horizontal. The centre of each square then represents the position of the MFM probe for this section of three adjacent linescans. The probe field function will be much sharper than the distance between successive pixels due to the low magnification used. Hence the response at a given pixel will depend on the position of the line feature within the pixel square relative to its centre. The signal will be greatest when the line intersects the centre of the square and

will fall as the line moves away from this position either up or down. Thus for line (1) the maximum response will be at pixel A and for line 2 it will be at pixel B. For either line the signal will fall on either side of A or B and this is clearly seen in the y-modulation image of Fig. 4.5.1.3. The horizontal distance between A and B in pixels will be given by (1/tan α) in terms of the number of pixels. For the data head image of Fig 4.5.1.1, α is estimated to be 1.6° and this gives ~36 pixels which is in agreement with the y-modulation image for a 256x64 format.

Shortly after the study of the data head the CoPt coated tip was inspected in a SEM and was found to be broken. This was disappointing since it was the most effective tip we identified for head field studies.

4.5.1.2 MESP Tip

Before the receipt of the two experimental hard CoPt tips from the University of Nebraska, the magnetically hardest tips available to us were the standard DI MESP tips. We have just seen the high quality images of the data head obtained with the Nebraska tips and a comparison with MESP tip imaging of the same specimen is clearly of interest. Experiments with the MESP tip were conducted at three drive current levels viz. 10mA, 20mA and 35mA. Only the images for the highest drive current are presented in Fig. 4.5.1.6a, but the linescans extracted at comparable positions in the scanned area are shown in Fig 4.5.1.6b, for all three drive conditions.

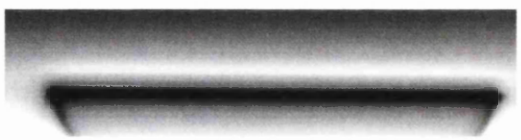

+35mA dc

-35mA dc

Fig 4.5.1.6a. The phase images taken with the MESP tip at an applied drive current of 35mA dc.

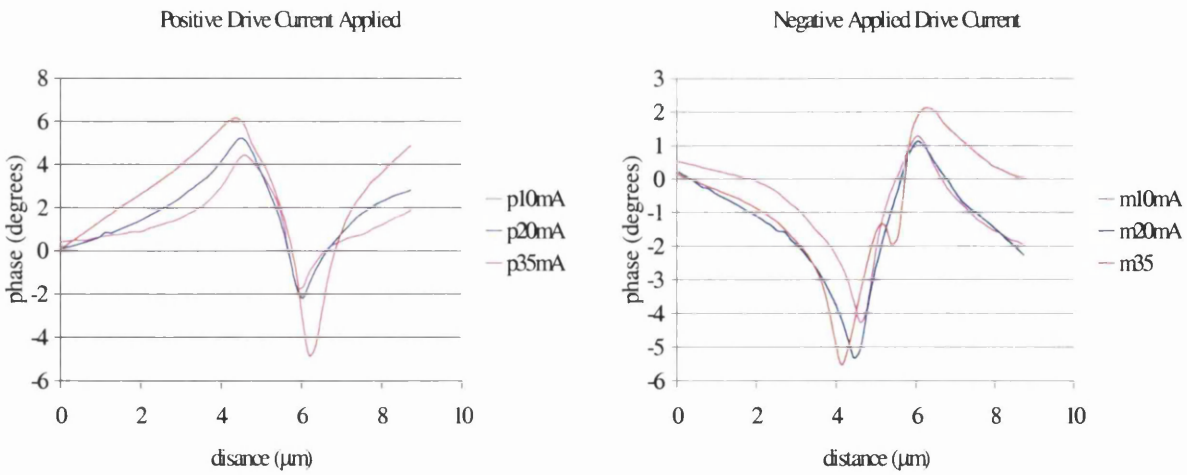

Fig.4.5.1.6b The linescans extracted from the middle of the lower pole, over the range of drive currents applied to the head.

There are a number of features, which require comment. Firstly there is clear indication of tip switching at the lower pole edge for the –35mA case; given previous studies on the Emboss heads at the normal drive currents used in the tape file, this is not surprising. A more surprising feature, in comparison with the CoPt results, is the much poorer resolution of the field gradient profile particularly at the upper pole edge. This is also seen in the profiles taken at the two lower drive currents and before tip switching was experienced. This would lead us to suspect that the particular MESP tip which was used was not exhibiting the imaging behaviour typical of this type of tip. Confirmation of this is also seen if we examine the magnitudes of the phase excursions at the pole edges under increasing drive current. It is clear that the maxima/minima do not scale with current magnitude. This particular tip was checked for its imaging performance with the NIST sample prior to these experiments and this indicated a slight tendency to sensitivity to an in-plane component of magnetic field. It was therefore surprising that such a large departure from the expected imaging behaviour with the recording head is obtained. This experience serves to show that such monitoring should be standard if we are to have confidence in the interpretation of the field images.

Due to a limited supply of the very hard magnetically tips, and the fact that the MESP tips were switching at 35mA, it was decided to use some of the softer magnetic tips to determine how useful these could be to our studies. The standard Low Coercivity (LC) tip

supplied by DI and two experimental tips were used in order. This would enable us to compare the standard tip against the experiment tips.

4.5.1.3 The Soft Magnetic Tips

As was the standard practice, the tip was scanned over the data head with the head driven at a d.c. value lower than the operating value all the while acquiring data to enable us to build up a profile of the tips response to the stray magnetic field. However, since the main interest was to study the head at its operation current value of 35mA only the data collected at this value will be presented.

The first soft magnetic MFM tip tried on the data head was the LC type manufactured by DI. The images at the maximum drive current and the linescans extracted at the centre of the lower pole are shown in Fig. 4.5.1.8. It is noteworthy that, although as expected the force experienced by the tip at each pole edge is attractive, the minima are not the same magnitude for the two drive currents. This suggests that there is probably a small degree of hardness in the tip coating. This may be compared to the results of imaging with another form of soft magnetic tip in this case coated with Metglas; these have been discussed earlier in section 4.3.1. The images obtained with two tips, one with a coating thickness of 10nm and the other with a thickness of 50nm are shown in Fig. 4.5.1.9

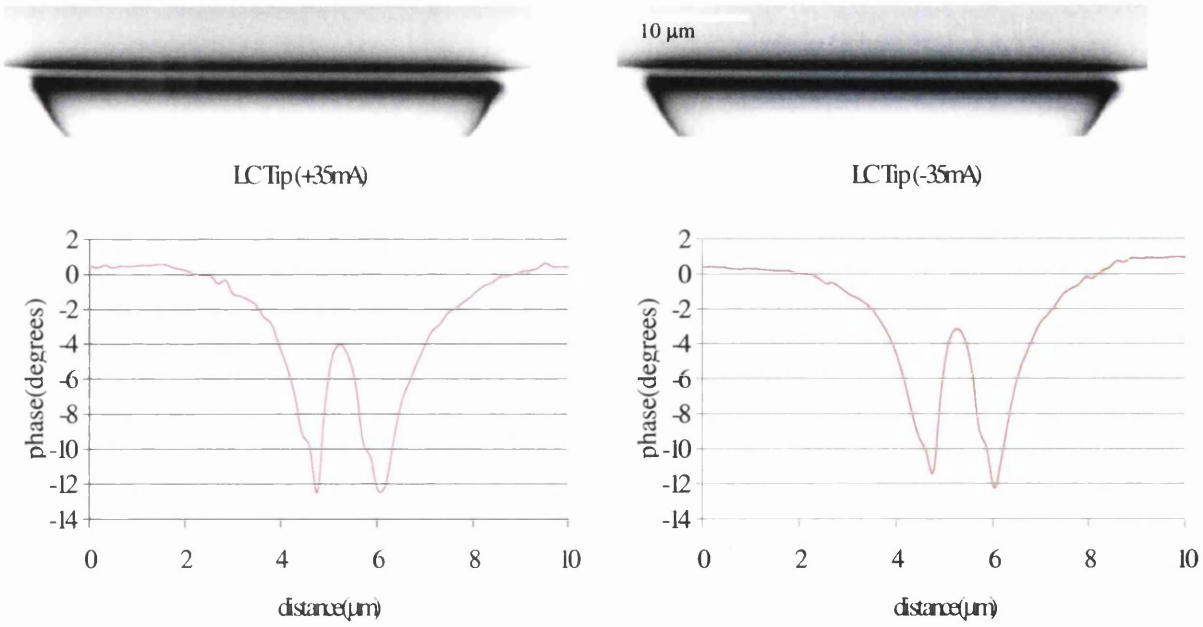

Fig. 4.5.1.8 Phase images taken with an LC tip and the corresponding linescans

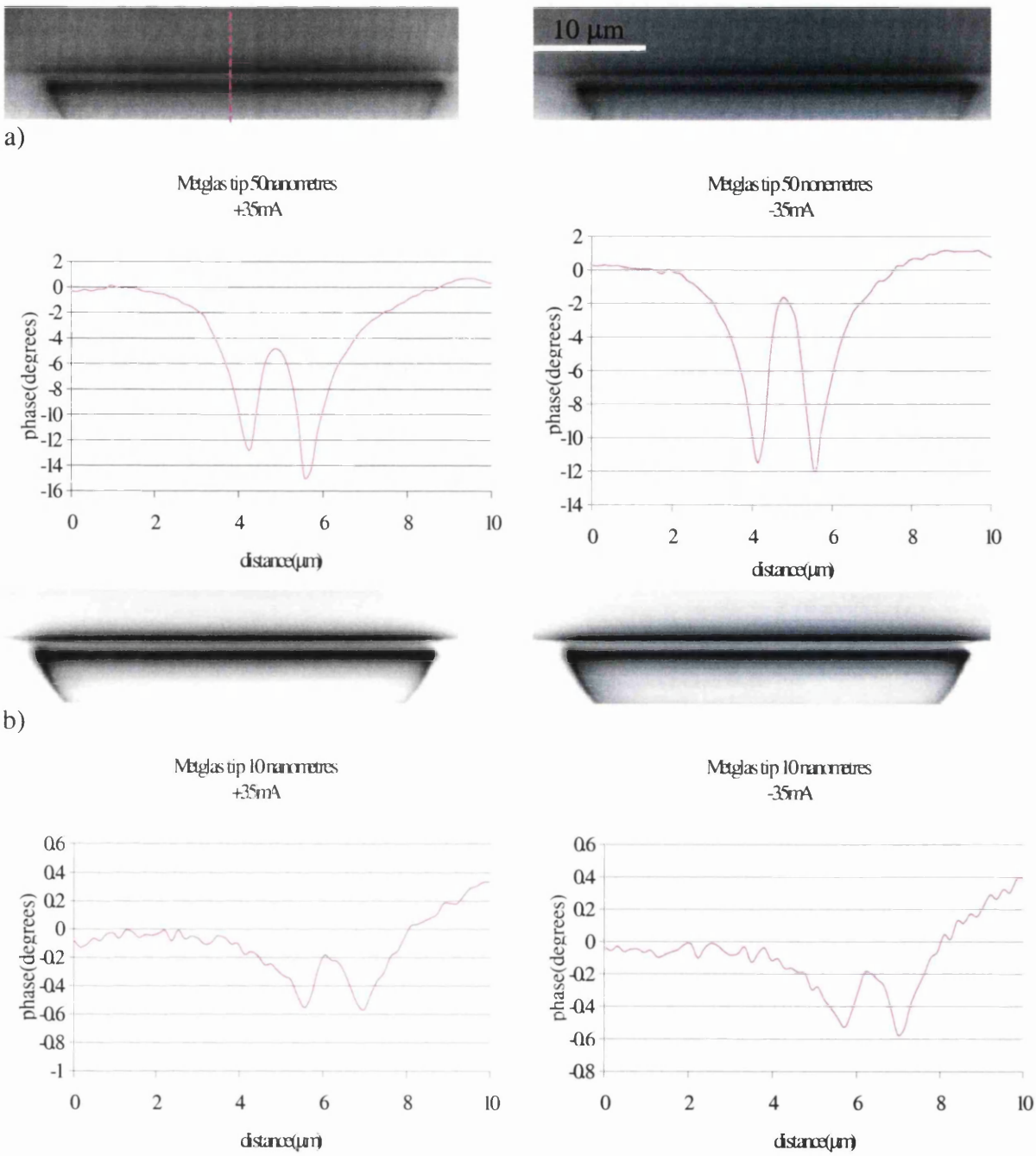

Fig.4.5.1.9 Image pair a), Phase images for the 10nm Metglas tip and corresponding linescans, and b) Phase images for the 50nm Metglas tip and the corresponding linescans.

The images taken with the 10nm-coated tip are quite noisy and this reflects the very small amount of magnetic material present on the tip. Nevertheless the field gradient contrast minima at the pole edges are clearly defined. The low signal to noise ratio with the 10 nanometre tip making it unsuitable for further studies of the heads. The images using the 50nm-coated Metglas tip are comparable in quality to those obtained with the LC tip. It

should be noted that there is asymmetry between the depths of the two minima and this varies slightly depending on the sign of the head drive current. The performance is thus similar to the LC tip. In this case however we do know that the coercivity of the Metglas coating does vary with coating thickness and this has been confirmed by switching-field experiments conducted in the CM20 microscope [4]. For Metglas thickness greater than 50nm, the MFM tips are very soft magnetically, those in the thickness range 30-50nm have ~twice the coercivity and this could account for the observed behaviour. It would be instructive to repeat these imaging studies with such tips.

Variations in the topographic data for the pole edges again plagued this experiment (see fig. 4.5.1.10), especially when the 50nm Metglas tip was used. It was difficult to determine why sometimes this occurred and other times behaved "normally". One possible explanation for this effect is that heating occurred within the head at the higher drive currents applied to it. The effect that has not been studied to date is the effect of temperature on the tips while being scanned over the samples.

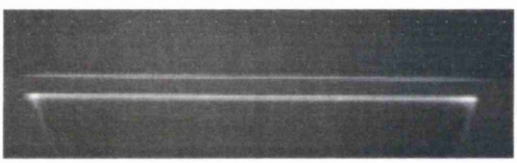

Fig.4.5.1.10 The topographic variations observed along the pole edges when the head was driven at 35mA.

In the above data the variation in sample height occurs along both pole edges on either side of the write gap. These have a similar effect on the phase data as surface features that are particularly high i.e. the tip is moved further away from the sample with the result that the recorded phase value is lower. More work needs to be carried out to determine the source of this change in topographic data when higher drive currents are applied to the head.

A higher magnification image of the central part of the pole gap imaged with the 50nm Metglas-coated tip is shown in Fig. 4.5.1.11 together with a selection of linescans. The uniformity of the field over this region is clearly established, as is the asymmetry in the minima depths depending on the pole and the sense of the drive current.

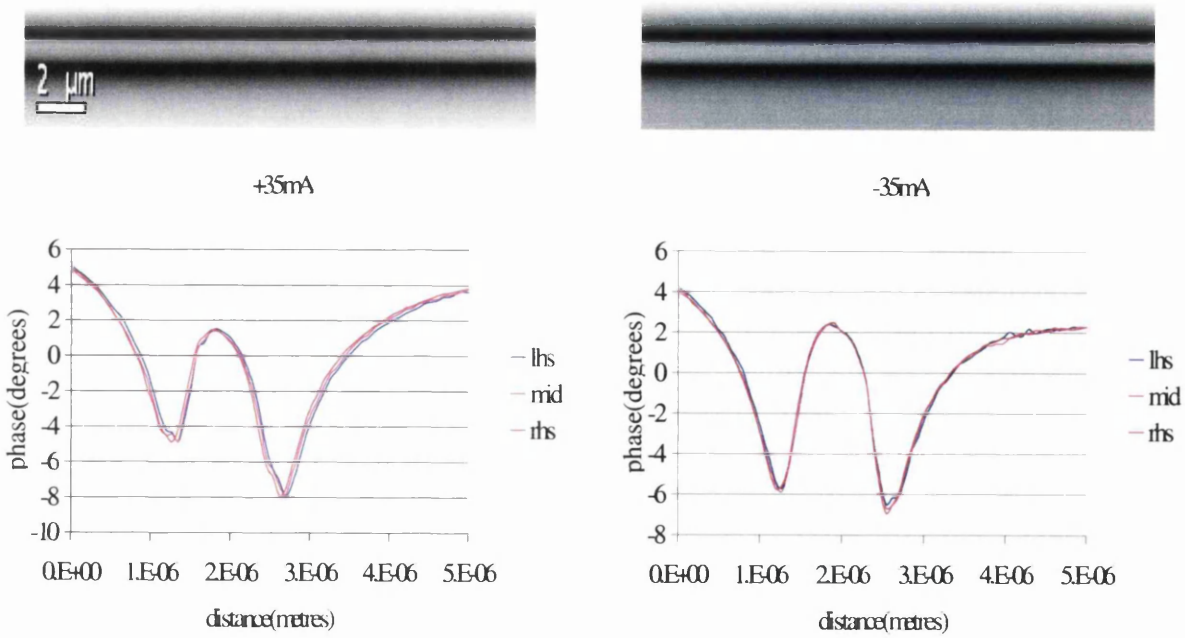

Fig. 4.5.1.11 Phase images taken with the Metglas tip in the region immediately around the pole gap. This pair of images was taken in the middle of the lower pole. The corresponding linescans are also presented.

The minima in the above graphs should be of similar magnitude to those in Fig. 4.5.1.9, but clearly they are not. The reason for this is probably due to variations in topography at the higher drive current applied to the recording head, which were more pronounced at this higher magnification. This data is included to highlight the effect of this problem on the phase data.

4.5.2 The study of the MR Element

This investigation was undertaken late in the study of the data head and unfortunately only the low coercivity tips were available. The MR elements were fully functional in that they could be biased. A series of experiments was performed with the MR element driven at ±10mA, with two bias currents of +4mA and +6mA. To avoid damage to the head, care had to be taken to ensure that the bias voltage was of the correct sign.

The first image pair (Fig. 4.5.3.1) show the height (a) and the phase (b) data for the head with no drive current or bias; this gives a baseline to compare the images in which the MR element was powered. The read gap is approximately 0.25µm in width and although it is

just resolved in the height image, it is much less clear in the phase image. The latter is rather noisy, as seen in the vertical line trace from the middle of the image and this is clearly a contributing factor to the poor gap definition. In an earlier attempt to study the MR element using the very hard magnetic tip, the read gap was clearly resolved in the phase image. Any stray magnetic field produced by driving the MR element with a d.c. current, should appear at the gap edges as the element is recessed from the TBS.

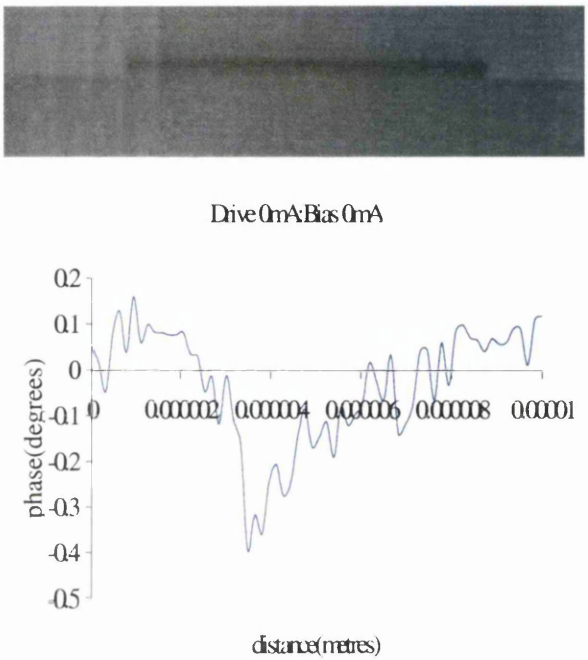

Fig.4.5.3.1 The undriven MR element and the corresponding linescan. The MR element can't be seen in the above image, what is shown is the upper pole and the common pole.

The first pair of images taken under drive currents of ±10mA and at a bias of +4mA are shown in Fig. 4.5.3.2. The first thing that is clear is the much increased contrast from the upper pole in comparison to the previous figure. In addition the line traces show a dip in contrast marked by the red circles. Since this feature appears at the same place in the line trace for both senses of drive current, it must be assumed that it is related to a topographic feature (Fig. 4.5.3.3) and not to any magnetic flux which may be emanating from the upper pole. It should be noted that there is a weak contrast feature along the top of the upper pole – its origin is undetermined

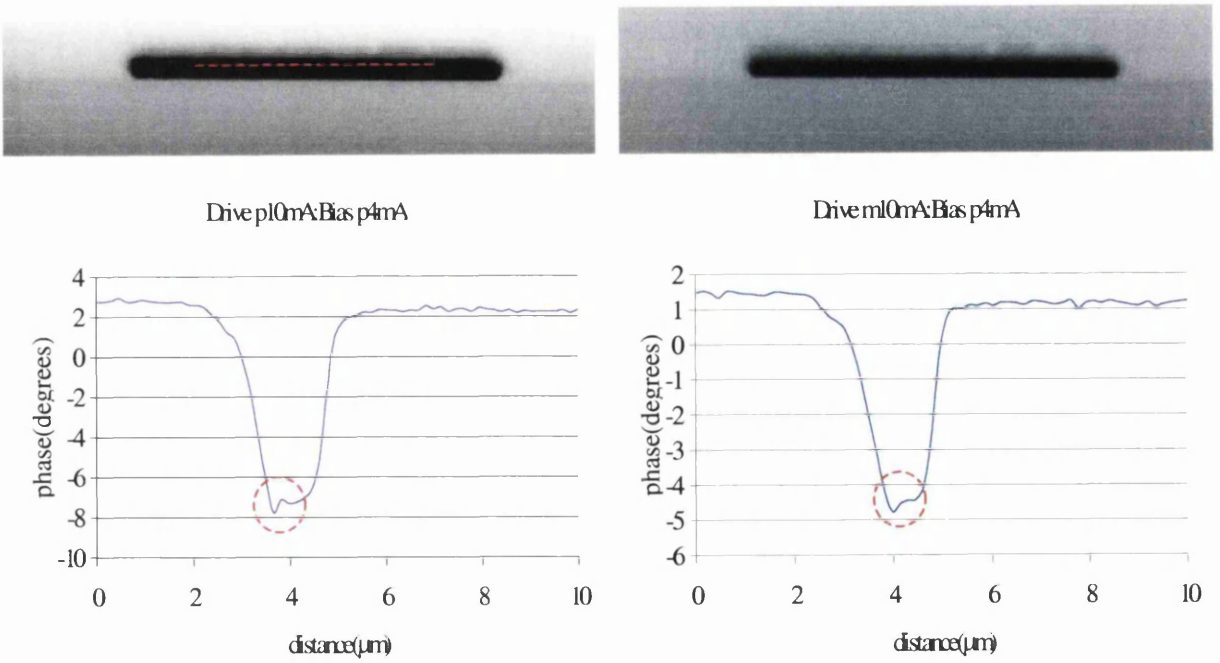

Fig.4.5.3.2 The Phase images of the Read gap taken with the LC tip and the corresponding linescans.

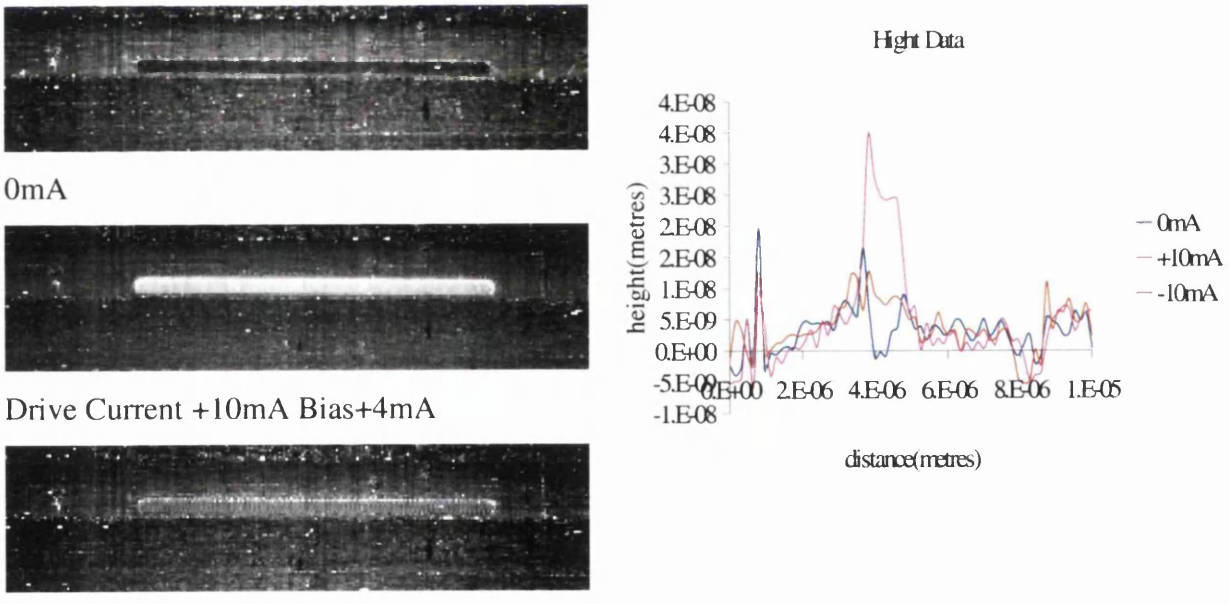

Fig.4.5.3.3 Height data for the images in fig.4.5.3.2.and an assessment of the height data.

At the end of the experiment the resistance of the MR element was checked and found to be ~88Ω compared to the value of ~74Ω at the start of the experiment. It seems likely that

some damage may have occurred to the element possibly due to heating arising from the d.c. drive conditions.

4.6 Discussion of Results

4.6.1 Emboss heads

The results for the Emboss head confirm that a side writing field was the source of the "spurious" stray field observed in the earlier DPC experiments. The MFM experiments confirm that, for a d.c. drive value, the field does not fall to zero in the gap region between two driven poles. It would have been interesting to compare this with results when both pole arrays were driven simultaneously, but with d.c. currents of opposite drive polarity, but this was not feasible.

The determination of a suitable tip for the study of tape recording heads indicates that the CoPt tip is the most promising. It retained its magnetic characteristics (i.e. it did not switch) when the Emboss head was at its full operating current of 400mA. The data from magnetically hard tips is also easier to interpret than for the soft magnetic tips, in that they are sensitive to a particular direction of magnetic induction and the results can be compared to studies carried out using DPC in the (S)TEM.

The MESP tip is not magnetically hard enough for the study of head fields under full head current operation due to tip switching. This is disappointing as it is commercially available from Digital Instruments and it is the standard type generally employed in MFM imaging. The cobalt-coated tip, prepared in our laboratory, showed similar characteristics to the MESP tip, but it was suspected that the performance had been effected by impurities in the coating [4]. Further work on the development of magnetically hard tips is indicated; in particular a preparation method that could be carried out locally would reduce substantially the operating cost of the MFM instrument. The soft magnetic tips were useful in determining the 2D map of the stray magnetic field on the Emboss head, but since the tip/sample force is always attractive, it is difficult if not impossible to determine the vector nature of the magnetic induction of the sample.

Subtracting images with opposite polarity drive currents in the head is at least partially successful in removing the background contrast, but only in the region around the pole gap; this is however the most important region in determining the head field. Improvements to the subtraction method will require further development of methods to remove the phase gradient across the images.

4.6.2 The Data Head

Once again for this sample the CoPt tip would have been the preferred tip for an extensive series of experiments, however we only had two of these prototype tips. An unusual problem occurred in imaging this head, a ripple appearing in the phase data at the pole edges. The source of this ripple was determined to be a pixilation/quantisation effect due to the head being mounted at a small angle with respect to the scan direction. This effect was not observed in the study of the Emboss head. Care must therefore be exercised in the alignment of the scan direction relative to the head geometry.

The soft magnetic tips map the stray field [5] only indirectly as only the magnitude of the tip interaction is observed. Our attempts to produce useful data were from time to time hampered by heating effects in the head. This issue will have to be addressed in future work on magnetic recording head samples.

An attempt was made to study the MR head by detection of the stray field, which should be present at the polegap when the element is subjected to a d.c. voltage; this however proved to be unsuccessful. Poor selection of tip type, combined with too low a magnification, did not help matters. There is however another method that can be employed to study this particular head design with the MFM. That is to scan the tip over the read gap and record the output of the MR element using the MFM hardware. This would give a map of the head read response. It may also be possible to determine the stay magnetic field from the tip in doing so and this could aid in the research on tip characterisation.

4.7 Conclusion

Research into the study of the stray magnetic fields from recording heads using MFM is in its infancy at Glasgow, but some ground rules have been established for the study of inductive write heads. The search for a suitable tip has been narrowed. The full potential of this scanning probe technique has yet to be established for the study of MR read heads. There are several interesting experiments that could be carried out on these samples, such as simultaneously driving both pole arrays for the Emboss head and observing the presence or otherwise of any interference effects. Also the application of a.c. drive currents, as opposed to the d.c. currents used exclusively in the present work, might be illuminating. This would involve changing the data collected from phase to frequency modulation, which directly determines the change in frequency shift. This work could be carried out in conjunction with developing suitable magnetic coatings for the tips. If this was carried out in-house this would not only reduce the cost of tips (as pointed out earlier), but would give the researcher greater control over the nature and the quality of the tips for the MFM.

4.8 References

1. Lohau J., Kirsch S., Carl A., Dumpich G. and Wassermann E.F., (1999), *J. Appl. Phys.*, **85,** 3410

2. Scott J., MacVitie S. and Ferrier R.P., (1999), *IEEE Trans. Mag.*, **35,** 3986

3. Liu Y., (1996) Electron Beam Tomography of Recording Head Fields, Ph.D. Thesis, University of Glasgow

4. J. Scott, (2000), private communication

5. Porthun S., Abelmann L., Vellekopp S.J.L., Lodder J.C. and Hug H.J., (1998), *Appl. Phys. A*, **66**, 1185

Chapter 5

5 Conclusion and Future Work

The work covered within this thesis involved an attempt to characterise the stray magnetic field from the Onstream tape recording heads using electron microscopy/tomography and magnetic force microscopy. Two types of Emboss heads that are used to format the tapes with servo information prior to sale and the data heads used in the tape drive, were studied. Unfortunately we were not involved in the experimental stages of the Onstream product development and hence we had to use production heads and this created difficulties for the electron microscopy investigations. There were no significant problems, with studying full size production heads in the MFM.

The initial DPC imaging studies of the Emboss heads carried out in the JEOL 2000 FX, led us to believe that there could be an undesirable stray field component of significant magnitude from the undriven section of the head. However modelling studies suggested that a more likely reason was the result of side fields from the driven poles. This was later confirmed in the MFM studies, which showed the presence of magnetic fields along the length of the common polepiece. The study of the Emboss heads was disappointing, since originally it was hoped to be able to collect DPC images over a rotation range ±60° and hence obtain useful field information from the tomographic reconstruction of the partial linescan data set; head mounting problems rendered this impractical. Only D.C. drive currents were applied to the head and only one pole array could be driven in any one experiment; studies where both head sections were excited with currents in both the same or opposite senses could have been instructive. An additional study of the domain configuration of the poles by backscattered imaging [1] was considered but could not be implemented due to the protracted microscope operational difficulties.

The experiments conducted on the modified data head, i.e. the single pole 'head', in the Philips CM20 were more promising. Electron beam tomography of recording heads had not previously been carried out on this (S)TEM, which because of its field emission gun, offered significantly higher spatial resolution than the JEOL. However the construction of the data head, which includes both the inductive write element and the MR read element,

has a similar structure to modern data heads for hard disk applications. Of particular concern for tomographic studies is the exceptionally long common pole required to shield the MR element from long range fields, which makes it very difficult to focus the electron probe at the centre of the pole gap. This and the fact that the writing pole was approximately 40μm in length, meant that undesirably low magnifications had to be used in DPC imaging; as a consequence the correction of descan could not be achieved with sufficient accuracy (this is an inherent electron optical problem). Despite these difficulties, a reasonable reconstruction of the stray magnetic field from the data head was achieved. Although future generations of Onstream tape files will have track widths significantly smaller than 40μm, there will still remain the problem of the long common pole between the inductive and MR components in the head. This will have to be overcome, possibly by careful mechanical polishing, if absolute field values close to the head surface are to be determined. The same of course is true for the current generations of hard disk heads, which combine inductive write and MR read elements.

Scanning probe microscopy, in particular MFM, is likely to play a much bigger role in the study of recording heads in the future. Whether this will be directly, as in the presented study, or indirectly, i.e. studying the tracks written by a head, it is difficult to say. However, the capability of working with production heads will clearly be an important consideration to head manufacturers. Not only will this reduce expensive specialised specimen preparation, but it can be part of the manufacture process itself. The extraction of quantitative information on the head field form, particularly close to head surface must be the goal. However for this to happen a number of improvements in technique will be required. The first problem, which will have to be overcome, is the variability of the MFM tip field form for nominally identical tips from the same production batch. The second problem is the variability of the mutual influence of the tip and head fields. The studies carried out in this thesis would indicate that MFM tip coatings, which are magnetically either very hard or very soft, could provide an answer, but no ideal form of either type has so far been identified. Improved performance MFM tips must therefore be sought; in this context the possible use of new improved Hall probes may well be relevant. In principal, the determination of the spatial variation of the vertical field component and its derivative at the head surface, together with a suitable algorithm, can provide a complete 3-D description of the head field. Whilst in the studies reported the lift height of the probe was

kept constant, studies of the signal variation as the lift height is varied would probably be necessary as a precursor to field reconstruction.

The apparent heating of the head samples under d.c. drive conditions in the MFM sometimes proved to be a problem and so the construction of a cooling stage and a means of monitoring the head temperature could be implemented. A more detailed study of the change in sample topography as a function of applied drive current should be undertaken to establish the reason why these changes occur.

Although the study of recording head fields by MFM has some advantages over electron microscopical methods, not least the much simpler specimen preparation, it will almost certainly not provide a complete answer to the characterisation of the head fields. Therefore it will be applied as part of a range of experimental investigations. If the specimen preparation problems can be overcome then electron microscopy can play an important role in these studies, due the complementary information it could provide. The study of the written tracks on the tape, both servo and data, by imaging techniques could also prove beneficial.

One method of studying the MRE that should be investigated is recording the output signal from the readback sensor while scanning a tip across the read gap. This method would enable the read response of the MR element to be investigated. The input connections are available on the MFM and the only additional piece of equipment required would be a pre-amplifier on the output from the readback sensor. This method has already been implemented by workers in Seagate [2], but the application is still very much in its infancy. Ideally the method requires an MFM tip with a field distribution which mimics the stray field from tracks written on the recording media i.e. the tip would have its magnetisation normal to the tip axis; this however is not a simple matter.

References

1. Ferrier R.P., McVitie S. and Nicholson W.A.P., (1990), *IEEE Trans. Mag.*, **26**, 1337 - 1339

2. Foss-Schroeder S. et al, (2001) Paper BD-05 presented at 8th Joint MMM-INTERMAG Conference, San Antonio (to be published in *IEEE Trans. Mag.*)

Appendix 1

1 Noise Studies

1.1 Reconstruction of data from an IBM Tamba Head

Due to the gun instability problems with the JEOL 2000 FX (see Chapter 2 section 2.4.1and Fig 1.1.1 below), it was decided to investigate how effectively the tomographic reconstruction method would cope with excessive noise in the input data. It was decided that the main emphasis should be through modelling with the input data subject to increasing noise levels. However prior to this, DPC data sets were collected for a IBM Tanba recording head [1], which had been studied by Liu [2]. Unfortunately the head was not correctly mounted on the sample stub, with the result that some shadowing occurred during the collection of the data and the field reconstruction is relevant to a plane probably no closer than ~1μm from the ABS. A set of four representative DPC images is shown in Fig. A1.1.1and the microscope parameters for the study are given in Table A1. The sample was rotated through 180 degrees at 5° angular increments and the linescans were extracted from a position 1 pixel beyond the edge of the specimen. The collected linsescans, which constitute the input data for tomographic reconstruction, are shown in Fig. A1.1.2.

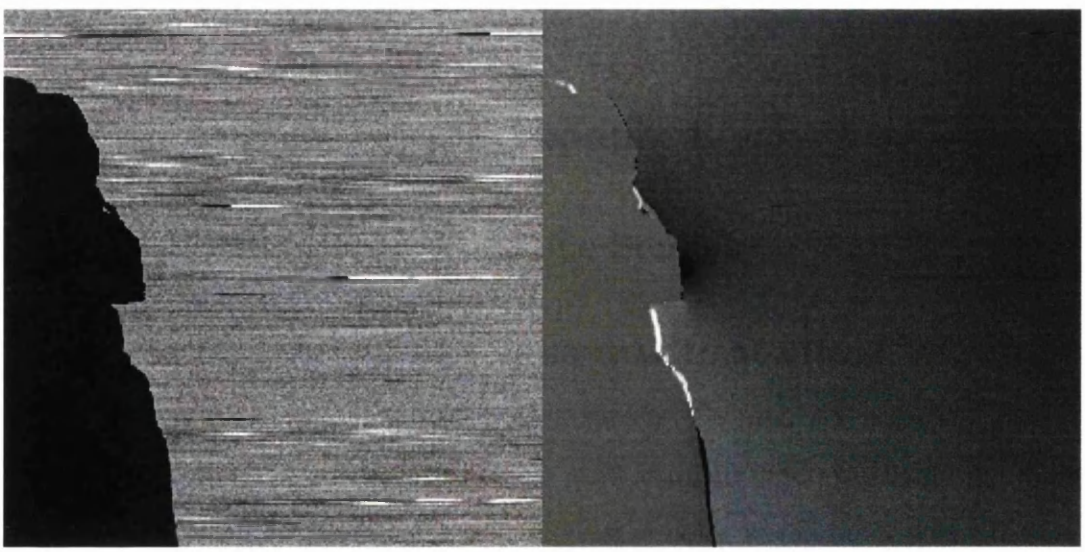

Fig.A1.1.1 Two DPC images showing the instability in the electron beam. The image on the left is a bright field image , i.e. the sum of all the detector quadrants. The other image is a differential phase image, which shows the noise in the data collected for the purpose of reconstruction.

TableA1. Experimental parameters.

Acceleration voltage (kV)	200
Displayed Image magnification	5000
Condenser aperture (μm)	70
Imaging resolution	256×256
Imaging A/D conversion precision	16 bit/pixel
Imaging integration	4
Head drive current (dc-mA)	±8

Lens set up	C1	C2	CM	OBJ	OM	I1	I2	I3	Proj
	7.83	5.28	0.02	3.65	4.18	3.03	2.76	0.07	8.07

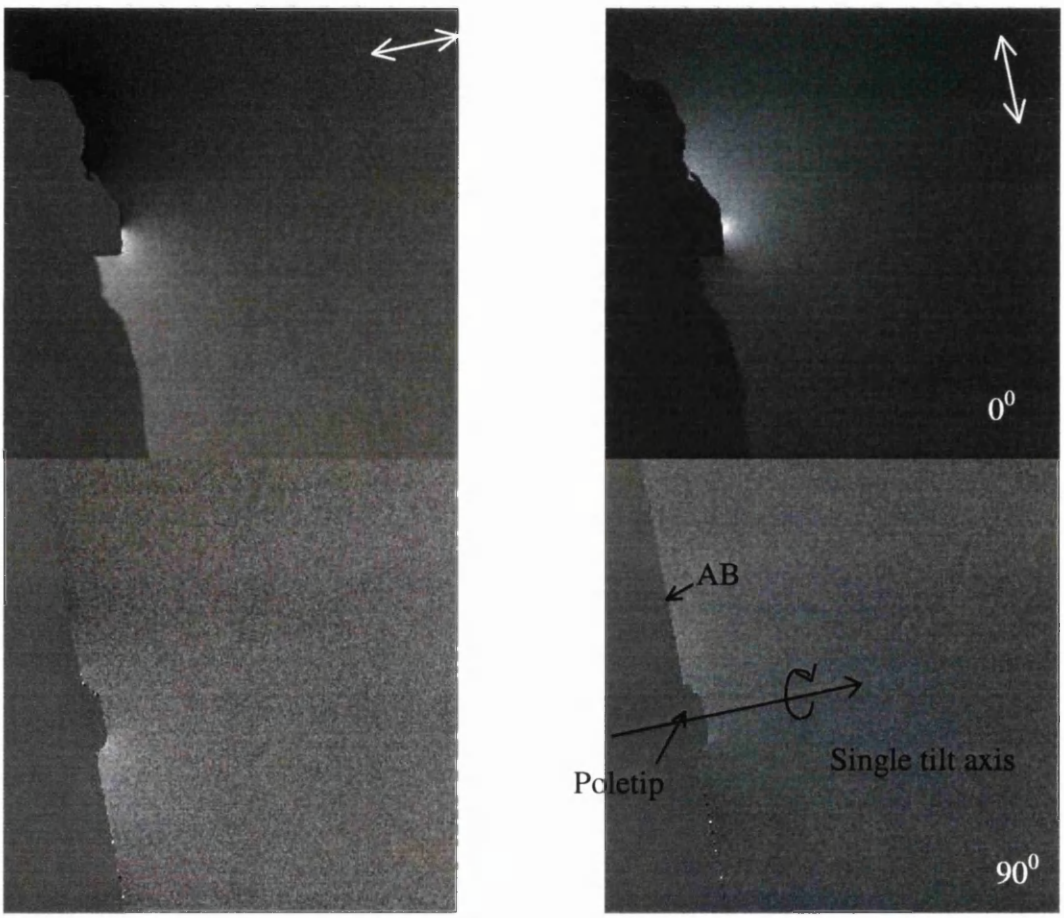

Fig.A1.1.2 DPC images for an IBM Tamba head. Two orthogonal angular rotation positions are shown, one looking down the pole gap (top pair) and the other across the pole gap (bottom pair). The double-ended arrows indicate the integrated field mapping directions of the contrast.

The tomographic data sets are poor in comparison to those collected by Liu. In particular there is a lack of detail around the 0° rotation position and there are apparently d.c. offsets between individual linescans. The fact that the data does not go to zero at the ends of the linescans was noted in the Liu data, but the effect is relatively greater in these data. Gun instability, both in the form of short-term fluctuation and drift in the mean beam current could explain the observed behaviour of the data. Using this data, the three magnetic field components were reconstructed. Given the nature of the data it was decided that the extra work necessary to put the reconstructed field on an absolute basis was not justified and hence the magnitude of the fields are in arbitrary units.

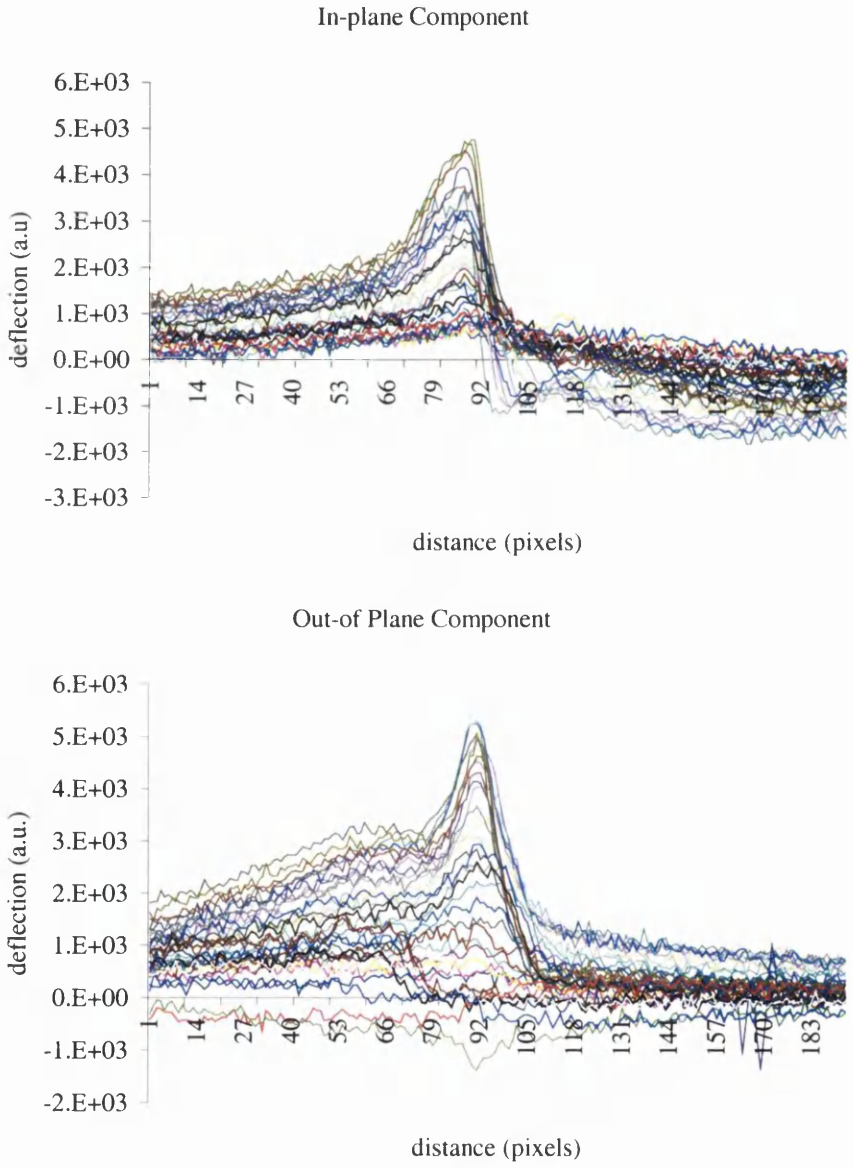

FigA1.1.2 Line scans extracted for the data set part of is presented in Fig.A1.1.1.

Both the ART and the RTM methods were used in the reconstruction; the former requires both data sets to provide the 3-D components of the field at each pixel in the reconstruction plane, whereas in the RTM method each data set gives an independent determination of the field. The results of the reconstructions are shown in Fig. A1.1.3 and the field profiles extracted from the data are shown in Fig. A1.1.4

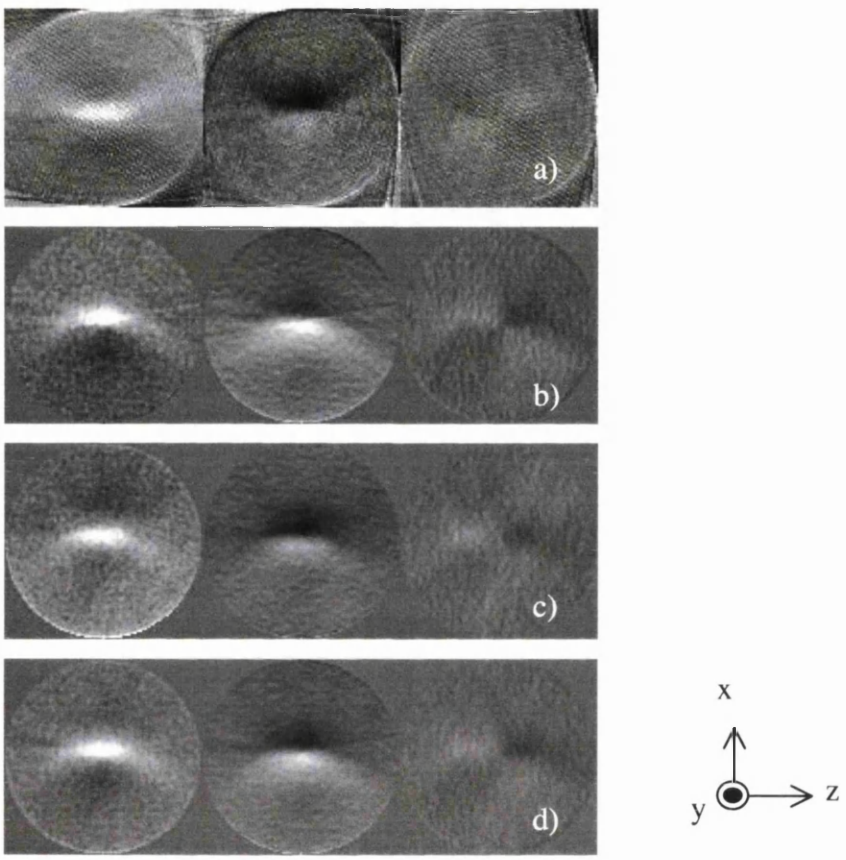

Fig.A1.1.3 The reconstructed magnetic fields, presented as a 2D grey scale image a) the ART reconstructed field, b) the RTM reconstruction using the in-plane component, c) the RTM reconstruction using the out-of-plane component and d) the average of the two RTM reconstructions.

It can been seen that the quality of the reconstructed field is rather poor, although the different methods show consistency in their results. The x and y components are rather better defined than the z component, indicating that the finer details of the field and in particular those that would determine the side writing performance, are largely absent. Given the gun problems, a more reliable assessment of the effect of random noise in the

DPC data on the reconstructed field, would best be obtained from model head field data; this investigated in the next section.

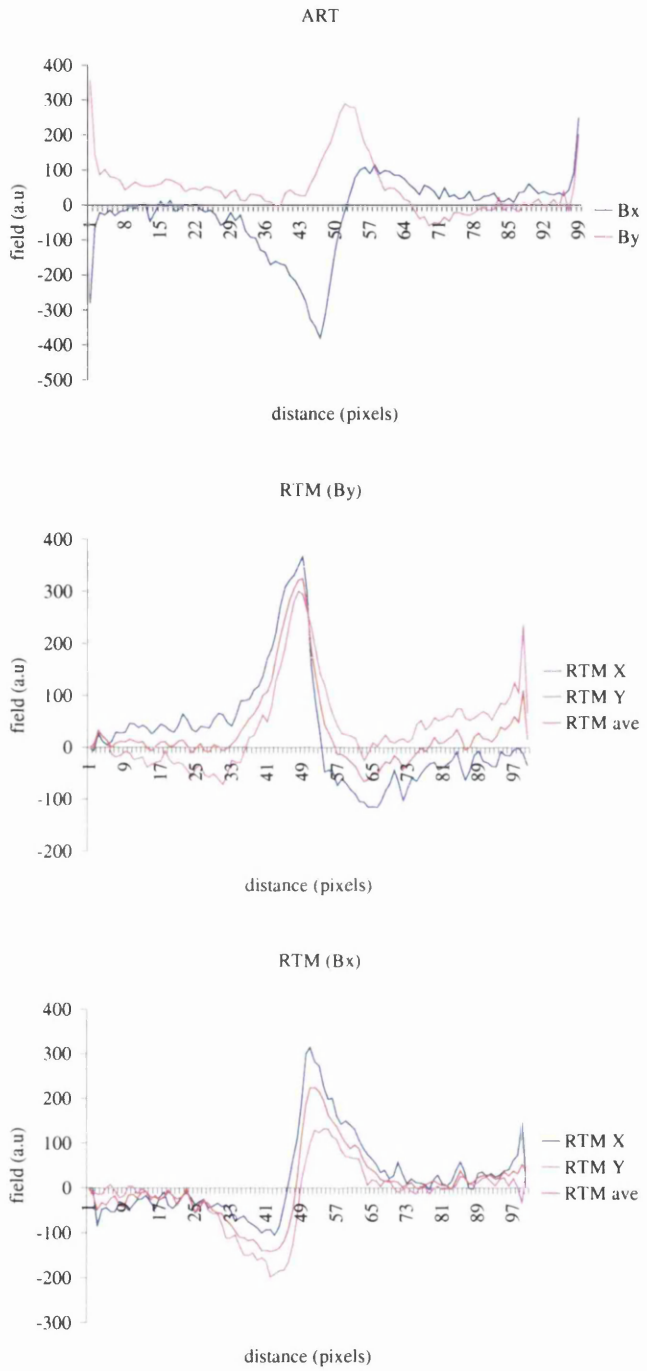

Fig.A1.1.4. Lines scans extracted from the images in fig.A1.1.3.

1.2 Reconstruction of Model Data with Noise

To determine the effect of noise in the (S)TEM DPC data on the reconstructed fields, it was decided to simulate noise in the imaging system. The field values for a head modelled using the TOSCA finite element programme [3] were used. The DPC linescan set, which would result from this field, was computed by integrating the relevant field components as the head rotation was performed. The level of shot noise in a signal is proportional to the square root of that signal. However, as a starting point, it was decided to add random numbers to the model deflection data. A small program was used to generate random numbers with the noise range determined by the experimenter, e.g. –0.1 - 0.1. Random noise over a range of levels was added to the model deflection data and then reconstructions by the ART and RTM methods were performed. The results were then compared with the reconstructions performed using the original 'noise free' data. The reconstructed field components for the differing input data sets are shown in Figs, A1.2.1 – 3, together with representative linescans from the input data sets. In this way the reader can visualise the influence of the level of noise on the quality of the reconstruction

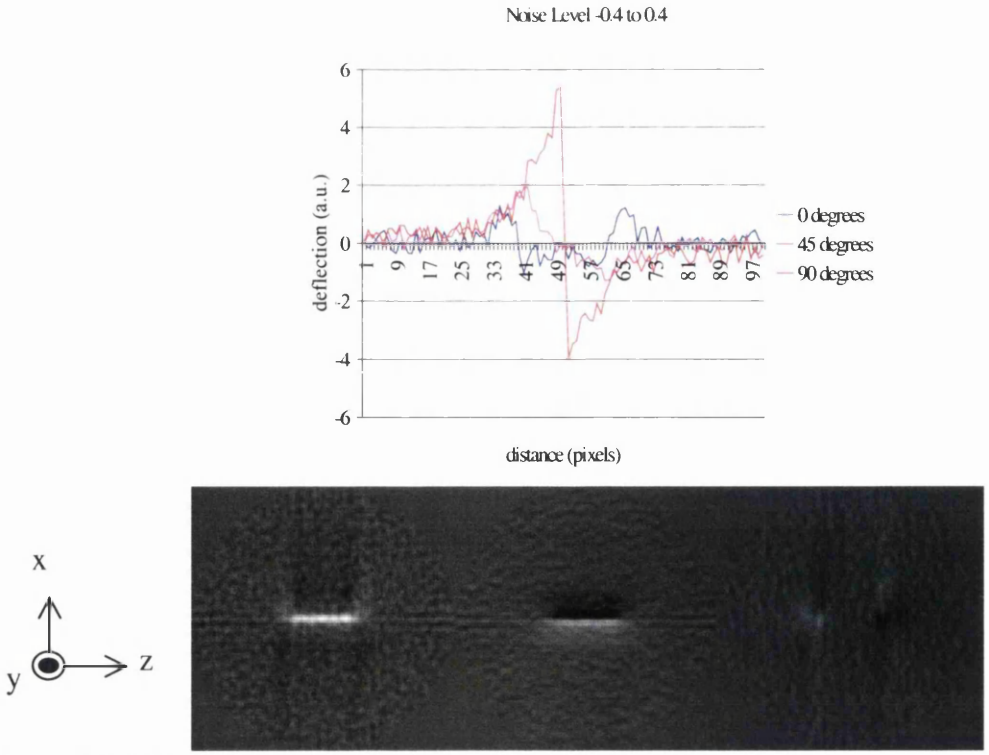

Fig.A1.2.1 RTM 1 reconstructed from the in-plane component of magnetic induction

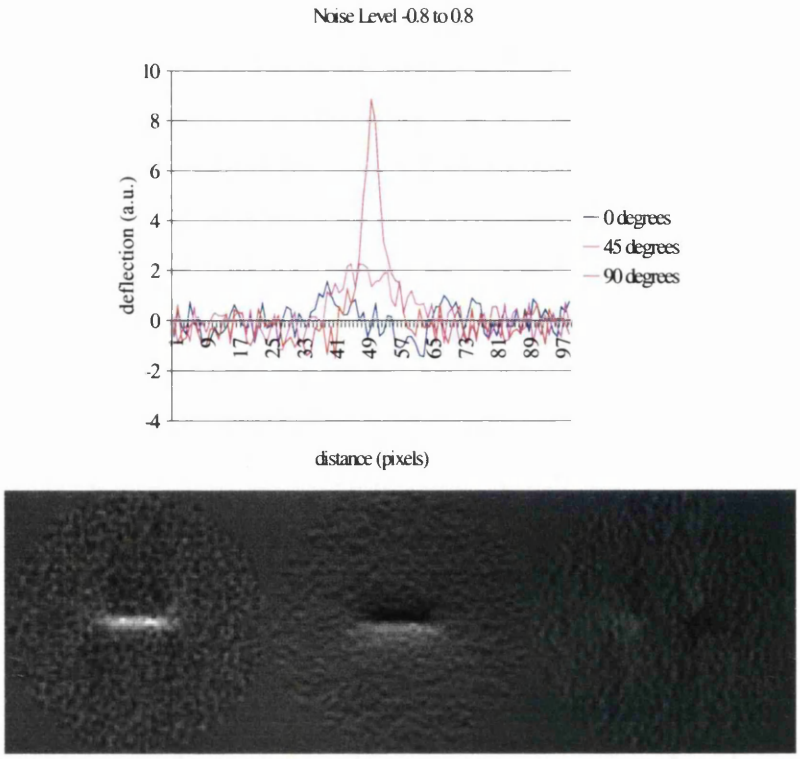

Fig. A1.2.2 RTM2 reconstructed from the in-plane component of magnetic induction.

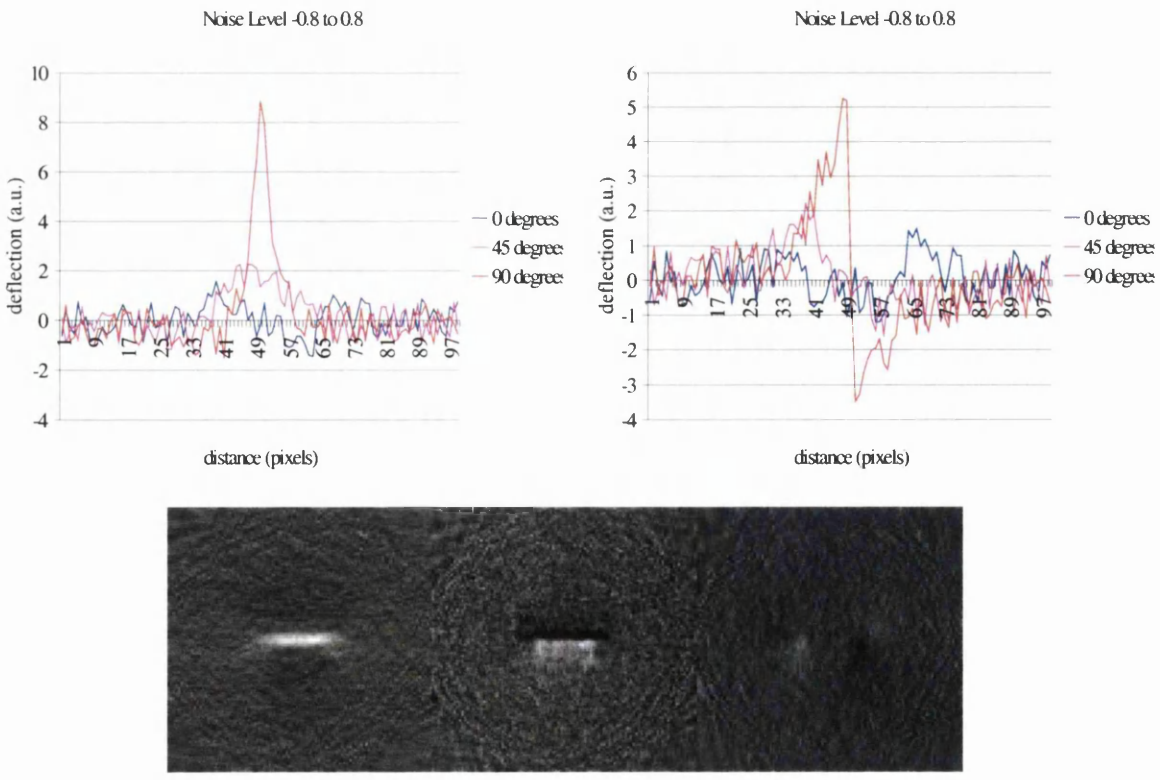

Fig. A1.2.3 ART reconstructed using both deflection components

From the above figures it is clear that both RTM and the ART programs give similar results as the noise level in the data is increased; recognition of the essential form of the head field and in particular the writing (x) component is possible even at relatively high noise levels. This is confirmed by a comparison of extracting the field component profiles extracted from the reconstructions. A comparison of the x component profiles for the ART and RTM methods using the noise free data is shown in Fig. A1.2.4 and apart from a small discrepancy in the maximum writing field value (always noted in previous work [4]) the results are very close. For this reason the development of noise in the reconstructed field components is shown only for the ART method in Fig. A1.2.5

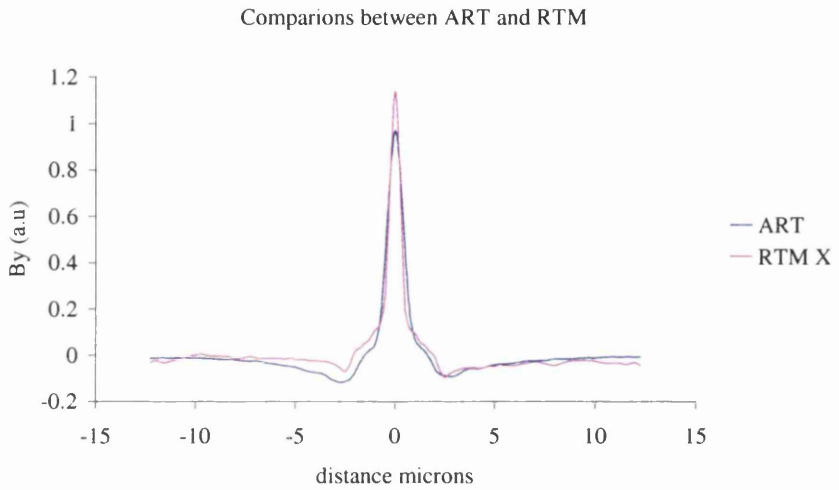

Fig.A1.2.4 A comparison between output of ART and RTM programs

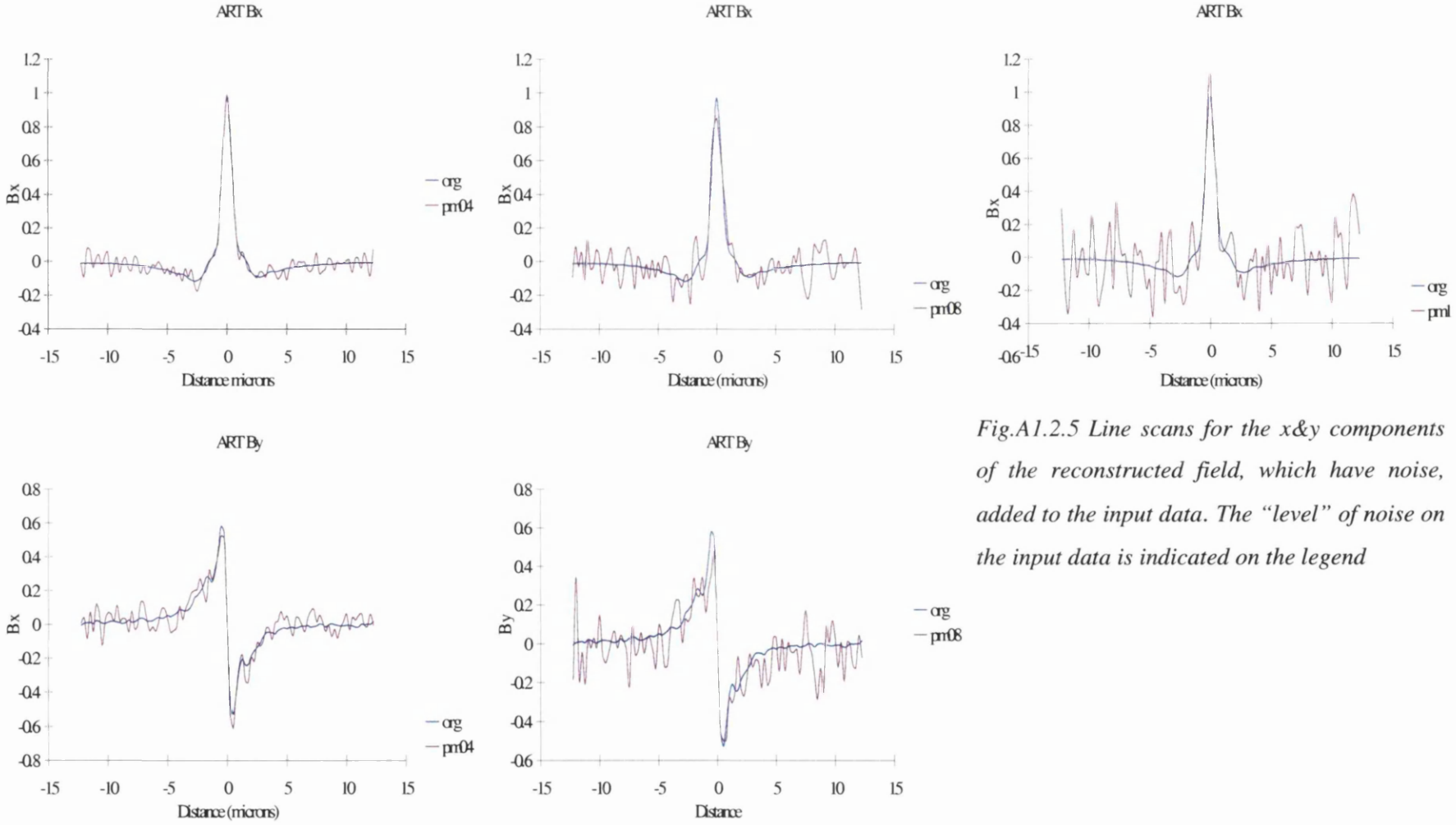

Fig.A1.2.5 Line scans for the x&y components of the reconstructed field, which have noise, added to the input data. The "level" of noise on the input data is indicated on the legend

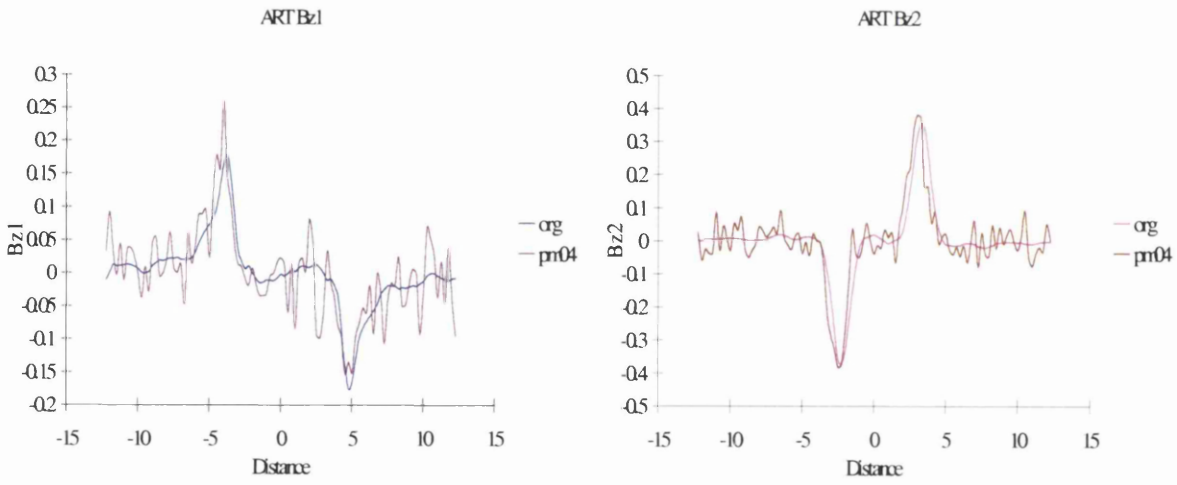

Fig.A1.2.5a Line scans for the Z component of the reconstructed field, which have noise, added to the input data.

The above graphs of the field component profiles reinforce the visual observations of the reconstructed fields. If a more realistic noise model had been employed, i.e. one which would have accounted for the shot noise aspect of the data, then a much smaller acceptable noise level would almost certainly have resulted

1.3 References

1. Chiu, A. et al. (1996), *IBM Journal of Research and Development*, **40**, 283-300

2. Liu, Y., (1996), *Electron Beam Tomography of Recording Head Fields*, Ph.D. Thesis, University of Glasgow

3. The model thin film head fields were computed using a finite-element package called TOSCA by Dr. David Heim at IBM Storage System Division, California

4. Ferrier, R.P., private commiunication